

**NASA
Reference
Publication
1080**

November 1981

NASA-RP-1080-VOL-1
19820008274

ATS-6 Final Engineering Performance Report

Volume I - Program and Systems
Summaries; Mechanical and
Thermal Details

LIBRARY COPY

NOV 17 1982
LANGLEY RESEARCH CENTER
LIBRARY, NASA
HAMPTON, VIRGINIA

NASA

**NASA
Reference
Publication
1080**

1981

ATS-6 Final Engineering Performance Report

Volume I - Program and Systems Summaries; Mechanical and Thermal Details

Robert O. Wales, *Editor*
Goddard Space Flight Center
Greenbelt, Maryland



National Aeronautics
and Space Administration

**Scientific and Technical
Information Branch**

An Engineering Evaluation

in

Six Volumes

- Volume I: Program and System Summaries; Mechanical and Thermal Details**
 - Part A: Program Summary**
 - Part B: Mechanical Subsystems**
 - Part C: Thermal Control and Contamination Monitor**
- Volume II: Orbit and Attitude Control**
 - Part A: Attitude Control**
 - Part B: Pointing Experiments**
 - Part C: Spacecraft Propulsion**
 - Part D: Propulsion Experiment**
- Volume III: Telecommunications and Power**
 - Part A: Communications Subsystem**
 - Part B: Electrical Power Subsystem**
 - Part C: Telemetry and Command Subsystem**
 - Part D: Data Relay Experiments**
- Volume IV: Television Experiments**
 - Part A: The Department of Health, Education and Welfare Sponsored Experiments**
 - Part B: Satellite Instructional Television Experiment (India)**
 - Part C: Independent Television Experiments**
- Volume V: Propagation Experiments**
 - Part A: Experiments at 1550 MHz to 1650 MHz**
 - Part B: Experiments at 4 GHz to 6 GHz**
 - Part C: Experiments Above 10 GHz**
- Volume VI: Scientific Experiments**

This document makes use of international metric units according to the *Système International d'Unités* (SI). In certain cases, utility requires the retention of other systems of units in addition to the SI units. The conventional units stated in parentheses following the computed SI equivalents are the basis of the measurements and calculations reported.

For sale by the National Technical Information Service
Springfield, Virginia 22161
Price

VOLUME I
CONTENTS

	<i>Page</i>
FOREWORD.....	xvii
INTRODUCTION.....	xxi

PART A
PROGRAM SUMMARY

CHAPTER 1 – MISSION SUMMARY	3
MISSION OBJECTIVES	3
MISSION OPERATIONS	4
CONCLUSIONS	10
CHAPTER 2 – SPACECRAFT SYSTEMS SUMMARY	11
REQUIREMENTS.....	11
Reliability	11
Launch Vehicle.....	12
OVERALL CONFIGURATION	13
TELEMETRY AND COMMAND SUBSYSTEM	16
Command and Telemetry Provisions.....	17
Command	17
Telemetry	17
ATTITUDE CONTROL SUBSYSTEM	18
SPACECRAFT PROPULSION SUBSYSTEM	19
COMMUNICATIONS SUBSYSTEM	19

VOLUME I
CONTENTS (continued)

	<i>Page</i>
ELECTRICAL POWER SUBSYSTEM.....	20
MECHANICAL SUBSYSTEM.....	21
THERMAL CONTROL SUBSYSTEM.....	22
RF COMPATIBILITY.....	22
OVERALL SPACECRAFT CHARACTERISTICS	23
CHAPTER 3 – SPACECRAFT TEST PROGRAM	27
TEST PROGRAM.....	27
SPACECRAFT TEST RESULTS.....	31
CHAPTER 4 – SPACECRAFT OPERATIONS SUMMARY.....	33
INITIAL MISSION OPERATIONS/PERFORMANCE	33
Launch	33
Ascent.....	36
Separation.....	38
Deployment	38
Sun Acquisition.....	39
Activation of Other Spacecraft Equipment.....	39
Earth Acquisition	40
Yaw Reference Maneuver	40
SPACECRAFT AND EXPERIMENT 30-DAY CHECKOUT.....	40
OVERALL MISSION/EXPERIMENT OPERATIONS.....	41
IN-ORBIT PERFORMANCE.....	49
IN-ORBIT ANOMALIES.....	54
TERMINAL MISSION OPERATIONS	56

VOLUME I
CONTENTS (continued)

	<i>Page</i>
Final Engineering Tests	56
Spacecraft Deorbit and Spinup Operations	58
Spacecraft Deactivation.	59
 CONCLUSIONS AND RECOMMENDATIONS.	 59
 PART B MECHANICAL SUBSYSTEMS	
 CHAPTER 5 – MECHANICAL DESIGN REQUIREMENTS	 67
 INTRODUCTION AND FUNCTIONAL REQUIREMENTS	 67
Earth-Viewing Module.	69
Fields of View.	71
Spacecraft Grounding Plan	71
Boom/Array Positive Latching Mechanisms.	72
 REFLECTOR SUPPORT ASSEMBLY	 73
Reflector Support Truss	73
Structural Hub	73
Hub Bridge Truss.	76
Magnetometer Boom Assembly	76
EME Adapter Assembly	76
 PARABOLIC REFLECTOR SUBSYSTEM	 76
Reflector Hub Assembly	77
Ribs and Mesh.	77
Release Mechanism	78
 SOLAR PANEL AND BOOM SUBSYSTEM	 78
Boom Assembly	78
Solar Array Panel Assembly	80
 EARTH-VIEWING MODULE SUBSYSTEM.	 82

VOLUME I
CONTENTS (continued)

	<i>Page</i>
Earth-Viewing Module Assembly	82
Communications Module	83
Service Module	83
Experiment Module	85
CHAPTER 6 – SEPARATION AND DEPLOYMENT MECHANISMS	87
SEPARATION MECHANISM	87
Separation Adapter Assembly	87
Separation Commanding	89
Separation Monitoring	91
SPACECRAFT DEPLOYMENT	91
Solar Array First-Motion Release	93
Solar Array First-Stage Deployment	96
Solar Array First-Stage Lockup	99
Solar Array First-Motion Monitoring	99
Solar Array Restraint and Release	99
Solar Array Second-Stage Deployment	101
Solar Array Second-Stage Lockup and Monitoring	103
Parabolic Reflector Deployment	103
Parabolic Reflector Deployment Monitoring	105
Solar Array Fourth-Stage Release	105
Solar Array Fourth-Stage Deployment and Monitoring	107
SQUIB INTERFACE UNIT AND AUTOMATIC DEPLOYMENT SEQUENCER	107
General Description	107
SIU/ADS Functional Description	108
ADS Operational Logic	109
CHAPTER 7 – DESIGN AND PERFORMANCE EVALUATION	115
INTRODUCTION	115

**VOLUME I
CONTENTS (continued)**

	<i>Page</i>
SPACECRAFT ENVIRONMENTAL TESTING REQUIREMENTS	115
Objectives	115
Implementation	115
SPECIAL TESTS	117
Spacecraft Separation	117
Adapter Release Test	118
Separation Test	118
Spacecraft Deployment	120
Solar Array Release	120
Damper and Hinge Cold Chamber Tests	121
Solar Array Zero-G Deployment Tests	121
Damper Development	122
THERMAL STRUCTURAL MODEL SPACECRAFT	123
IN-ORBIT PERFORMANCE AND OPERATIONS	123
Overview	123
Performance Evaluation of Structural/Mechanical/Reflector Subsystems	123
IN-ORBIT ANOMALIES—NORTH ARRAY PANEL DELAYED DEPLOYMENT	125
CONCLUSIONS AND RECOMMENDATIONS	128
CHAPTER 8 – TELEVISION CAMERA REFLECTOR MONITOR	131
FUNCTIONAL REQUIREMENTS	131
DESIGN DESCRIPTION	131
IN-ORBIT PERFORMANCE	132

**VOLUME I
CONTENTS (continued)**

	<i>Page</i>
IN-ORBIT ANOMALIES.....	133
CONCLUSIONS AND RECOMMENDATIONS.....	133
PART C THERMAL CONTROL AND CONTAMINATION MONITOR	
CHAPTER 9 – THERMAL CONTROL SUBSYSTEM	143
INTRODUCTION.....	143
Design Description	143
General Considerations	143
Thermal Design Hardware.....	146
CHAPTER 10 – THERMAL CONTROL DESIGN VALIDATION.....	155
INTRODUCTION.....	155
Mathematical Modeling.....	155
Louvers Analysis.....	155
Heat Pipe Modeling.....	155
EVM Math Model	157
TESTING	158
Thermal-Structural Model.....	158
Verification and Qualifications Tests.....	159
CHAPTER 11 – THERMAL CONTROL SUBSYSTEM PERFORMANCE.....	167
DATA COMPILATION AND EVALUATION.....	167
THERMAL CONTROL SUBSYSTEM PERFORMANCE	167
Early Mission Performance	167

VOLUME I
CONTENTS (continued)

	<i>Page</i>
Orbital Temperature	169
SPECIAL IN-ORBIT TESTS	184
Heat Pipe Performance	184
Louver Performance	187
ANOMALIES	188
Battery Temperature	189
Earth Sensor	194
CONCLUSIONS AND RECOMMENDATIONS	196
CHAPTER 12 – ADVANCED THERMAL CONTROL FLIGHT EXPERIMENT	201
INTRODUCTION	201
EXPERIMENT OBJECTIVES	201
SYSTEM DESCRIPTION	201
FLIGHT PERFORMANCE AND EXPERIMENT RESULTS	206
Normal Mode Performance	207
Feedback Versus Passive Control	210
Normal Versus Passive Mode Performance	210
Feedback Control at an Elevated Set Point	211
COMPARISON OF FLIGHT AND 1-g PERFORMANCE	213
Long Term Performance	216
Telemetry	216
Degradation of Second-Surface Mirrors	216
Phase-Change Material	219
Thermal Diode Heat Pipe	219
Feedback-Controlled Heat Pipe	221

**VOLUME I
CONTENTS (continued)**

	<i>Page</i>
END OF MISSION	221
SUMMARY	222
REFERENCES	223
CHAPTER 13 – QUARTZ-CRYSTAL MICROBALANCE CONTAMINATION MONITOR ..	225
INTRODUCTION	225
SYSTEM DESCRIPTION	225
DATA MEASUREMENT AND EXPERIMENT RESULTS	225
SIGNIFICANT RESULTS AND SUMMARY	227
APPENDIX—ACRONYMS AND ABBREVIATIONS	229
BIBLIOGRAPHY	243

LIST OF ILLUSTRATIONS

<i>Figure</i>	<i>Page</i>
Frontispiece—ATS-6 Spacecraft Undergoing All Up RFC Tests at Fairchild Space and Electronics Company	xxiv
1-1 ATS-6 Earth-Pointing Reference Orientation (Local Vertical/Orbit Plane)	8
2-1 Configuration and Nominal Orientation in Orbit	14
2-2 Launch (Stowed) Configuration	15
3-1 TSM Spacecraft (Launch Configuration)	28
3-2 Protoflight Spacecraft Test Program—Schedule	30
4-1 Launch of ATS-6 on a Titan III-C Launch Vehicle	34

LIST OF ILLUSTRATIONS (continued)

<i>Figure</i>		<i>Page</i>
5-1	Design Load Requirements	68
5-2	Structural and Reflector Subsystems.	70
5-3	Reflector Support Assembly	74
5-4	Reflector Support Assembly (Detail A and Detail B)	75
5-5	Technicians Furl Large ATS-6 Antenna Reflector.	77
5-6	Truss Frame (Boom) Assembly	79
5-7	Solar Array Panel Assembly	81
5-8	Earth-Viewing Module.	82
5-9	Service Module Structural Assembly	84
6-1	Separation Adapter Assembly	88
6-2	Spacecraft/Titan III-C Arm/Fire Separation Interface.	90
6-3	Separation Sequence Diagram	92
6-4	Deployment Sequence.	93
6-5	Deployment Mechanisms.	94
6-6	Center-Line Lock (Prerelease).	95
6-7	Restraint Assemblies	95
6-8	Center-Line Lock (Post-Release).	96
6-9	First-Stage Deployment Mechanism	97
6-10	First-Stage Lockup Mechanism	98
6-11	Solar Array Restraint and Release Mechanism.	100
6-12	Second-Stage Deployment and Lockup Mechanisms.	102

LIST OF ILLUSTRATIONS (continued)

<i>Figure</i>		<i>Page</i>
6-13	Parabolic Reflector Assembly: Release and Deployment Mechanism	104
6-14	Fourth-Stage Release and Deployment Mechanisms	106
6-15	Simplified Schematic of the SIU, ADS, and External Connections	110
6-16	Command Decoder-Distributor/SIU/ADS Interface Functional Diagram	111
6-17	Automatic Deployment Sequencer, Logic Block Diagram	112
6-18	ADS Input Configuration	113
7-1	TSM and Adapter/Transtage Mass Simulator Configuration for Separation Tests . .	119
7-2	ZAZ During Deployment	127
8-1	TV Camera Outline Drawing	133
8-2	TV Camera Reflector Monitor Configuration	134
8-3	TV Camera Monitor Ground Station Configuration	135
8-4	Progress of EVM Shadow Across Antenna-0255	136
8-5	Progress of EVM Shadow Across Antenna-0505	137
8-6	Progress of EVM Shadow Across Antenna-0822	138
8-7	Progress of EVM Shadow Across Antenna-0959	139
9-1	Thermal Control Subsystem	145
9-2	EVM Thermal Design	146
9-3	Interferometer Horn Thermal Design (Typical Interface with EVM Blankets).	147
9-4	GFRP and Solar Array Harness Insulation.	148
9-5	ATS-6 Louvers	149
9-6	EVM Average Temperatures	150

LIST OF ILLUSTRATIONS (continued)

<i>Figure</i>		<i>Page</i>
9-7	Heat-Pipe Design	152
10-1	Louver Characteristics.	156
10-2	Thermal Model for Heat-Pipe-Honeycomb Panel with Exterior Louvers	157
10-3	Predicted vs. Test Temperatures for Heat Pipes in Communications Module.	159
11-1	Average EVM Temperature (Heat Pipe Panels)	169
11-2	Launch Solar Array Boom Temperature	170
11-3	Launch GFRP, Fitting, and EME Truss Temperature	172
11-4	Launch Damper Temperature	174
11-5	Launch Reflector Temperature	176
11-6	Launch Solar Array Temperature	178
11-7	Experiment Module Average Temperature	182
11-8	Service Module Average Temperature	183
11-9	Communications Module Average Temperature	184
11-10	Service Module Heat Pipe No. 3 Flight Data	185
11-11	ATS-6 Five-Year Temperature Comparison.	186
11-12	Telemetry Transmitters/DOC 1 Temperature	187
11-13	Battery Case Temperature.	188
11-14	Solar Array Booms and Deployment Dampers Temperatures	189
11-15	External Structure Temperature	190
11-16	Service Module Heat Pipe No. 3 Flight Data	191
11-17	Communication Module—North Wall Temperature Sensor Locations	192

LIST OF ILLUSTRATIONS (continued)

<i>Figure</i>		<i>Page</i>
11-18	Communication Module Heat Pipe No. 3 Test.	193
11-19	Service Module Temperature vs. Power Dissipation.	194
11-20	Battery Orbital Temperature (August 28, 1976).	195
11-21	Battery Orbital Temperature (September 7, 1976).	196
11-22	Earth Sensor Temperature (August 28, 1976).	199
11-23	Earth Sensor Temperature (September 7, 1976).	200
12-1	Diode Heat Pipe	202
12-2	PCM Box.	202
12-3	Feedback Control	203
12-4	Feedback Control Heat Pipe	203
12-5	Functional Diagram.	204
12-6	Typical Daily Solar Cycle for ATFE	205
12-7	Typical Transient Response in Normal Mode (10 Days Post-Launch)	208
12-8	Axial Temperature Profiles, June 9, 1974	209
12-9	Comparison of Feedback and Passive Transient Control	211
12-10	Comparison of Axial Profiles in Normal and Passive Modes.	212
12-11	Comparison of Feedback and Passive Control at an Elevated Set Point.	213
12-12	Comparison of Flight and Ground Transient Performance—Normal Mode	214
12-13	Comparison of Flight and Ground Axial Temperature Profiles	215
12-14	Daily Temperatures, OSR Absorptivity, and Maximum Solar Intensity vs. Days in Orbit.	217

LIST OF ILLUSTRATIONS (continued)

<i>Figure</i>		<i>Page</i>
12-15	Diode PCM Temperature Drop vs. Days in Orbit.	220
13-1	Quartz-Crystal Microbalance Data.	226

LIST OF TABLES

<i>Table</i>		<i>Page</i>
1-1	Summary of ATS-6 Experiments.	5
2-1	Maximum Predicted External RF Fields (Volts/Meter)	23
2-2	ATS-6 Subsystem Weight Breakdown	24
2-3	ATS-6 Spacecraft Sequenced Mass Properties	25
4-1	Spacecraft Launch Configuration	35
4-2	Times of Major Events During Ascent Phase	37
4-3	Chronology of Spacecraft Activity (June 1 to June 17, 1974)	42
4-4	Experiment Operations Summary – First Year.	47
7-1	ATS-6 Separation/Deployment Timelines.	124
7-2	ATS-6 Deployment Temperatures.	125
7-3	ATS-6 Deployment RGA Rates (Actual Values are in Degrees/Second)	126
9-1	ATS-6 Temperature Specifications (°C)	144
10-1	ATS-6 Components, Structure Qualification, and Actuals.	160
11-1	Component Base Temperatures.	168
11-2	Launch Phase Temperatures	181
11-3	Battery Main and C/60 Charge Rate Temperature Gradients (°C).	197

LIST OF TABLES (continued)

<i>Table</i>		<i>Page</i>
11-4	Shunt Dissipation Data (°C)	197
11-5	Spacecraft Roll Angle vs. Battery Temperature.....	198
11-6	Millimeter Wave Experiment	198
12-1	ATFE Operational Modes	206

FOREWORD

ATS-6 has been referred to as Arthur C. Clarke's "Star," because Mr. Clarke originated the idea for synchronous communications satellites in an article that he wrote in 1945. In 1975, Mr. Clarke was actively engaged in monitoring the Indian Satellite Instructional Television Experiment on ATS-6 and giving feedback to the Indian Space Research Organization. We, therefore, felt that it would be appropriate for him to contribute the foreword for this report.

An excerpt from his response to our request and selected paragraphs from his contribution, "School-master Satellite," follow.



ශ්‍රී ලංකා මොරටුව විශ්වවිද්‍යාලයේ
කුලපති කාර්යාලයෙනි

FROM THE DESK OF THE CHANCELLOR
UNIVERSITY OF MORATUWA, SRI LANKA

ආචාර්ය ඩී. ක්ලර්ක්
බී.ඒ.සී.සී., ඒ.ඒ.ඒ.ඒ.ඒ., ඒ.ඒ.බී.ඒ.ඒ.ඒ.
ලන්ඩනයේ කිංග්ස් විද්‍යාලයේ අධ්‍යාපන සාමාජික
Arthur C. Clarke
B.Sc., F.R.A.S., F.B.I.S.
Fellow of King's College, London.

දුරකථන අංකය: 94255
කේබල්: අන්ඩර්සී
කොළඹ 7
Tel: 94255
Cable: Undersea
Colombo

"ලෙස්ලිගේ නිවස"
25, බාර්න්ස් ප්ලේස්,
කොළඹ 7.
"Leslie's House"
25, Barnes Place,
Colombo 7.

24th September 1980

The extracts that follow are from an essay that was written in 1971, almost five years before the SITE program became fully operational, and originally appeared in the *Daily Telegraph Colour Magazine* for 17 December 1971. It was later read into the *Congressional Record* (27 January 1972) by Representative William Anderson, first commander of the nuclear submarine *Nautilus*, and now forms Chapter 12 of *The View From Serendip* (Random House, 1977; Ballantine, 1978).

To me, it brings back vivid recollections of my meetings with Dr. Sarabhai, the chief instigator of the program. I would like to dedicate it to his memory – and to that of another good friend, also closely associated with the project – Dr. Wernher von Braun.

Chancellor
University of Moratuwa
Sri Lanka

Arthur C. Clarke
Vikram Sarabhai Professor, Physical Research
Laboratory, Ahmedabad
India

SCHOOLMASTER SATELLITE

“For thousands of years, men have sought their future in the starry sky. Now this old superstition has at last come true, for our destinies do indeed depend upon celestial bodies—those that we have created ourselves . . .

“In 1974 there will be a new Star of India; though it will not be visible to the naked eye, its influence will be greater than that of any zodiacal signs. It will be the satellite ATS-F (Applications Technology Satellite F), the latest in a very successful series launched by America’s National Aeronautics and Space Administration. For one year, under an agreement signed on September 18, 1969, ATS-F will be loaned to the Indian Government by the United States, and will be “parked” 22,000 miles above the Equator, immediately to the south of the sub-continent. At this altitude it will complete one orbit every 24 hours and will therefore remain poised over the same spot on the turning Earth; in effect, therefore, India will have a TV tower 22,000 miles high, from which programmes can be received with almost equal strength over the entire country . . .

“ATS-F, now being built by the Fairchild-Hiller Corporation, represents the next step in the evolution of communications satellites. Its signals will be powerful enough to be picked up, not merely by multi-million dollar Earth stations, but by simple receivers, costing two or three hundred dollars, which all but the poorest communities can afford. This level of cost would open up the entire developing world to every type of electronic communication—not only TV; the emerging societies of Africa, Asia and South America could thus by-pass much of today’s ground-based technology, and leap straight in to the space age. Many of them have already done something similar in the field of transportation, going from ox-cart to aeroplane with only a passing nod to roads and railways.

“It can be difficult for those from nations which have taken a century and a half to slog from semaphore to satellite to appreciate that a few hundred pounds in orbit can now replace the continent-wide networks of microwave towers, coaxial cables and ground transmitters that have been constructed during the last generation. And it is perhaps even more difficult, to those who think of television exclusively in terms of old Hollywood movies, giveaway contests and soap commercials to see any sense in spreading these boons to places which do not yet enjoy them. Almost any other use of the money, it might be argued, would be more beneficial . . .

“Those who actually live in the East, and know its problems, are in the best position to appreciate what cheap and high-quality communications could do to improve standards of living and reduce social inequalities. Illiteracy, ignorance and superstition are not merely the results of poverty—they are part of its cause, forming a self-perpetuating system which has lasted for centuries, and which cannot be changed without fundamental advances in education. India is now beginning a Satellite Instructional Television Experiment (SITE) as a bold attempt to harness the technology of space for this task; if it succeeds, the implications for all developing nations will be enormous.

“Near Ahmedabad is the big 50-foot diameter parabolic dish of the Experimental Satellite Communication Ground Station through which the programmes will be beamed up to the hovering satellite. Also in this area is AMUL, the largest dairy co-operative in the world, to which more than a quarter of a million farmers belong. After we had finished filming at the big dish, our camera team drove out to the AMUL headquarters, and we accompanied the Chief Veterinary Officer on his rounds.

SCHOOLMASTER SATELLITE

“At our first stop, we ran into a moving little drama that we could never have contrived deliberately, and which summed up half the problems of India in a single episode. A buffalo calf was dying, watched over by a tearful old lady who now saw most of her worldly wealth about to disappear. If she had called the vet a few days before—there was a telephone in the village for this very purpose—he could easily have saved the calf. But she had tried charms and magic first; they are not always ineffective, but antibiotics are rather more reliable . . .

“I will not quickly forget the haggard, tear-streaked face of that old lady in Gujerat; yet her example could be multiplied a million times. The loss of real wealth throughout India because of ignorance or superstition must be staggering. If it saved only a few calves per year, or increased productivity only a few per cent, the TV set in the village square would quickly pay for itself. The very capable men who run AMUL realise this; they are so impressed by the possibilities of TV education that they plan to build their own station to broadcast to their quarter of a million farmers. They have the money, and they cannot wait for the satellite—though it will reach an audience two thousand times larger, for over 500 million people will lie within range of ATS-F . . .

“And those who are unimpressed by mere dollars should also consider the human aspect—as demonstrated by the great East Pakistan cyclone of 1971. That was tracked by the weather satellites—but the warning network that might have saved several hundred thousand lives did not exist. Such tragedies will be impossible in a world of efficient space communications.

“Yet it is the quality, not the quantity, of life that really matters. Men need information, news, mental stimulus, entertainment. For the first time in 5,000 years, a technology now exists which can halt and perhaps even reverse the flow from the country to the city. The social implications of this are profound; already, the Canadian Government has discovered that it has to launch a satellite so that it can develop the Arctic. Men accustomed to the amenities of civilisation simply will not live in places where they cannot phone their families, or watch their favourite TV show. The communications satellite can put an end to cultural deprivation caused by geography. It is strange to think that, in the long run, the cure for Calcutta (not to mention London, New York, Tokyo), may lie 22,000 miles out in space . . .

“The SITE project will run for 1 year, and will broadcast to about 5,000 TV sets in carefully selected areas. This figure may not seem impressive when one considers the size of India, but it requires only one receiver to a village to start a social, economic and educational revolution. If the experiment is as great a success as Dr. Sarabhai and his colleagues hope (and deserves), then the next step would be for India to have a full-time communications satellite of her own. This is, in any case, essential for the country’s internal radio, telegraph, telephone and telex services . . .

“Kipling, who wrote a story about “wireless” and a poem to the deep-sea cables, would have been delighted by the electronic dawn that is about to break upon the sub-continent. Gandhi, on the other hand, would probably have been less enthusiastic; for much of the India that he knew will not survive the changes that are now coming.

SCHOOLMASTER SATELLITE

“One of the most magical moments of Satyajit Ray’s exquisite Pather Panchali is when the little boy Apu hears for the first time the Aeolean music of the telegraph wires on the windy plain. Soon those singing wires will have gone forever; but a new generation of Apus will be watching, wide-eyed, when the science of a later age draws down pictures from the sky—and opens up for all the children of India a window on the world.”

A. C. Clarke

INTRODUCTION

ATS-6 (ATS-F before launch) was the final satellite in a series of six of the Applications Technology Satellite Program of the National Aeronautics and Space Administration. It was designed and built by Fairchild Space and Electronics Company, Germantown, Maryland, under NASA Contract NAS5-21100 from NASA Goddard Space Flight Center.

At the time of its launch, it was the largest and most powerful communications satellite to go into orbit.

The mission of ATS-6 was to demonstrate and evaluate the application of new technologies for future satellite systems. This it accomplished by demonstrating the first direct-broadcast television from geosynchronous orbit; by demonstrating many new communications technologies; by relaying data from, and tracking, low-orbiting satellites; by relaying communications and positions of ships and aircraft; and by supporting a variety of other experiments involving communications, meteorology, particle and radiation measurements, and spacecraft technology.

The purpose of this report is to document the lessons learned from the 5-year ATS-6 mission that might be applicable to spacecraft programs of the future. To satisfy this purpose, the six volumes of this report provide an engineering evaluation of the design, operation, and performance of the system and subsystems of ATS-6 and the effect of their design parameters on the various scientific and technological experiments conducted.

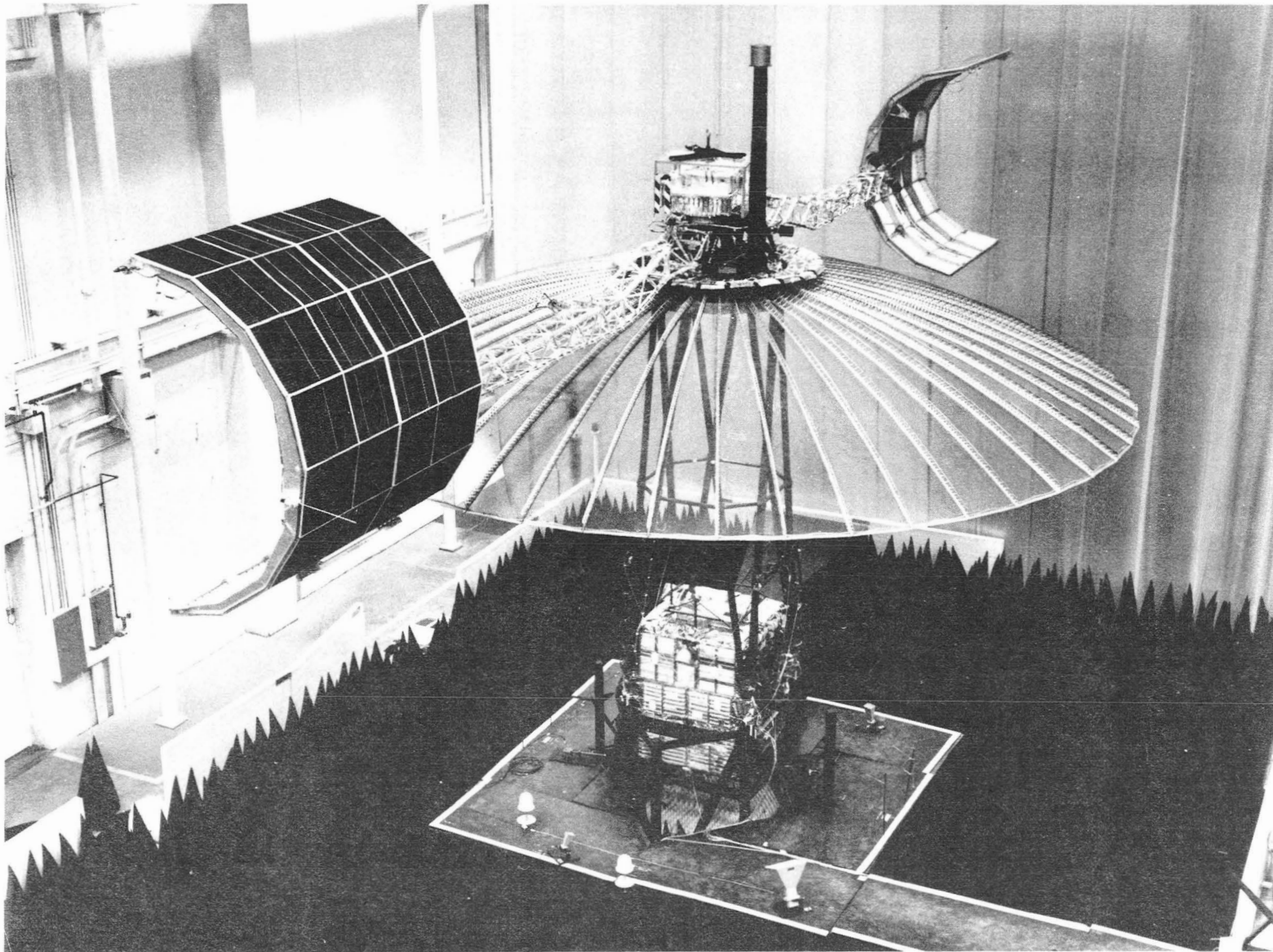
The overall evaluation covers the following:

- A summary of the ATS-6 mission objectives, operations, and results
- A summary description of the spacecraft system and subsystem requirements, the designs evolved to meet these requirements, and special analyses and ground testing performed to validate these designs and to confirm the flight integrity of the spacecraft
- A comparative evaluation of the 5-year performance and operations in orbit relative to those specified and demonstrated during ground tests prior to launch
- A summary of anomalies that occurred in the hardware, probable causes, and recommendations for future spacecraft systems
- A summary evaluation of the various technological and scientific experiments conducted
- A summary of conclusions and recommendations at the spacecraft system and subsystems levels that address considerations that might be relevant to future spacecraft programs or similar experiments.

ACKNOWLEDGMENTS

Many scientists, engineers, and technicians, too numerous to mention by name, have contributed to these volumes. Engineers at Fairchild Space and Electronics Company and Westinghouse Defense and Electronic Systems Center composed the chapters from material supplied by subsystems designers of the various systems and experiments, and have worked closely with the editors to complete this report. They have the editor's gratitude.

In particular, thanks go to Mr. Ralph Hall at Fairchild Space and Electronics Company and Mr. James Meenen of Westinghouse Defense and Electronic Systems Center for their patient cooperation, thorough review, and constructive comments and suggestions.



ATS-6 Spacecraft Undergoing All Up RFC Tests at Fairchild Space and Electronics Company

Part A
Program Summary

CHAPTER 1

MISSION SUMMARY

MISSION OBJECTIVES

The Applications Technology Satellite-6 mission objectives were to:

- Demonstrate the deployment in near-geosynchronous orbit of a 9.14-meter (30-foot) diameter parabolic reflector antenna, with an associated communications system, that is capable of providing good quality TV signals to small, inexpensive ground receivers, and to measure and evaluate the performance of such a system.
- Stabilize the spacecraft using a 3-axis attitude control system, with a slewing capability in roll and pitch off the local vertical, permitting antenna pointing with an accuracy commensurate with the antenna characteristics.
- Support and demonstrate user-oriented applications experiments using the spacecraft capabilities.
- Meet a 2-year mission lifetime (specification) with a 5-year design goal.

Mission success was to be judged on the basis of meeting these objectives.

In addition, there were numerous secondary mission objectives as follows:

- To demonstrate new technology in space appropriate to:
 - aeronautical and maritime traffic control
 - infrared Earth observation
- To acquire useful systems data for application to communications in space by:
 - demonstrating a two-axis, steerable antenna beam
 - measuring radio frequency interference in shared frequency bands
 - measuring propagation characteristics of millimeter waves, measuring ionospheric/exospheric electron content, and studying ionospheric propagation effects
 - performing spacecraft-to-spacecraft communications and tracking experiments.
- To test and obtain useful data on the following spacecraft technologies:
 - three-axis stabilization with a Z-axis (reflector boresight) Earth-pointing capability to an accuracy of ± 0.1 degree (3-sigma) over a roll/pitch angle range of ± 10 degrees off

- the local vertical and a roll/pitch slewing capability over 17.5 degrees (Earth angle) in 30 minutes
- microwave interferometer attitude sensor with a precision compatible with the 0.1-degree pointing objective
 - control of spacecraft attitude by a ground computer (precision pointing and slewing)
 - ion microthruster propulsion system to control thrust vectoring and attitude/orbit inclination
 - quartz-crystal microbalance contamination monitor to provide data on extremely small mass accretions on the surface of the spacecraft
 - advanced thermal control system that will stabilize temperatures of spacecraft components.
- To make particle and radiation measurements in the geosynchronous environment.

To meet the mission objectives, ATS-6 was designed to support some 28 experiments. These experiments were broadly classified as being of four types: communications, technological, meteorological, and scientific. Table 1-1 presents a summary description of these experiments. Additional experiments were conceived and performed after ATS-6 was placed in orbit, using the communications and experiment capabilities already designed into the spacecraft.

MISSION OPERATIONS

ATS-6 was launched from the Eastern Test Range at the NASA Kennedy Space Center on May 30, 1974 at 13:00 GMT (09:00 EDT) by a U.S. Air Force Titan III-C launch vehicle. It was injected 6.48 hours later into a near-perfect, 1.8-degree inclined geosynchronous orbit above 94° West longitude.

Following the separation of the spacecraft from the third stage (transtage) of the Titan III-C launch vehicle, the solar arrays and the 9.14-meter parabolic reflector were automatically deployed. The attitude control subsystem and the spacecraft propulsion subsystem were activated by command from ground personnel. Using propulsion subsystem thrusters as torquers, the attitude control subsystem was commanded to sequentially perform the Sun, Earth, and yaw attitude acquisition maneuvers. The Earth-pointing reference attitude, as depicted in Figure 1-1, was realized by 02:10 GMT on May 31, 1974. Two small orbit error correction maneuvers were subsequently executed.

At the end of the first month of flight, all subsystems had been successfully evaluated with very few anomalies encountered, and ATS-6 was declared operational. For the next 10½ months, from July 1, 1974 to mid-May 1975, ATS-6 successfully supported a full schedule of experiment and spacecraft operations from 94° West longitude, with highest priority devoted to the Health, Education, Telecommunications experiment. It was during this period, on September 26, 1974, that the mission was officially declared a success by NASA. Other key experiments included the Position Location and Aircraft Communications Experiment, the Satellite Tracking and Data Relay Experiment, the Environmental Measurements Experiments, the Radio Beacon Experiment, Radio Frequency Interference Experiment, Millimeter Wave Propagation studies, Cesium Ion Engine, and the Very High Resolution Radiometer. For many of these experiments, the spacecraft was maneuvered to point at specified locations on the Earth.

Table 1-1
Summary of ATS-6 Experiments

Experiment	Type of Experiment	Major Objectives
Health, Education, Telecommunications (HET) (S-Band)	Communications	Evaluate a system that will permit relay of television programs through the satellite to inexpensive ground stations at facilities such as schools, remote hospitals, CATV systems, etc.
Satellite Instructional Television Experiment (SITE)	Communications	Demonstrate relay by geosynchronous satellite of CCIR quality television programs from a high-powered transmitting station to small, modified standard television receivers located throughout rural India and to urban rebroadcast stations.
Television Relay Using Small Terminals (TRUST) (UHF)	Communications	Advance state-of-the-art in space communications by demonstrating CCIR quality wideband signaling between ATS-6 and inexpensive ground stations.
Position Location and Aircraft Communications Experiment (PLACE) (L-Band)	Communications	Develop improved air and sea traffic control, communications, and location techniques.
Tracking and Data Relay Experiment (TDRE) (S-Band)	Communications	Demonstrate technology necessary for an operational tracking and data relay satellite system.
Radio Frequency Interference (RFI) (C-Band)	Communications	Investigate C-Band terrestrial noise sources (geographical noise power distribution).
Millimeter Wave (MMW) (20 and 30 GHz)	Communications	Investigation of atmospheric propagation of MMW frequencies; feasibility of applications of MMW communications systems.
Apollo-Soyuz Test Program (ASTP) (S-Band)	Communications	Track the Apollo-Soyuz spacecraft and relay voice, television, and telemetry to the Earth.

Table 1-1
Summary of ATS-6 Experiments (Continued)

Experiment	Type of Experiment	Major Objectives
Building Attenuation Measurement (UHF, L-Band and S-Band)	Communications	Measure rf attenuation as produced by various building constructions.
Comsat Propagation Experiment (13 and 18 GHz)	Communications	Collect data on attenuation due to precipitation; determine power margins needed in spacecraft communications systems.
Cesium Bombardment Ion Engine (CIE)	Technological	Verify and obtain data on ion microthruster propulsion system; demonstrate thrust vectoring and attitude/orbit inclination control.
Quartz-Crystal Microbalance (QCM) Contamination Monitor	Technological	Provide data on extremely small mass accretions on the surface of the spacecraft.
Advanced Thermal Control Flight Experiment (ATFE)	Technological	Evaluate the performance of an advanced thermal control system and demonstrate its effectiveness in stabilizing temperatures of spacecraft components.
Spacecraft Vibration Accelerometers	Technological	Provide data for verifying basic spacecraft mode shapes and frequencies during flight.
Television Camera	Technological	Monitor the condition of the reflector.
Spacecraft Attitude Precision Pointing and Slewing Adaptive Control (SAPPSAC)	Technological	Investigate ground-computer-controlled spacecraft attitude control performance.
Interferometer High Data Rate Acquisition (300 to 1,000 kHz)	Technological	Collect data on all of the phase quantities measured by the interferometer, for wide-band spacecraft attitude jitter and vibration sensing.
Very High Resolution Radiometer (VHRR) (1 Hz to 250 kHz)	Meteorological	Measure cloud cover; determine wind field, ocean temperature, Earth resources.

Table 1-1
Summary of ATS-6 Experiments (Continued)

Experiment	Type of Experiment	Major Objectives
Radio Beacon Experiment (RBE) (40, 140, and 360 MHz)	Scientific	Measure ionospheric/exospheric electron content; study ionospheric propagation effects.
Magnetometer	Scientific	Study the magnetic field at synchronous orbit altitude.
Solar Cosmic Ray	Scientific	Study solar cosmic rays, entry and propagation within magnetosphere ; make detailed measurements of trapped electronics.
Auroral Particles	Scientific	Study the distribution of low-energy electrons and protons.
Electron-Proton Spectrometer	Scientific	Investigate the origin of the Van Allen trapped radiation.
Omnidirectional Spectrometer	Scientific	Measure omnidirectional fluxes and spectra of electrons and protons.
Low-Energy Proton-Electron	Scientific	Make swept and pitched angle measurements of low energy electrons and protons in the magnetosphere.
Low-Energy Proton	Scientific	Study low energy protons and heavier ions.
Solar Cell Radiation	Scientific	Measure life characteristics and performance degradation of solar cells in space.
U.S./U.S.S.R. Magnetic Correlation Experiment	Scientific	Provide a means of correlating worldwide magnetic field measurements.

Z-AXIS TARGET IS EARTH CENTER

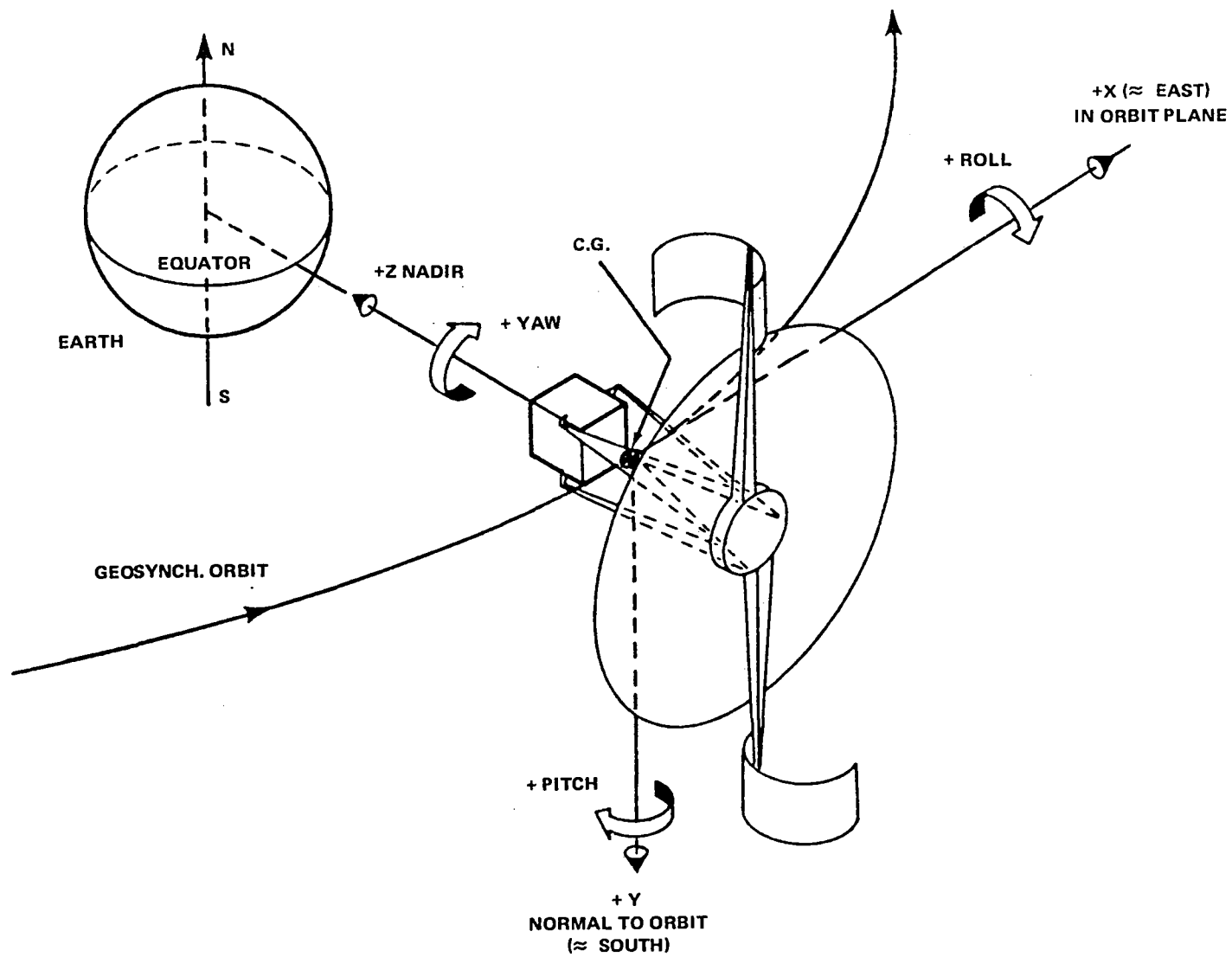


Figure 1-1. ATS-6 Earth-Pointing Reference Orientation (Local Vertical/Orbit Plane)

The next major phase of the mission was initiated on May 21, 1975, by firing an orbit control jet on command for approximately 9½ hours in two burns that established an eastward drift rate of 3.85 degrees per day. Command and telemetry communications with ATS-6 were switched from the ground station at Rosman, North Carolina, to the one near Madrid, Spain, as the satellite drifted within line-of-sight of the latter. This transfer operation, which placed ATS-6 at 35° East longitude, was completed 40 days later as a result of drift-removal firings on June 21, 25, and 29.

Even during this drift phase, ATS-6 continued to support a heavy load of experiment operations, including Tracking and Data Relay Experiment operations with GEOS-3 and Nimbus-6, Position Location and Aircraft Communications Experiment, Radio Frequency Interference Experiment, and Millimeter Wave Propagation. Also, during this period, ATS-6 served as a launch-critical data relay satellite for the OSO-8 launch.

Operations at 35° East longitude were highlighted by the spectacularly successful voice and live television relay for the Apollo-Soyuz rendezvous mission in July of 1975 and the twice-daily, direct-broadcast television coverage provided for the Indian Satellite Instructional Television Experiment from August 1, 1975 through July 31, 1976. Other major experiment operations conducted during this period included Tracking and Data Relay Experiment operations with Nimbus-6, European Millimeter Wave experiment, European Space Agency L-band, and the U.S.S.R. magnetometer experiment.

Due to the capability and flexibility of ATS-6 and ground support systems, none of the anomalies encountered during the first 2 years of in-orbit operations precluded ATS-6 from meeting all of its mission objectives, nor did they jeopardize the useful lifetime goal of 5 years.

To conserve its hydrazine propellant for subsequent operations, a relatively slow westward drift rate of 1.5 degrees per day was imparted to ATS-6 on August 1, 1976, to move it to its next orbital station above 140° West longitude. During the 120-day drift period, a joint NASA/U.S. Agency for International Development experiment was conducted. This major experiment involved a series of two-way color television broadcasts on the potential benefits of satellite technology to a number of developing nations. During a 90-day period, demonstration broadcasts were sequentially beamed into 27 nations in Asia, Africa, the Caribbean, and South and Central America.

During the final 2½ years of experiment operations above 140° West longitude, the spacecraft was used for a variety of societal, communications, and scientific/technical experiments in the continental United States, Alaska, and the Pacific Basin. While many of these experiments were similar to those performed during the first 2 years of ATS-6 operations, a number of the experiments demonstrated the use of the L-band mobile communications for natural disasters, search and rescue, and for traveling field units such as trucks and ships.

In February 1977, the first of an extended series of failures of the spacecraft propulsion subsystem thrusters was observed. These failures took various forms, including reduced or zero thrust capability and spontaneous leak or "hang-fire" operations. Various modified and contingency operations procedures were developed to compensate for these jet failures, thereby permitting experiment

operations to continue. Because of NASA's commitment to remove ATS-6 from geosynchronous orbit at the conclusion of its mission, the failure by May 1979 of three of the four orbit control jets was a major factor in deciding to terminate the mission.

ATS-6 operations during July 1979 were primarily devoted to final engineering tests on each of the spacecraft subsystems. These tests were designed to provide engineering data on the various subsystems that would be useful for future spacecraft programs.

On July 31, 1979, a 28-hour continuous burn of the remaining westward-firing orbit control jet was initiated to lower the ATS-6 orbit and to give the spacecraft a large eastward drift rate. On August 2, 1979, an 11-hour firing of the one remaining roll jet, coupled with a 9-hour burn of the orbit control jet, and a 6-hour burn of a yaw jet was performed to yield a 9.6 degree per second spin rate and to deplete the hydrazine propellant. The final westward drift rate thus obtained was about 6 degrees per day, corresponding to an orbit altitude about 500 kilometers below the geosynchronous altitude of 35,800 kilometers.

On August 3, 1979, the spacecraft was powered down (except for a few components that included power control elements and the command receivers that are hard-wired to the power subsystem), and the telemetry transmitters were commanded off at 0144 Z. This marked the formal end of a spectacular 5-year mission that witnessed the successful completion of all planned experiments and of a number of additional experiments that were conceived and executed while ATS-6 was in orbit. Subsequent to its turnoff, it was decided to turn ATS-6 telemetry back on from November 1979 to February 1980. The objective was to collect particle data for correlation with similar data being collected by other geosynchronous satellites as ATS-6 drifted past them. The operation was performed successfully.

CONCLUSIONS

ATS-6 fully demonstrated the technology of direct-broadcast television by relaying high quality, color video signals from a central transmitting ground station directly to a large number of small Earth terminals.

In addition, it demonstrated many communications technologies by acting as a data relay and tracking satellite in conjunction with low-orbiting satellites, by conducting communication and position location operations with ships and aircraft, and supporting a variety of other experiments involving communications, meteorology, particle and radiation measurements, and spacecraft technology. It completed over 5 years of highly successful operations, fully satisfying its specified 2-year mission lifetime before its mission was terminated on August 3, 1979.

CHAPTER 2

SPACECRAFT SYSTEMS SUMMARY

REQUIREMENTS

The major spacecraft requirements in support of the overall mission objectives were to:

- Demonstrate the deploying of the 9.14-meter diameter reflector with good radio frequency (rf) performance up to 6 gigahertz (GHz)
- Provide Earth pointing of the spacecraft Z-axis (reflector boresight) to an accuracy of ± 0.1 degree (3 sigma) over a roll/pitch angle range of ± 10 degrees off the local vertical, and slewing of the Earth-pointing Z-axis over the Earth-subtended angle range of 17.5 degrees in 30 minutes
- Demonstrate a precision attitude measuring capability and closed loop Earth-pointing attitude control to an accuracy of ± 0.1 degree (3-sigma) using an rf interferometer
- Demonstrate the capability of forming high-gain steerable antenna beams
- Demonstrate the capability of providing a relay for two-way command/telemetry and ranging data between ground stations and low-orbiting spacecraft for the following cases:
 - Z-axis tracking of one low-orbit spacecraft
 - steerable antenna beams to simulate track of two low-orbiting spacecraft
- Provide the required communications capability for the Position Location and Communication Experiment (PLACE), the satellite Tracking and Data Relay Experiment (TDRE), the Health, Education, Telecommunications (HET) experiment and the Satellite Instructional Television Experiment (SITE)
- Provide an oriented, stable platform at geosynchronous altitude for the support of additional experiments

An additional primary requirement of the design was to preclude any single-point failure that could prevent a successful 2-year mission lifetime.

Reliability

The reliability requirements for the program were established when it was planned to launch two spacecraft ATS-F, (called ATS-6 after its launch) and ATS-G, after integration and test of a (third) prototype spacecraft. Instead, the prototype was eliminated; ATS-F (6) was integrated, tested and

launched as a *protoflight* spacecraft; and the ATS-G fabrication was terminated when it became clear that ATS-6 was an outstanding success in orbit, fully capable of fulfilling all of its mission objectives.

The reliability requirements were stated as follows in the "GSFC Reliability Assurance Program Plan for ATS-F & -G" of March 1969: "To accomplish the basic goal of the Applications Technology Satellite F and G program of establishing the feasibility of long life, 3-axis stabilized flight of a minimum of 2 years duration . . .

"The minimum operating life of ATS-F and -G shall be 2 years in orbit after the required prelaunch testing and storage of up to 1 year. The operating life shall be defined as that life in orbit up to which the basic spacecraft can no longer adequately support its experiment complement in the normal mission sequence. Subsystem operating life shall be defined within this context. Experiment operating life shall be defined as that life within which all significant experiment goals for that particular payload can continue to be achieved. The design goal for synchronous spacecraft life shall be 5 years or more with life limited only by propellant loading.

"One-time operations, which must succeed to achieve injection into orbit (separation, solar panel deployment, antenna deployment, initial capture sequence, etc.), have a reliability requirement that is very close to unity."

Launch Vehicle

The major requirements imposed on ATS-6 by the Titan III-C launch vehicle were the following:

- The overall launch weight of the spacecraft, including adapter, shall be no more than 1,406 kilograms (3,100 pounds).
- The stowed spacecraft in its launch configuration shall fit within the 8.84-meter long by 3.05-meter diameter (29-foot by 10-foot diameter) Titan payload fairing.
- The spacecraft shall be designed to withstand the environment of the Titan III-C launch, including acceleration, acoustic, thermal, shock, and pressure decay effects.
- There shall be no degradation of launch vehicle or spacecraft performance due to the effects of the mutual electromagnetic interference or radio frequency interference.
- The spacecraft shall be designed to provide a separation velocity from the Titan third stage (transtage) that lies between 0.6 meter per second (2 feet per second) and 0.99 meter per second (3.25 feet per second) and with angular rates less than or equal to 1 degree per second.

- The spacecraft shall be designed to achieve its desired position in geostationary orbit above 94° West longitude with a nominal 1.8° orbit inclination with the following 3-sigma Titan injection errors:

Subsatellite Location	93.3° to 98° West longitude
Apogee Altitude ¹	±198 nautical miles
Perigee Altitude ¹	±176 nautical miles
Orbit Period ¹	±11 minutes
Eccentricity	0.0066

The spacecraft launch window was defined so as to cause the right ascension of the ascending node of the final geosynchronous orbit to lie between 260 degrees and 280 degrees. In this way the action of the solar/lunar gravitational perturbations acting on the ATS-6 orbit, coupled with an initial inclination of 1.8°, would cause the orbit inclination to remain within 2° for the projected 5-year orbit lifetime.

OVERALL CONFIGURATION

The ATS-6 requirements resulted in a large rigid spacecraft design with deployable solar arrays and parabolic reflector, multiple space and Earth-viewing provisions, and an integrated, multifrequency rf transponder and reflector prime-focus feed. This led to the general design concept of a rigid structural hub supporting the reflector, solar arrays, and space-viewing experiments, interconnected by a stiff tubular truss with an Earth-viewing module that supported the elements of the prime-focus feed and that contained most of the subsystem operating elements and experiments. Figure 2-1 illustrates the overall spacecraft design in its deployed orbital configuration and nominal Earth-pointing orientation.

The deployed spacecraft measured 15.8 meters (51.7 feet) from tip to tip of the deployed solar arrays and 8.2 meters (27 feet) from the bottom (Earth-viewing face) to the top of the magnetometer boom. The gross launch weight was 1,396.3 kilograms (3,078.3 pounds), including the 48.1-kilogram (106.1-pound) adapter structure that remained with the transtage.

For launch, the spacecraft had to be designed to be stowable in a compact configuration so as to fit within the Titan payload fairing as shown in Figure 2-2. The parabolic reflector design was a furlable rib-and-connecting-mesh design that could be coiled into a compact torus-shaped package for launch. The stowed spacecraft had a maximum static diameter of 2.7 meters (9.0 feet), excluding adapter mounting provisions to the transtage, and an overall length of 8.4 meters (27.4 feet), including adapter.

The solar boom and arrays were locked around the main body of the satellite, the Earth-viewing module (EVM), during launch. After injection into the final geosynchronous orbit, restraining cables for the booms/arrays were cut by pyrotechnics following separation from the transtage of

¹Deviations relative to geosynchronous orbit.

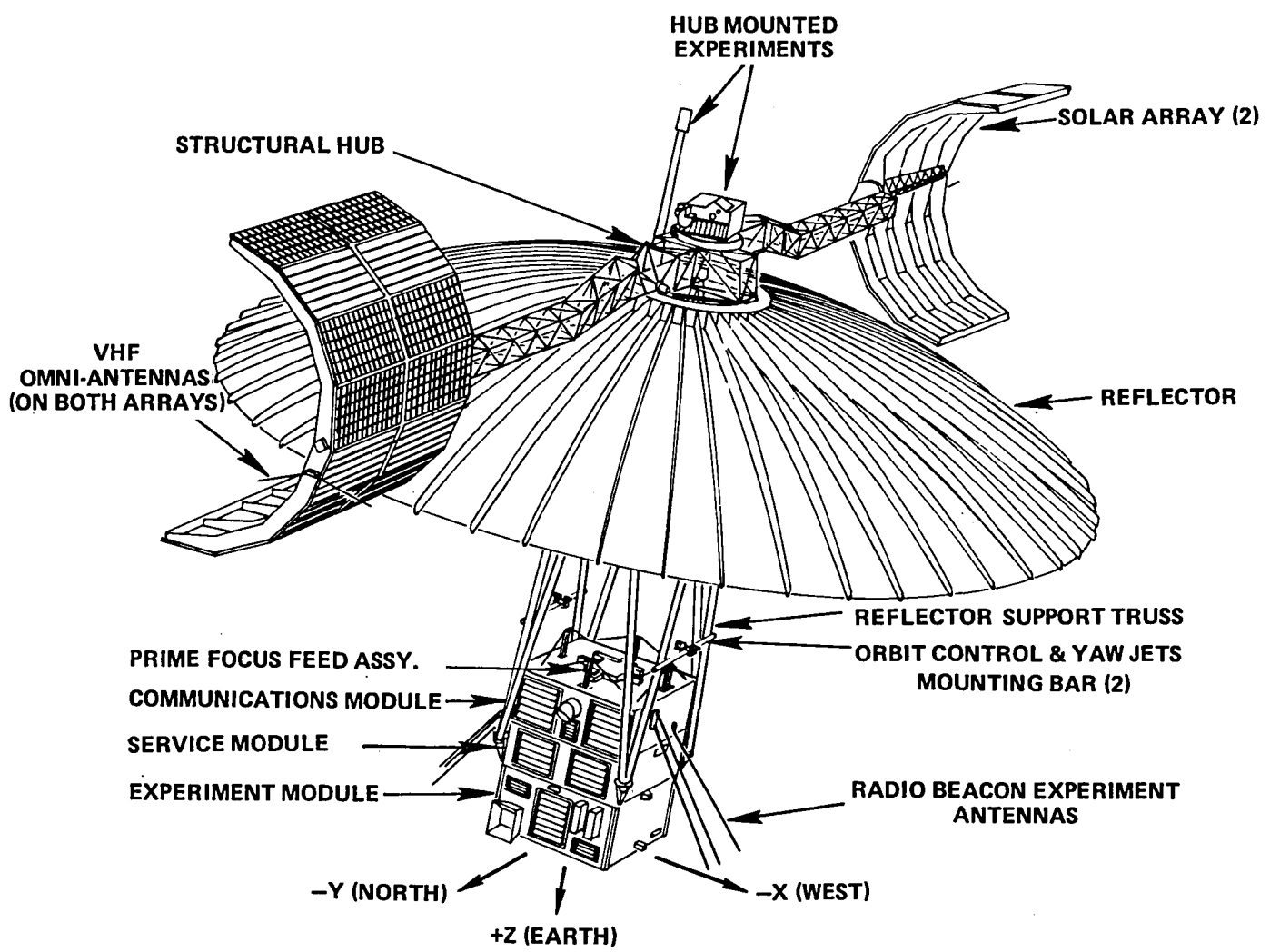


Figure 2-1. Configuration and Nominal Orientation in Orbit

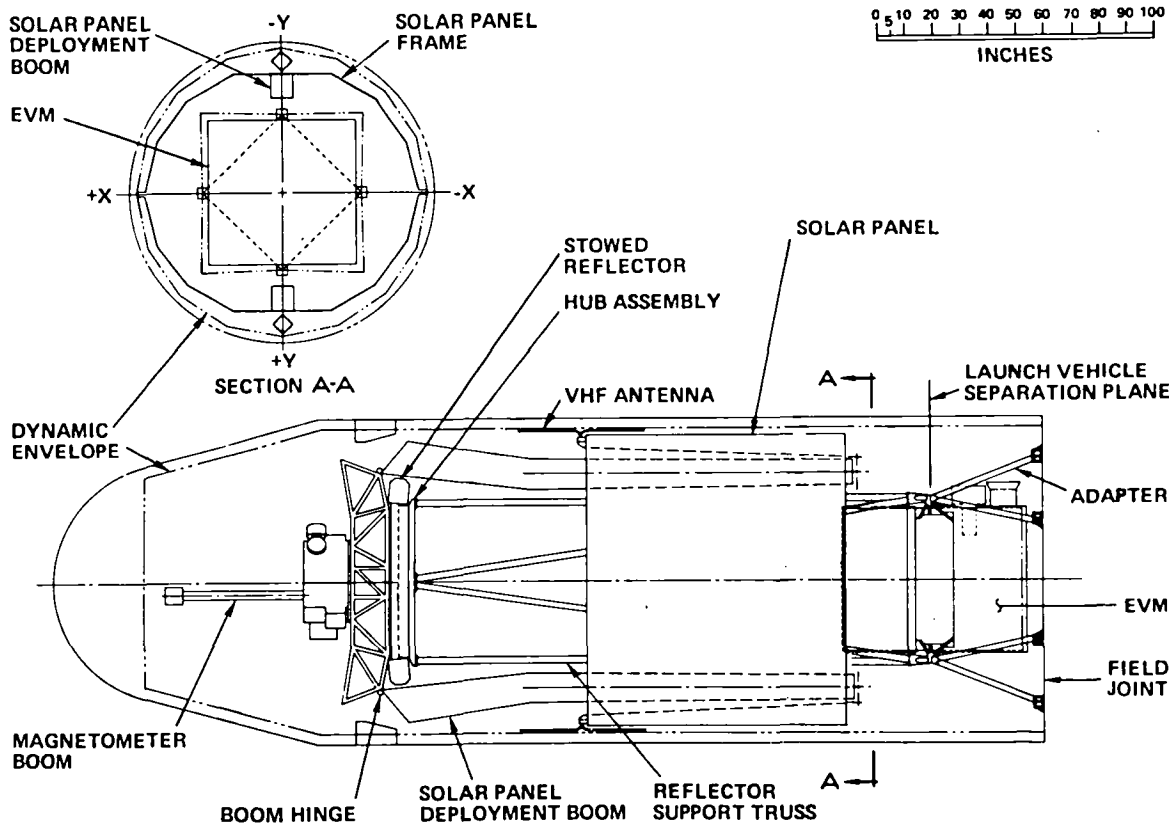


Figure 2-2. Launch (Stowed) Configuration

the launch vehicle. Spring and damper mechanisms at the hub end of each boom provided a rate-controlled deployment to the high-locked position. When the arrays were subsequently released, similar spring and damper mechanisms caused a 180-degree rotation of each semicylindrical array about a skewed-hinge line to yield oppositely-facing arrays.

The reflector was deployed, following array lockup, by cutting a cable holding spring-loaded doors around the sides of the torus container. The strain energy resident in the coiled position of the reflector ribs caused deployment to occur as the restraining doors were opened.

The array booms were then lowered from their high position (chosen to ensure safe reflector deployment even under possible array unfold failure conditions) to their lower, final orbital position to minimize the dominant solar pressure disturbance torques.

To satisfy the ATS-6 mission objectives and requirements, the several major communications experiments (e.g., HET, SITE, PLACE, RFI, TDRE) were implemented within the design of the spacecraft's integrated rf transponder-feed assemblies. Other spacecraft support subsystems were provided to meet the electrical power, command and telemetry, thermal control, attitude control, and propulsion requirements.

The ATS-6 subsystems and their suppliers to Fairchild Space and Electronics Company (Fairchild) as the spacecraft prime contractor were as follows:

- Electrical power subsystem – Fairchild
- Telemetry and command subsystem – IBM Corporation
- Attitude control subsystem – Honeywell
- Spacecraft propulsion subsystem – Rocket Research Company
- Communications subsystem – Ford Aerospace and Communications Corporation
- Electrical power subsystem – Fairchild
- Parabolic reflector subsystem – Lockheed Corporation
- Structural/mechanisms subsystems – Fairchild
- Thermal control subsystem – Fairchild
- Environmental measurements experiments subsystem – supplied as government furnished equipment from Westinghouse Defense and Electronics Center

TELEMETRY AND COMMAND SUBSYSTEM

The telemetry and command subsystem (T&CS) provided the space communication links between the ground operations controllers at ATS Operations Control Center (ATSOCC) and ATS-6². The T&CS command capability included receiving, decoding, and distribution of discrete and data-word commands to the spacecraft support subsystems and the spacecraft experiments. The T&CS also provided the command link between the ground station computers and the spacecraft attitude control subsystem in the ground-attitude-control mode associated with the Spacecraft Attitude Precision Pointing and Slewing Adaptive Control experiment. The T&CS telemetry capability included the multiplexing, formatting, and transmission of analog and digital data from the spacecraft support subsystems and the experiments. A special data link was also provided for voice-bandwidth analog data communication between ATS ground stations.

The T&CS used multiple units and extensive cross-strapping to provide dual and quad redundancy for high reliability. The telemetry and command subsystem used two pairs of vhf dipole antennas located at the edges of the solar arrays. These provided near-omnidirectional coverage in the stowed configuration during the launch, ascent, and final orbit injection phases, during the various stages of the spacecraft deployment, and for the fully deployed operational configuration. Once the spacecraft was Earth-oriented, command and telemetry data were normally transmitted at vhf through the 9.14-meter reflector with about a 15-degree field of view.

²Further design details and performance analysis are found in Volume III.

Commands were normally sent at vhf frequencies, but could also be uplinked at C-band. The command decoder and distribution (CDD) units had a capacity of decoding and distributing 512 discrete commands and 45 data-word commands. Each data word transmission carried nine bits of data. Before command execution, ground personnel verified by telemetry that the command had been received. An execute command was then transmitted from the ground. In a special mode, a second pair of tones was used to provide ground attitude control and high-speed execute command capability. The ground attitude control and high-speed execute commands were executed immediately without ground verification. The CDD performed an address check and parity check on the command prior to issuing the ground attitude control discrete execute pulse.

The data acquisition and control units (DACU) provided for a maximum capacity of 368 nine-bit words. Five of these words were reserved for telemetry functions, including frame synchronization and status. The remaining 363 words were used for analog and digital data. In the normal telemetry mode, one of the two DACU's was commanded on. The DACU sampled the input lines from the digital and analog levels sampled in a 9-bit analog-to-digital converter, and serialized the digital bits into a nominal 391-bits per second (bps) biphasic bit stream. These data were switched by the data switching unit to the frequency division multiplex unit or one of the four transmitters, by ground command control.

The prime mode of telemetry operation was frequency modulation/phase modulation (FM/PM), with normal telemetry (DACU), EME, and voice-bandwidth-analog data frequency-division multiplexed onto the carrier of one of the two transmitters associated with the prime-focus feed. This mode took advantage of the high quality link performance. Normal telemetry or EME data could modulate either of the omnidirectional antennas associated transmitters or the prime-focus feed associated transmitters directly in backup modes. Telemetry data could also use the C-band transponder as a backup downlink.

Command and Telemetry Provisions

The command and telemetry provisions for the entire spacecraft are summarized as follows:

Command

- 446 discrete commands used (512 available)
- 8 data-word commands used (45 available)
- Command bit rate — Normal 128 bps (28 bits per command)
— Hi-speed 1200 bps (13 bits per command)

Telemetry

- 368 9-bit words at 391 bps

- 65 analog words (70 available) and 42 digital words at a once-per-3-second sampling rate (minor frame)
- 198 analog (208 available) and 45 digital (48 available) at once-per-48-second sampling rate (16 channels subcommutated 16 deep on the 128-by-16-word major frame)

A dwell capability was supplied that provided a higher sampling rate for a single telemetry channel. Except for the insertion of the first 16 spacecraft status words every minor frame (3-second intervals), this mode provided repetitive sampling of the selected channel every 23 milliseconds.

ATTITUDE CONTROL SUBSYSTEM

The attitude control subsystem (ACS) served to stabilize and orient the spacecraft after separation from the transtage.³ It also provided the precision pointing and slewing control required for the various experiments. The ACS was composed of three main elements: sensors, controllers, and torquers.

The control reference signals were obtained from the following sensors. The redundant 3-axis rate gyro assemblies provided spacecraft angular rate data for rate damping and rate compensation during the acquisition modes. Analog and digital Sun sensors provided pitch/yaw Sun angle data for all attitudes for use during the initial Sun and Earth acquisition modes when the positive or negative X-axis was aligned to the Sun. The Earth sensor assembly was used for measuring roll/pitch angles of the spacecraft Z-axis off the local vertical (up to ± 14 degrees) during the initial Earth-acquisition mode and subsequent operational modes. The yaw inertial reference unit and the Polaris sensor were used for measuring angular motions around the spacecraft (yaw) Z-axis.

The C-band interferometer, when illuminated by rf energy from a ground transmitter, measured the spacecraft roll and pitch angles over a primary angle range of ± 17.5 degrees (and over a secondary angle range 3 to 4 times this value) relative to the line-of-sight vector from the spacecraft to the transmitters. When two ground transmitters were used, precise measurements of the spacecraft roll, pitch, and yaw angles could be obtained by ground processing of telemetered interferometer outputs.

The communications subsystem monopulse mode provided roll and pitch error signals that enabled the ACS to boresight the 9.14-meter reflector to a ground station emitting a vhf, S-band, or C-band signal. The S-band monopulse mode could also be used for a closed-loop satellite track mode based on S-band transmissions from the target satellite.

The ACS featured two redundant digital computers, called digital operational controllers. The basic control laws for the various acquisition and operational modes were programmed into their memory, which could be reprogrammed by ground command. The digital operational controller accepted mode and pointing commands from the ground, and orbit ephemeris data for the purpose of holding a fixed-ground aim point (by compensating for nongeostationary orbit effects) or for tracking a low-orbiting satellite in an open-loop programmed track mode. The analog backup controller was a simple, low power analog controller that was used during the acquisition modes and also served as a backup to the digital operational controllers for the local vertical and station point (monopulse) operational modes.

³Further design details and performance analysis are found in Volume II.

The actuator control electronics included the wheel drive electronics, the wheel momentum unload logic and the spacecraft propulsion subsystem control electronics and associated power supplies. The actuator control electronics drove the inertia wheels or the spacecraft propulsion subsystem thruster valves in response to attitude error signals from one of the two digital operational controllers or from the analog backup controller or in response to direct torquer commands from the ground. The three inertia wheels served as the prime torquers for all modes of operation except acquisition, orbit control, and 3-axis jet-only control.

The choice of any control mode and ground aim point (in latitude-longitude coordinates or roll and pitch angles off the local vertical), or roll and pitch slew maneuver (angle changes and rate), were established by ground command, as were the elements of the ACS (sensors, controllers, torquers) to be used for executing these commands. Clearly, the ACS was very versatile and complex in nature, with a large number of commandable modes and element configurations to execute these modes.

SPACECRAFT PROPULSION SUBSYSTEM

The spacecraft propulsion subsystem provided a fully redundant capability for east-west and north-south orbit control (the latter as a time-limited experiment only) and for 3-axis attitude control, including inertia wheel momentum unloading.⁴ It used 16 catalytic hydrazine thrusters arranged in two functionally redundant half-subsystems that were fed from two propellant tanks with positive expulsion bladder control operating in a single blown-down mode. The thrust levels for all thrusters decreased from an initial thrust of 0.56 Newton (0.125 lbf) to a final thrust at propellant depletion of 0.22 Newton (0.05 lbf).

The propulsion subsystem included seven latching valves for isolating the tanks, the eight Earth-viewing module (EVM) thrusters, and the eight truss-mounted thrusters. The eight EVM thrusters provided redundant roll and pitch control. The eight truss-mounted thrusters were located near the XY plane of the spacecraft center-of-mass and were used for redundant yaw control, redundant east-west orbit control, or (fired in pairs) north-south orbit control.

COMMUNICATIONS SUBSYSTEM

The communications subsystem was an integrated, multifrequency rf repeater capable of receiving up to three signals in any of four frequency bands (C-, S-, L-band, and vhf) and amplifying, processing, and retransmitting them on any commanded frequency in four frequency bands (C-, S-, L-band, and uhf).⁵ The communications subsystem consisted of a complex transponder and antenna feeds. The transponder provided the basic interface between the experiments in the satellite and the ground terminals, and performed frequency generation, translation, and power amplification functions. The transponder was thus an essential part of many of the communication experiments.

The transponder was functionally divided into four major elements: the receivers, the i.f. amplifier assembly, the frequency synthesizer, and the transmitters. Supporting these major elements were the rf input-output circuitry, wideband data unit, monopulse detector, command decoders, and dc-dc converters.

⁴Further design details and performance analysis are found in Volume II.

⁵Further design details and performance analysis are found in Volume III.

With certain exceptions, all active components were fully redundant. This included the synthesizer, transmitters, receivers (except L-band), monopulse, wideband data unit, and transponder command decoder. The intermediate frequency (i.f.) was triply redundant. Upconverters and downconverters, with the exception of the uhf upconverter, were not redundant. Operational redundancy was provided in the case of the Health, Education, Telecommunications experiment with one transmitter at each HET frequency. All transmitters were solid state with the exception of the C-band power amplifiers which were 10-watt traveling wave tube amplifiers.

The communications subsystem operated in various commandable modes to fulfill the requirements of the ATS-6 experiments. In the coherent mode, all local oscillator signals were derived from a single oscillator phase-locked to the C-band signal carrier transmitted from the ground to the spacecraft. In the noncoherent mode, the local oscillator frequencies were generated within the spacecraft by a highly stable fixed-frequency oscillator with an initial frequency tolerance of ± 10 parts per million (ppm) and a long term stability of better than ± 3 ppm in three months.

The primary mode of transponder operation was frequency translation with hard limiting in the intermediate frequency section. Another mode of transponder operation involved demodulation of incoming signals to baseband and then remodulation by phase modulation for subsequent transmission. These modes could be used with any combination of receivers and transmitters. A second mode of frequency translation with automatic gain controlled linear amplification was available via the 3950-megahertz (MHz) channel of the C-band transmitter only.

The antenna-feed assemblies provided radiating and receiving elements for the communications subsystem. The prime-focus feed was located on the top surface of the communication module at the focal plane of the high-gain, 9.14-meter parabolic reflector. Multiple feeds were used to accommodate the various spacecraft rf frequencies and to permit beam shaping and scanning. In addition to the prime-focus feed, Earth-viewing horns were located on the bottom surface of the EVM to transmit and receive wide-beam C-band signals directly to and from the Earth.

ELECTRICAL POWER SUBSYSTEM

The electrical power subsystem provided a well-regulated 30.5-volt supply for most of the spacecraft subsystems.⁶ The two fixed hemicylindrical solar arrays, consisting of 16 flat panels each, provided a near-constant power output. Two 19-cell, 15-Ah, nickel-cadmium batteries provided power for housekeeping during Sun occult and supported peak load conditions when the power demands of the spacecraft exceeded the capability of the solar array. The power subsystem had numerous automatic protective features, extensive redundancy, and operated in a shunt, charge, or boost mode to handle the large variations in power demanded by the operating modes. When solar array power exceeded that required for the spacecraft equipment and for charging batteries, partial shunt regulation was provided by 12 shunt regulators located within the EVM.

The power subsystem met or exceeded performance specifications and preflight predictions in all areas. Total solar array power capability for spacecraft use was approximately 595 watts, 40 watts

⁶Further design details and performance analysis are found in Volume III.

higher than the specified value for the summer solstice. Power bus regulation remained within specification through the entire range of operation including the batteries only (array occulted), array only (batteries being charged), and battery share modes. Bus voltage for all experiments was 28 volts, ± 0.1 volt (specification value was 28 volts, ± 0.45 volt).

The degradation of solar panels resulted in a 26.8 percent reduction of the power output compared with 28.9 percent predicted after 5 years in orbit. Battery temperatures rose to 31°C after the eclipse season due to Sun angles, heavy shunt dissipation, extended millimeter-wave experiment operations, overcharging, and spacecraft pointing.

MECHANICAL SUBSYSTEM

The mechanical subsystems consisted of six major elements: (1) parabolic reflector subsystem, (2) reflector support truss, (3) Earth-viewing module, (4) solar array and boom assemblies, (5) separation adapter, and (6) the separation and deployment mechanisms.⁷

The parabolic reflector was 9.14 meters in diameter and had 48 ribs to which was attached a copper-coated Dacron mesh. The reflector was coiled into a compact, torus-shaped package (2-meter outer diameter) for launch.

The Earth-viewing module (EVM) that housed most of the electronics was below the reflector. It was connected to the reflector by a truss made of graphite fiber reinforced plastic. This material was chosen because of its excellent stability over wide temperature variations. It had a coefficient of thermal expansion of 0.2×10^{-6} cm/cm/°C.

The EVM consisted of three sections: the experiment module, containing Earth-viewing equipment, such as the Earth sensors, the interferometer, and smaller aperture antennas; the service module, containing housekeeping equipment, such as the power, telemetry and command, and attitude control subsystems; and the communications module containing rf equipment. The prime-focus feed assembly was an integrated feed farm for vhf, uhf, L-band, S-band, and C-band frequencies.

There were two solar array and boom assemblies. In orbit, one assembly was extended north from the spacecraft and the other south. Each solar array was in the form of a hemicylinder and faced in the opposite direction from the other so that a complete cylinder of solar cells provided a constant solar energy input to the power system (except during eclipse periods) over the course of any 24-hour period. During launch, these assemblies were folded into the stowed position and were deployed by spring damper mechanisms through a sequence of motions.

The separation adapter was bolted to the Titan III-C and provided the mounting for ATS-6 at each of the four corners of the EVM. The adapter also provided the pyrotechnic release mechanism and springs to separate the spacecraft from the launch vehicle.

There were no problems associated with the mechanical subsystems in orbit.

⁷Further design details and performance analysis are found in Chapter 5 of this volume.

THERMAL CONTROL SUBSYSTEM

Because of the large power capability of ATS-6 and the variety of operating modes, there was a wide fluctuation in the amount of power that had to be dissipated from the components within the EVM. The thermal control subsystem maintained the temperatures of the mounting surfaces in the EVM within an excursion of 5° to 35°C.⁸ To achieve this, the subsystem made use of superinsulation, thermal louvers, heat pipes, thermal coatings, and the heat dissipating shunts of the power subsystem located within the EVM. The thermal louvers were located on the north and south faces of the EVM, the primary mounting surfaces for high-power spacecraft equipment. Superinsulation blankets covered the other faces of the EVM, and the heat pipes were bonded within the EVM north and south panels and within the transverse bulkheads connecting these panels.

RF COMPATIBILITY

Because of the nature of the ATS-6 configuration, the bulk of the spacecraft operating equipment was located in the Earth-viewing module that was directly exposed to the high rf transmitting fields produced by the reflector. Table 2-1 lists the worst case predicted values for these rf fields for the various transmitting frequencies for the exterior of the EVM and several other spacecraft locations.

To minimize the possibility of any resulting EMI/RFI problems, a number of actions were taken, including the following:

1. Imposition of an overall EMI/RFI Control Plan
2. Noise immunity design for the command subsystem by the choice of a 5-volt level for the active (1) state and a -5 volt level for the quiescent (0) state
3. A single point spacecraft electrical ground with separate power, signal, and chassis ground lines for each component with a few exceptions
4. An electromagnetic interference compatibility (EMIC) design and test review by a central EMIC Board, based on a comprehensive component, subsystem, and system EMIC test program tied to a stringent requirement on emission and susceptibility (1 volt/meter for all interior EVM components)
5. Continuous ground paths linking all of the structure, bridging moving joints as well
6. Grounding of outer and inner conductive sheets of the thermal blankets to the structure and grounding of all conductive sheets on open edges of the blankets

⁸Further design details and performance analysis are in Chapter 9 of this volume.

Table 2-1
Maximum Predicted External RF Fields (Volts/Meter)

Operating Mode	Freq. Band (MHz)	Over PRS (EME/SS)	Along Truss (SPS Thrusters)	EVM N-S Face	EVM E-W Face	EVM Earth View Face	S/A Booms (Omni/Power)
RBE	40	—	1.5	5.4	43	6.1	0.6
T&C	137	2.8	4.8	1.3	—	—	16.8 ¹
RBE	140	—	3.5	1.3	18	1.4	1.4
RBE	360	—	10	1.5	33	1.5	3.9
SITE	860	3.5	56	20	20	—	2.0
L	1600	2.5	39	14	14	—	8.7
S	2200	1.8	29	10	10	—	12.7
C	4000	1.2	19	6.6	6.6	20.4	5.9
K	20,000	—	—	—	—	6	—
K	30,000	—	—	—	—	9	—

¹Value at DSS location and solar array boom is 6.5 V/m.

7. Shielding of all external harnesses (avoiding in particular the conducting of surface rf fields into the EVM) and appropriate shielding, twisting, etc., of all interior harnesses
8. Rf closure of all significant EVM apertures by use of rf gaskets, honeycomb plugs, or conductive mesh/tape.

Two additional potential problems were also minimized by virtue of the foregoing actions: the buildup of differential charges on the spacecraft during ground operations (particularly on the launch pad at the Cape) and during occult periods in orbit. The large static charge potentials which can be experienced during the latter periods (as high as -15,000 volts on ATS-6) could, and have on some spacecraft, produced static discharges which could damage spacecraft operating subsystems or cause spurious commands or telemetry data. No such problems were evidenced by ATS-6.

OVERALL SPACECRAFT CHARACTERISTICS

A breakdown of the spacecraft weight by subsystem is presented in Table 2-2. The total weight of the GFE experiments, apart from the communications experiments that are incorporated into the transponder design, is also included.

The overall spacecraft mass properties are given in Table 2-3, covering the several intermediate spacecraft configurations during the deployment sequence and a full, intermediate and depleted propellant load for the fully deployed configuration.

Table 2-2
ATS-6 Subsystem Weight Breakdown

Subsystem	Weight	
	(kg)	(lb)
Electric Power Subsystem	256.0	564.5
Power control	99.9	220.4
Utility electronics	16.5	36.3
Harness	139.6	307.8
Telemetry and Command Subsystem	42.5	93.6
Attitude Control Subsystem	98.5	217.2
Spacecraft Propulsion Subsystem	88.3	194.7
Hardware	37.4	82.4
Propellant/pressurant ¹	50.9	112.3
Spacecraft Communication Subsystem	147.8	325.7
Transponder	121.1	266.8
Prime focus feed	26.7	58.9
Parabolic Reflector Subsystem	86.7	191.2
Structural/Mechanisms Subsystems	356.3	785.5
Primary structure	192.4	424.2
Solar array/deployment mechanisms	144.2	317.8
Equipment mounting provisions	19.7	43.5
Thermal Control Subsystem	56.0	123.5
GFE Experiments	183.9	482.5
Spacecraft Mass Properties Test Adjustment ²	-2.8	-6.2
SPACECRAFT SEPARATED WEIGHT	1348.2	2972.2
Titan III-C/Spacecraft Adaptor	48.1	106.1
SPACECRAFT LAUNCH WEIGHT	1396.3	3078.3

¹ Included 0.8 kg of N₂ pressurant

² Correction per integrated spacecraft weighting

Table 2-3
ATS-6 Spacecraft Sequenced Mass Properties

Condition	Weight (lb)	Center of Mass (inches)			Moment of Inertia (slug-ft ²)			Product of Inertia (slug-ft ²)		
		Roll	Pitch	Yaw	Roll	Pitch	Yaw	Roll/ Pitch	Roll/ Yaw	Pitch/ Yaw
Launch	3078.3	-0.41	0.39	286.9	4792.4	4675.1	596.4	-7.2	14.9	26.7
Separation	2972.2	-0.41	0.39	284.6	4671.8	4551.0	548.3	-7.2	15.0	26.9
Solar array booms moved to 121.4°	2972.2	-0.41	0.38	260.9	9784.5	7831.0	2381.8	3.4	9.9	33.6
Solar array panels unfolded	2972.2	-0.40	0.37	256.2	12760.1	9126.3	3959.1	-98.3	8.2	37.1
Reflector deployed	2972.2	-0.42	0.37	256.8	12802.3	9168.6	4198.7	-98.3	9.4	36.6
Solar array booms moved to 90° (Spacecraft fully deployed)	2972.2	-0.42	0.37	269.3	10856.0	6187.8	5233.0	-110.8	12.5	33.8
Intermediate propellant load	2913.1	-0.43	0.38	267.8	10783.3	6112.2	5230.0	-110.8	12.1	34.2
Propellant depletion	2862.4	-0.44	0.38	266.4	10718.4	6044.7	5227.4	-110.8	11.6	34.5
Titan III-C/ATS-6 adapter	106.1	-0.42	0.27	350.4	25.3	28.7	48.1	—	—	—

The Z-axis stations of the roll and pitch thrusters were 344.6 and 345.8, respectively; hence, for the case of the intermediate propellant load condition, with an indicated center-of-mass station of 267.8, the roll and pitch thruster lever arms were 1.95 m (6.4 ft) and 2.0 m (6.5 ft), respectively. The lever arm for the yaw thrusters was a constant 0.75 m (2.5 ft) for all of the indicated spacecraft configurations.

CHAPTER 3

SPACECRAFT TEST PROGRAM

TEST PROGRAM

During the hardware phase (Phase D of the phased procurement cycle) for ATS-F and -G, the program was changed from one involving a prototype and two flight spacecraft to one with ATS-F (ATS-6 after launch) as the protoflight spacecraft and ATS-G as its backup. However, the program did benefit substantially from the use of a thermal structural model (TSM) spacecraft. The TSM structure, separation and deployment mechanisms, and overall thermal control were identical or equivalent to the flight designs. It contained mass/thermal dummies of all other spacecraft components. A photograph of the TSM on a Ransome table is given in Figure 3-1.

The TSM was subjected to a 14-month test program which included the following accomplishments:

- Qualified the structure and thermal control subsystem designs
- Verified the design of the separation and deployment mechanisms
- Characterized the dynamic structural modes of the spacecraft (modal survey) and the vibration environments to which the spacecraft components would be subjected
- Confirmed proper deployment of the parabolic reflector under vacuum conditions (no unacceptable dynamic interactions in suspended test at Lyndon B. Johnson Space Center)
- Proved out spacecraft handling and test procedures and fixtures through the environmental test sequence, transport operations by aircraft, and all mechanical operations at the launch site

The general approach for design qualification and flight validation for the protoflight spacecraft and its constituent subsystems/components was as follows:

- Qualify component designs, if required, by use of a separate prototype unit. The prototype spacecraft propulsion and communications subsystems were subjected to qualification level environmental tests as complete subsystems.
- The flight units were subjected to acceptance test levels as components; i.e., except for the communications and propulsion subsystems which were acceptance tested as complete subsystems.

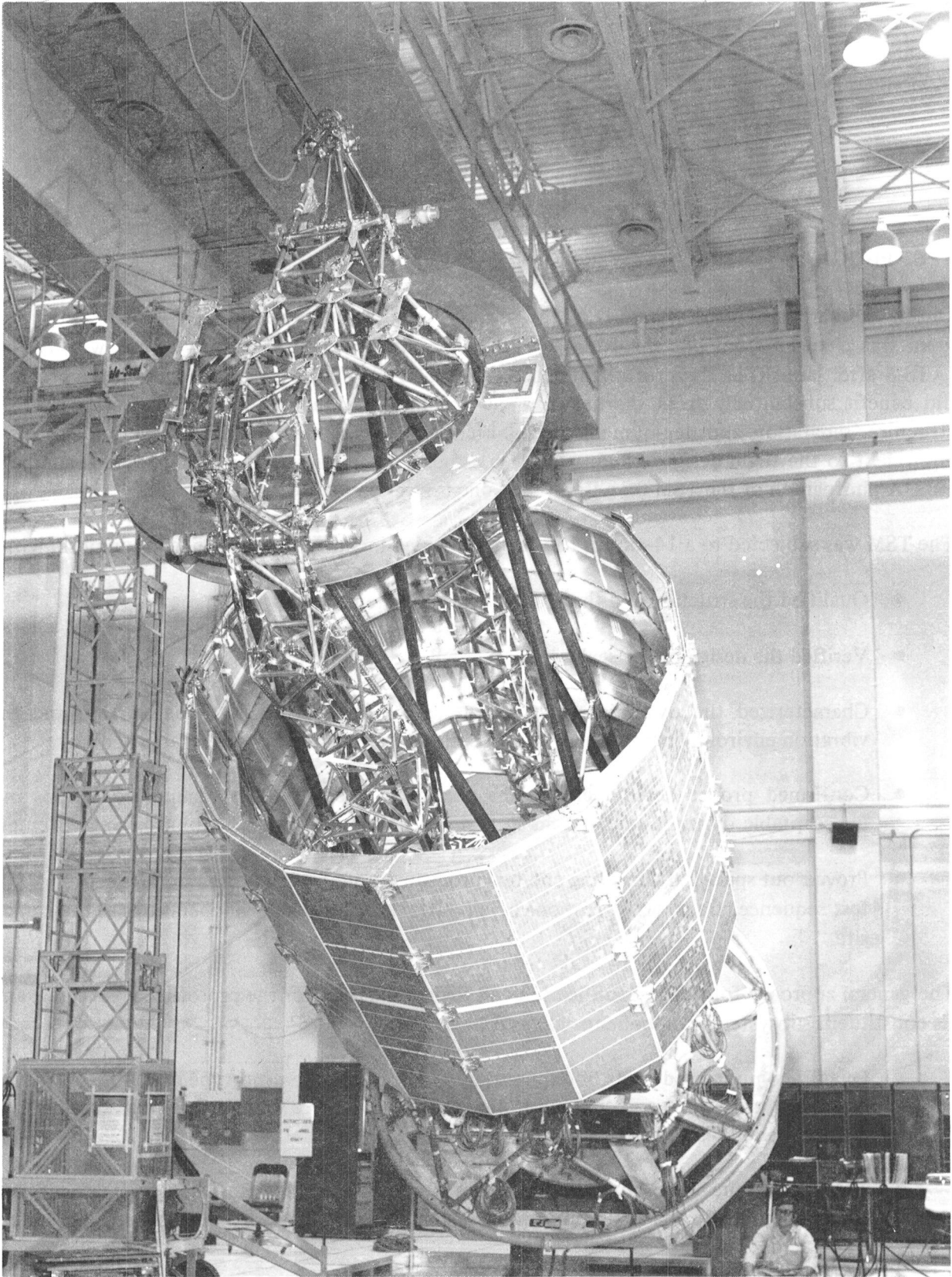


Figure 3-1. TSM Spacecraft (Launch Configuration)

- The protoflight spacecraft was integrated using formal, approved procedures; performance tested in a semiautomated manner under computer control from a central System Test Complex with software essentially identical to the subsequent flight operations software; and subjected to environmental tests (thermal vacuum, acoustic, vibration) performed to qualification levels for flight acceptance durations.

Figure 3-2 presents a summary overview of the protoflight spacecraft test program and schedule. The following comments are offered in explanation of the approach and content of this test program:

- The bench test was used to perform a combined test of the power subsystem and telemetry and command subsystem prior to their integration into the service module and experiment module.
- The long form test provided a performance test of the entire spacecraft (including GFE experiments) for its various operating modes. The long form test was designed to be primarily an end-to-end performance test for each of the spacecraft subsystems and experiments configured in accordance with planned operational modes. Additional special tests were performed to cover unique requirements not verifiable in this manner. Except for the long form tests performed during the EVM radio-frequency compatibility test, the last thermal balance phase of the thermal vacuum test, and the all-up deployed spacecraft radio-frequency compatibility test, external stimulators were used for the various spacecraft elements as required for the execution of end-to-end performance tests (e.g., hoods for the attitude control subsystem Sun sensors, Earth sensor, and Polaris star sensor; stimulators for the interferometer horns; a hat coupler for the prime-focus feed; etc.). Full performance tests were performed for prime components and for functionally redundant components; functional verification tests were conducted for standby redundant components.
- The radio-frequency compatibility test of the EVM was performed in an anechoic chamber with a reduced-diameter test reflector to provide an early confirmation of system rf compatibility in the high rf fields produced during the various communications transmit modes.
- The thermal vacuum test included a thermal cycle test of the EVM without louvers and blankets and a thermal balance test with same. Spacecraft compatibility with ATSOCC, Spaceflight Tracking and Data Network, and various experiment ground equipments was also demonstrated during this test by landline connections into the chamber.
- The all-up spacecraft rf interference test (with the spacecraft supported over an anechoic carpet) incorporated a final long form performance test that verified there were no performance changes as a result of all the environmental tests and that confirmed the rf integrity of the deployed spacecraft in its operational, radiating modes.
- As part of the launch operations, ATS-F was shipped directly to the launch pad and mated with the Titan III-C launch vehicle. The spacecraft prelaunch checkout was remotely

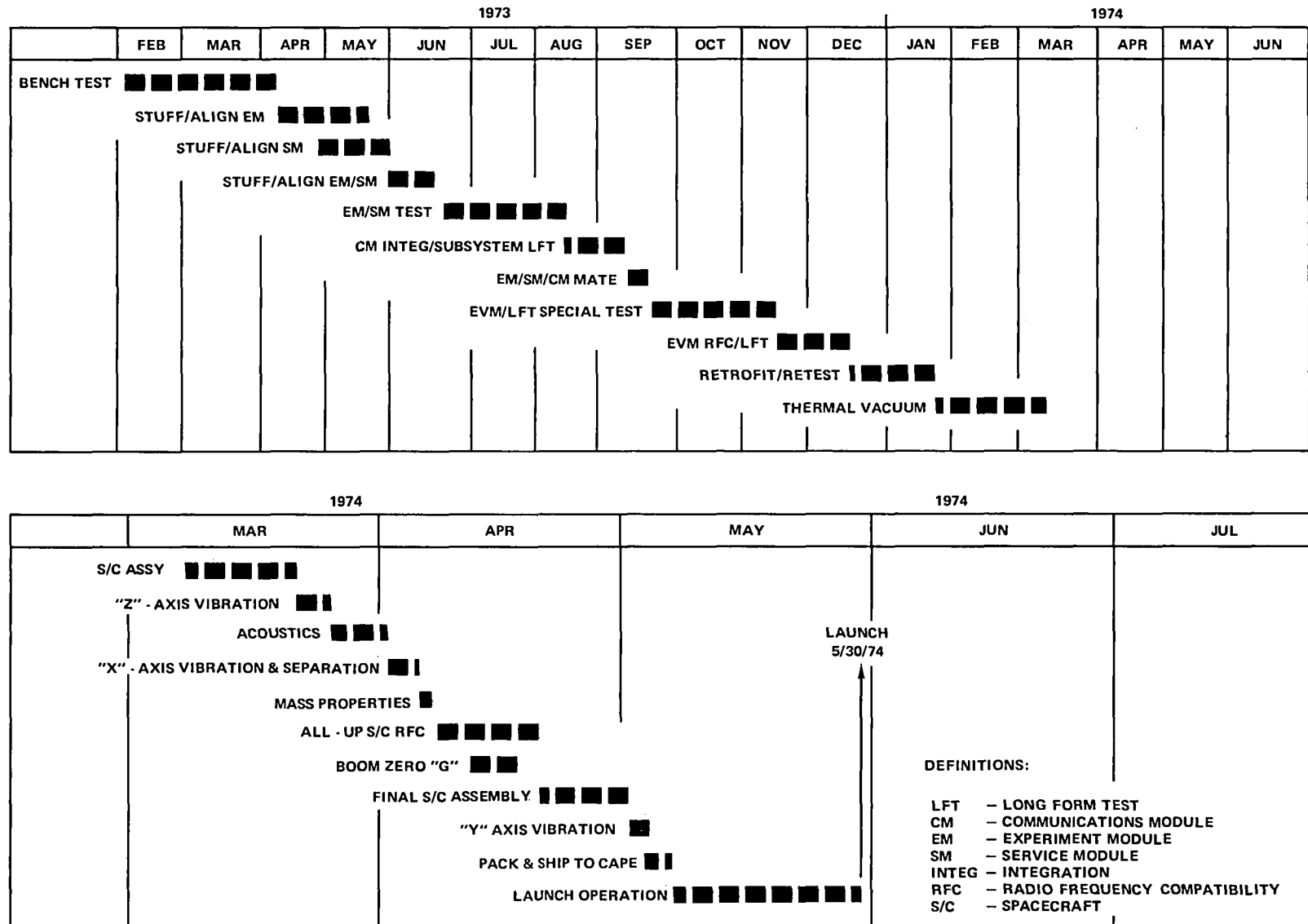


Figure 3-2. Protflight Spacecraft Test Program—Schedule

controlled from the System Test Complex which had been relocated in Hangar AE. The peripheral test/support equipment required in close proximity to the spacecraft (e.g., communications subsystem aerospace ground equipment, propulsion subsystem loading cart, etc.) were housed within the environmental control shelter that enveloped the spacecraft.

SPACECRAFT TEST RESULTS

The integration and test effort for the protoflight spacecraft proceeded in a remarkably smooth manner despite the fact it was not preceded by a prototype spacecraft. Apart from the design and interface reviews and controls imposed during the program to ensure overall system compatibility, including a formal EMI/RFI Compatibility Control Board, the following items of the system level test program undoubtedly contributed to its efficiency:

- Special early interface tests were performed for components of different subsystems with complicated interfaces to verify compatibility.
- Mechanical and thermal environments for each component were established by tests of the TSM. At the same time the associated spacecraft handling and test aerospace ground equipment and procedures were validated.
- Formal integration, handling and test procedures were used at all times.
- An experiment interface test unit was used to confirm the compatibility of all GFE experiments with spacecraft simulated power, command, and telemetry interfaces prior to the experiments being integrated into the spacecraft.
- A semiautomated test approach was used to expedite the testing of performance in planned operational modes. This also served to prove out equivalent software to be used subsequently for control of in-orbit flight operations.

Very few of the limited number of failures exhibited during the total test program could be attributed to its protoflight nature (first fully functional spacecraft) or special environment tests (e.g., vibration test to qualification levels and test durations to flight acceptance requirements), rather than to random hardware failures. A summary listing of the major spacecraft tests and possible "protoflight-relatable" failures follows:

- No failures of this nature were observed during the EVM rf compatibility tests. Some rf field interference was observed on temperature sensors of the spacecraft propulsion subsystem but this was largely alleviated by additional metal tape shielding of the associated harnesses.
- During the first portion of the thermal vacuum tests, the EVM ground-plane attachment failed due to thermal distortions; it was successfully redesigned. The spacecraft propulsion subsystem propellant lines, near the point of exit from the EVM, ran colder than desired.

The propellant-line thermal control provisions were improved and successfully retested in the final phase of the thermal vacuum test.

- No protoflight-relatable failures occurred during the vibration tests.
- During the acoustic test, the leads from the temperature sensor on the solar array broke loose. As a result, an improved potting procedure was introduced.
- During the shock and separation tests, a hub-mounted flight accelerometer failed and was replaced.
- No protoflight-relatable failures occurred during the undeployed (launch configuration) rf compatibility and simulated pad functional tests that confirmed spacecraft compatibility with specified Titan and Kennedy Space Center range rf environments and requirements. High concentrated power levels, produced by L-band pencil-beam test, did cause local charring of the hat coupler for the prime-focus feed.
- During special final calibration tests prior to the deployed rf compatibility tests, above-specification leak rates were observed on several propulsion subsystem thruster valves, a latch valve, and two fill-drain valves. The fill-drain valves were successfully reworked, while the other leak rates were waived since they were acceptable from an overall mission standpoint.
- During the deployed rf compatibility test, several of the radio-beacon antenna feed-through connectors were found to be broken; the design fault was rectified and successfully retested.
- No protoflight-relatable failures were experienced during the prelaunch and launch operations at the Kennedy Space Center.

CHAPTER 4

SPACECRAFT OPERATIONS SUMMARY

INITIAL MISSION OPERATIONS/PERFORMANCE

Launch

ATS-F (designated ATS-6 after launch) was successfully launched at 13:00:01 GMT (9:00 EDT) on May 30, 1974, from the Eastern Test Range aboard a Titan III-C launch vehicle (Figure 4-1). Prior to launch, the spacecraft was subjected to a series of launch preparation operations and tests at the launch complex culminating in the terminal countdown. During these operations, the spacecraft was commanded and monitored from the Fairchild System Test Complex located in the A&E Hangar at Kennedy Space Center. Spacecraft telemetry data was also processed and displayed at the ATS Operations Control Center (ATSOCC) at the Goddard Space Flight Center via the NASA Communications Network during prelaunch and launch operations. This permitted final calibration at ATSOCC's data processing system and verification of ATSOCC launch readiness.

The spacecraft launch configuration was established in accordance with the following criteria:

- Launch with spacecraft on internal power (batteries)
- Minimize load to avoid excessive battery discharge
- Provide for telemetry status monitoring
- Avoid requirement to transmit commands to spacecraft prior to separation from Titan transtage
- Minimize commands required to effect acquisition of the Sun immediately after separation and deployment
- Verify the performance of the Sun sensor prior to separation
- Power-up selected components for vibration protection
- Minimize commands required to establish in-orbit baseline configuration

The resultant launch configuration is presented in Table 4-1.

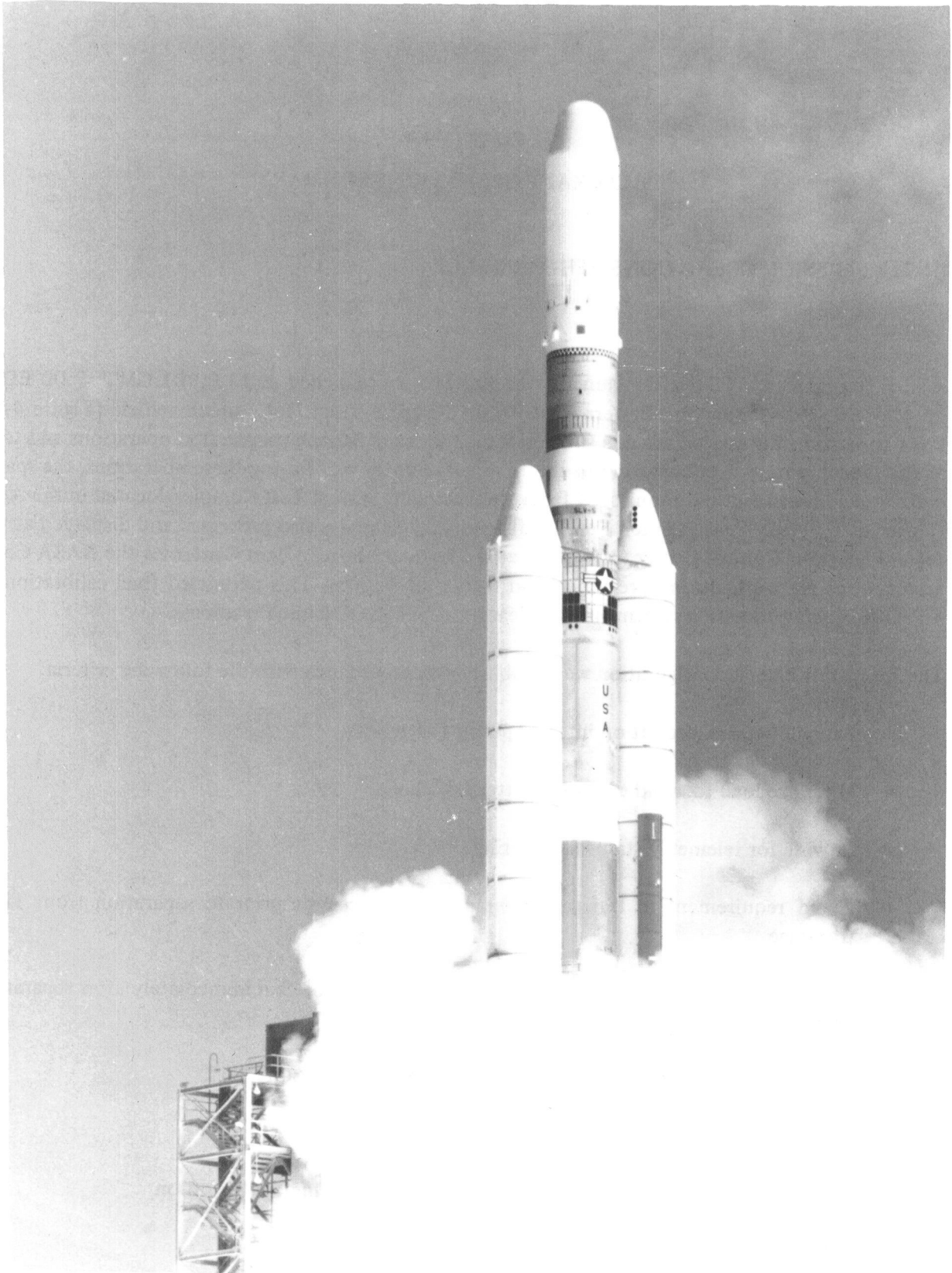


Figure 4-1. Launch of ATS-6 on a Titan III-C Launch Vehicle

Table 4-1
Spacecraft Launch Configuration

SUBSYSTEM		
Spacecraft Propulsion Subsystem (SPS)	1. SPS 1 and 2 powered on	Provide power for SPS instrumentation and valve heaters
	2. Tank 1 and 2 valves open; Truss 1 and 2 valves closed; EVM 1 and 2 valves closed; Cross line latch valve closed	Permits hydrazine in SPS lines up to thruster latch valves; nitrogen in lines between thruster latch valves and thruster
	3. SPS 1 and 2 prime valve heaters powered on	Maintains acceptable valve temperatures
	4. Signal conditioning box power on	Provides telemetry for line heaters and thermal subsystem
	5. SPS 1 and 2 prime and backup line heaters powered on, automatic, in low heat	Maintains acceptable temperatures for SPS truss lines; minimizes possibility that a single point failure will result in unacceptably high (explosive) or low (freezing) hydrazine temperature
	6. SPS 1 and 2 catalyst bed heaters off	Not required until acquisition phase; off to reduce power requirements
Attitude Control Subsystem	1. Analog, digital, and auxiliary digital Sun sensors powered on	Enables verification of sensors during ascent and minimizes commands required for Sun acquisition
	2. Polaris 2 Sun shutter powered on	Protects sensor optics from Sun damage
	3. Rate gyro assembly 1 and 2 powered on	Protects against launch vibration damage, enables verification during ascent, minimizes commands required for attitude acquisition
	4. All other components off	Minimizes spacecraft power requirements and battery discharge when solar panels are not illuminated
Telemetry and Command	1. DACU in normal and connected to 136-MHz and 137-MHz transmitters on omni antennas	Ensures full coverage, regardless of spacecraft attitude during ascent, separation, and acquisition
	2. EME, Earth sensor pitch radiance signal, and DACU 2 are connected to the FDM, but are off	Minimizes commands after launch. Conserves power during launch
	3. Command receivers and CDD's are connected to the omni antennas	Ensures full coverage, regardless of spacecraft attitude during ascent, separation, and acquisition
Communications	Communications subsystem is not powered (but is preconfigured for the standby mode)	Minimizes power requirements from launch through acquisition as well as minimizing commands required when the standby mode is eventually commanded
Power	Power subsystem is in the normal mode (main regulating circuits and main chargers will be on with both batteries connected; C/10 charge rate will be on; all fault detecting circuits and nonessential loads will be on)	Power subsystem can be launched in the normal mode thereby not requiring any commands under nominal mission operations
Experiments	1. VHRR chopper motor powered on	Protects experiment against launch vibrations
	2. VHRR Sun shutter powered on	Protects experiment optics from Sun damage
	3. QCM powered on	Obtain experiment data during Titan maneuver
	4. All other experiments off	Minimize power requirements

Ascent

The ascent trajectory was composed of four orbital phases: launch into park orbit, park orbit, transfer orbit, and injection into near geostationary orbit (with a nominal 1.8° inclination).

The first phase, launch into parking orbit, required approximately eight minutes. The internal batteries provided all spacecraft power during the first five minutes at which time the payload fairing was jettisoned. During the remainder of the launch phase and parking orbit phase, the batteries and arrays both provided power, depending on the Sun aspect angle. The transtage and spacecraft remained in the parking orbit for approximately one-half orbit (66 minutes). During that time, the spacecraft Z-axis was pointed along the direction of motion and the X-axis pointed southward.

At the second equatorial crossing, the transtage engines were fired to inject the spacecraft and the transtage into the transfer orbit. During the transfer orbit phase, a period of approximately 316 minutes, the transtage held the spacecraft Z-axis to within 30 degrees of the normal to the Sun line to ensure sufficient illumination of the solar arrays to provide spacecraft power and to recharge the batteries. In addition, the transtage maintained a roll rate (spacecraft yaw rate) of approximately 1 degree per second. This "rotisserie" maneuver was designed to provide a thermal balance for spacecraft components external to the Earth-viewing module. The nominal transtage attitude was interrupted three times during the transfer orbit for transtage telemetry readouts. These telemetry maneuvers, which lasted approximately 10 minutes each, occurred at approximately 100, 152, and 204 minutes after liftoff. At approximately liftoff plus 386 minutes, the transtage was reoriented for the second burn. At liftoff plus 391 minutes, this second burn was accomplished, and the transtage and spacecraft were injected into a near perfect, 1.8° inclined geosynchronous orbit as targeted. The spacecraft separation command was issued by the transtage programmer approximately 3 minutes later.

The predicted and actual times for the major events during this period are presented in Table 4-2. Spacecraft performance during the ascent period was nominal with no problems encountered. Good quality telemetry data were received continuously, except for the periods when the spacecraft was not in the field of view of a tracking station. The spacecraft battery state-of-charge remained above 75 percent, and booster efficiency was calculated at approximately 89 percent. The attitude control subsystem rate gyros and Sun sensors appeared to be operating properly and readings correlated well with Titan-predicted and telemetered attitudes and rates. During the rotisserie maneuvers, and attitude control subsystem yaw gyros indicated a rate of $0.98, \pm 0.04$ degree per second; the rotation rate was actually $1.00, \pm 0.05$ degree per second. The thermal control system operated satisfactorily and temperatures internal and external to the EVM were in the ranges predicted.

The final orbit parameters were as follows:

Inclination	1.76° (specification $1.8^\circ, \pm 0.165^\circ$)
Eccentricity	0.0008 (specification less than or equal to 0.0066)
Subsatellite Position	93.9° West longitude (specification: 93.3° West longitude to 98.0° West longitude)
Drift	0.27 degree per day west (specification: within ± 2.76 degrees per day)

Table 4-2
Times of Major Events During Ascent Phase

Predicted Time	Actual Time	Event	Spacecraft Source
13:00:00	13:00:02	Liftoff	roll, pitch, yaw gyros*
13:00:06	13:00:08	Begin Titan roll	yaw gyro
13:00:10	13:00:13	Begin Titan pitch	roll gyro
13:00:15	13:00:16	Begin Titan yaw	pitch gyro
13:00:30	13:00:31	Begin gravity turn	roll gyro
13:02:01	13:02:03	Jettison solid rocket motors	yaw gyro
13:04:14	13:04:12	Stage two ignition	roll, yaw gyros
13:05:05	13:05:05	Jettison payload fairing	-Z ADSS, roll, pitch, yaw gyros
13:07:42	13:07:45	Stage two tail off	roll, pitch, yaw gyros
13:47:50	13:26:52	Enter shadow (?)	-Z auxiliary digital Sun sensor
14:21:50	14:22:39	Already left shadow	-X digital Sun sensor
14:16:54	14:22:39	Already started thermal yaw	yaw gyro
14:40:10	14:40:03	Start reor for TM#5 dipout	pitch, yaw gyros
14:41:24	14:41:40	Reached TM#5 dipout	roll, pitch, yaw gyros
14:45:02	14:15:04	Start reor for thermal yaw	roll, pitch, yaw gyros
14:46:06	14:46:03	Start thermal yaw	roll, pitch, yaw gyros
16:24:20	16:24:21	Start reor for TM#7 dipout	pitch, yaw gyros
16:25:48	16:26:10	Reached TM#7 dipout	roll, pitch, yaw gyros
16:29:20	16:29:22	Start reor for thermal yaw	roll, yaw gyros
16:30:06	16:29:57	Start thermal maneuver	yaw gyros
18:08:38	18:08:42	Start reor for TM#9 dipout	pitch, yaw gyros
18:10:06	18:10:17	Reached TM#9 dipout	pitch, yaw gyros
18:13:38	18:13:40	Start reor for thermal yaw	yaw gyro
18:14:12	18:14:04	Start thermal yaw	yaw gyro
19:26:19	19:26:01	Start reor for T/S burn	roll, yaw gyros
19:27:21	19:27:06	Reached T/S burn attitude	roll, pitch, yaw gyros
19:28:49	19:28:30	T/S small limit cycle	roll, pitch, yaw gyros
19:28:55	19:28:35	Start T/S engines	yaw gyro
19:30:48	19:30:37	End T/S burn and reor for separation	roll, pitch, yaw gyros
19:31:09	19:30:59	Reached separation attitude	roll, pitch, yaw gyros
19:33:15	19:32:54	T/S large limit cycle	yaw gyro
19:33:41	19:33:21	Separation movement	roll, pitch gyros

*Gyros are the spacecraft rate gyros.

Note: Times are accurate within ± 3 seconds, GMT.

Because of the excellent orbit provided by the Titan, some 7.9 kilograms of propellant were saved that had been budgeted for correcting the specified 3-sigma in-plane orbit injection errors.

Separation

Spacecraft separation was successfully initiated by the transtage at 19:33:21 GMT. The relative separation velocity was approximately 0.6 meter per second. Spacecraft tip-off rates, as indicated by the rate gyros of the attitude control subsystem, were as follows:

Roll:	0.22 degree per second
Pitch:	0.11 degree per second
Yaw:	-0.06 degree per second

It was subsequently determined that roll-rate gyro 1 had an offset error of 0.19 degree per second. Since its output was being averaged with roll-rate gyro 2 during this period, the actual tip-off rate in roll was approximately 0.13 degree per second rather than 0.22 degree per second as indicated by telemetry.

Deployment

The automatic deployment sequence was initiated when microswitches indicated that ATS-6 had separated and cleared the rails attached to the transtage. The rails were cleared at about 19:33:21 GMT according to the rate-gyro output changes. At 19:39:18 GMT, the 6-minute deployment timer completed its count to start the first deployment motion of releasing both booms from their launch configuration. Based upon rate-gyro information, 6 minutes and 2 seconds had elapsed from separation to the start of motion. The first motion was nominally predicted to last 50 seconds, but actually took 74 seconds to boom lock-up.

Following microswitch indication of the completion of the boom first-deployment motion (as for all subsequent deployment operations), the deployment timer again counted to about 6 minutes and enabled the start of the second motion, the array skewed hinge release, at 19:46:34 GMT. The +Y boom locked into position at 19:50:03 GMT; however, the -Y boom did not lock until 20:02:00 GMT. The predicted duration of both events was 200 seconds. The actual deployment time for the +Y boom array was 203 seconds, but the deployment time for the -Y boom array was 802 seconds. The deployment timer again counted to about 6 minutes and the reflector deployment began at 20:08:03 GMT. The reflector deployment duration was less than 3 seconds, according to the rate gyro and the timer.

The deployment timer counted for the fourth and last time and enabled final boom motion at 20:14:14 GMT, 6 minutes and 11 seconds after deployment of the reflector. The deployment motion was complete at 20:14:32 GMT. Fourth motion duration was actually 18 seconds versus the predicted 10 seconds.

The body rates during the entire deployment sequence, starting at separation, never exceeded 0.23 degree per second in roll, 0.10 degree in pitch, and 0.49 degree in yaw. The following listing summarizes the separation and deployment timelines (derived from ATS-6 discrete event telemetry):

Event	Time (GMT)
SEPARATION ENABLE	19:33:18
CLEAR SEPARATION RAIL	19:33:21
BOOM RELEASE ENABLE	19:39:18
BOOM RELEASE	19:39:23
+Y BOOM AT 121°	19:40:25
-Y BOOM AT 121°	19:40:34
ARRAY UNFOLD ENABLE	19:46:34
+Y BOOM UNFOLDED	19:50:03
-Y BOOM UNFOLDED	20:02:00
REFLECTOR RELEASE ENABLE	20:08:03
REFLECTOR DEPLOYED	20:08:12
BOOM DROP TO 90° ENABLE	20:14:14
+Y BOOM DROP TO 90°	20:14:29
-Y BOOM DROP TO 90°	20:14:32

Sun Acquisition

Following deployment, the attitude control subsystem was activated, the spacecraft propulsion subsystem-1 (SPS-1) lines were purged of nitrogen, and the +X axis was successfully pointed to the Sun as planned using the analog backup controller, the rate-gyro assembly (RGA), the course/fine Sun sensors and jets. Sun acquisition was completed in 10 minutes.

Activation of Other Spacecraft Equipment

After Sun acquisition was completed, the digital operational controller 1 was powered on (in the monitor mode) and its status was confirmed. The EME, including heaters, and the Magnetometer Experiment were powered on. The quality of the EME data could not be ascertained since the spacecraft had not been configured to transmit EME telemetry. The Advanced Thermal Control Flight Experiment (ATFE) was also activated at this time. The communications subsystem was commanded into the "standby mode" in preparation for activating the interferometer. The very high resolution radiometer (VHRR) cone and patch heaters were also powered on during this sequence.

Earth Acquisition

The Earth sensor assembly (ESA) was turned on 19 minutes prior to the start of Earth acquisition. At 21:10, the analog backup controller was commanded to acquire the Earth. At the start of Earth acquisition (accomplished by rotating the spacecraft about the Sun-oriented roll axis), the roll jets fired to develop an apparent spacecraft roll rate of -0.27 degree per second. The Earth was acquired at approximately 21:20, but with a 2-degree limit cycle and 7-degree offset in roll. RGA 1 indicated an apparently erroneous roll rate of 0.19 degree per second. When rate control was switched from RGA 1 to RGA 2, the attitude control subsystem successfully completed the Earth acquisition maneuver to within 0.35 degree of local vertical. Spacecraft control, after Earth acquisition, was accomplished with the analog backup controller using the Earth sensor for roll and pitch control and the coarse/fine Sun sensors for yaw control. Torquer control was switched from jets to wheels after the spacecraft had settled. Because Earth acquisition was commanded during the evening (twilight) hours as planned, the spacecraft +Y axis was pointed southward. Since the nominal flight attitude requires the +X axis to point eastward, and the -Y axis to point northward, the flight plan required a near 180-degree yaw maneuver (rotation) to properly orient the spacecraft.

Yaw Reference Maneuver

Following completion of Earth acquisition, the yaw inertial reference unit (YIRU) was checked out prior to its use as the yaw axis sensor. The telemetry and command subsystem was configured at this time into its normal orbit mode: (1) data acquisition and control unit 2/EME on frequency division multiplex on the 137-MHz transmitter No. 2 over the prime-focus feed using the 9.14-meter reflector; and (2) the 154-MHz command receiver switched to the prime-focus feed. When the telemetry and command subsystem was switched to the prime-focus feed, approximately 11 dB increase in carrier-to-noise ratio was measured both at the ground and the spacecraft.

At approximately 23:45, the spacecraft yaw maneuver was begun by commanding the analog backup controller, using jets and the rate gyro assembly (RGA) 2. When the spacecraft X-axis was pointed to approximately 20 degrees below the Sun (placing the +X axis nearly due east), yaw control was commanded from the RGA to the YIRU. The total time for the completion of the 200-degree yaw maneuver was 33 minutes.

SPACECRAFT AND EXPERIMENT 30-DAY CHECKOUT

Following completion of the initial acquisition sequence, the spacecraft was reconfigured for orbital operations. The 6-hour timer was checked out and digital operational controller (DOC) 2 was powered on. Ephemeris data blocks were loaded into both DOC's followed by memory dumps. Analysis of the memory dumps showed both on-board digital controller memories unperturbed by the launch. At 13:56 on May 31, 1974, DOC 1 was placed in the attitude control subsystem control loop using the Earth sensor assembly and YIRU as sensors and the wheels as torquers in the local vertical pointing mode. In this local-vertical-orbit-plane-east mode, the +X axis is aligned in the orbit plane nominally due east and the +Z axis is aligned along the local vertical.

ATS-6 checkout procedures were conducted from the ATS Operations Control Center using an automated computerized test procedure. These procedures, previously "debugged" against a spacecraft simulator, were used from launch through the entire 30-day spacecraft checkout time period. A summary chronology of the activities from June 1 through June 17, 1974, is given in Table 4-3.

Upon completion of the spacecraft and experiment 30-day checkout phase with very few anomalies recorded, ATS-6 was declared operational and commenced full-scale experiment operations according to mission schedules.

OVERALL MISSION/EXPERIMENT OPERATIONS

Support of experiment operations during the ATS-6 mission required constant reconfiguring of the communications and experiment subsystems into the desired modes of operation, and maneuvering the spacecraft in pitch and roll to point at the desired ground location. Because of the capability of the spacecraft, the extensive software support system at ATSOCC, and the ability and experience of the operations team, these operations quickly became routine and enabled ATS-6 to consistently meet the requirements of tight experiment schedules.

A summary of the experiment operations during the first year at 94° West longitude is presented in Table 4-4. Consistently successful spacecraft support was provided for all such experiment operations.

The principal experiment during this period was the Health, Education, Telecommunications (HET) experiment. The HET experiment actually consisted of six different experiments into three geographical areas: Pacific Northwest, Rocky Mountains, and Appalachia. On July 2, 1974, the first HET education program was broadcast over the Appalachian Regional Commission network of 16 ground terminals. On July 3, the first HET medical program was broadcast over an 11-ground-terminal network for the Veterans Administration, also in the eastern section of the country. By the fall of 1974, HET programs were being broadcast to the Rocky Mountain area, the Pacific Northwest, and large portions of Alaska in accordance with daily and weekly broadcast schedules.

For a period of 3 weeks in December 1974 and January 1975, Galena and Fort Yukon, Alaska, had no contact with the outside world except through ATS-3 and ATS-6 due to extreme adverse weather conditions. During this period, two emergency medical cases were handled through the ATS-6 Indian Health Service—Alaska experiment, featuring duplex video communications, and was credited with saving the lives of the two patients.

With few exceptions, the other experiment operations conducted at 94° W longitude were also highly successful. Continuous data was obtained for the EME, Radio Beacon, ATFE, and Quartz-Crystal Microbalance experiments, although the University of New Hampshire (Low-Energy Proton-Electron) Experiment failed shortly after turn-on on June 18, 1974, and again on August 1, and remained off thereafter. Extensive data was obtained on the Propagation, MMW, RFIME, and PLACE experiments. A large number of meteorological pictures was obtained on the VHRR experiment from mid-June until August 15, 1974, at which time the chopper motor failed, precluding further picture taking.

Table 4-3
Chronology of Spacecraft Activity (June 1 to June 17, 1974)

Date	Activity	Remarks
June 1	In-orbit configuration	Configured spacecraft to support planned checkout 6-hour timer checkout DOC 2 turn-on and checkout DOC ephemeris update and memory dumps YIRU calibration DOC control using ESA/DSS and ESA/YIRU
	Interferometer checkout	Active checkout nominal for 6150 and 6155 MHz frequencies in both modes (coarse and vernier) and both ground stations (Rosman and Mojave) Closed loop functioned well for both frequencies Interferometer/DOC interface works well for pitch and roll control
	<ul style="list-style-type: none"> ● Passive/active ● Closed loop 	
June 2	Additional spacecraft checkout	DOC local-vertical control mode DOC offset point, ground coordinates (0° lat, 94°W long) Vhf monopulse (monitor only) Radio beacon checkout (no interference problem)
June 3	Polaris turn-on	Polaris successfully acquired using gate 3 No evidence of arcing or corona Bright object disturbances caused repeated losses of star acquisition Decreased sensitivity forced constant usage of gate 3
	ATS ranging	C-band checkout showed 0.12 to 2.0 dB glitches* as reported by both Rosman and Mojave ground stations

*Power dips in ground station receiver automatic gain controls.

DSS—Digital Sun sensor

ESA—Earth sensor assembly

Table 4-3
Chronology of Spacecraft Activity (June 1 to June 17, 1974) (Continued)

Date	Activity	Remarks
June 3 (Cont)	ATS ranging (continued) <ul style="list-style-type: none"> ● C-band checkout ● TV camera on ● ATS Ranging 	TV camera turn-on was successful. Early pictures showed fully deployed antenna and booms. C-band "glitches" do not affect the quality of the TV pictures Ranging was conducted for 15 hours for orbit determination
June 4	C-band TWTA's and Polaris turn-off	High voltages were turned off to permit further outgassing and to permit analysis of "glitches"
June 5	Offset point to Rosman	Spacecraft commanded to offset point at equator. Slewed to Rosman and offset-point ground coordinates at Rosman
	Monopulse checkout (passive)	Low jitter mode then commanded. Operation was excellent Comprehensive checkout of vhf, S-band and C-band monopulse performed while slewing spacecraft to different angles around Rosman. Vhf showed significant interference from other Earth radiating ground stations
June 6	C-band turn-on	"Glitches" still present
	Initial orbit correction maneuver	Fired westward control jet for 480 seconds to reduce orbital drift from approximately 0.27° W per day to 0.20° W per day using approximately 0.136 kilograms of fuel
	ATS-ranging	Ranging for 24 hours to measure accuracy of initial orbit correction maneuver
	C-band glitch investigation	Conducted 16 hour of cycling all equipment on and off to ascertain cause of C-band "glitches." Equipment cycling and use of redundant equipment did not affect the glitches. Commanding the 10-dB attenuator pad into the i.f. decreased the frequency and amplitude of the glitches in both transmitters. This was the normal mode of operation for C-band

Table 4-3
Chronology of Spacecraft Activity (June 1 to June 17, 1974) (Continued)

Date	Activity	Remarks
June 7	Polaris turn-on and Polaris yaw control	Bright object disturbances were still present Polaris sensor assembly was used successfully for yaw control Slewed from local vertical to Rosman with Earth sensor assembly and Polaris sensor assembly as sensors
	VHRR/Interferometer high-speed data link checkout	Successfully completed. VHRR pictures were of good quality. The Interferometer high-speed data link worked well. Spacecraft was in low-jitter mode on interferometer during this exercise. VHRR checkout was nominal
June 8	Final orbit correction maneuver	Fired for 31 minutes for final orbit correction. Total fuel consumption was approximately 0.59 kilograms of fuel for both maneuvers. Final drift was 0.05° East per day
June 9	Calibration of spacecraft axes	Calibration of interferometer. Relative sensor misalignments were recorded
June 10	Monopulse checkout (active)	Checked vhf, S-band, and C-band monopulse in the control loop S-band worked well; needed better pointing at Rosman to fully evaluate C-band (sensor misalignments)
	Propagation checkout	Nominal
	Advanced Thermal Control Flight Experiment checkout	Nominal
June 11	L-band and S-band solid state transmitter turn-on	Nominal—no problems
June 12	C-band Earth-coverage horn receive antenna pattern	C-band Earth-coverage horn receive antenna pattern was completed

Table 4-3
Chronology of Spacecraft Activity (June 1 to June 17, 1974) (Continued)

Date	Activity	Remarks
June 12 (Cont)	S-band on-axis antenna pattern	Antenna patterns completed for <ul style="list-style-type: none"> ● S-band on-axis receive ● S-band on-axis 3° transmit pattern ● S-band on-axis 5° transmit pattern
June 13	Position Location and Aircraft Communication Experiment checkout	Successfully completed
	Tracking and Data Relay Experiment checkout	Satellite relay link using Nimbus simulator at Rosman completed
	Satellite track	Satellite track mode was successfully completed using Nimbus-5 ephemeris data
June 14	Uhf turn-on	Nominal—no problems
	Health, Education, Telecommunications experiment checkout	Ground terminals were righthand circular polarized as opposed to the spacecraft which is lefthand circular polarized. All seven sections of checkout were successfully demonstrated
	MMW (communications mode) checkout	Compatibility of MMW/communications subsystem interface successfully demonstrated
June 15	Rfi checkout	Nominal
	Television Relay Using Small Terminals (TRUST) experiment checkout	Spacecraft configured to TRUST mode while ground station performed TRUST experiment. Proper spacecraft operation was demonstrated
June 16	Uhf antenna pattern	Uhf 5° transmit antenna pattern successfully completed
	EME checkout	Successfully completed
	Two-station interferometer	Successfully demonstrated
	S-band and C-band transmit antenna patterns	Successfully completed using 3° cloverleaves for S-band off-axis and 5° patterns for C-band horn transmit

Table 4-3
Chronology of Spacecraft Activity (June 1 to June 17, 1974) (Continued)

Date	Activity	Remarks
June 17	S-band cross-axis antenna pattern	Antenna patterns successfully completed by slewing 6° E, W, N, and S
	L-band pencil transmit antenna	Successfully completed
	L-band fan transmit and receive antenna patterns	Successfully completed
	MMW antenna pattern	Antenna patterns successfully completed for 30-GHz horn and 30-GHz parabolic antenna. No pattern for 20-GHz horn was received due to high voltage failure

Problems also forced premature curtailment of the Cesium Ion Engine experiment. Ion engine 2 was operated successfully for 1½ hours on July 17; however, subsequent attempts to operate it were unsuccessful. Similarly, ion engine 1 was operated for a 4-day period starting on October 19, 1974. Operation was satisfactory. As was the case for engine 2, all subsequent efforts to operate the engine failed.

On April 16, 1975, ATS-6 achieved a major mission objective by conducting successful tracking and data relay operations with the GEOS-3 spacecraft. Synchronization and lock-up to the pulse-code modulation data received at the GEOS control center was instantaneous, and data quality was reported good.

The orbit transfer maneuver from 94° West longitude to 35° East longitude was initiated on May 20, 1975.

During the 40-day drift phase, a full schedule of experiment operations was maintained, including:

- Tracking and Data Relay Experiment (GEOS-3, Nimbus-6, and Apollo Soyuz Test Project simulations)
- Position Location and Aircraft Communication Experiment, Radio Frequency Interference, Electromagnetic Environmental Survey
- Millimeter Wave Experiment, during first few weeks of drift
- Building Attenuation Measurements experiment

Table 4-4
Experiment Operations Summary – First Year

Operation	No. of Times Conducted	Total Time* (Hours)
Health, Education, Telecommunications experiment	1,063	1,529
Radio Frequency Interference experiment	197	1,174
Millimeter Wave experiment	445	1,132
Position Location and Aircraft Communication Experiment	235	1,073
SSE (GEOS)	109	380
Tracking and Data Relay experiment (Nimbus) checkout	51	273
Very High Resolution Radiometer	61	273
Ion Engine	21	137
Electromagnetic Environmental Survey	25	115
Apollo-Soyuz Test Project checkout	26	101
Lewis Research Center–Bldg. Attenuation Measurements	38	75
Spacecraft Attitude Precision Pointing and Slewing Adaptive Control	10	56
Television Relay Using Small Terminals experiment	21	51
Brazil Educational Television	45	38
U.S.S.R. Data Collection Platform	8	22
SITE Checkout	10	17
Demonstrations	48	77
Special Tests	159	751
Maneuvers	9	23
Eclipse	95	182
Range and Range Rate	24	576
Total Operations:	2,700	8,055

*The operational hours shown above represent mission support time and include ground setup, spacecraft slew, configuration, and transmit times.

From July 14 through July 24, 1975, at 35° East longitude, ATS-6 provided full time TDRE coverage for the historic American-Russian space rendezvous of Apollo and Soyuz, the Apollo-Soyuz Test Project. Spacecraft performance was consistently excellent, and continuous tracking and communications coverage was provided whenever Apollo was in view. ATS-6 successfully tracked the Apollo spacecraft for 130 of 138 orbits as planned, including the entire period relating to the linkup with Soyuz. The program track mode was used when Apollo was on the far side of the Earth or when the Apollo S-band antenna was not pointed at ATS-6. Monopulse track was used whenever the Apollo S-band signal was available. Because of its position at synchronous altitude, ATS-6 was able to provide approximately 55 minutes of support for each Apollo orbit, thereby providing extended periods of TV coverage of the linkup and rendezvous ceremonies between the two crews for viewers around the world.

On August 1, 1975, ATS-6 achieved another major milestone, for on that date the Indian Satellite Instructional Television Experiment (SITE) became operational. Spacecraft and communications subsystem performance were excellent as uhf TV reception at Ahmadabad was TASSO-1 with a 3-dB noise figure receiver. Approximately 80 percent of the 2400 Indian remote stations were operational with picture quality reported at TASSO-2 or better. SITE operations were conducted daily, 7 days a week, for 2¼ hours in the morning and 3¼ hours in the afternoon. Typical programming subject matter included agriculture, family planning, news, science, and cultural events.

ATS-6 successfully experienced its third and fourth eclipse seasons during that period with no adverse affects encountered. The extreme conditions recorded during the eclipse periods were as follows:

<u>Item</u>	<u>Third Eclipse (9-1 to 10-17-75)</u>	<u>Fourth Eclipse (2-27 to 4-12-76)</u>
Maximum spacecraft charge	-16,000 volts	-12,000 volts
Minimum battery voltage	21.4 volts	21.4 volts
Peak umbra period	67.9 minutes	68.02 minutes

Other experiment operations conducted during the second year of the mission included Nimbus-6 and GEOS-3 TDRE operations, European Millimeter Wave, L-band Electromagnetic Environmental Survey (EES), and EME.

On July 31, 1976, ATS-6 formally completed the SITE broadcasts to India. Its orbit was subsequently modified to give it a 1.5 degree per day westward drift relative to the Earth in a planned 4-month transfer to 140° West longitude.

During the first 3 months of this drift phase, ATS-6 supported a series of HET-type demonstration broadcasts to 26 countries in Asia, Africa, and South America. The purpose of the demonstration series, which was conducted by NASA for the Agency for International Development (AID), was to

encourage the useful application of space technology in underdeveloped countries of the world. Portable ground stations were set up in the participating countries on a rotating basis as ATS-6 drifted from east to west. Each ground station cluster consisted of one receive/transmit terminal and five receive-only terminals. Each demonstration included a film broadcast that illustrated the benefits of space communications and related technology, and a two-way video relay of a question and answer session between officials of the host governments and those of the United States.

After arrival at its designated 140° West longitude location on December 1, 1976, ATS-6 successfully supported a heavy schedule of societal, communications, and scientific and technical experiments (similar to those conducted during its first 2 years of flight) until the end of its operations on June 30, 1979. These experiments included HET-type broadcasts to Appalachia, Pacific Northwest, and Alaska; uhf broadcasts to Puerto Rico; Public Broadcast Service television relay at S-band to Alaska and Samoa; a uhf propagation experiment; geopotential mapping of the Earth's gravitational field via TDRE operations with GEOS-3; and a new type experiment involving L-band mobile communications for trucks on the highway, search and rescue operations, and emergency communications following major accidents and natural disasters. Further details of all experiment operations and performance for the entire ATS-6 mission are contained in a separate volume.

IN-ORBIT PERFORMANCE

ATS-6 was considered to be an unqualified success in meeting its specification requirements and all mission objectives. Spacecraft operation was consistently excellent from launch on May 30, 1974 until June 30, 1979, despite the anomalies and failures encountered. Further, due to the capability of the spacecraft and a sophisticated ground operations and software system, ATS-6 proved to be dependable and relatively easy to control with a minimum number of operations personnel required. At the completion of the initial 30-day evaluation period, all satellite subsystems were fully operational with no loss of redundant or back-up capability. Further, as a result of the excellent initial orbit provided by the Titan III-C launch vehicle, only a small portion of the onboard propellant was used for orbit correction, extending the usable life of the spacecraft beyond the 5 year design goal.

The excellent performance evidenced by ATS-6 in meeting its major mission requirements is summarized by the following:

- The 9.14-meter parabolic reflector was deployed 7 hours and 8 minutes after launch. This was confirmed by a picture of the reflector taken by a television camera aboard the spacecraft and transmitted to the ground some three days into the ATS-6 mission. Also, all communications links using the reflector (from 137 MHz to 6150 MHz) were successfully supported throughout the mission.
- The attitude control subsystem achieved a pointing accuracy of 0.05 degree with a pointing stability of 0.01 degree in the offset-point mode using the Earth sensor (roll/pitch) and Polaris sensor (yaw). The attitude control subsystem achieved controlled slew rates of 1.2 degrees per minute that demonstrated a capability of slewing the spacecraft Z-axis 17.5 degrees in less than 15 minutes.

- When the rf interferometer (with its 0.00142-degree resolution) was used in the attitude control subsystem control loop for roll and pitch attitude control, pointing accuracy and pointing stability were within specification and comparable in performance with the Earth sensor. When the interferometer was configured in its dual-frequency mode to receive rf transmissions from two ground stations, spacecraft roll, pitch, and yaw information was computed in real time at the ATS Operations Control Center, based on telemetered interferometer phase measurements.
- All antenna beams on ATS-6 were initially pointed at Rosman and performance data were obtained. Subsequently, all such beams were successfully used for experiment operations; e.g., the antenna beams for the Health, Education, Telecommunications experiment (beam-widths of 0.85 degree) were successfully used to support live TV broadcast programs for the Appalachian Regional Commission (ARC), Veterans Administration, the Federation of Rocky Mountain States, and Regionalized Medical School, Health, and Education in Alaska. TV reception was consistently excellent.
- ATS-6 tracked the Nimbus-5/6 and GEOS-3 satellites with a roll and pitch accuracy of better than 0.2 degree. During the S-band cross-antenna-pattern measurement operations, successful beam switching and performance was demonstrated by sequentially selecting each of the 21 individual beams as the spacecraft Z-axis was slewed ± 6 degrees about Rosman, first in the east-west direction and then in the north-south direction. In July 1975, ATS-6 tracked 130 of the 138 Apollo-Soyuz orbits, supporting a television and data-link relay to the Apollo-Soyuz Test Project control center at Houston.
- The communication links for each of the communication experiments were successfully demonstrated using ground communication equipment located at Rosman. On July 2, 1974, ATS-6 was declared operational and began daily HET broadcasts, covering three different geographical locations. In July 1975, after being moved to 35° E longitude, ATS-6 provided daily support of SITE programming, a series of health and educational broadcasts to the Indian subcontinent. A wide variety of experiments were successfully supported through the end of operations on June 30, 1979.

In summary, all of the major objectives imposed on ATS-6 were fully satisfied. This high level of ATS-6 performance was the culmination of superior performance by the spacecraft subsystems. The objectives and requirements of the various subsystems were almost universally satisfied and in most cases exceeded as next summarized and detailed in the subsystem chapters.

The structural/deployment subsystem met its basic flight requirements. The spacecraft successfully withstood the launch environment and deployed in space with no structural failures. Alignment of the various sensors (Earth sensor, interferometer, and monopulse) was preserved. (A capability was provided in the attitude control subsystem for compensation of sensor misalignments as determined by in-orbit calibration procedures.)

The separation subsystem worked very well. The spacecraft angular rates after separation were 0.13, 0.11, and -0.06 degree per second in roll, pitch and yaw, compared to specified rates of ± 1 degree per second about the three axes. Automatic deployment of the spacecraft was successfully achieved.

The thermal control subsystem met or exceeded temperature control specification requirements, indicating that the louvers and heat pipes were fully operational and that the external insulation satisfactorily survived the launch environment. The excellent temperature control provided for mounting surfaces within the EVM over all of the various spacecraft modes of operation enhanced the performance and operating life of the equipments.

The electrical power subsystem met or exceeded performance specifications and preflight predictions in all aspects. The total initial solar array power for spacecraft use was 595 watts, 40 watts higher than specified for the summer solstice. The solar array capability over the ATS-6 mission closely matched prelaunch predictions.

Power bus regulation remained within specification through the entire range of operations, including the batteries-only (array occulted), array-only (batteries being charged), and battery-share modes. The highest spacecraft load encountered was 656 watts during a two-frequency HET mode with C-band monitor. Bus voltage for all GFE experiments was 28.0 volts, ± 0.1 volt (specification was 28.0 volts, ± 0.45 volt). No failures were experienced throughout the entire mission.

The telemetry and command subsystem performed in a highly successful manner, providing for normal telemetry (via the omnidirectional and prime-focus feed antennas), dwell telemetry, and the Environmental Measurements Experiments telemetry in the frequency division multiplex mode via the prime-focus feed and the 9.14-meter reflector. Spacecraft commanding was completely successful at vhf (via the omnidirectional and prime-focus feed antennas) and at C-band (via the reflector/prime-focus feed). In addition, the ground attitude control decoder successfully supported the Spacecraft Attitude Precision Pointing and Slewing Adaptive Control experiment. Regarding all of the redundancy provision in the telemetry and command subsystem, the only use of the capability was that necessitated by a failure of DACU-1 in August 1975 (rendering it useable only for limited periods of time) and a failure of DACU-2 in May 1979 (requiring its replacement by DACU-1).

The attitude control subsystem met or exceeded specifications in all categories and, with the aid of a sophisticated software system at ATSOCC, proved to be relatively easy to monitor and control from the ground. The ability of the onboard digital operational controller (DOC) to be reprogrammed by ground command proved invaluable in developing new control modes to compensate for a partial failure in the roll-wheel drive electronics in June 1975. Functionally redundant yaw sensors (the YIRU and the digital Sun sensors) were used to replace the Polaris sensor that failed in October 1975.

For the offset point-ground mode, the latitude and longitude coordinates of the target point, and the orbit ephemeris for ATS-6 were sent to the DOC. The latter were used by the DOC to automatically correct the spacecraft pointing angles for nongeostationary orbit effects (inclination, eccentricity, longitude station, and drift, etc.).

To provide the programmed satellite track operation for the Tracking and Data Relay Experiment, the orbit ephemeris data for both ATS-6 and the low altitude satellite were transmitted to the DOC. The DOC then calculated the time-varying roll and pitch angles required for the ATS-6 reflector boresight to track the target satellite, and controlled the reaction-wheel torquers so as to produce signals representing these angles at the outputs of the Earth sensor. A more accurate closed-loop

satellite track mode was provided by commanding the DOC to null the roll- and pitch-error signals developed by monopulsing on S-band transmissions from the target satellite. This mode was demonstrated many times during TDRE operations.

Ground station pointing using the monopulse roll- and pitch-error signals was successfully accomplished at vhf (158 MHz), S-band (2253 MHz), and C-band (6150 MHz).

The performance of the spacecraft propulsion subsystem was well within specification requirements although a series of thruster failures were experienced starting in February 1977. Despite these jet failures, which were initially compensated by the use of backup thrusters and then by special spacecraft contingency maneuvers to provide the requisite wheel momentum management and spacecraft orbit control, experiment operations were supported as desired through June 30, 1979 when formal experiment operations were terminated.

The communications subsystem generally met or exceeded all of its specification requirements and very successfully supported the following major experiments:

- Health, Education, Telecommunications
- Television Relay Using Small Terminals
- Position Location and Aircraft Communication Experiment
- Tracking and Data Relay Experiment
- Very High Resolution Radiometer
- Radio Frequency Interference Measurement Experiment
- Comsat Propagation Experiment

In addition, monopulse operation at vhf, S-band, and C-band was successfully demonstrated, although the vhf error-curve slopes were lower than specified.

Despite a partial failure in the S-band transmitter for TDRE, it remained operational throughout the mission. In fact, none of the redundant transmitters were even turned on until the final engineering tests during the terminal mission operations.

During its outstandingly successful 62-month mission, ATS-6 pioneered a number of firsts in space communications, including the following:

- The first educational course ever taught by satellite television was conducted in 1974. More than 600 elementary school teachers in 8 Appalachian states participated in graduate-level studies.
- The first social experiments in health and educational telecommunications by satellite were offered to hundreds of small communities in remote areas of the Rocky Mountain states, the Appalachian region, and Alaska.
- The first medical-information network experiments to demonstrate medical techniques for doctors and health care techniques for people in remote areas were conducted jointly by the Veterans Administration; the University of Washington; the Alaska Health Department;

the Department of Health, Education and Welfare; and NASA. Through telemedicine, physicians actually prescribed treatment to patients through two-way, voice-video communication.

- The first satellite air and sea traffic control and communications experiments were conducted using ATS-6. The Federal Aviation Administration, the U.S. Coast Guard of the Department of Transportation, and the Maritime Commission participated.
- The first successful satellite-to-satellite communications experiments proved the feasibility for a tracking and data relay system that will support future low-Earth orbit missions.
- The direct TV support provided by ATS-6 for the Apollo-Soyuz Test Project permitted live coverage of this historic space rendezvous for viewers in both the United States and the Soviet Union in July 1975.
- From August 1975 to August 1976, ATS-6 transmitted the first satellite broadcasts to inexpensive ground receivers throughout India, bringing educational and health information to millions of viewers in 1,500 remote villages.
- The first full-duplex teleconferencing (two-way color TV and audio) with 27 lesser-developed countries of the Third World was conducted by the State Department, NASA, and other U.S. agencies using ATS-6 to demonstrate the usefulness of satellite technology.

In addition to the foregoing experimental demonstrations, and a wide variety of other successful scientific and technological experiments, the data collected through ATS-6 relating to climatological studies, the use of millimeter waves (in selected frequencies), and radio frequency interference studies are expected to provide information that will permit more effective use and regulation of radio transmissions by satellite and ground communications systems. This knowledge will contribute substantially to the improvement in design of future communication satellites.

In addition to its historic experimental contributions, ATS-6 reflected many significant design firsts as well:

- Largest geosynchronous communications satellite launched to date
- First 3-axis stabilized communications satellite
- First spacecraft to use
 - A 9.14-meter parabolic reflector
 - A digital computer for attitude control
 - Solid state high power rf transmitters
 - Graphite composite material for primary structure
 - Heat pipes for primary thermal control
 - Monopulse tracking for attitude control
 - Rf interferometer for attitude determination and control

IN-ORBIT ANOMALIES

A number of flight anomalies were observed during the ATS-6 mission, including some hardware failures. However, because of the extensive functional and standby redundancy provisions in the ATS-6 design, and the operational flexibility of many of its components (in particular the command reprogrammable digital operational controller), these flight anomalies and failures did not compromise the ATS-6 experiment support capabilities until its design goal of a 5-year mission lifetime had been exceeded. In May 1979, the cumulative failure of a number of thrusters was a major factor in deciding to terminate experiment operations on June 30, 1979, and to deorbit the spacecraft as desired by NASA while the requisite thrusters were still operational.

The flight anomalies associated with the various subsystems and experiments are discussed in greater detail in their related chapters. A brief description of the more significant anomalies and failures follows:

- May 1974 (at launch): The north solar array took 802 seconds to unfold compared to 203 seconds for the south array.

The attitude control roll channel developed a 0.19 degree per second rate bias during the launch phase.

- June 1974: The Polaris sensor tracked false targets that appeared to be stray dust particles and solar reflections from the north array. The number of false tracks decreased significantly with time, and the resultant yaw perturbations were generally of such short duration that they had no effect on experiment operations.

Dips of 2 to 3 dB were observed in C-band downlink power, probably due to epoxy contaminant outgassing in an output filter.

A failure occurred in the EME telemetry system following turn on of the UNH experiment.

- July 1974: The second frequency channel of the interferometer failed after several intermittent operations in June.

The SPS-2 prime-thruster valve heaters became inoperative.

The Auroral Particles Experiment (University of California at San Diego) experienced an electronic failure.

The operation of the south ion engine lasted about 1 hour. It failed to restart.

- August 1974: The VHRR instrument ceased functioning due to the failure of the chopper motor.

- Fall 1974 to Spring 1979 (Eclipse Seasons): Higher than anticipated temperatures were observed on the Earth sensor for several hours around spacecraft midnight during eclipse seasons.
- September 1974: First the EW detector stopped rotation on the UCSD EME experiment, then the NS rotation became intermittent.
- October 1974: The number 2 driver of Health, Education, Telecommunications experiment could not be turned off.

The north ion engine was started and ran for 92 hours. It could not be restarted.

- October 1974 to December 1975: The prime data and acquisition control unit (DACU) exhibited problems in dwelling on odd channels in October 1974, so dwell operations were discontinued. From August 1975 to December 1975 an increasing number of "doublet" errors were observed (even channel words assuming the value of the next odd channel).
- December 1974: More electronic failures on the UCSD Auroral Particles Experiment.
- June 1975: The roll-wheel drive electronics of the attitude control subsystem became unable to drive consistently in the positive rpm direction (negative torque), particularly for protracted, intermediate duty cycle operations.
- September 1975: The magnetometer Y-axis failed.
- October 1975: The Polaris sensor indicated large rapid transients in yaw angle, accompanied by noise transients in the Earth-sensor outputs probably caused by arcing or corona near the Polaris sensor assembly's high voltage image dissector tube and noise coupling onto the Earth sensor assembly signal ground lines.
- November 1975: All 9 bits of DACU-2 word 98 (MMW) failed in the zero state.
- February 1976: The UCSD particles experiment suffered mechanical failure.
- May 1976: The power output of the north solar array suddenly dropped about 20 watts, and remained consistently low by this amount relative to the south solar array throughout the rest of the mission.
- October 1976: The SPS-1 prime and backup truss thruster valve heaters failed while in a combined power mode, a mode not planned prior to launch.
- November 1976: The S-band power output of the Tracking and Data Relay Experiment dropped by 2 to 3 dB.

- May 15, 1977: Final failure of the UCSD Auroral Particles Experiment.
- May 1979: Some DACU-2 telemetry words successively read zero and then normal, with the number of affected words increasing with time and with sustained periods of good and bad data for 10 days and more.
- February 1977 through August 1979 (End of Mission): Throughout this period, a progressive series of thruster failures/anomalies were experienced wherein 13 of the 16 thrusters evidenced various combinations of sudden inoperability; low, variable or degrading thrust; or intermittent leakage or protracted firing. At the end of the mission, only SPS-1 thrusters were operative. They included one pitch, one roll, and one orbit control thruster operating normally, and one yaw thruster performing at a degraded level. A probable cause was contaminants that accumulated in the thruster capillary feed tubes (8-mil diameter) until they became plugged. The likely sources of contaminants were zinc and silicon oxide leached from the tank diaphragms, trace impurities in the hydrazine, and/or deposits from clean-and-flush operations after hydrazine exposure during ground tests (not recommended for future programs). Corrective actions for these failures (which permitted satisfactory experiment operations through June 1979) first involved use of redundant thrusters, and then specially devised contingency procedures that used spacecraft pointing maneuvers between experiment operations to unload control wheel momentum as required. These maneuvers involved controlled use of the dominant solar-pressure torques (also gravity-gradient torques) or operative thrusters in reoriented attitudes to remove accumulated spacecraft momentum as required). The sudden failure of two out of three of the still operative orbit control thrusters in May 1979 was a significant factor in the decision to terminate the mission, while the operative thrusters were still available to deorbit the spacecraft.

As indicated in the preceding paragraphs, use was made of standby or functionally redundant equipments to preserve the performance capability for ATS-6 for over 5 years. The overall ATS-F and -G program reliability requirement for a 2-year mission lifetime (5-year goal) was fulfilled in an outstanding manner with the single ATS-6 flight.

TERMINAL MISSION OPERATIONS

Final Engineering Tests

Following the decision in May 1979 to terminate the ATS-6 mission, formal experiment operations were concluded on June 30, 1979. During the month of July, a variety of special engineering tests were conducted. The objectives and results of these tests are briefly summarized as follows:

1. To verify the integrity and performance of redundant components in the communications subsystem (e.g., transmitters) and the power subsystem that were never used during the basic mission. All such components proved to be fully operational and met their performance requirements.

2. To verify unused modes in the power subsystem (e.g., failure protection provisions) and the attitude control subsystem (e.g., monopulse mode for the analog controller). All such modes were demonstrated to operate properly.
3. To obtain end-of-mission performance data to the extent possible for all subsystems to compare with similar begin-of-mission data obtained during the initial 30-day check-out phase.

No significant performance degradation was evidenced by any of the subsystems thus tested as reflected by the following:

- Telemetry and Command Subsystem—Transmitter frequencies remained well within specification values, the initial and final effective isotropic radiated power (e.i.r.p.) values were in good agreement, the downlink bit rate was unchanged, and the two sets of command threshold data were closely comparable.
 - Communications Subsystem—The measured beginning and end of mission e.i.r.p. and gain/temperature (G/T) values were in reasonably good agreement.
 - Power Subsystem—Performance specifications were satisfied throughout the mission. The array power degradation at the end of the 5 years was 26.8 percent compared to the 28.9 percent predicted.
 - Attitude Control Subsystem—There was no discernible degradation in performance of the sensors, controllers (analog and digital), or actuators beyond the anomalies/failures previously discussed. There was a slight increase in the reaction wheel friction and windage torque from 3.53×10^{-4} Nm (0.05 in-oz) to 1.059×10^{-3} Nm (0.15 in-oz) depending upon speed, and the change in the uncompensated drift rate of the yaw inertial reference unit over the mission was less than 0.05 degree per hour.
 - Thermal Control Subsystem—Temperature data taken over the full mission indicate proper performance of the heat pipes and the louvers (with no evidence of any detrimental leakage of ammonia or buildup of noncondensable gas).
4. To perform special tests of several attitude control subsystem sensors, namely:
 - Polaris Sensor—During an end-of-mission power-on test of the Polaris sensor assembly, it appeared to still produce noise transients in the Earth sensor.
 - Yaw Inertial Reference Unit—A number of successful power-off and power-on cycles were conducted, with proper operation of the gas-bearing gyro being indicated each time.

Spacecraft Deorbit and Spinup Operations

Because of the concern over the continued operability of the SPS-1 thrusters, a number of contingency procedures were developed for accomplishing a major orbit-change maneuver depending on which of the thrusters were available for use. Since some of these procedures involved protracted, many-day operations, it was decided to lower the ATS-6 orbit instead of raising it as initially planned. The resultant eastward drift rate would permit longer visibility and control from the primary ground station near Rosman, and would also add to the existing small eastward drift.

At 1720Z on July 31, 1979, the orbit-change maneuver was initiated by commanding on the remaining (prime) SPS-1 westward-thrusting, orbit-control jet. During the subsequent 28-hour sustained burn of this jet, the positive yaw jet returned to operation (at a degraded thrust level) after a previous failure on July 13, 1979. The use of this jet and the normally-operative negative pitch and positive roll jets, coupled with use of the inertia wheels, permitted control of spacecraft attitude throughout the maneuver. The maneuver was completed at 2126Z on August 1, 1979.

It had previously been decided to spin up the spacecraft about its roll axis just prior to terminating the mission for several reasons:

- It was desired to obtain magnetometer calibration data over several complete rotations of the spacecraft.
- A spinning spacecraft would provide a more stable target for subsequent orbit determination by NORAD.
- It was desired to deplete the remaining 2.77 kilograms of onboard hydrazine propellant before relinquishing control of the spacecraft.

At 1429Z on August 2, 1979, with the command and telemetry links tied to the omnidirectional antennas, the spinup maneuver was initiated by a steady burn of the positive roll jet. After several hours, when the roll rate had reached 2 degrees per second, the west prime orbit jet was commanded on to further deorbit the spacecraft and to help deplete the hydrazine propellant. Nearly 3½ hours later, at a roll rate of 4 degrees per second, the positive yaw jet was also commanded on to further aid in propellant depletion. Some 5 hours later, a sudden drop in tank pressure and reductions in catalyst bed temperatures indicated that the hydrazine had been essentially depleted. The maneuver was terminated at this time, although the west jet was left powered on to help ensure the elimination of any residual hydrazine in the system.

At the conclusion of these maneuvers, ATS-6 was determined to be drifting eastward with a rate of 6.05 degrees per day and with a positive (clockwise) rotation at 9.6 degrees per second about its roll axis. The general orientation of this axis (with coning/nutation motions of several degrees amplitude clearly evident) was judged to be:

Right ascension	—	132.1 degrees
Declination	—	17.8 degrees

Spacecraft Deactivation

Following the completion of the terminal spacecraft maneuvers, the spacecraft was configured as follows for shutdown:

Attitude Control	—	Earth sensor assembly, yaw inertial reference unit, and analog backup controller all on (to obtain possible extended life data) All other units off
Propulsion	—	SPS-1 on, and west prime jet on SPS-2 and all heaters off
Communications	—	All off
Experiments	—	All off
Power	—	Normal configuration with main charger and under-voltage detectors enabled
Telemetry and Command	—	Command receivers (hardwired on) and telemetry transmitters tied to the omnidirectional antennas

At 0144Z on August 3, 1979, the telemetry transmitters were commanded off, formally concluding an eminently successful mission that had started over 5 years earlier at 1300Z on May 30, 1974.

CONCLUSIONS AND RECOMMENDATIONS

As an element of the NASA/GSFC Applications Technology Satellite Program, ATS-6 required the development and successful demonstration in orbit of the spacecraft, its subsystems, and the experiment technology needed to satisfy its multimission objectives. ATS-6 was an outstanding success in this regard. Substantial benefits were obtained from the various communications, scientific, meteorological, and technological experiments. However, to profit from its contributions as an Applications Technology Satellite, the lessons derived from its design, test, and operations are next identified for use in future programs.

From a management standpoint, a number of elements undoubtedly contributed to the success of the ATS-6 program; e.g., configuration management, reliability, quality assurance efforts; control documentation such as interface control drawings, power profiles, mass properties reports,

command/telemetry lists; etc. However, concentrating more on the direct technical aspect of the programs, some of the more important conclusions and recommendations pertinent to future programs of this complexity are the following:

1. A protoflight program is a technically viable, cost, and schedule effective approach to spacecraft programs, even though they may be as complex as ATS-6. Careful definition, control, and documentation of hardware requirements and characteristics, and thorough evaluation of the design and performance verification efforts are particularly crucial.
2. The thermal structural model spacecraft was an important element of the ATS-6 protoflight program for qualifying the designs of the structural, thermal, and mechanisms subsystems; for providing an early definition of the mechanical environments for which the other spacecraft operating subsystems had to be designed; and for validating critical spacecraft handling, and test hardware, software, and procedures.
3. Another vital element of a successful protoflight program is the early assurance of compatible system and subsystem interfaces. This involves analysis and formal definition and control of all such interfaces. Advance interface compatible tests were conducted for ATS-6 with breadboard and qualified components that had particularly complex or sensitive interfaces, either within or between subsystems. Several incompatibilities were identified by such tests, permitting their resolution in a timely manner, and thus avoiding any significant impact on the protoflight spacecraft schedule. Use of a standard interface test unit to verify command, telemetry, and power interface compatibility for government furnished equipment, experiment and spacecraft hardware prior to integration was also very beneficial, as was the use of formally defined and controlled spacecraft integration and test procedures.
4. Functional and standby redundancy and operational flexibility for all of the critical spacecraft elements is important for the realization of an extended successful mission. Incorporation of a central digital computer, capable of being reprogrammed on command from the ground, can be an important factor in continued mission success. Required changes in operational modes, such as modification of attitude control laws, data processing algorithms, etc., can be accommodated thereby.
5. Potential emi/rfi and spacecraft charging problems can be prevented by a strong emi/rfi control program (the ATS-6 approach featured a review committee with a central responsibility for defining design and test requirements, evaluating test results, and providing critical judgments as to necessary corrective action indicated); careful definition and control of spacecraft grounding provisions (ATS-6 used grounding straps for isolated structural elements and all conductive layers of thermal blankets); design of a telemetry and command subsystem with appropriate noise immunity (ATS-6 had a 10-volt differential between "0" and "1" states); and thorough verification of spacecraft electromagnetic and radio frequency compatibility in its launch and orbital configurations and planned operational modes.
6. Technical, schedule, and cost advantages can be realized by defining and developing common software to be used for automated or semiautomated spacecraft testing and for the control of

in-orbit operations. Realization of an effective and successful mission for ATS-6 was ensured by early involvement of flight operations personnel in the definitions of system and subsystem design and test requirements; by an operations-oriented spacecraft ground test program that verified all planned prime and backup operational modes; by the use of common command and telemetry procedures and displays for spacecraft ground test and flight operations; by the sequential involvement of a core of key personnel through the total flow of spacecraft test and flight operations; by direct involvement of all flight operations personnel during several phases of spacecraft testing operations (by remote communications links); and by advance preparation of comprehensive command, telemetry, and operations handbooks that were verified during spacecraft ground-test operations.

7. The propellant to be used by the spacecraft propulsion subsystem for attitude and orbit control functions is the major expendable of the mission; hence, conservative design practices for sizing the propellant loading and for maximum flexibility in its use are very important. As an example, the ATS-6 propellant budget included provisions for correction of predicted, 3-sigma, in-plane orbit injection errors that could affect the success of its mission. When a near flawless orbit injection condition was realized, the propellant allocated was available to be used for unforeseen attitude and orbit-control contingencies, such as for a mixed wheel-jet mode to compensate for a partial failure in the roll-wheel drive electronics, east-west stationkeeping at 140° West longitude for the final 3 years (instead of being located at the planned 105° West longitude stable point with no stationkeeping required), and an unplanned major deorbit maneuver at the conclusion of the mission.
8. In designing satellite power generation and storage capabilities, careful consideration must be given to the number of times and extent to which the batteries will be required to help support spacecraft loads. ATS-6 flight experience indicated that when mission support requirements imposed more and deeper discharge cycles on the batteries than anticipated, the energy storage capacities of the latter are significantly degraded.
9. Considerable effort and money were expended during the ATS-6 program to provide attitude sensors and controllers that could provide an absolute pointing accuracy within 0.1 degree (3-sigma) over a 5-year mission. It would appear that the pointing requirements of the various experiments could have been addressed more effectively by specifying tight short-term drift performance by the attitude control subsystem, and by emphasizing in-orbit calibration techniques to eliminate any long-term bias effects detrimental to experiment objectives. It is noted that one of the major relative angle variation effects experienced during the mission appeared to be due to thermal distortions of the parabolic reflector, due to varying solar inputs, that caused off-axis "squinting" of the rf boresight.
10. The all-attitude relative Sun-direction information provided by the five wide-angle, two-axis digital Sun sensors proved invaluable during periods when the spacecraft became disoriented and major Sun and Earth reacquisition maneuvers had to be performed. While dynamic graphics displays were provided for operations personnel for reference during slewing and satellite tracking maneuvers, enhanced displays that would more directly depict the relative spacecraft, Sun, and Earth orientation and location would have been very helpful.

11. The rf interferometer proved to be a very effective sensor for relative Earth-pointing attitude because of its fine resolution (0.0014 degree), tight accuracy (0.018 degree, 3-sigma) and wide-angle measurement capability (several repetitive cycles of the unambiguous coarse-angle range of 35 degrees in pitch and roll). Because of the lack of moving parts and potentially high reliability, this sensor would appear to be worthy of consideration for mission applications where the requisite rf reference signal from a ground station can be provided on a continuous basis.
12. Following the Polaris sensor noise anomaly in October 1975, the yaw inertial reference unit (featuring a single-degree-of-freedom, gas bearing, rate integrating gyro), in conjunction with reference updates from the $\pm X$ axis digital Sun sensors, was used successfully as a backup yaw sensor for the rest of the mission. Its accuracy and ease of operation could have been enhanced, however, by a greater rate bias torquing capability (to fully compensate for orbital rate pickup at large roll offset angles from the local vertical) and by onboard torquing control via the digital controller to compensate for dynamic rate coupling effects during slewing and tracking maneuvers.
13. Extreme care was exercised in the design of all deployable structural elements to ensure positive lockup with no residual free play in the hinge joints. This effectively precluded any deleterious dynamic coupling between the structure and the attitude control subsystem that would have compromised the stringent attitude stability requirements imposed on the latter. However, possible inadequate provisions for moving element edge clearances and thermal distortion effects may have led to the interruption of the initial normal deployment motion of the north array. If the array had not finally deployed properly, this could have seriously impacted the ATS-6 mission.
14. The outstanding performance of the thermal control subsystem in controlling the temperatures of the Earth-viewing module and its complement of components was due in large measure to the use of multiple heat pipes buried in the north and south EVM faces (primary mounting surfaces of EVM equipment components) and the connecting heat pipes buried in the north-to-south transverse beams. These thermally conductive heat pipes, working in concert with the thermal louvers on the north and south sides, the thermal insulation blankets on the remaining faces, and the internal shunt dissipators of the power subsystem, maintained close temperature control throughout a wide range of solar aspect angles, solar flux levels, and diverse operational powered configurations of EVM mounted experiments and support equipment.
15. While higher than anticipated temperatures were experienced by equipment mounted on the Earth-viewing face, largely due to solar flux inputs through the many cutouts required and poor thermal coupling of the ground-plane mounting surface to external faces, this effect could be alleviated by improving the thermal coupling from the mounting surface to the north and south external surfaces.
16. The reflector support truss, which was constructed of graphite fiber reinforced plastic (GFRP), demonstrated the feasibility of using GFRP for primary structural elements and the unique thermal stability and structural/mass property advantages of this material.

17. The module EVM configuration permitted separate communications and attitude control subsystem integration and testing, remote from the remainder of the spacecraft, permitting simultaneous performance of subsystem level operations in the communications module, service module, and experiment module. The spacecraft propulsion subsystem, fabricated and tested as a hermetically sealed system (except for fill, drain, and pressurizing valve ports), was mounted totally within the EVM (except for yaw and orbit control thrusters mounted on the reflector support truss). The modular structural design of the EVM contributed to the feasibility and ease of installation and integration of the spacecraft propulsion subsystem.
18. While the telemetry and command subsystem provided considerable capability and flexibility in its design and operation, it was difficult to accommodate new command and telemetry requirements that were identified late in the program. A next generation improvement is the current distributed, multiplex data-bus approach that couples remote command and data interface units to a central bus that runs throughout the spacecraft. The integration of additional hardware elements requires only local harnessing to their nearby interface units.
19. Despite the prime-focus feed arrangement for the parabolic reflector, the rf perturbations and losses introduced by the truss and EVM blockage did not appear excessive. This effect had to be accounted for, however, in rf characterization tests using "hard" and "soft" (flight-type) reflectors. Test problems were particularly evident for the vhf frequency and for monopulse operations, which suffered from a lack of integrated system testing and precision phase adjustments. The use of a hat coupler during various phases of integrated spacecraft testing, permitting signals to be coupled via the antenna feeds rather than merely hardline connections with the transponder, was of significant benefit.
20. The series of thruster anomalies and failures that occurred during the period from February 1977 through the end of the mission in August 1979, contributing significantly to the decision to terminate the mission at that time, are judged to have been largely caused by propellant feed blockages due to system contaminants. The likely sources of these contaminants were residual deposits remaining after clean and flush operations following exposure to hydrazine during subsystem-level, hot-firing ground tests (strongly recommended to be avoided on future programs), zinc and silicon oxide leached from the tank diaphragms (to be countered by selection of diaphragm materials with proven low-contaminant generation or by elimination of elastomeric tank diaphragms as a propellant expulsion aid), and/or trace impurities in the loaded hydrazine (to be addressed by carefully specifying and controlling the purity of the flight propellant to the best state-of-the-art levels). Susceptability of the thruster to contamination should also be diminished by selecting higher thrust levels and, therefore, larger capillary feed tubes if allowed by mission requirements; using larger capillaries to feed the catalyst bed; and minimizing the number of pulses on any particular thruster as permitted by mission attitude control requirements.

Part B
Mechanical Subsystems

CHAPTER 5

MECHANICAL DESIGN REQUIREMENTS

INTRODUCTION AND FUNCTIONAL REQUIREMENTS

The ATS-6 mechanical subsystems were considered to include the structural subsystem, the parabolic reflector subsystem, and the separation and deployment mechanisms.

The structural subsystem of the spacecraft was required to house, support, and maintain the relative alignment of all spacecraft from subsystem integration and test through launch, separation of the spacecraft from the launch vehicle, deployment, and all operations while in orbit. The structure was also a critical element for some of the communication experiments because it was required to position and maintain the 9.14-meter (30-foot) diameter parabolic reflector with respect to its prime-focus feed assembly that was located at the focal plane of the reflector.

The structure requirements included the necessary fields of view for each experiment, control subsystem sensors, and the power subsystem solar arrays. The structure of the spacecraft and reflector were also required to be physically compatible with the Titan III-C launch vehicle and its payload fairing.

The structure and mechanisms designs provided facilities for retaining the spacecraft to the launch vehicle, release of the spacecraft (upon command) from the launch vehicle adapter, and separation of the spacecraft from the adapter under controlled tip-off conditions with sufficient velocity to prevent physical interference between the spacecraft and the launch vehicle.

The spacecraft structure and mechanism designs also incorporated the means to restrain the solar arrays and parabolic reflector during launch, to sequentially deploy them upon command, and to lock these elements into position for the operational life of the vehicle, with no free motion allowed that could perturb the attitude of the spacecraft.

The structure also had to be compatible with the requirements for the installation of an integrated, hermetically-sealed spacecraft propulsion subsystem.

Figure 5-1 summarizes the most significant design load requirements imposed on ATS-6.

The structural subsystem of ATS-6 was designed to accommodate the electronic and electromechanical apparatus necessary to fulfill the spacecraft mission and to provide the physical means for integrating the packaged apparatus with two solar panel assemblies, a parabolic rf reflector, and the

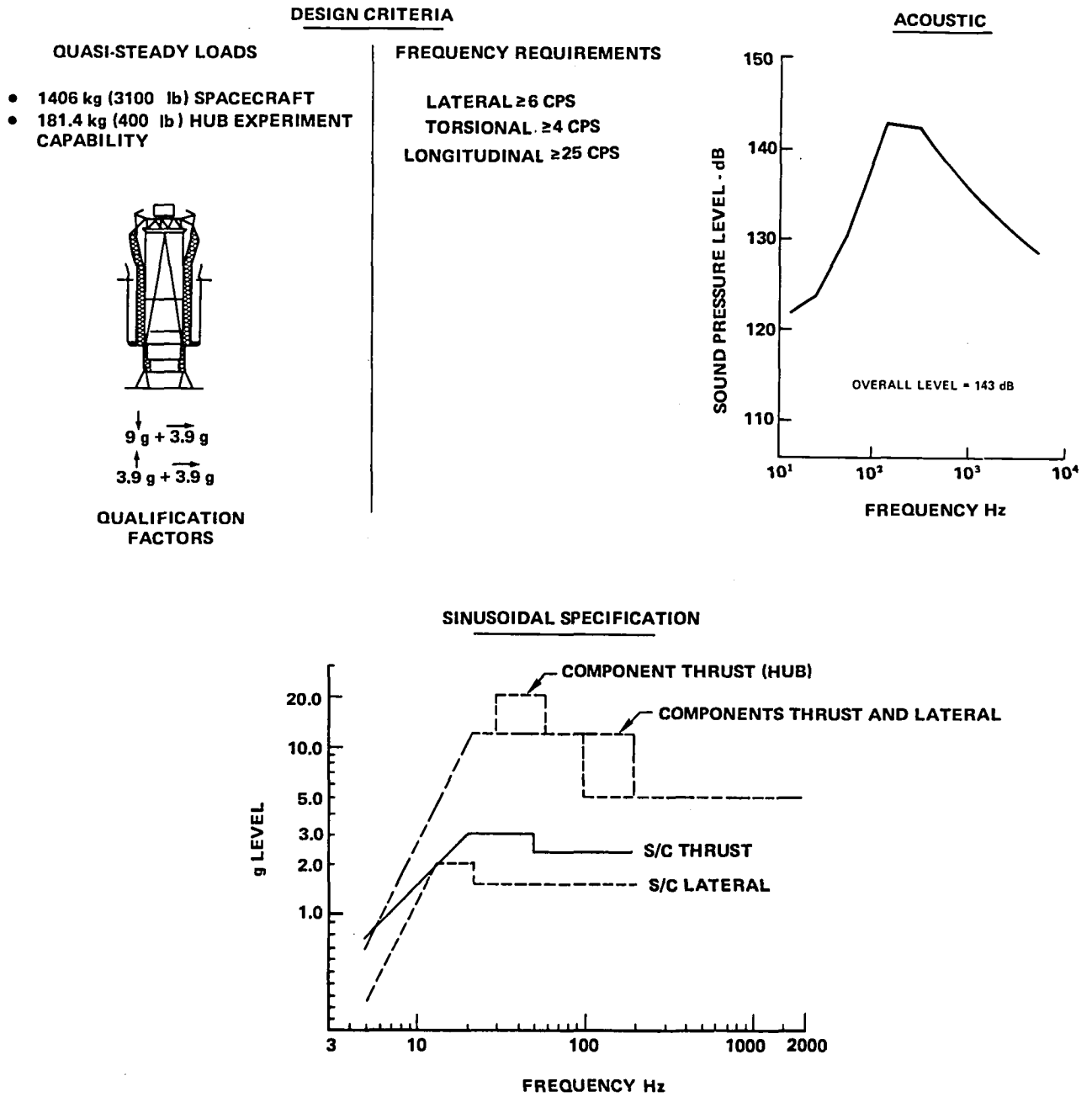


Figure 5-1. Design Load Requirements

Titan III-C launch vehicle. The structural/reflector subsystems consisted of five major component assemblies. These assemblies, shown in Figure 5-2, consisted of the reflector support assemblies, parabolic reflector, two solar array and boom assemblies, separation/adaptor assembly, and Earth-viewing module.

The structural subsystem design incorporated two functional mechanisms for separation and deployment. Separation involved the release and ejection of the spacecraft from the adaptor/separation assembly that remained with the Titan III-C third stage (transtage). Deployment consisted of the release and sequential deployment of the solar panel boom assemblies, solar panels, and the parabolic reflector.

Pyrotechnic firing signals for separation originated in the Titan. The automatic deployment sequencer, located in the service module, provided automatically sequenced deployment signals. Backup ground command capability for manually initiated deployment was provided through the normal ground-to-spacecraft command link if the automatic deployment sequencer failed, or if anomalies occurred that required stopping the sequencer to obtain time for analysis.

Earth-Viewing Module

The configuration of the EVM developed from trade studies that considered mission, subsystem, and component requirements. The more significant requirements and constraints follow:

- Operational requirements, such as fields of view of experiments and sensors
- Maximum communication power efficiencies
- Subsystem and system integration and test requirements
- Minimum spacecraft weight
- Thermal control requirements

To comply with these requirements and constraints and to permit parallel integration and test of spacecraft subsystems, the EVM was separated into three modules. The service (central) module was a major load carrying structure, acting to stabilize the base of the reflector support truss and to resist launch and separation loads induced by the spacecraft/launch vehicle adaptor. It also provided the base for mounting the communications module near the large parabolic reflector and for mounting the experiment module on the opposite side.

The design of the experiment module (EM) was determined primarily by operational requirements of the experiments and of the Sun, star, and Earth sensors of the attitude control subsystem.

The communications module (CM) was located nearest the reflector and supported the reflector prime focus feed (PFF) assemblies on its top surface. The equipment within the CM was composed primarily of communications equipment, located close to the PFF to minimize power losses.

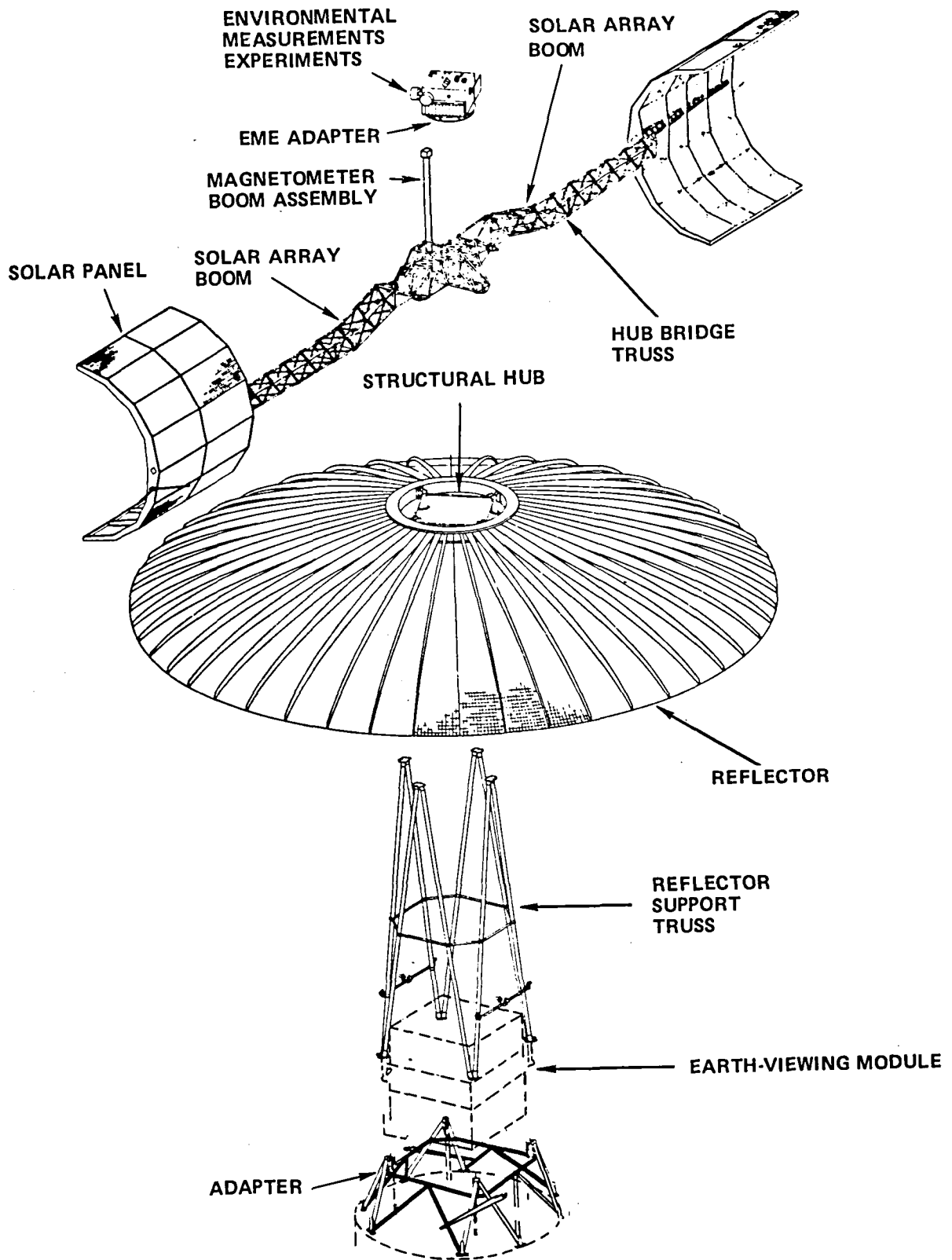


Figure 5-2. Structural and Reflector Subsystems

The EVM configuration permitted communication subsystem installation, integration, and test at the subsystem level and remote from the remainder of the spacecraft, thereby permitting simultaneous performance of subsystem level operations in the CM and in the remainder of the EVM. The spacecraft propulsion subsystem (SPS), fabricated and tested as a hermetically sealed system (except for fill, drain, and pressurizing valve ports) was mounted within the EVM (except for orbit control thrusters on the reflector support truss). The modular design of the EVM contributed to the ease of installation and integration of the SPS.

The outstanding performance of the thermal control subsystem of the EVM and its complement of components is due in large measure to the use of multiple heat pipes buried in the north and south EVM faces (primary mounting surfaces of EVM components) and the heat pipes buried in the north-to-south transverse beams. These thermally connected heat pipe systems worked in concert with the thermal louvers on the EVM north and south sides and the thermal insulation on the remaining faces to maintain close temperature control throughout a wide range of solar aspect angles, solar flux levels, and multiple operational configurations of EVM mounted experiments and equipment.

Fields of View

The desired fields of view (FOV) established the location of most of the experiments. The Earth direct viewing experiments were located in the base of the EVM; the space and environmental experiments were packaged into the environmental measurements experiments (EME) package and were mounted above the large reflector that provided shielding from much of the high power rf energy. The magnetometer was mounted at the tip of a Beryllium tubular mast that extended above the reflector hub, again to achieve maximum separation from spacecraft generated disturbances and noise. The communication subsystem omnidirectional antennas were placed at the extreme north and south ends of the deployed solar arrays to enhance 4π steradian coverage.

Spacecraft Grounding Plan

The electrical potential between any locations on the spacecraft was minimized by implementing a comprehensive grounding plan in the early phases of the structural design.

The spacecraft used separate lines for signal and power returns with all lines grounded to the structure at one central "star" grounding point. The structural elements of the EVM were electrically grounded to each other and rf seals were used on every joint or opening to reduce stray rf fields within the EVM.

Shields were used on lines sensitive to noise and, where possible, filters were used to reduce noise at entry points to the EVM. The exterior case of boxes and components mounted to the honeycomb core sandwich panels of the EVM were grounded to the structure by using silver-filter epoxy to firmly attach one or more of the mounting screw panel inserts to the panel.

The solar array boom hinges were locations that could produce high electrical impedance between major structural elements. Flexible grounding straps were used across all hinges. Other moving elements were analyzed to find potential trouble spots and suitable grounding provided.

The spacecraft used multilayer thermal insulation over many surfaces, such as the EVM, reflector support truss, solar array booms, and deployment hinge mechanisms. All metallized surfaces of the insulating blanket were grounded together and to the structure at frequent intervals to minimize build-up of potential differences on the spacecraft as static charges were accumulated in orbit.

Following the first week in orbit, during which spacecraft initial outgassing occurred, the spacecraft performance did not exhibit any anomalies that could be traced to a difference in electrical potential between spacecraft components. (In this regard, it was noted that during eclipse periods spacecraft charge levels as high as -14,000 volts were measured.)

Boom/Array Positive Latching Mechanisms

A critical operational mode of the ACS, the low-jitter mode, affected the spacecraft structural and mechanical subsystem designs. In this operational mode, the spacecraft was required to exhibit a pointing accuracy of less than 0.5 degree, pointing stability of less than 0.01 degree, and rate stability of less than 0.001 degree per second. The deployed spacecraft was required to have sufficient stiffness so that no element of the structure would have natural frequencies of vibration low enough to resonate with motions of the spacecraft produced by ACS controlled operations and thereby cause the spacecraft to exceed the low-jitter mode stability requirements.

The structural elements of the spacecraft were sufficiently stiff so as to pose no problem; however, the rotating hinge joints of the solar array deployment system were identified in the early design phases as a potential source of trouble. To minimize bearing lubrication problems and to achieve a simple and low-weight design, journal type bearings were used for the deployment system first-, second-, and fourth-motion hinges. The necessary clearance in these hinges if not deleted, cancelled, or made nonoperative after final lockup, would provide a hinge-joint-motion deadband that could interact with the ACS system. Furthermore, the hinge-motion-lockup latches were also a potential source of relative motion in the hinge.

The ATS-6 hinge and lockup designs were developed using the following guidelines:

1. Hinge-pin clearance should be minimized and consistent with predicted temperature gradients to prevent binding during deployment.
2. Hinge-pin clearances should be negated by drive spring forces continuing to act after lockup; i.e., the deployment spring action should drive the hinge to a known configuration of hinge elements and pin under normal conditions with zero clearances.
3. Lockup should be accomplished using tapered locking plungers or pins in wedge-shaped or conical holes to reduce mating clearance to zero.
4. Locking-pin mechanisms should have minimum clearances consistent with predicted temperature gradients to prevent binding during operation.
5. Deployment forces should continue to act following locking-pin seating to drive locking pins into a designated position with zero clearances.

The solar array deployment and lockup mechanism designs met these requirements (Figures 6-6, 6-7, 6-9, and 6-11). In each case, deployment springs continued to act to seat hinge pins and lockup plungers after lockup was accomplished. Multiple drive springs provided redundancy for this action. Two lockup pins, acting redundantly, ensured that lockup would occur. In the unlikely event that lockup plungers did not enter their seats, over-travel stops on each mechanism positioned the hinge very close to the position of design lockup. Deployment spring forces were sufficient to maintain the hinge at the final deployed position against any torques that could be applied to the hinge-system by the spacecraft in normal operation.

The hinge and latch mechanisms provided a backlash-free system that had no detectable deleterious effects on the spacecraft response to the ACS low-jitter mode operations.

REFLECTOR SUPPORT ASSEMBLY

The reflector support assembly (Figure 5-3) consisted of a reflector support truss, structural hub, a hub bridge truss, a magnetometer boom assembly, and the Environmental Measurements Experiments adapter assembly.

Reflector Support Truss

The reflector support truss consisted of eight 7.1 centimeters (2.8-inch) outside diameter graphite fiber reinforced plastic tubes arranged in a symmetrical tower-type configuration approximately 4.67-meters (15 feet, 4 inches) high and were terminated at both ends by titanium end fittings (for thermal compatibility) that were bonded to the tubes.

The tubes were wrapped with superinsulation to ensure that temperature variations on the truss would not produce thermal distortions that could cause degradation of the reflector rf patterns. The structural tower was composed of four A-frame structures with interconnecting, stabilizing tubes forming a complete ring at their approximate midpoint.

Orbit control jet (OCJ) support assemblies were located on both the east and west sides of the structural truss near the Z-axis station of the spacecraft center of mass. These assemblies provided mounting facilities for orbit control and yaw thrusters of the spacecraft propulsion subsystem. Each of these assemblies (Detail B, Figure 5-4) consisted of a length of square aluminum tubing attached between two tubular legs of the truss of clamp-type titanium sleeves. These sleeves were also held in place by spring-loaded bolts and adhesive bonding.

The truss maintained structural integrity and performed satisfactorily throughout the 5-year mission.

Structural Hub

The aluminum structural hub (Figure 5-3) consisted of four fittings bolted to four strut assemblies, all of which were aluminum. The four fittings of the structural hub were bolted to the end fittings at the top of the truss. The structural hub fittings provided the four-point mounting for the parabolic reflector and the interface between the reflector support truss and the hub bridge truss.

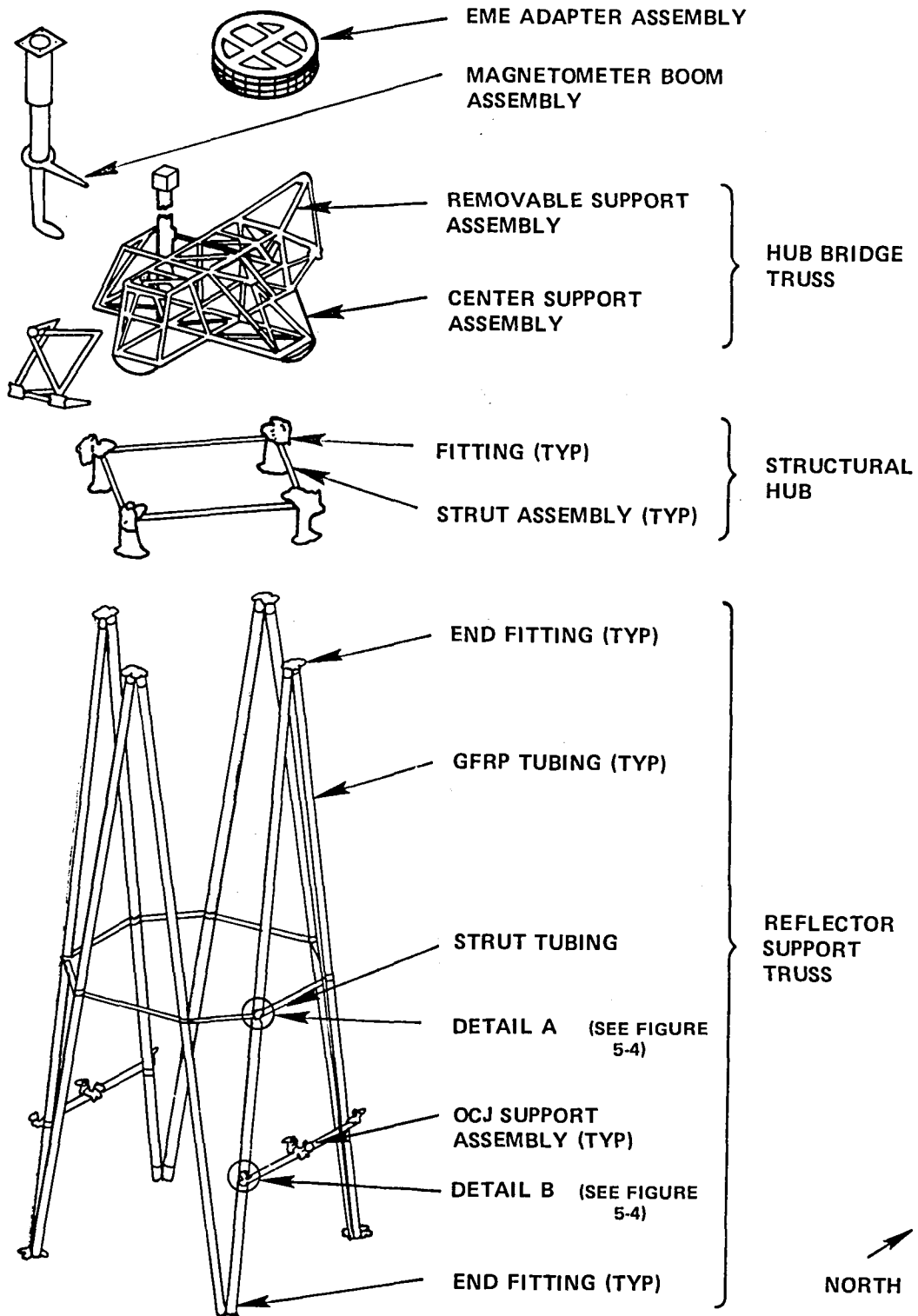
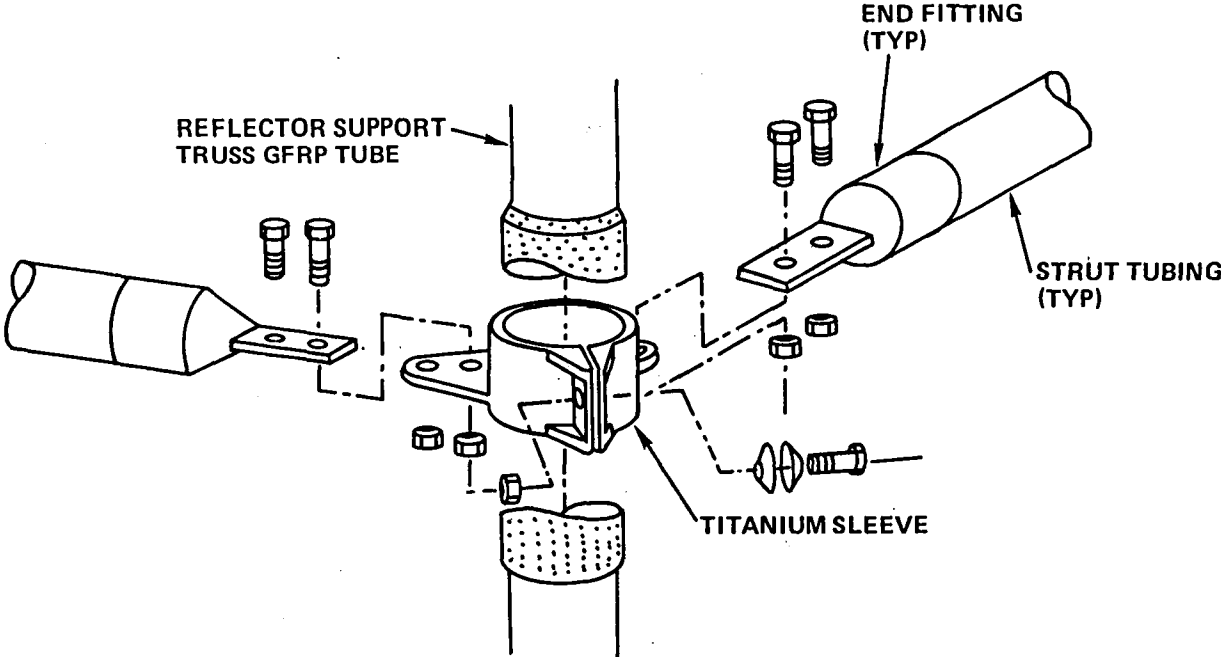
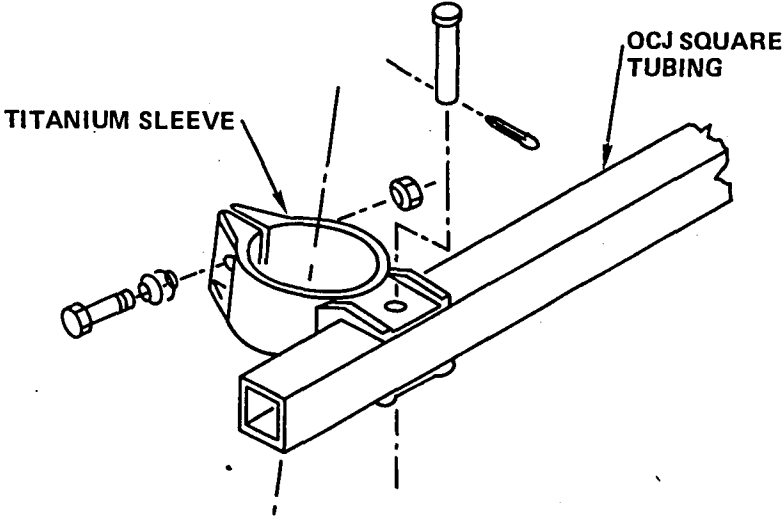


Figure 5-3. Reflector Support Assembly



DETAIL A. TRUSS STABILIZATION DETAILS



DETAIL B. OCJ STRUT DETAILS

Figure 5-4. Reflector Support Assembly (Detail A and Detail B)

Hub Bridge Truss

The hub bridge truss (Figure 5-3) consisted of a center support assembly and two identical removable support assemblies. The center support assembly consisted of a space structure of aluminum tubing and fittings interconnected by a combination of rivets, bolts, and welding. The top-center of the hub bridge truss contained the mounting facilities for the Environmental Measurements Experiments (EME) adapter assembly and provisions for attaching the magnetometer boom assembly. The two removable support assemblies were also a combination of aluminum fittings and tubing, with hinge fittings for interfacing with the solar array booms. They also provided part of the mounting facilities and integrating structure for the spacecraft deployment and latching mechanisms.

Magnetometer Boom Assembly

The magnetometer boom assembly (Figure 5-3) consisted of a tapered tubular beryllium boom with a mounting plate at the top and two mounting brackets located near the lower portion. The boom was approximately 2.13-meters (7-feet) long and 11.4 centimeters (4½ inches) in overall diameter. The plate bonded to the top of the boom provided a mounting base for the magnetometer. The boom assembly mounting brackets were attached to the top and bottom truss members of the north-west side of the center support assembly of the hub bridge truss.

EME Adapter Assembly

The EME adapter assembly was a 7.6-centimeter (3-inch) high truncated cone with external flanges at each end, fabricated as an aluminum weldment 76.2 centimeters (30 inches) in diameter at the top and 71.1 centimeters (28 inches) in diameter at the bottom. Numerous lightweight intercostals were connected to both flanges and the cone for stiffness. The underside of the adapter assembly was bolted to the center support assembly of the hub bridge truss. The top of the adapter assembly provided the mounting facility for the EME.*

PARABOLIC REFLECTOR SUBSYSTEM

The parabolic reflector assembly was a 9.14-meter (30-foot) diameter parabola ($f/d = 0.44$). The reflector shape was established by ribs to which the mesh was sewn, hinged from an aluminum hub assembly. The reflector was stowed before deployment in a 1.98-meter (78-inch) outside diameter torus by winding the ribs around each other in a "maypole" fashion with the mesh folded between and retained by doors hinged to the top of the torus. A cable encircling the torus held the doors closed; this was cut by a pyrotechnic cable cutter for deployment. The reflector is shown being furled in Figure 5-5.

*The EME is described in Volume VI of this report.

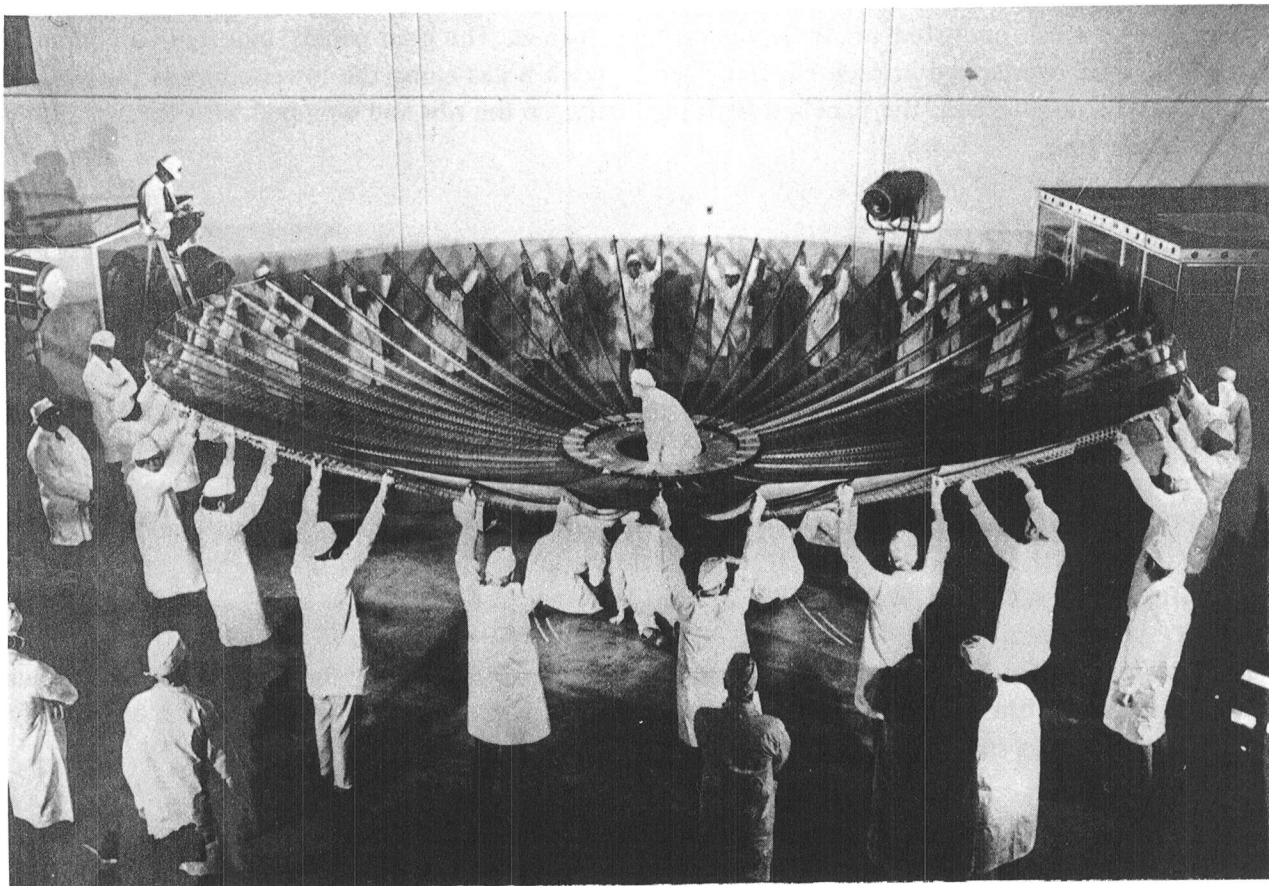


Figure 5-5. Technicians Furl Large ATS-6 Antenna Reflector

Reflector Hub Assembly

The hub assembly was a C-shaped structural ring with the recess facing away from its center. The recess provided the mounting for 48 equally spaced clevis hinges to which the antenna ribs were attached. The recess also provided stowage for the ribs and mesh. The top of the hub was the mounting surface for the hinged brackets of the multipanel release mechanism. The hub assembly interfaced with the reflector support assembly at four mounting points. These points were located on the inner perimeter of the hub and bolted to the four fittings of the reflector support assembly structural hub.

Ribs and Mesh

The 48 radial thin-gauge aluminum ribs of the reflector were of a semicylindrical configuration forming an approximate 10.8-centimeter ($4\frac{1}{2}$ -inch) segment of an arc at the larger or hinge end. Each rib, chemically milled and perforated with diagonally-oriented hold patterns, was tapered at a 2:1 ratio from the hinge end to the outer tip.

A copper-coated dacron mesh (coated with silicone) supported by the ribs, formed the rf reflecting surface. The mesh consisted of 48 pie-shaped gore panels. The gore panels, adjusted to eliminate wrinkles, were overlapped at each rib and sewn through holes along the lower edges of the ribs. In the stowed configuration, the panels were folded between the ribs and wrapped with the ribs in the recess of the hub.

Release Mechanism

The antenna release mechanism consisted of 24 panels or doors with spring-loaded hinged brackets, a single cable, a cable clamp, and two cable cutters. In the stowed configuration, the panels held the antenna ribs and mesh in the recess of the hub. The panels, or doors, were held closed by the single cable that encircled them. This cable was routed through an aluminum tube mounted on 23 of the doors and through both cable cutters on the 24th door, with the cable ends terminated in the adjustable cable clamp. The terminated cable ends and cable clamp were assembled between the two chisel-type pyrotechnically actuated cable cutters on the same panel.

SOLAR PANEL AND BOOM SUBSYSTEM

There were two identical solar panel and boom assemblies oriented along the plus (south) and minus (north) Y-axes of the spacecraft. These assemblies were pyrotechnically released and mechanically deployed to expose the solar panels to the Sun.

In the normal orientation in orbit, one assembly was extended north from the spacecraft and the other south. Each solar array formed a hemicylinder facing in the opposite east-west direction from the other, so that a cylinder of solar cells provided a constant solar energy input to the power subsystem (except during eclipse periods) over the course of any 24-hour period. During launch these assemblies were folded into the stowed position.

Each solar panel and boom assembly consisted of three integral parts: the truss frame or boom assembly, the integral second-stage deployment mechanism, and the solar array panel assembly.

Boom Assembly

Each boom assembly (Figure 5-6) was an offset structure spanning approximately 4.42 meters (174 inches) between the hinge point that interfaced with the hub bridge truss interface, the offset, the boom structure, and the solar panel hinge fitting.

The offset and boom structure formed a rectangular framework with the hub bridge truss interface structure welded to one end and the solar panel hinge fitting bolted to the other end. This framework was a gradually decreasing armtype structure starting from a 27.9-centimeter by 29.4-centimeter (11-inch by 11 9/16-inch) rectangle at the end of the offset span and terminating in a 20.3-centimeter by 20.3-centimeter (8-inch by 8-inch) square at the solar panel hinge fitting. The boom was constructed from a riveted framework consisting of four segmented lengths of 1-inch square aluminum alloy tubing interconnected by aluminum channels and combinations of gussets arranged in triangular patterns on all four sides of the boom.

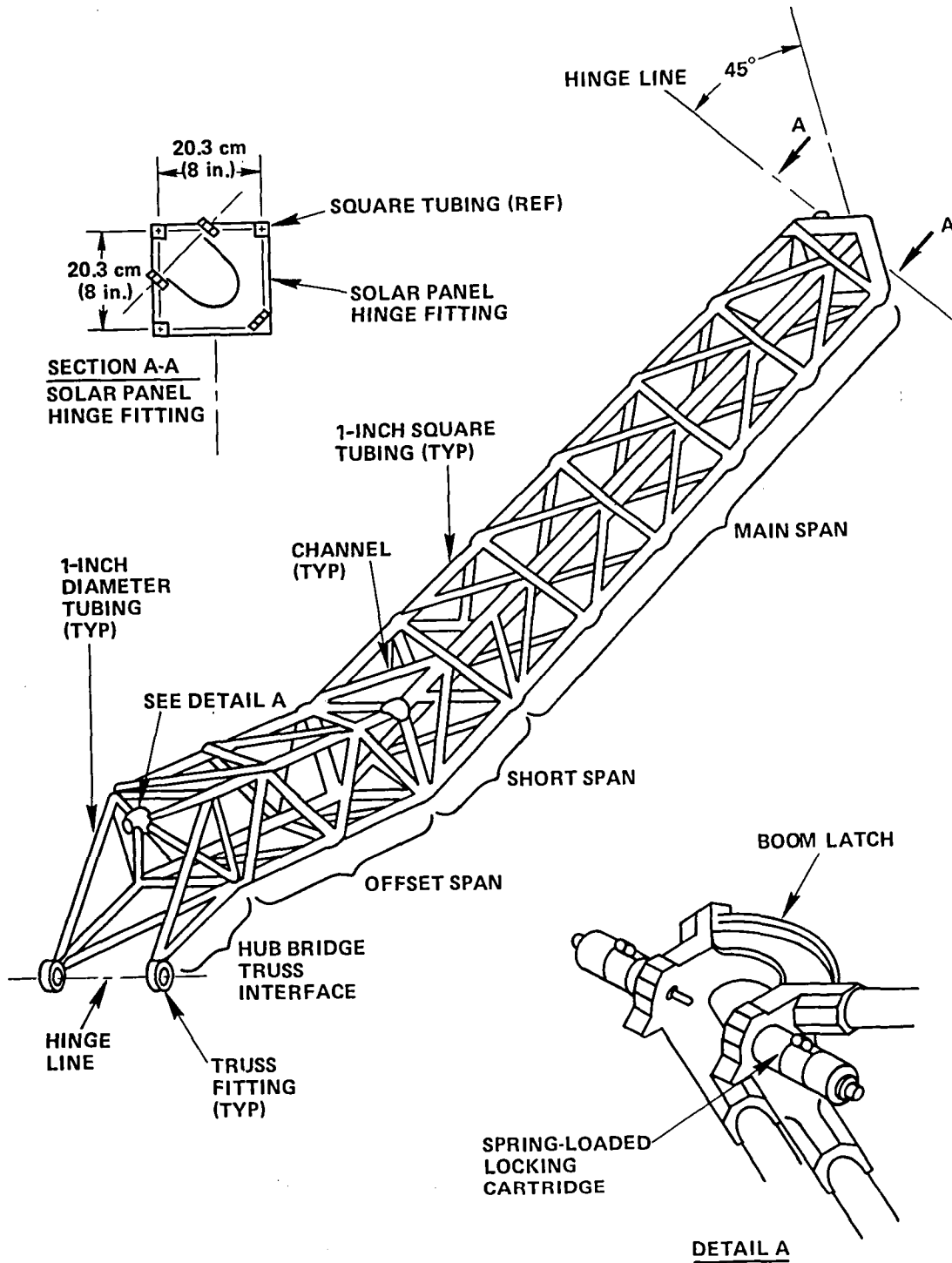


Figure 5-6. Truss Frame (Boom) Assembly

The solar panel hinge fitting (Section A-A, Figure 5-6) was a functional part of the solar panel deployment mechanism. This hinge, skewed angularly at 45 degrees from the spacecraft vertical, provided the hinge point and part of the locking apparatus for the deployment mechanism.

The hub bridge truss interface structure connected the solar panel and boom assemblies to the spacecraft. This structure was a welded arrangement of 2.54-centimeter (1-inch) diameter tubing, truss fittings, and a boom latch. The boom latch (Detail A, Figure 5-6) consisted of a horseshoe-shaped latch and two springloaded locking cartridges that locked the solar panel boom assemblies at the completion of the first-stage deployment.

Solar Array Panel Assembly

Each solar array panel assembly consisted of structural elements and solar panel assemblies integrated into a 2.29-meter (7½-foot) high semicylinder of 137.2-centimeter (54-inch) radius (Figure 5-7). There were three groups of aluminum alloy structural elements, each consisting of five eight-sided, semicylindrical frames (frames A to E), perpendicularly oriented with, and riveted to, eight interconnecting stringers and a structural spar assembly. Sixteen solar panel assemblies were attached by screws to this framework. The spar assembly was the central structural member of the solar array panel assembly. It provided the central support for the entire solar array panel assembly and was cantilevered from the boom assembly through the second-stage deployment mechanism. It was a rectangular riveted framework constructed from four lengths of aluminum alloy L-shaped angles interconnected by multiple aluminum channels. The spar was 237.5-centimeters (93½-inches) long and started with a 15.2-centimeter (6-inch) square cross section at one end and decreased to a 7.5-centimeter (3-inch) square at the other end.

Each solar panel assembly consisted of two groups of components: those of a structural nature and those related to a solar cell stack. The structural components (Section A-A, Figure 5-7) consisted of a rectangular aluminum frame with flanges on all four sides, an aluminum foil bottom face sheet, a honeycomb panel, a rectangular top aluminum frame also with flanges on all four sides, an aluminum foil top face sheet, and a polyvinyl fluoride insulated substrate sheet integrated into a structural assembly by interspaced layers of adhesive. A solar cell stack consisted of a 2-centimeter by 4-centimeter gridded silicon negative on positive solar cell, 0.36-millimeter (0.014-inch) thick, and its antireflection coated microsheet coverglass with blue filter. Each solar cell was bonded to the insulated substrate by a resilient adhesive.

On each solar panel assembly, 675 solar cells (2 centimeters by 4 centimeters) were subdivided into module and submodule groups. Each submodule consisted of three parallel connected solar cells. Each module consisted of a row of 25 series connected submodules, totaling 75 solar cells, and each solar panel had 9 modules totaling 675 solar cells. Consequently, each of the two solar array panel assemblies contained 10,800 solar cells. Solar cell electrical connections were made with a network of silver mesh that provided relief from strain due to temperature variations.

The electrical performance of this solar cell assembly is discussed in Volume III and in Part A, Chapter 2, in this volume.

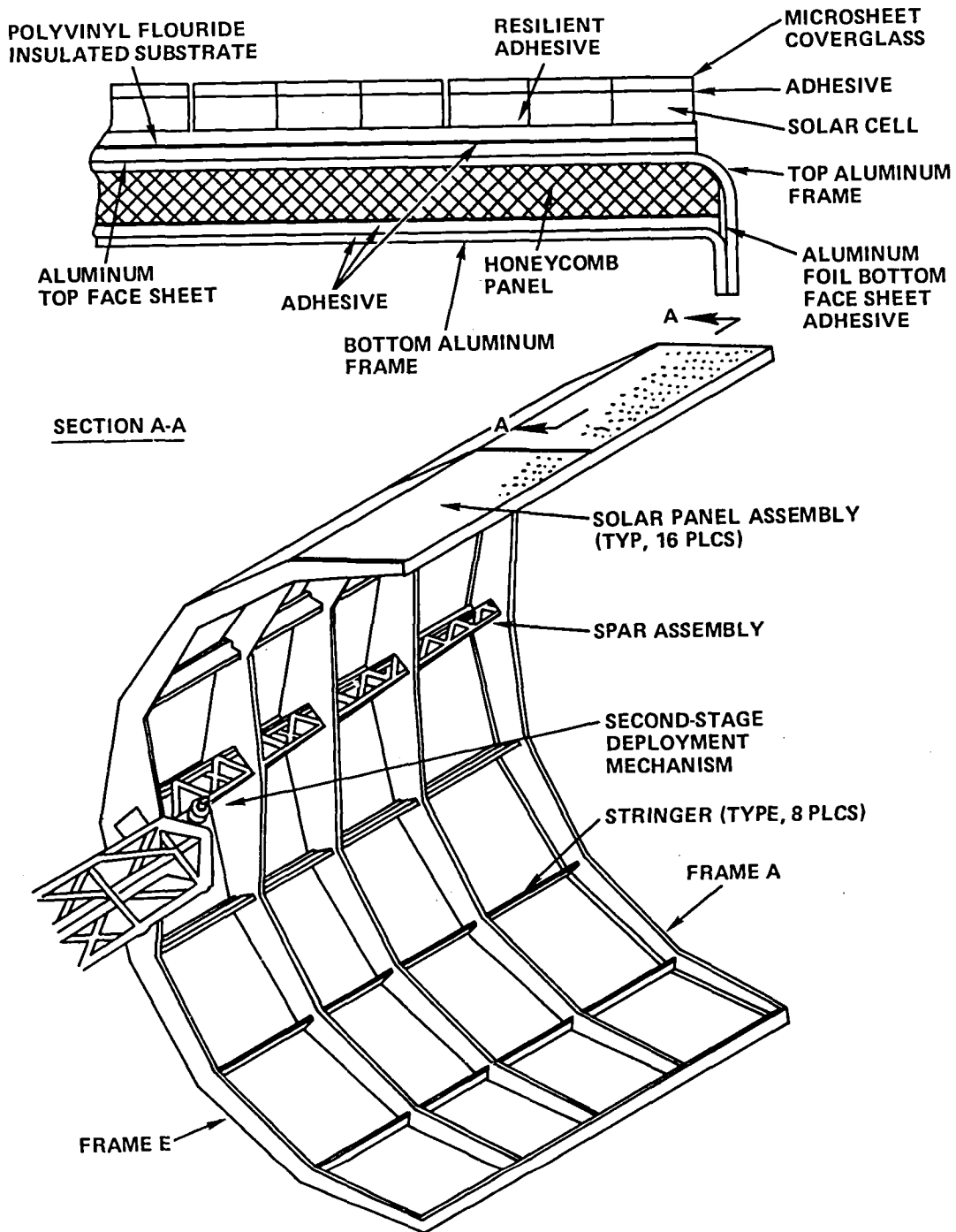


Figure 5-7. Solar Array Panel Assembly

EARTH-VIEWING MODULE SUBSYSTEM

Earth-Viewing Module Assembly

The Earth-viewing module (EVM) was a temperature-controlled enclosure that was approximately 1.4 meters X 1.4 meters X 1.7 meters. External and internal panels employed bonded sandwich panel construction with aluminum honeycomb core and face sheets. It housed all of the spacecraft electronics and experiments (except for the hub-mounted Environmental Measurements Experiments assemblies). Thermal control was maintained at 20°C , $\pm 15^{\circ}\text{C}$ by the use of internal heat pipes, thermal louvers on the north and south sides and superinsulation on all other surfaces. The prime-focus feed was mounted on the top face of the EVM nearest the reflector. The bottom face was used to mount Earth-viewing experiments (millimeter wave, propagation, radiometer) the C-band Earth-coverage horns, the interferometer horns, and the Earth sensor heads. The radio beacon antennas were mounted on the east and west sides of the EVM.

A sketch of the EVM is shown in Figure 5-8 that identifies various elements associated with this module. As indicated in this figure, the EVM is composed of three separate modules: communications, service, and experiment.

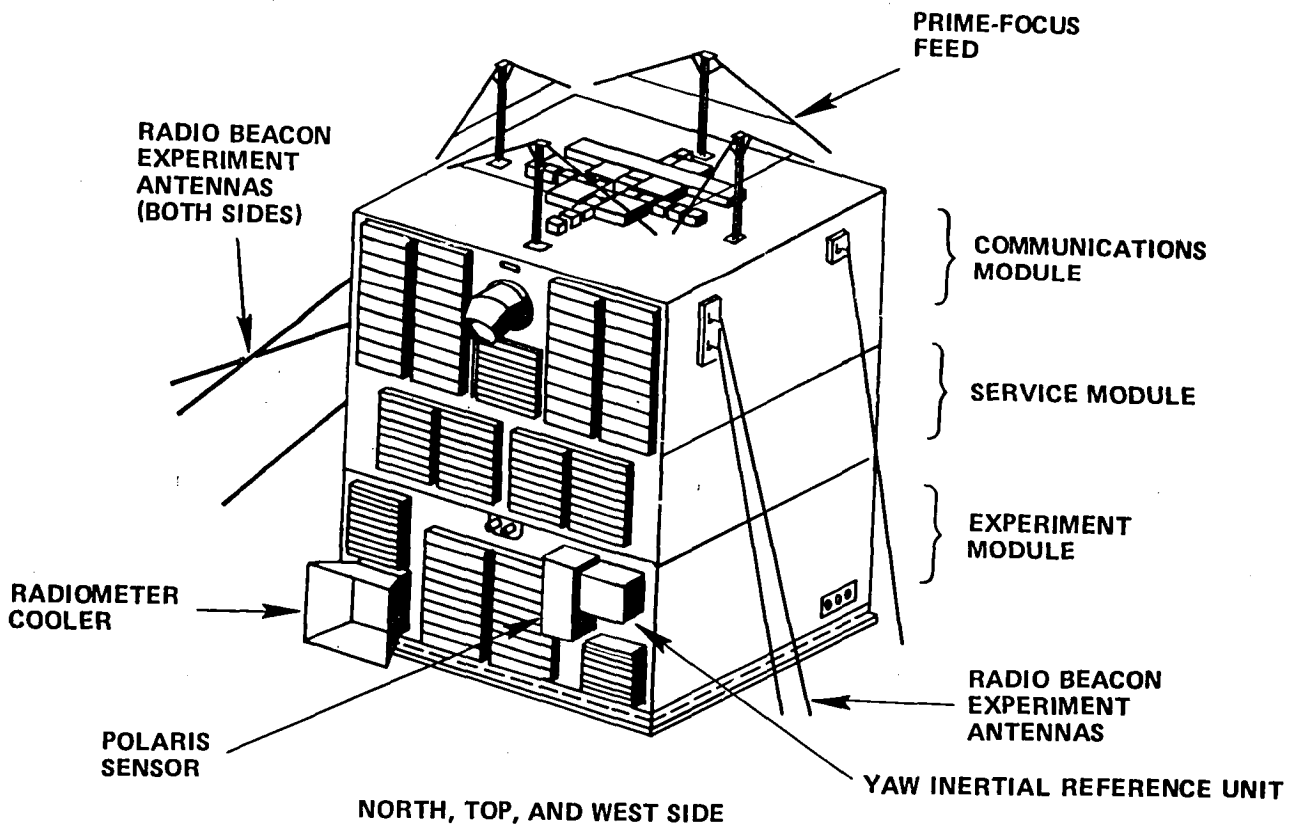


Figure 5-8. Earth-Viewing Module

Communications Module

The communications module faced the reflector and accommodated the communications subsystem, with its prime-focus feed elements mounted on its top surface. The module consisted of a basic structural framework and a combination of internal and external panels. The basic framework consisted of four L-shaped aluminum alloy supports assembled into a square table-type structure with corner brackets and L-type upright frames integrating the assembly at each of the four corners. A foot bracket at the base of each upright framework attaches to each corner of the service module. The internal panels were a center beam and an intercostal panel that were equipment mounting bulkheads. The center beam panel contained heat pipes recessed within a honeycomb core that was sandwiched between two light gauge aluminum alloy face sheets. This panel attached to the north and south frame supports. The intercostal panel was connected from the west side of the center beam panel to the module's west frame support. The feed panel, which formed the top of the communications module, was aluminum honeycomb panel upon which the parabolic reflector's prime-focus feed is mounted.

Service Module

The service module (Figure 5-9) housed the equipment for many of the support subsystems and was at the center of the EVM. The module was the central structure of the EVM and the structural interface for the communications module and the experiment module. The structural interfaces between the service module and both the communications and experiment modules were bolted in each of the four corners, and the external panels of each module were attached to a common frame member of the service module. The storage tanks, propellant lines, and electromechanical hardware of the spacecraft propulsion subsystem (SPS) were assembled on a platform. This platform and components of the attitude control, telemetry and command, power, and pyrotechnic subsystems were mounted within the service module.

The service module was constructed from two stable frameworks approximately 1.37 meters (54 inches) square and interconnected at the four mating corners by cast aluminum corner fittings that placed the frames approximately 48.3 centimeters (19 inches) apart. Each framework consisted of four H cross-section edge beams stabilized diagonally by rectangular tubes. The upper frames and diagonal supports provided the mounting facilities for the electrical connector panels (for interconnecting EVM modules and for external harness connections), auxiliary equipment mounting shelves lying in the plane of the framework, SPS mounting plate, and various bracketry. The service module also had a thermally controlled (with heat pipes) transverse beam between the north and south panels. The service module internal corner casting provided a support to which the EVM support fittings were attached on the outside of the module. These fittings integrated the separation adapter assembly, the EVM, and the reflector support truss assembly. The four support fittings, containing pyrotechnically actuated separation nuts, were also a part of the spacecraft separation mechanism.

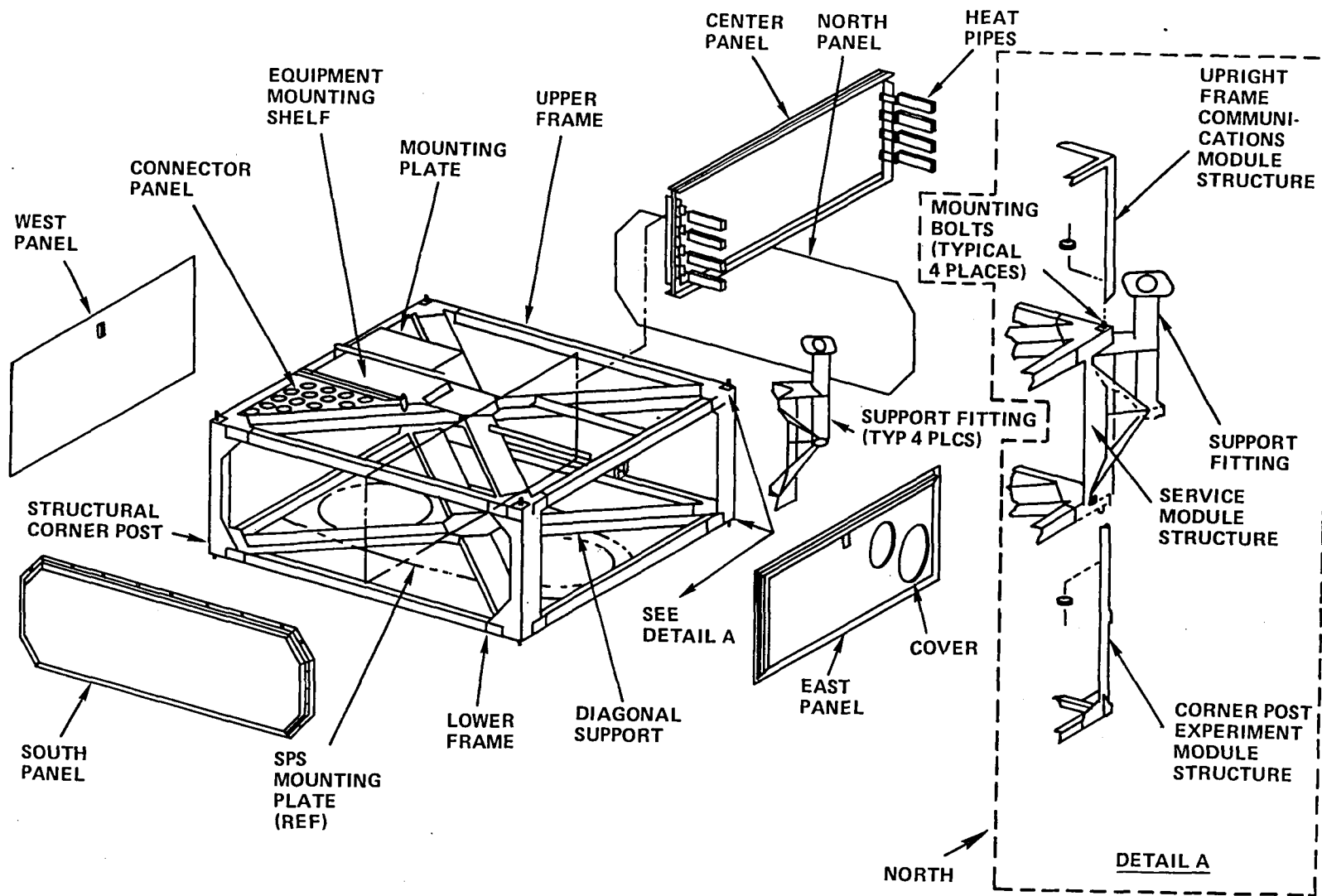


Figure 5-9. Service Module Structural Assembly

Experiment Module

The experiment module consisted of a structural framework, several internal structural elements, and a group of external panels. The framework was constructed from four channel-type edge members in an inverted table-type configuration. The edge members and corner bracketry were assembled to the four corner posts. This framework was completed with the base panel and aluminum honeycomb sandwich panel containing numerous holes for Earth-viewing experiments and equipment sensors. The base panel was attached to the top flange of the four edge members. The internal elements of the module consisted of east and west intercostal beams, radiometer support frame, and a center beam panel. The center beam panel had six heat pipes recessed within a honeycomb core and sandwiched between aluminum alloy face sheets. The radiometer support frame was an equipment mount consisting of an aluminum alloy sheet with stiffeners and equipment access holes. It connected between the center beam panel and external panel. The east and west intercostal beams were flanged aluminum alloy sheets with stiffeners and provided a structural interface between sides of the center beam panel and their external panels. There were four external or side panels and an external rf ground panel. Each of the external side panels was attached to the corner posts of the module's framework. The rf ground panel was not a structural element of the experiment module, but acted as an rf shield providing a common rf ground for the experiment module's antennas. It had a polished, highly reflective Earth-viewing surface that was attached to the bottom flange of the four edge members. It also was attached to the base panel at nine points with standoffs that compensated for the height of the edge members and allowed for a layer of insulation between the two panels. The four separation guide rails were a physical part of the experiment module. These rails were attached to pads on the outer edge of each of the module's four corner posts.

CHAPTER 6

SEPARATION AND DEPLOYMENT MECHANISMS

SEPARATION MECHANISM

The release and ejection of the spacecraft was accomplished by four identical groups of components that comprised the separation mechanism. Each group was located at a corner of the Earth-viewing module. The separation mechanism included the four adapter assemblies of the separation adapter assembly, the support fittings of the service module, the separation guide rails of the experiment module, and the associated pyrotechnically actuated releasing nuts that retained the spacecraft to the adapter.

Separation Adapter Assembly

The separation adapter assembly was bolted to the third stage (transtage) of the Titan III-C launch vehicle and attached to ATS-6 at each of the four corners of the EVM. The adapter assembly provided the pyrotechnic release mechanisms and springs that separated the spacecraft from the transtage. (This assembly remained on the transtage after separation.) Four adapter assemblies mated with the support fittings and tracks located at each of the four corners of the Earth-viewing module. Each mechanism included two 5.08-centimeter (2-inch) diameter aluminum alloy adapter legs, two base fittings, and an adapter assembly with spring and Spirator ejection mechanisms and the associated pyrotechnically-actuated releasing nuts. When these nuts were released, the four springs and Spirators drove the spacecraft and transtage apart, with their relative motion controlled by four roller/guide rail elements. The base fittings were drilled for attachment to the Titan interfacing structure. The separation adapter assembly is shown in Figure 6-1. The sheaths that stowed the Radio Beacon Experiment whip antennas were mounted on the northwest and southeast corners of the adapter assembly.

The spacecraft was mated to the adapter by inserting the bearing rollers of each adapter housing into the guide rails at each corner of the experiment module. The spacecraft and adapter were brought together until the support fittings and adapter housings were mated. During this operation, the support fittings compressed the spring-loaded ejector rod of each adapter housing a distance of 7.62 centimeters (3 inches) that produced an initial separating force of 2224 Newtons (500 lbf) at each fitting. Each support fitting was locked to the mating adapter housing by an adapter separation stud gripped at each end by a pyrotechnically-actuated releasing nut.

Additional separation forces were provided by the Spirator system at each of the four adapter housing assemblies. The Spirator system was composed of two Spirator spring-drive devices and an interconnecting tension cable. The Spirator drive consisted of a housing having a drum with one end of the interconnecting cable attached to the drum. With spacecraft and adapter mated, the cable

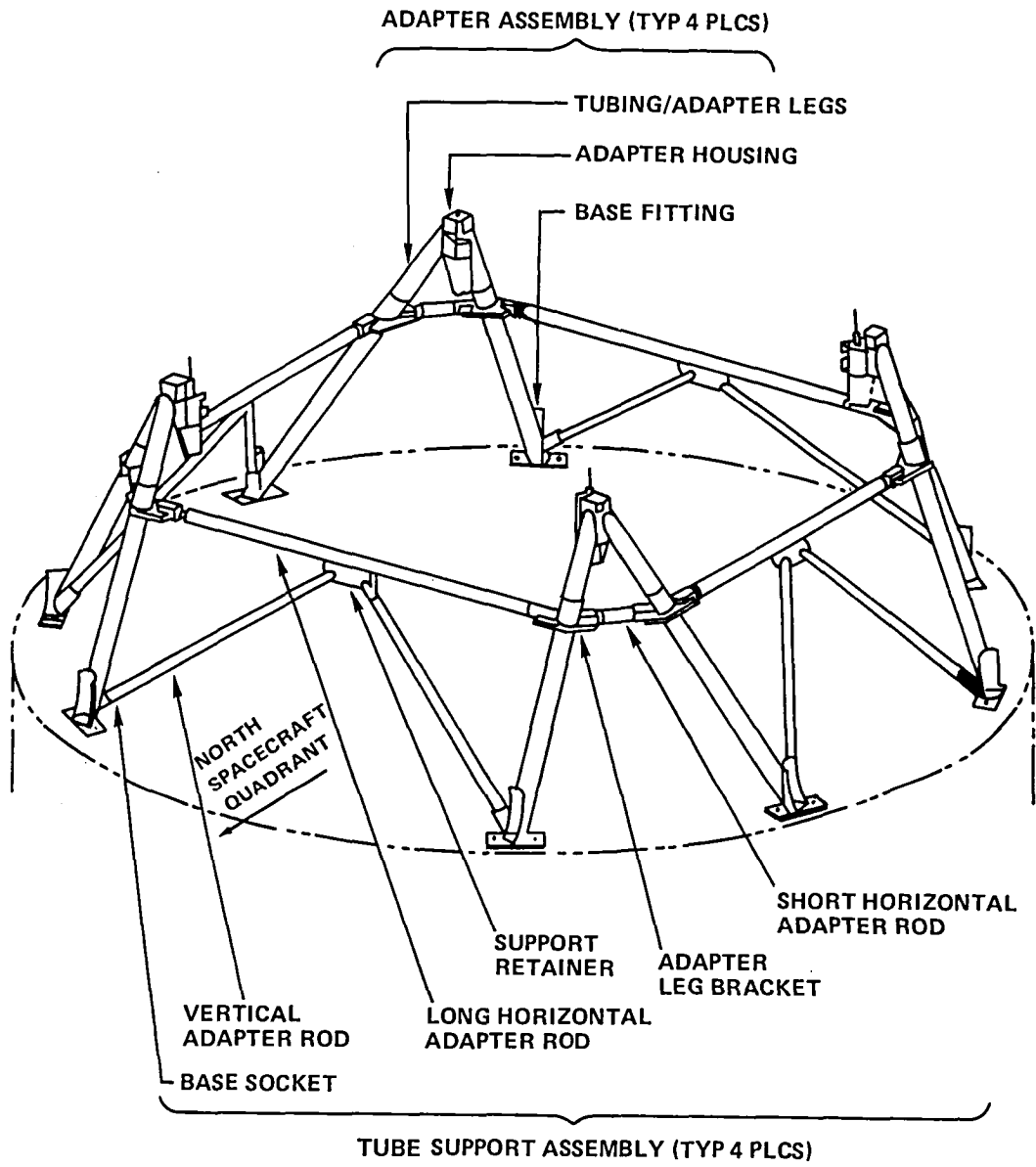


Figure 6-1. Separation Adapter Assembly

was withdrawn approximately 76.2 centimeters (30 inches) simultaneously and equally from the two drums and installed in a cable groove across the bottom of the separation guide rail. Each Spirator imparted a pull of approximately 40.0 Newtons (9 lbf) to the cable. Thus the two drums of each Spirator system caused the cable to apply a separation force of 80.0 Newtons (18 lbf) between spacecraft and adapter with the force acting for the duration of engagement of the EVM and the adapter; i.e., approximately 76.2 centimeters (30 inches).

Separation of the spacecraft from the launch vehicle was initiated by applying power to simultaneously ignite (within 10 to 12 milliseconds) the four squibs in the adapter housings and the four squibs in the EVM support fitting. With the squibs fired, the gases from the ignited cartridge were channeled by the separation nut housing to apply a force of approximately 6670 Newtons (1500 lbf) to the piston, causing it to move forward, compress the spring, and simultaneously remove the restraint to radial motion of the three segments of the nut. The spring forced the separator to expand the three-piece nut, which disengaged from the threads of the adapter stud.

Separation Commanding

Until spacecraft separation had occurred, the squib interface unit functioned only as a switching device, providing firing current to the separation nuts on the spacecraft. The automatic deployment sequencer was not operational until after separation, although power was applied to the sequencer upon activation of the separation enable relays. The spacecraft separation nuts were activated as follows: concurrent Titan/spacecraft separation enable and separation fire commands were generated by the Titan guidance computer (Figure 6-2). The enable command from Titan to the squib interface unit (SIU) activated redundant relays K27 and K28. These relays provided ground returns that activated the coils of enable relays K2 and K14. The closure of these enable relays applied battery power to the separation fire relay (K1 and K13) coils and contacts. Upon receipt of the separation fire command from Titan, relays K25 and K26 were activated. This provided ground returns for the fire relay coils K1 and K13, and activated them. Once activated, separation squib firing current for the four spacecraft squibs was provided by the spacecraft batteries. This interlocking of enable and fire relay coil grounds through relays controlled by Titan was a reliability feature to prevent inadvertent separation of the spacecraft.

The interlocking feature resulted in a spacecraft separation fire-delay time relative to the Titan side-fire signal. When the Titan fire relay closed, power was transferred to the four separation nuts on the Titan side of the separation plane. At the same time (no delay), power was transferred to the fire ground interlocking relays K25 and K26, which in turn activated fire relays K1 and K13. The delay between the Titan-side and spacecraft-side separation nut release was a function of relay transfer time and the simultaneity of separation nut activations.

The relays in the SIU activated by Titan were Babcock BR-26 and had a specified maximum actuation time of 4.0 milliseconds (ms) at 26 volts, direct current (Vdc). The SIU fire relays were Babcock BR-15 and had a specified maximum actuate time of 7.5 ms at 26 Vdc. The simultaneity specification of the separation nuts was 5 ms; thus, at a nominal 26 Vdc, the maximum delay time would be $4 + 7.5 + 5 = 16.5$ ms. Actual separation fire delay measurements with a Titan transtage resulted in a 10- to 12-ms delay time.

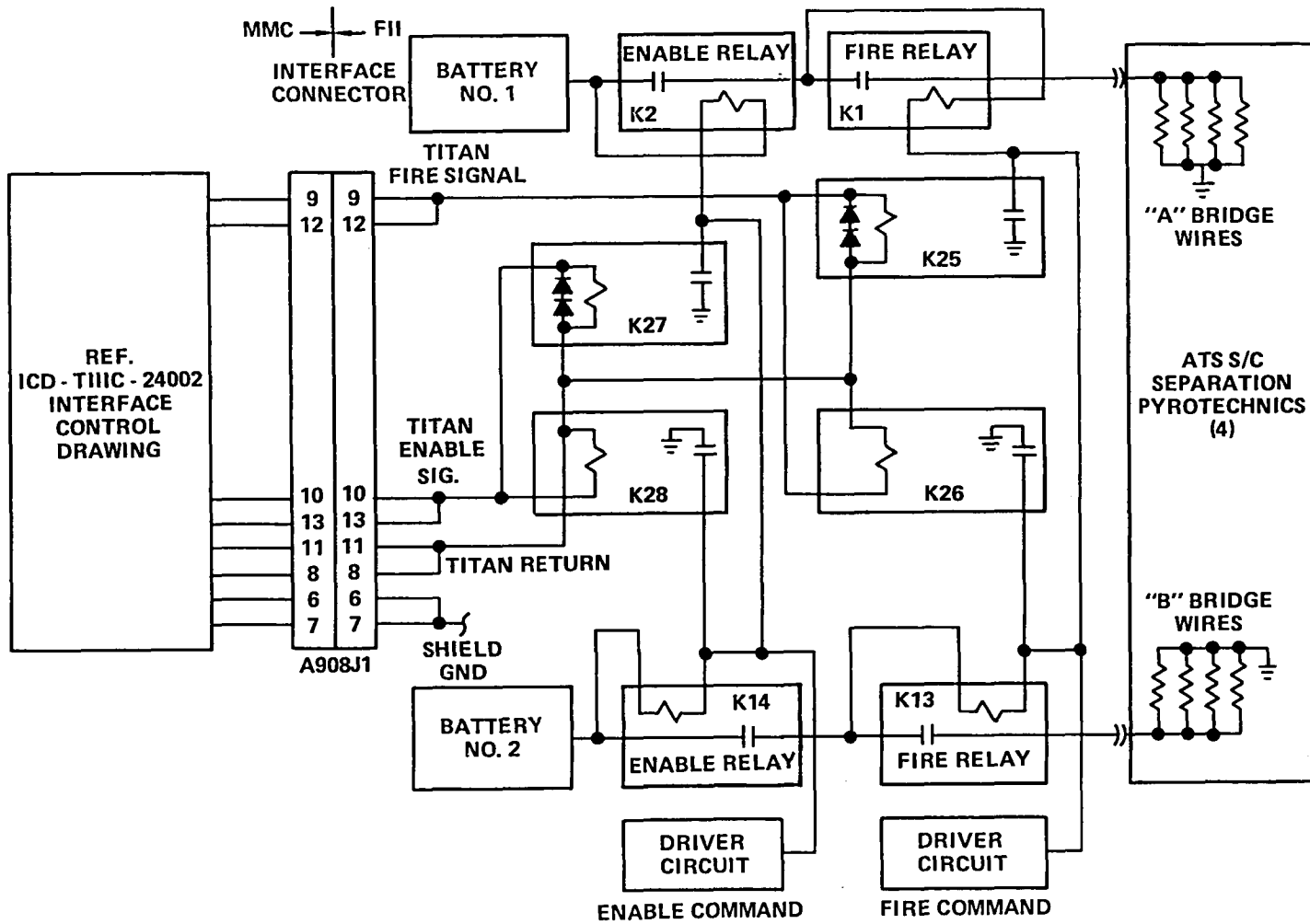


Figure 6-2. Spacecraft/Titan III-C Arm/Fire Separation Interface

Separation Monitoring

Separation was monitored with two redundant switch assemblies, as shown in Detail A, Figure 6-3. One of the devices was located on the northeast corner, and the other on the southwest corner of the EVM.

The separation switch assemblies had their actuator arms depressed prior to separation. The actuator was released at separation. Two microswitches verified separation by telemetry while the remaining switches redundantly initiated operation of the automatic deployment sequencer.

SPACECRAFT DEPLOYMENT

Following separation from the Titan transtage in geosynchronous orbit with ATS-6 in the stowed configuration, deployment of the spacecraft was initiated. The parabolic reflector, the solar array, and booms had to be deployed prior to the initiation of the spacecraft Earth acquisition mode. Four sequential functions deployed the spacecraft. In order of occurrence they were as follows: (1) solar array booms launch-lock release, first-stage deployment (boom 120-degree rotation up about hub hinge), and first-stage lockup; (2) solar array paddle release, deployment and lockup; (3) parabolic reflector deployment; and (4) boom drop, fourth-stage deployment (boom 30-degree rotation down about hub hinge), and fourth-stage lockup. (See Figure 6-4.)

Following pyrotechnically-actuated releases, the first, second, and fourth deployment motions were effected by redundant spring and constant-rate damper mechanisms at each of the indicated hinges. The deployment of the reflector was accomplished by virtue of the spring energy resident in the coiled reflector ribs, after their restraining doors were spring-opened following pyrotechnic cutting of the cable holding them shut.

Positive lockup mechanisms were provided for the booms and arrays to preclude any free play in their hinges after deployment that could cause deleterious relative motion effects on the attitude control performance of the attitude control subsystem.

The automatic deployment of the spacecraft was controlled by an automatic deployment sequencer and a squib interface unit located in the electrical power subsystem.

Backup ground control capability for manual deployment of the spacecraft was provided in the event of failure of the sequencer. If other contingencies should arise, the sequencer could also be commanded off and deployment controlled by ground command.

The squib interface unit and automatic deployment sequencer were essentially command generator and switching devices that provided enable (arm) and fire commands in the proper sequence to activate enable and fire relays. These relays provided the firing current path from the batteries to the pyrotechnic devices used to initiate each deployment motion.

The sequencer provided a resettable, six-minute timer command generator that was initiated by actuation of the various event-enable microswitches for the four deployment motions. Correct squib

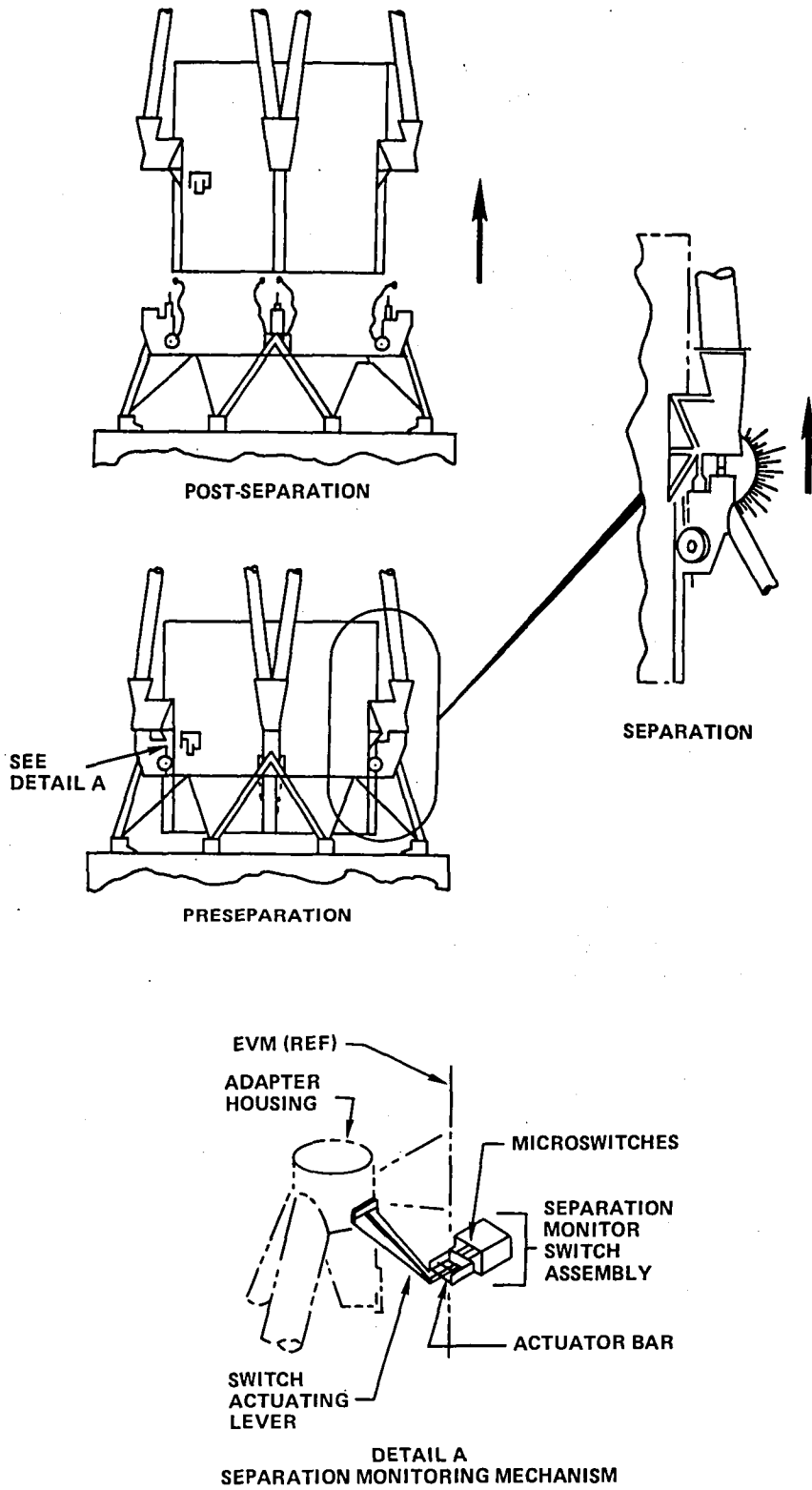


Figure 6-3. Separation Sequence Diagram

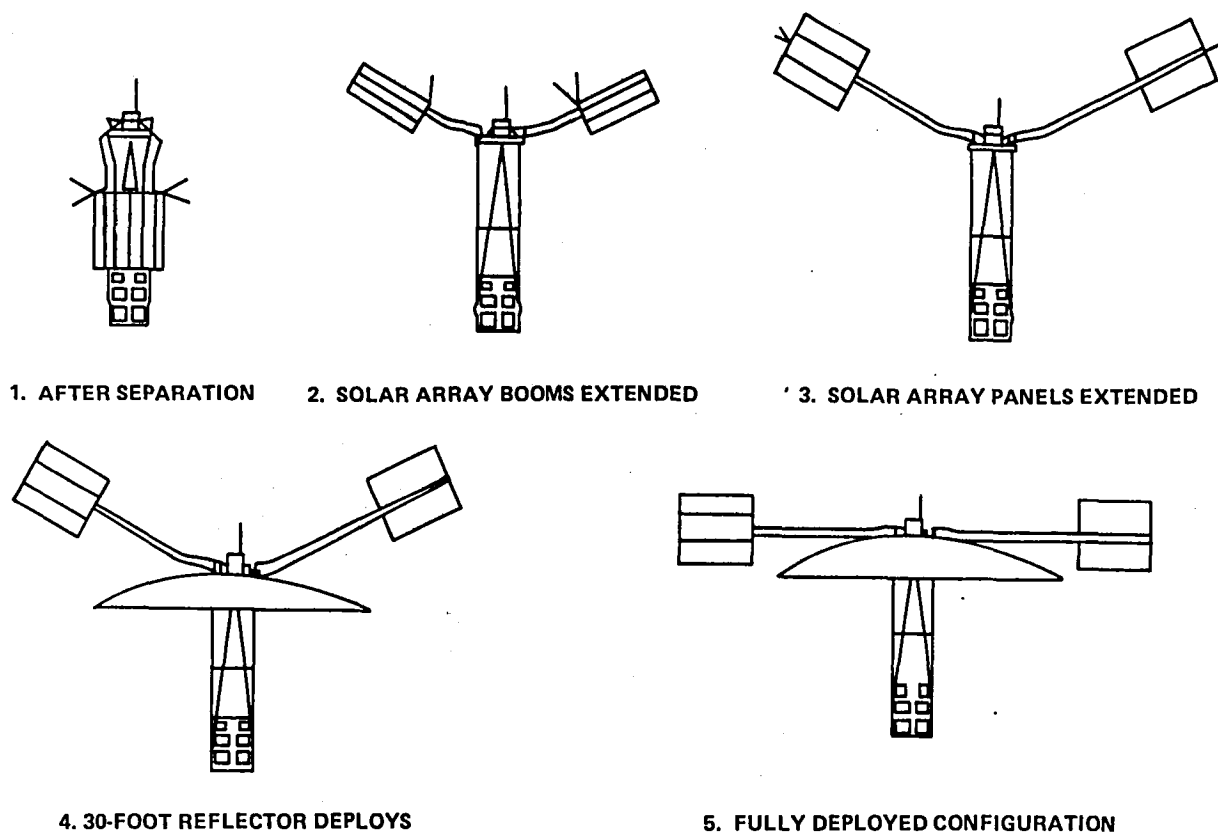


Figure 6-4. Deployment Sequence

firing order was ensured in the automatic sequence mode by performing an “and” function between the sequencer “fire” signal and all previous event-enable commands and event-completion micro-switch signals. All timer fire commands were “or” functions combined with ground control commands to maintain a backup capability.

By means of the design approach selected for the indicated mechanisms and controls, a high level of confidence was established that the critical spacecraft separation and deployment functions would be properly effected with or without ground command control capability.

Solar Array First-Motion Release

Prior to launch, the solar arrays and booms were secured by the first-motion launch-lock and release mechanisms. The mechanisms consisted of the two sets of two center-line locks (total of four) and four X-Y-Z restraint assemblies.

The center-line locks held the two semicylindrical solar arrays in a cylinder and opposed the deployment forces of the first-stage deployment mechanism springs. One set of center-line locks was installed at frame A and D on the east side of the spacecraft and the remaining set on the west side at corresponding locations on the same frames. (See Figure 6-5.)

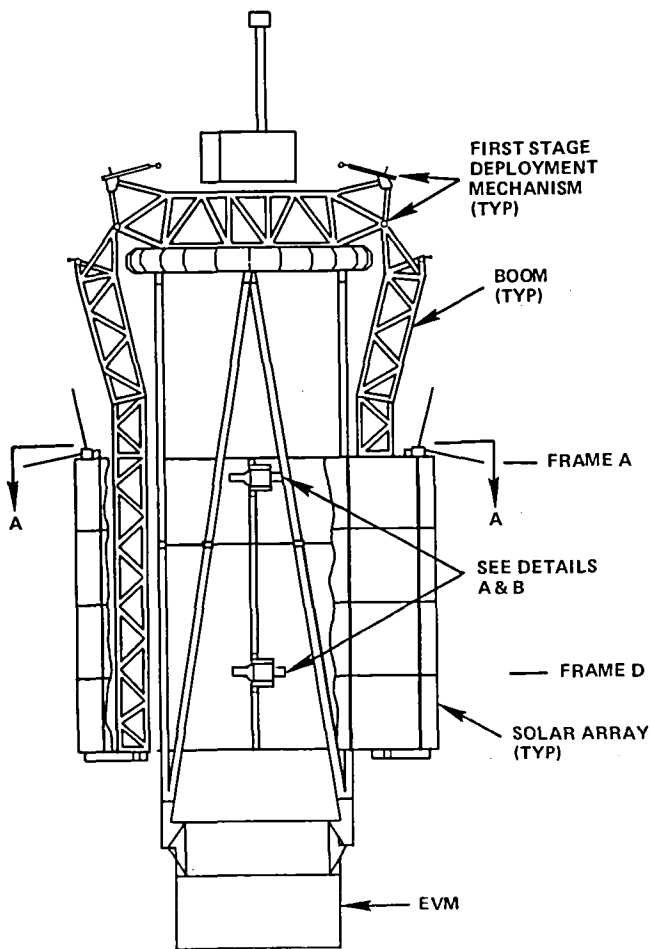


Figure 6-5. Deployment Mechanisms

spring-loaded plunger, and the solar array mounted bracketry with tapered pin. The tapered pin was inserted into the mating receptacle of the corner bracket. The spring-loaded plunger applied pressure to the tapered pin and bracketry to aid disengagement of the pin/socket at the initiation of the deployment of the solar array.

After the separation of the spacecraft was completed, release of the solar array center-line locks initiated the first motion of the deployment sequence of the solar array boom. Power was applied to ignite the cartridges actuating the cable cutters of the center-line locks. The cable cutters were hot-gas actuated guillotine blades that sever the cable by driving a chisel-type plunger through the cable against an anvil. With the cables severed (Detail B, Figure 6-8), the actuating spring forces of the first-stage deployment mechanism caused the booms to pivot about the hub hinges and to swing away from the sides of the EVM. Initial motion was aided by the spring-loaded plungers in the X-Y-Z fitting.

Each center-line lock (Figure 6-6) consisted of nine primary functional components: the main body, socket, cable and retaining hardware, two force washers, two cable cutters, and associated power cartridges. The main body and socket of each center-line lock were aligned, and the cable was routed through the semicylindrical socket and fastened in place by the retaining hardware, securing the solar arrays in the stowed configuration. Two compression force washers, one at each end of each cable assembly, were used to indicate cable tension.

The X-Y-Z restraint assemblies prevented motion of the solar arrays in the vertical ($\pm Z$) axis, in the horizontal ($\pm X$) axis, and parallel to the Y-axis for motion inboard only. The four X-Y-Z restraint assemblies interconnected for four corners of the EVM and the solar arrays, as shown in Detail A of Figure 6-7. Each X-Y-Z restraint had two primary functional elements (Detail C of Figure 6-7): the EVM corner bracket and

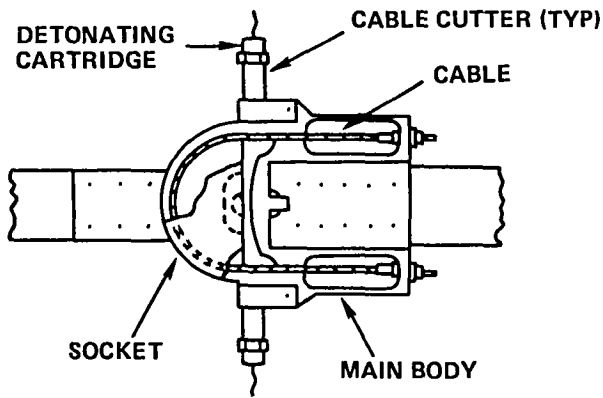


Figure 6-6. Center-Line Lock (Prerelease)

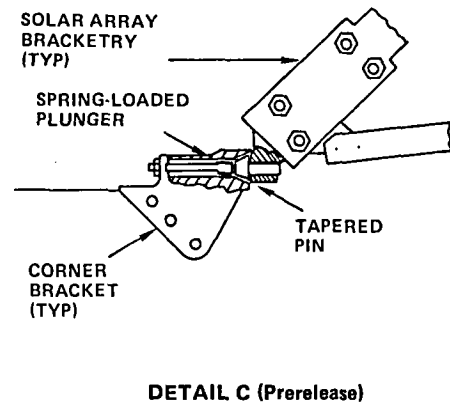
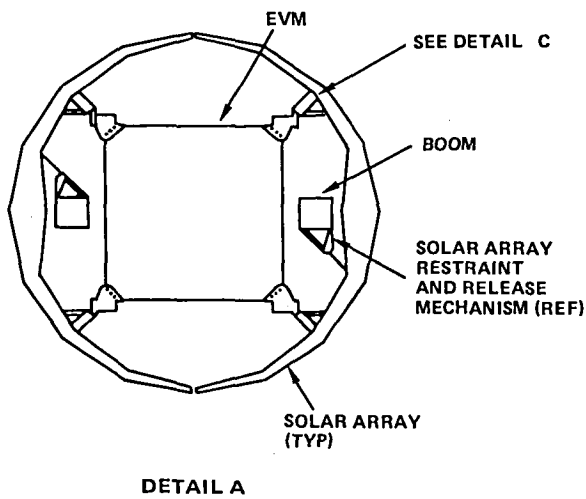


Figure 6-7. Restraint Assemblies

Solar Array First-Stage Deployment

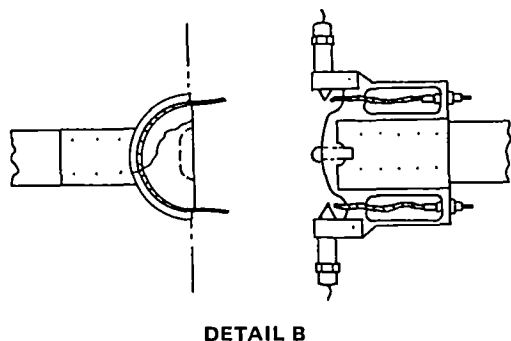


Figure 6-8. Center-Line Lock (Post-Release)

Following first-motion release, first-stage deployment of the spacecraft's booms was accomplished automatically. Each first-stage deployment mechanism was composed of a drive-spring group to furnish motive power, and two damper assemblies (Section A-A, Figure 6-9) to control the rate of deployment.

A drive-spring group consisted of four spring assemblies fastened to a main spool that was free to turn on the hub hinge pin. Each spring assembly (Section B-B, Figure 6-9) was a laminated eight-leaf spring. The main spool was anchored to the hub bridge truss and was prevented from rotating on the hinge pin by a torque arm fastened to the main spool and to the extension bar head (Figure 6-10). The extension bar was firmly attached to the bridge truss. The separate takeup spools of each drive-spring group were also mounted on a common shaft that was part of the boom assembly. Each individual spring, forming an S or reverse-curve configuration, was bolted on one end to the main spool with the opposite end partially wrapped around the takeup spool.

Upon initiation of first-stage deployment, the 56.5 N·m (500 in.-lb) of torque applied to the takeup spools by the springs caused the boom to pivot about the hub hinge. As the boom rotated, the unattached ends of the springs coiled around the takeup spools, as shown in Section B-B of Figure 6-9. This process continued until the boom lockup occurred (1.2-minutes to 4-minutes duration).

During the deployment sequence, the angular velocity of each boom was controlled by the two damper assemblies. Each damper assembly consisted of an adapter assembly and damper with cover, as shown in Section A-A of Figure 6-9. The adapter assembly used a thermal isolating coupling to attach the damper shaft to the hinge pin, and a thermal isolating housing that connected the damper housing to the boom truss. The damper was a temperature compensated, rotary, viscous device that had an essentially constant damping rate over the temperature range of -34°C to 49°C (-30°F to $+120^{\circ}\text{F}$). This type of damper was rate sensitive; i.e., as the angular velocity decreased, so did the restraining torque. The dampers contained a silicone fluid having a viscosity of 2000 centistokes at 25°C .

The damper consisted of a housing, a fixed barrier (dam) that acted with the shaft and vane to divide the housing into two cavities; a vane affixed to the damper shaft, sealed tightly to the damper housing and end plates; and a port, through the damper shaft, that interconnected the two cavities of the damper that were separated by the vane and the dam.

The damper contained a reservoir of fluid, pressurized by a spring-loaded diaphragm, that was ported to the working cavities of the damper through checkvalves. This arrangement forced fluid from the reservoir into the body cavities as the volume of the fluid contracted during decreases in temperature. Excessive buildup of fluid pressure in the damper body cavities due to increases in temperature was relieved through a valve, ported to the reservoir, and located in the damper shaft

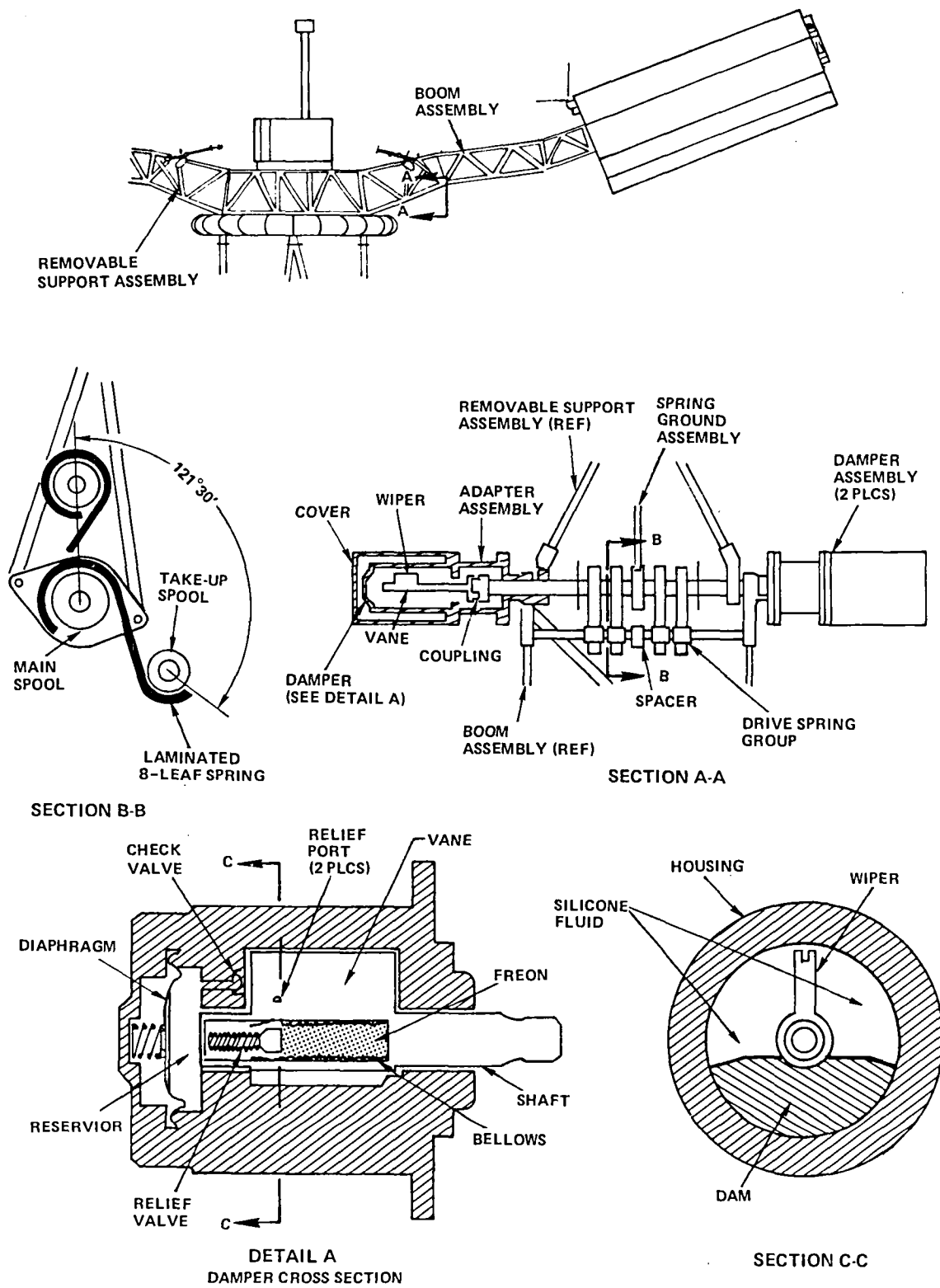


Figure 6-9. First-Stage Deployment Mechanism

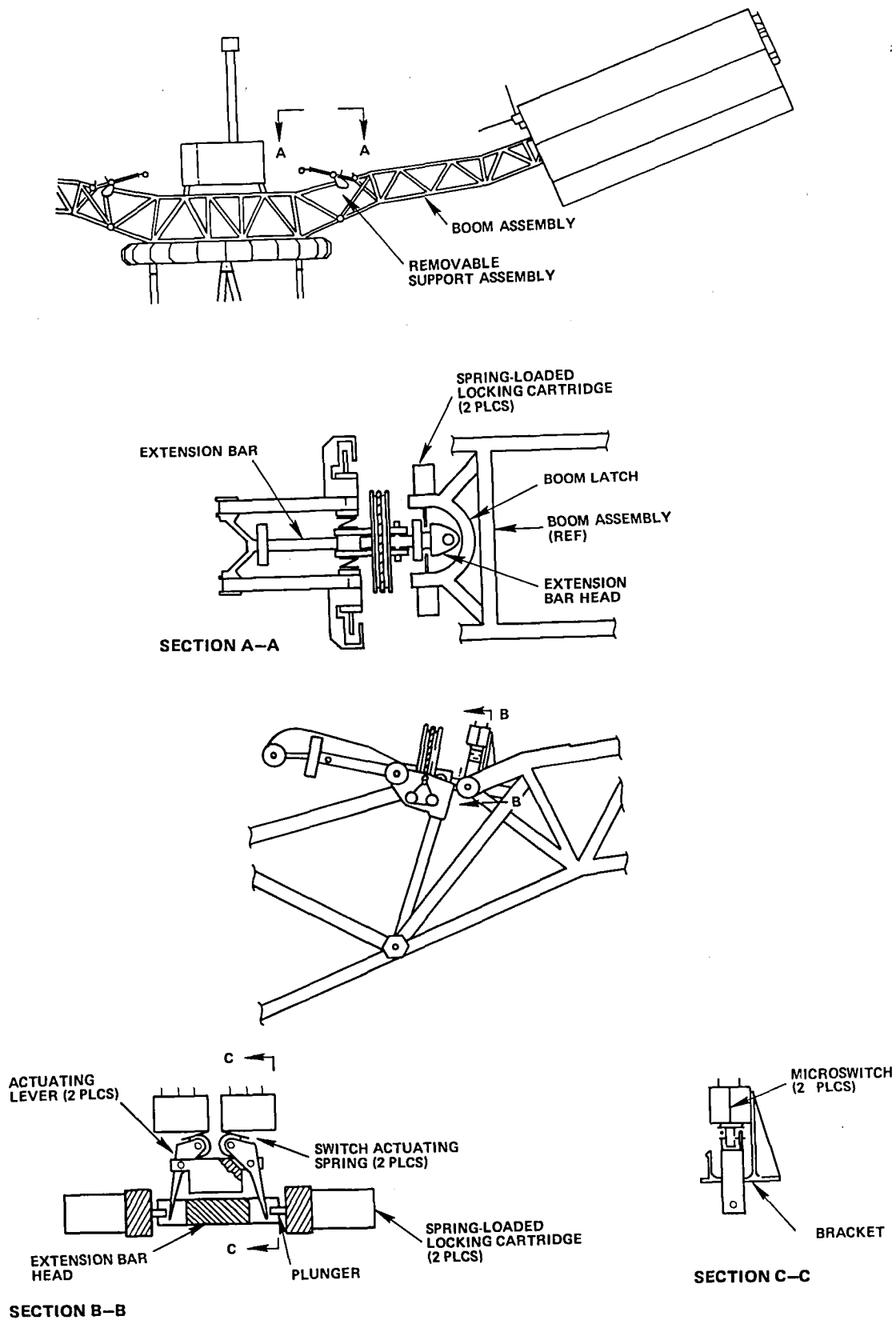


Figure 6-10. First-Stage Lockup Mechanism

that was the downstream (low pressure) side of the working cavity fluid exit port. The damper shaft was hollow and contained a Freon-filled bellows actuator that moved a tapered plug axially in the region of the cavity exit ports. The length of the bellows varied as a function of the volume of the Freon fluid, which expanded and contracted with the increase or decrease of temperature, thereby moving the plug and varying the working area of the chamber exit port. The change in restriction to the flow of the fluid compensated for the change in the viscosity of the fluid due to temperature variations and thus maintained an essentially constant damping characteristic over the design range.

Solar Array First-Stage Lockup

First-stage lockup of the boom occurred upon completion of its 121.5-degree motion. Lockup was accomplished when the spring-loaded locking cartridges, located on the sides of the boom receiver, engaged the extension bar head as shown in Section A-A of Figure 6-10.

As the boom completed the deployment arc, the plunger of each locking cartridge struck the arrow-shaped head of the extension bar. The plungers were depressed into the locking cartridges, compressing the springs within the cartridges as the plungers traveled the length of the gradually increasing width of the extension bar head until they reached the locking recesses on its sides. At this point, the plungers were thrust into the locking recesses by the compressed springs of the locking cartridges, completing the positive lockup process.

Solar Array First-Motion Monitoring

The first motion of deployment was monitored at its inception by the launch-lock release monitor circuits. At completion, first-stage lockup was monitored with switches shown in Section C-C of Figure 6-10.

Solar Array Restraint and Release

Restraint of the solar array booms during first-stage deployment and release of the solar arrays for second-stage deployment was accomplished by identical solar array restraint and release mechanisms located on each boom. These mechanisms were structurally interconnected between frame A of each undeployed solar array and the adjacent boom structure (Section A-A, Figure 6-11).

Each mechanism consisted of a restraint assembly and release apparatus. The restraint assembly was a hollow slotted tube that contained a movable spring-loaded plunger held within the tube by a bar (Section B-B, Figure 6-11). The restraint assembly also had a U-shaped latch surrounding the center, top, and both sides of the slotted tube that pivoted from the end of the tube that connected to the boom. Restraint of the solar arrays was required between the completion of the first-motion release and first-stage boom deployment. Prior to first-motion release, the restraint assembly latch was in its pivoted position and permitted relative motion between the boom and the array frame during launch. This approach prevented the booms and reflector support truss from loading the array except at the EVM interface. The latch rested on the bar that was attached to the plunger. When first-motion release was accomplished, and the booms swung away from the sides of the reflector support truss, the spring of the second-stage deployment mechanism caused the upper ends of the

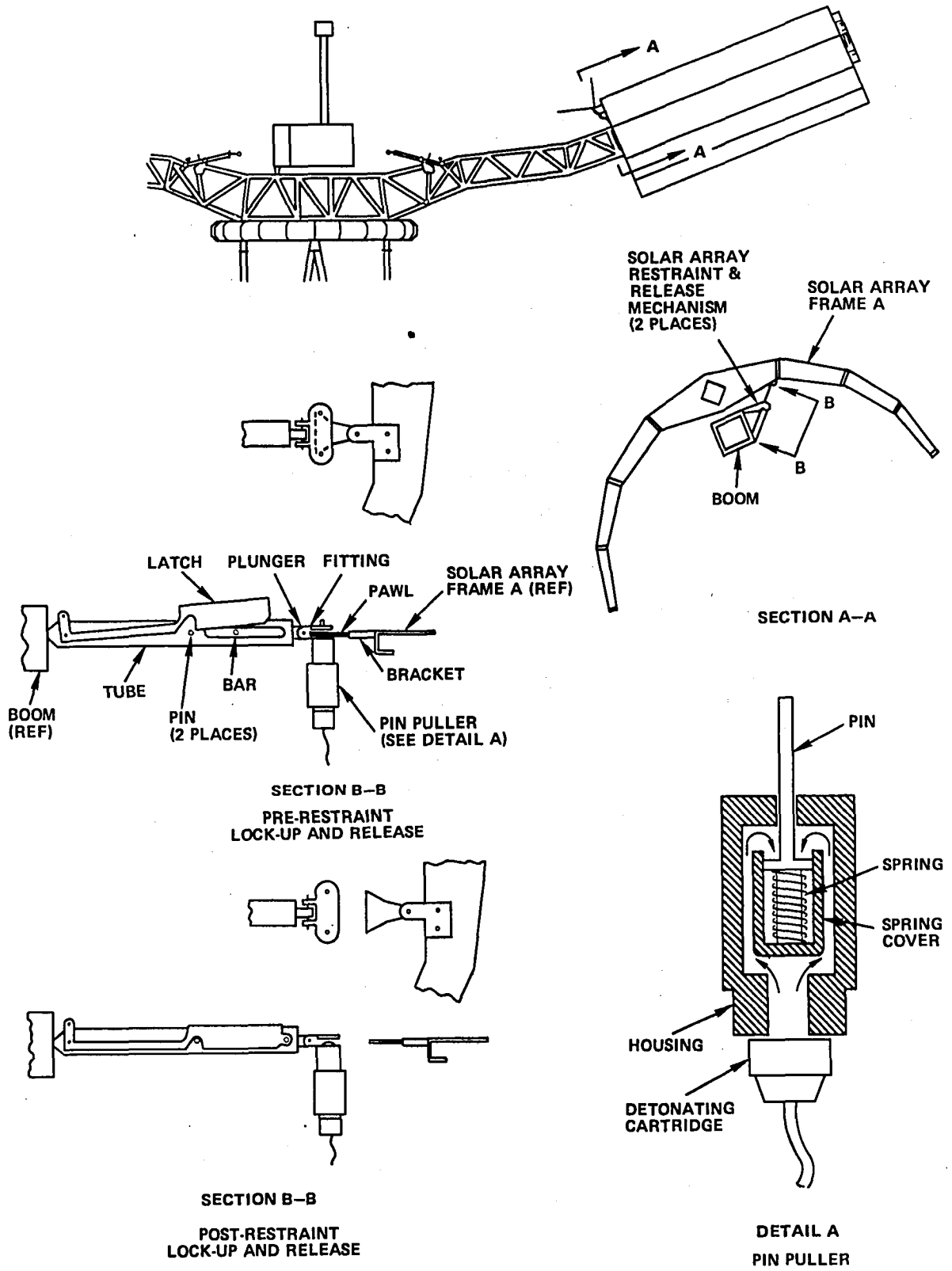


Figure 6-11. Solar Array Restraint and Release Mechanism

solar arrays to swing away from the booms. The outward motion of the booms pulled the restraint assembly plunger forward, using the release apparatus as a linkage. This allowed the latch to be forced downward by the plunger's spring until it struck the pins on the sides of the tube and locked in place. When locked in place, the solar array movement was restricted until the pin pullers of the release apparatus were actuated. The release apparatus consisted of two groups of hardware: (1) a triangular-shaped pawl attached to a bracket by a pin and cotter pins (the bracket was riveted to Frame A of the solar array), and (2) two pin pullers with detonating cartridges mounted on a fitting attached to the end of the restraint assembly plunger by a pin and cotter pins.

In the stowed configuration, the release apparatus was connected to hold each solar array in place. The pawl was inserted into the fitting (Section B-B, Figure 6-11) and both pin pullers of each apparatus were installed. This locked the triangular pawl between the extended pins of the pin pullers, securing the array in place.

When first-stage deployment was completed, the power cartridges on the pin pullers were electrically actuated. Gas from the cartridges (Detail A, Figure 6-11) was routed between the pin-puller housing and spring cover, applying a downward force to the pin. The spring was compressed and the pin was retracted into the housing, releasing the pawl. Actuation of either pin puller accomplished this.

Solar Array Second-Stage Deployment

Deployment of the solar arrays was accomplished after actuation of the solar array release mechanisms. The deployment mechanisms were located at the structural interface between the booms and the solar array panel assemblies. They interconnected between the hinge fitting on the end of each boom (Section A-A, Figure 6-12) and Frame E of each solar array panel assembly.

Each mechanism consisted of a drive-spring group, two damper assemblies and structural elements connected between the boom and array, as shown in Detail A of Figure 6-12.

A drive-spring group consisted of a main spool, three takeup spools and three laminated, seven-leaf, constant torque springs (Section B-B of Figure 6-12). The main spool of the drive-spring group was assembled on the shaft supported by the two hinge journals of the hinge fittings (Detail A, Figure 6-12). The three takeup spools were assembled on a shaft that was a part of the spring bracket. This in turn was connected to the spar hinge fitting, structurally interfacing with Frame E of the solar array. The three springs were connected between the main and takeup spools. Each spring was bolted to the main spool on one end, with the remaining end partially wrapped around a takeup spool held in place by its residual spring tension.

At solar array second-motion release, 33.9 N·m (300 in.-lb) of torque applied by the drive springs caused each solar array to rotate about its hinge. As the solar array rotated, the unattached ends of the springs coiled around the takeup spools. The spring torque forced the array to swing diagonally away from the boom through a 180-degree arc. When the arc was completed, one of the solar energy-absorbing surfaces faced the spacecraft +X axis (nominally east) and the other faced the -X axis. (The north array on the -Y axis faced west when the spacecraft was normally Earth oriented.)

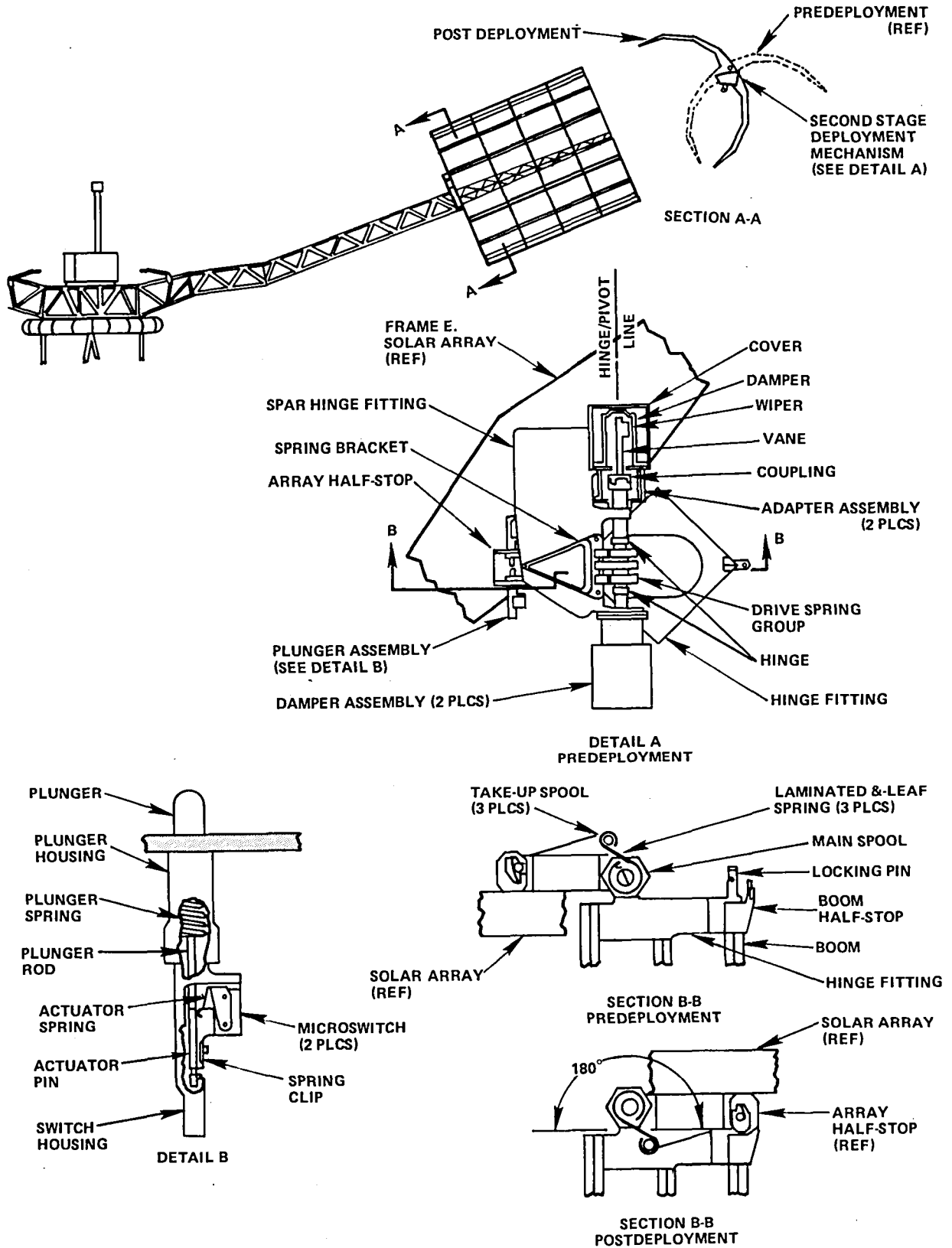


Figure 6-12. Second-Stage Deployment and Lockup Mechanisms

The movement of each solar array panel assembly was maintained at a constant rate by the two damper assemblies. Each damper assembly consisted of an adapter assembly and damper with cover, as shown in Detail A of Figure 6-12. The adapter assembly consisted of a thermal isolating coupling, and a housing that connected to the damper on one side and to the spar hinge fitting on the other. The damper was fundamentally a housing filled with a high viscosity silicone fluid, and a vane with a wiper. It was attached to the stationary shaft of the hinge fitting. The housing of both the damper and adapter were connected to the spar hinge fitting, so that when the solar array motion began, both housings, connected together, rotated through a 180-degree arc.

Solar Array Second-Stage Lockup and Monitoring

When each solar array completed its 180-degree arc, second-stage lockup occurred. Lockup was accomplished by the dual plunger assemblies mounted on the array halfstop. Each plunger assembly consisted of a rod, spring, and plunger contained within a plunger housing (Detail B, Figure 6-12). Integrated with each plunger assembly was a lockup monitoring device consisting of two microswitches, an actuator spring, pin, and spring clip assembled with a switch housing.

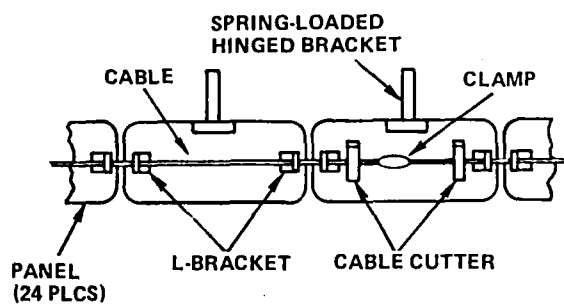
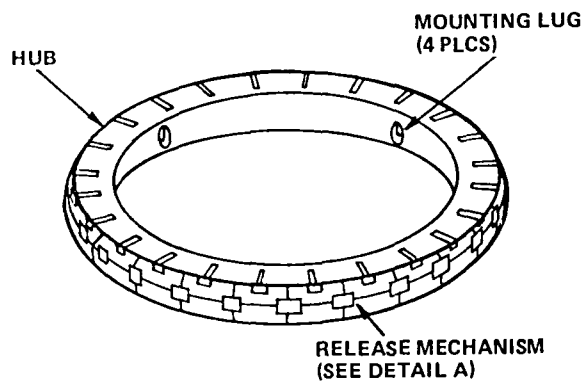
As the solar arrays completed the 180-degree arc, the plungers struck the chisel-pointed locking pin, compressing its plunger spring and forcing the plunger rod outward. The plunger rod struck the actuator pin and caused the spring clip to release the pin, driving the end of the actuator pin from under the actuator spring and replacing it with the plunger rod without operating the actuator spring. As the 180-degree arc was completed, the plunger traveled down the sides of the locking pin until it reached the hole on the sides of the locking pin. At this point, compressed springs forced the plungers into the holes, locking the solar array in the deployed configuration. When this occurred, each plunger spring extracted its plunger rod. This allowed the actuator spring to expand, releasing the pushbutton of both microswitches. This produced redundant open-circuit lockup monitor switch configurations.

Parabolic Reflector Deployment

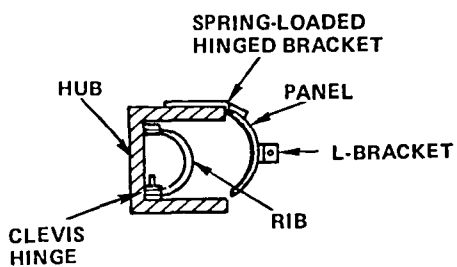
With the solar arrays locked into position, the deployment of the parabolic reflector was initiated. Third-stage deployment (pyrotechnic release and automatic parabolic reflector deployment) was initiated by a release mechanism. This mechanism consisted of 24 panels with spring-loaded hinged brackets, a single cable, a cable clamp, and two cable cutters.

In the stowed configuration, the 24 panels of the release mechanism, surrounding the outer periphery of the hub, held the reflector ribs and mesh in the recess of the hub. The panels were held closed by a single cable encircling them. The cable was routed through aluminum tubes on 23 of the panels and through both cable cutters on the 24th panel, with the cable ends terminated in an adjustable cable clamp (Figure 6-13).

When power was applied to the cable cutter's detonating cartridges, gases drove chisel-type plungers through the cable. With the cable cut, the 24 panels were raised by their spring-loaded hinged brackets. The natural resilience of the 48 attached ribs caused them to unwind circumferentially around the hub, carrying the interconnecting mesh of the reflector with them. As the ribs attained a deployed position in which they were essentially straight, the ribs, through the clevis hinges, were also



DETAIL A



STOWED CONFIGURATION

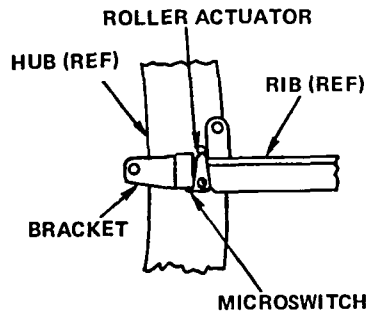


Figure 6-13. Parabolic Reflector Assembly: Release and Deployment Mechanism

in a position tangential to the reflector hub. The ribs continued to deploy, rotating the clevis hinge 90 degrees and thereby, at full deployment, attained a radial configuration from the hub centerline and formed a 9.14-meter (30-foot) diameter parabolic reflector.

Parabolic Reflector Deployment Monitoring

Switch mechanisms monitored deployment of the 44th and 46th ribs. Each mechanism consisted of a microswitch with a flexible roller type actuator attached to a bracket mounted to the parabolic reflectors' hub.

When the 44th and 46th ribs were deployed, the end of each rib attached to the clevis hinge struck the roller actuator of the switch mechanism and depressed its pushbutton.

Solar Array Fourth-Stage Release

During deployment of the parabolic reflector, the solar array booms were located at an angle 31.5 degrees above the horizontal. This position was selected to provide extra clearance for the whipping action of the reflector's ribs during deployment. The booms were then repositioned to the horizontal after the reflector was deployed.

Each boom was retained by a latching mechanism that included a release assembly. The latching mechanism (Section A-A, Figure 6-14) consisted of a pivot-mounted, claw-type latch loaded by two torsion springs. The release assembly (Section B-B, Figure 6-14) consisted of two pin pullers with detonating cartridges mounted side by side on a bracket, a cable with a triangular pawl at one end and a cable restraint at the other, and a cable guide mounted on the top of the latch.

Prior to launch the extension bar was locked into position (Section A-A, Figure 6-14) by the latching mechanism and release assembly. The pawl of the release assembly was inserted into a slot in the bracket, and both pin pullers were installed. This locked the pawl between the extended pins of the pin pullers. When the pawl was inserted into the bracket, the cable of the release assembly was drawn taut. The taut cable pulled the cable guide downward, which forced the latch downward in opposition to the torsion springs until it hooked over the lugs on both sides of the extension bar, locking it in place.

When the detonating cartridges on the pin pullers were actuated, the gases from each pin puller were routed between the pin puller's housing and spring cover, applying a downward force to the pin. The springs of each pin puller were compressed and the pin was retracted into the pin-puller housing, releasing the triangular pawl. With the pawl release, the torsion springs caused the latch to pivot upwards, releasing the lugs on the sides of the extension bar and initiating final deployment of the boom.

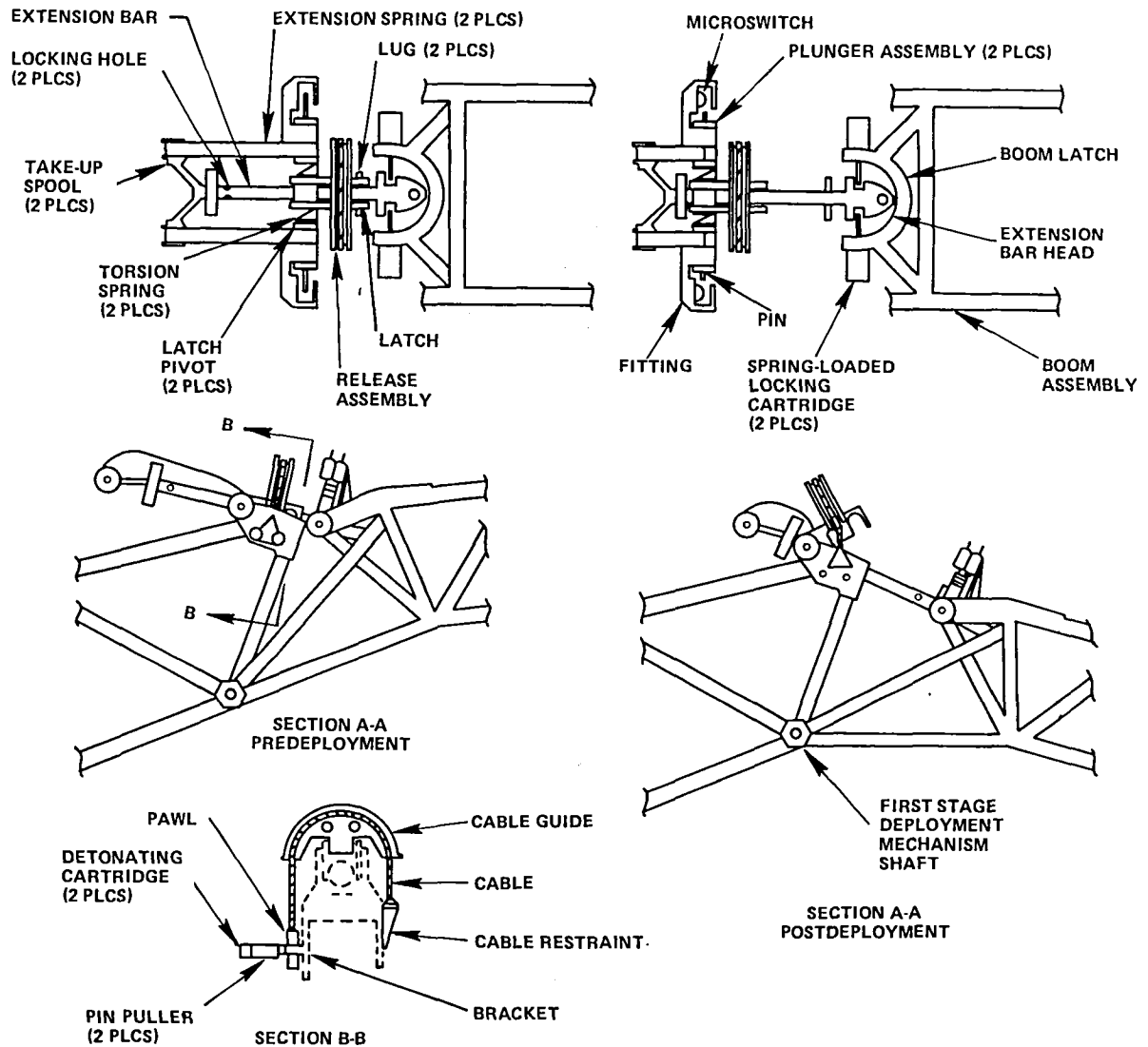


Figure 6-14. Fourth-Stage Release and Deployment Mechanisms

Solar Array Fourth-Stage Deployment and Monitoring

Deployment was accomplished by two drive-spring groups, two plunger assemblies, and the extension bar. The drive-spring group consisted of two takeup spools, two multileaf laminated extension springs, and two attachment pins that were colinear with the latch pivot centerline. The plunger assemblies each consisted of a spring-loaded plunger encapsulated within a housing and fitting containing a microswitch, all also colinear with the latch pivot centerline.

When release was completed, a constant force of 111 Newtons (25 pounds) applied by each extension spring forced the extension bar in the direction of the arrow head. Each boom was pivoted downward about its main hinge. The extension bar head rotated on the plungers of the two locking cartridges on the sides of the head. The extension bar slid through a journal that was normal to, and pivoted about, the latch pivot centerline. When the holes in the extension bar body were aligned with the plunger assemblies that were colinear to the latch pivots, the spring-loaded plungers engaged the holes on the sides of the extension bar. The extension bar was then locked in the post-deployment configuration, as shown in Section A-A of Figure 6-14. As each plunger seated into the extension bar body, the pin attached to the plunger was retracted from the opening of the fitting attached to the plunger assembly. When this pin was retracted, the microswitch actuator in the fitting was released.

SQUIB INTERFACE UNIT AND AUTOMATIC DEPLOYMENT SEQUENCER

General Description

The deployment of the spacecraft was initiated after separation from the Titan transtage in geosynchronous orbit. Enable and fire signals from the Titan initiated firing of the pyrotechnic separation nuts on both the transtage and spacecraft sides of the separation adapter. After separation, the squib interface unit/automatic deployment sequencer (SIU/ADS), located in the service module of the EVM, automatically deployed the spacecraft. Backup ground control capability for manual deployment was provided in the event of failure of the ADS or other contingencies. Thus, the SIU/ADS was essentially a command generator and switching device that provided enable and fire commands in the proper sequence to activate enable and fire relays. These relays provided the firing current path from the batteries to the pyrotechnic devices that initiated the various deployment motions.

The ADS was included as a safety feature to guard against a possible spacecraft orientation that might block ground command signals to the spacecraft omnidirectional antennas. These antennas were located at the outboard center of each solar array panel. In the launch configuration, and for all spacecraft normal configurations except that following first-motion lockup, the antennas provided essentially omnidirectional receive capability. But for the configuration attained at deployment first-motion lockup, both omnidirectional antennas were shielded from line of sight to the Earth by a set of spacecraft orientations generally defined by the spacecraft centerline lying with a 31-degree half-angle cone whose centerline pointed toward Earth (with the EVM facing the Earth). This situation was possible due to the location of the omnidirectional antennas, coupled with location of the solar array panels and the solar array booms being then positioned approximately

31 degrees above the horizontal (normal to the spacecraft centerline). In this position, the antennas were shielded from the sight of the Earth by the solar arrays. This unique orientation would not normally be attained but could happen if, for some reason, spacecraft deployment was delayed and the spacecraft rotated relative to its separation attitude.

The separation/deployment events occurred in sequence and are summarized as follows:

- Separation—The spacecraft was separated from the Titan transtage adapter. Eight separation nuts were provided: four on the Titan side and four on the spacecraft side of the separation adapter. Enable and fire relay activation signals were provided by the Titan for both Titan and spacecraft switching circuits. Firing current was provided by the Titan batteries for Titan side squibs; spacecraft batteries provided firing current for the spacecraft side squibs. Separation squib redundancy was thus provided at each of the four corners on the separation adapter.
- Solar Array/Booms Release—The two solar array panels and support booms were released from their stowed configuration. After the solar array constraints were released, the solar array support booms deployed about the knee joints at the structural hub truss. Eight cable cutters (four primary and four secondary) severed the restraining cables and effected launch-lock release.
- Solar Array Deployment—Following lockup of the knee joints, the solar arrays rotated about their skewed hinges, assuming positions above and outboard of the parabolic reflector deployment envelope. Four cable cutters (two per solar array panel) severed restraining cables to effect the release of the array.
- Reflector Release—After solar array deployment was complete, the reflector restraint was severed by two cable cutters to allow the deployment of the parabolic reflector.
- Boom Second Motion—The knee joints were released, allowing the solar array booms to rotate downward 31.5 degrees and lock in their final position. Four cable cutters (two for each solar array boom) allowed this motion.

SIU/ADS Functional Description

The ADS provided a resettable 6-minute timer command generator that was sequentially initiated by actuation of the various event enable microswitches for the four deployment motions. Correct squib firing order was ensured in the automatic sequence mode by performing an “and” function between the sequencer “fire” signal and all previous event enable commands. All timer enable and fire commands were “or” functioned with ground control commands to maintain a backup manual deployment capability.

Ground commands could be used to stop automatic deployment once it was initiated. In addition, a timer reset capability could be used to reset the deployment sequence if it was desired to reactivate the automatic sequence.

A more detailed explanation of how the SIU/ADS accomplished the spacecraft separation and deployment functions may be obtained by referring to Figure 6-15, which is a simplified schematic of the SIU, ADS, and external connections.

ADS Operational Logic

Figure 6-16 contains a simplified schematic of the ADS and its interface with the event-enable microswitches, enable relays, and fire relays for the first deployment motion (initiated by launch-lock release). This interface was typical of those for all four deployment motions, the only difference being in the electrical arrangement of the event enable-microswitches. Depending upon the deployment motion involved, the microswitches were connected in one of the following configurations: (1) quad-H, (2) series-parallel, or (3) series.

After separation, the separation microswitches changed state from their launch configuration and provided an enabling signal (battery voltage) to reset the counter and to restart its 6-minute timing sequence. At the end of the 6-minute interval, the counter transmitted an enable and fire command in accordance with the timing sequence shown on the simplified ADS block diagram (Figure 6-17). These signals were logically "ANDED" in separate gates with the separation microswitch event-enable signal. Thus, the ADS provided the equivalent of a CDD-generated XY enable and fire command that was applied to the enable and fire relay switch matrices. The enable signal was generated 2 seconds prior to the fire signal. Activation of the enable relay transferred battery power to the fire relay switch matrix, and to the next set of event enable microswitches. Activation of the fire relay completed the firing current path from the spacecraft batteries to the launch-lock release pyrotechnic devices, thus initiating the first-deployment motion. At the completion of this motion, another set of event-enable microswitches changed state from its stowed configuration and another ADS cycle was initiated for the skewed hinge, or second deployment motion. The outputs of the second ADS cycle were logically "ANDED" with the first motion and second motion event-enable microswitches. This interlocked the start of the spacecraft second-deployment motion with the completion of the previous deployment motion, preventing out-of-sequence deployment. The remaining spacecraft automatic deployments were accomplished in a similar manner as indicated in the simplified diagram of Figure 6-18.

In the event of ADS failure, deployment could be ground commanded.

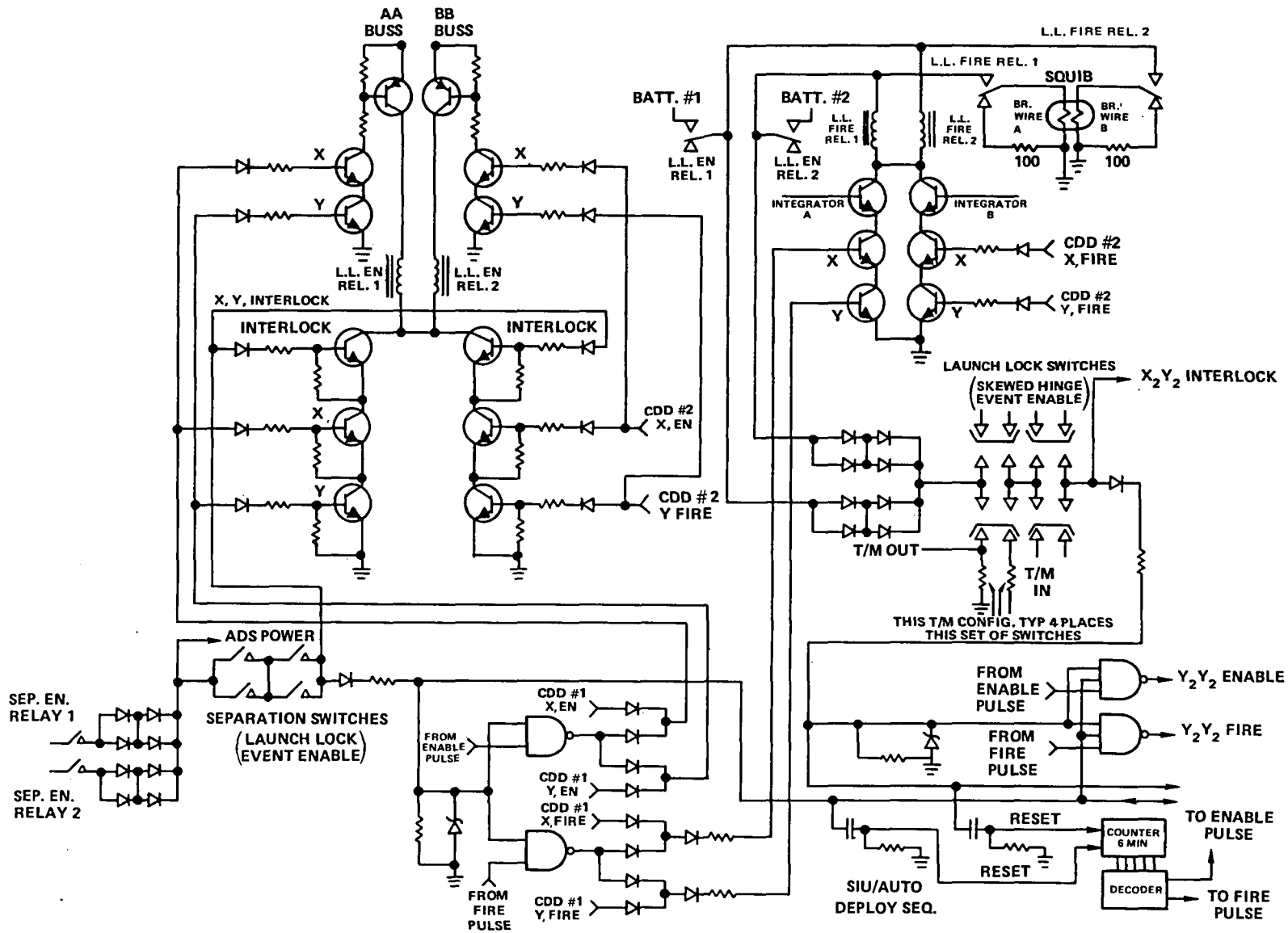


Figure 6-15. Simplified Schematic of the SIU, ADS, and External Connections

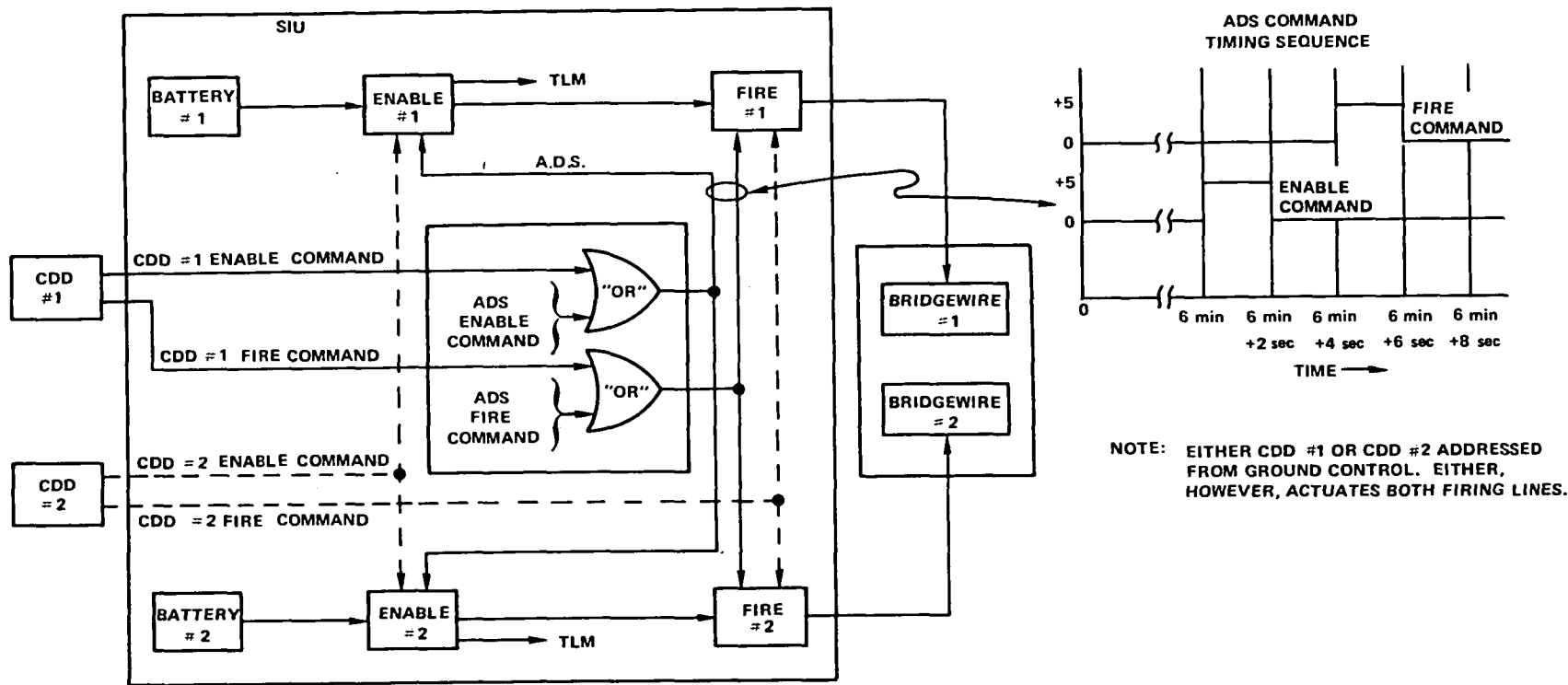


Figure 6-16. Command Decoder-Distributor/SIU/ADS Interface Functional Diagram

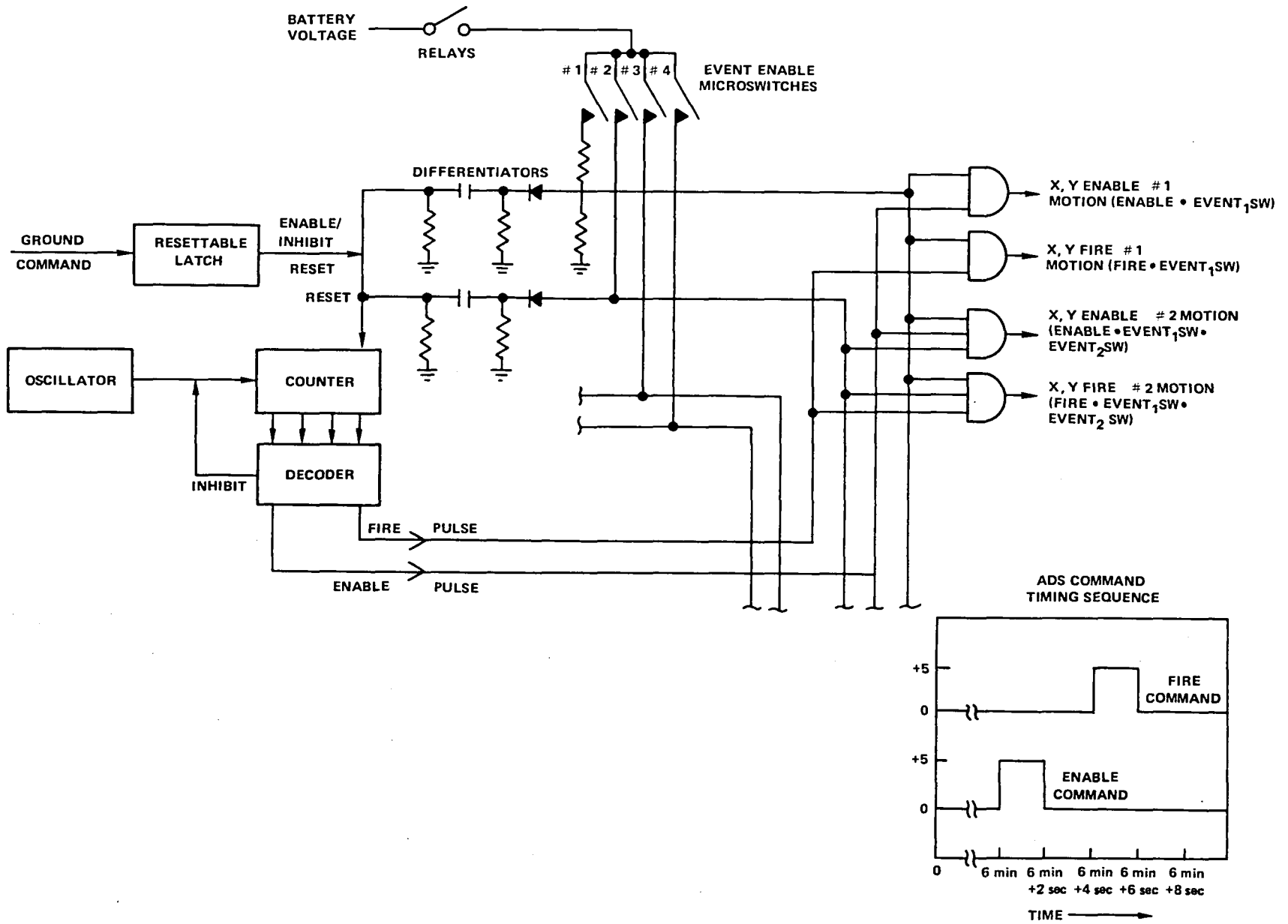


Figure 6-17. Automatic Deployment Sequencer, Logic Block Diagram

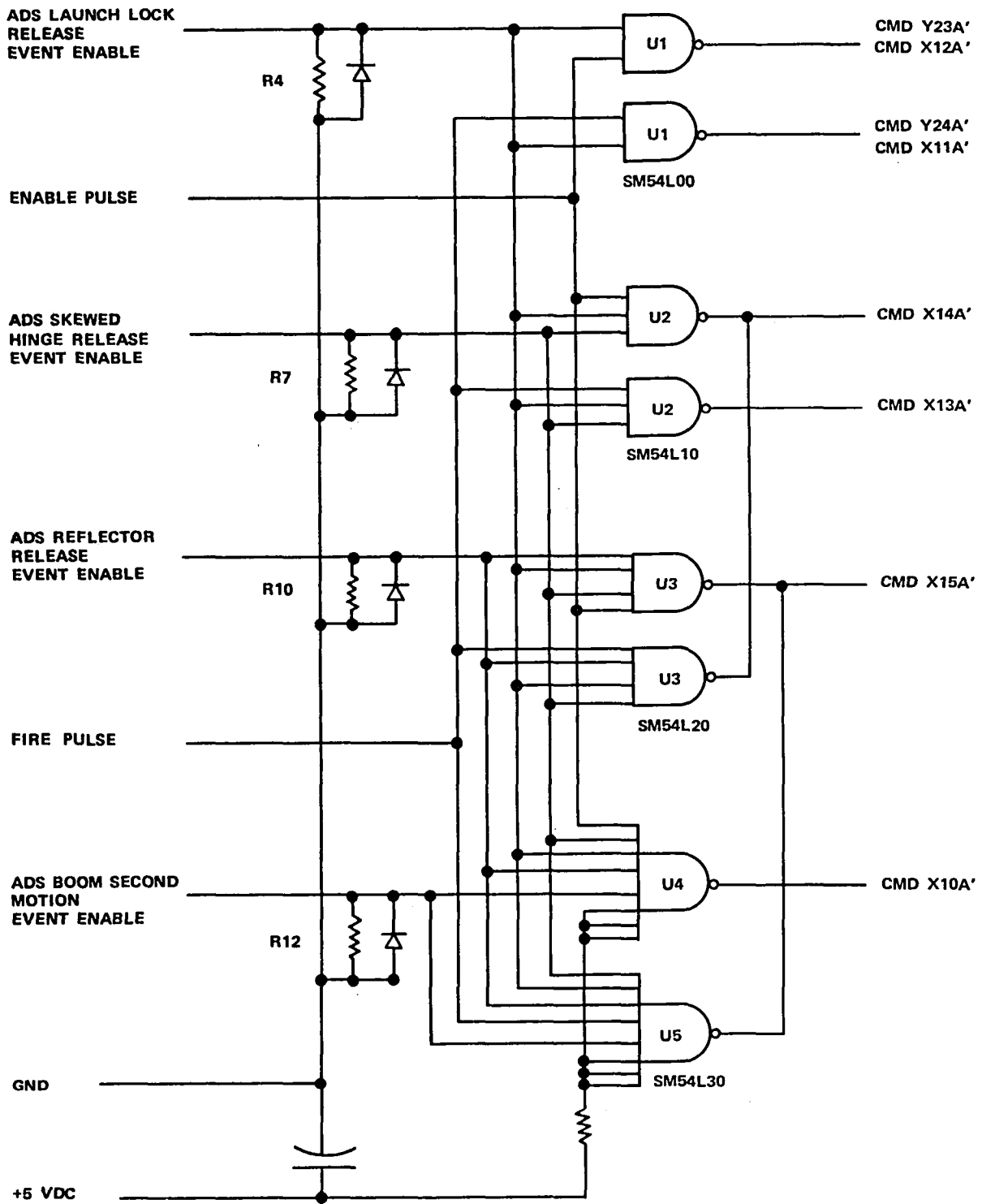


Figure 6-18. ADS Input Configuration

CHAPTER 7

DESIGN AND PERFORMANCE EVALUATION

INTRODUCTION

The spacecraft mechanical subsystem designs were subjected to a series of tests at the major assembly and system levels to validate the designs and to ensure that the flight vehicle would perform satisfactorily. After launch, the performance and operation of the mechanical subsystems in orbit were evaluated.

SPACECRAFT ENVIRONMENTAL TESTING REQUIREMENTS

Objectives

The objectives of the environmental test program for spacecraft level testing were:

1. *Engineering and Development Testing*

a. *Structural Model*—To demonstrate the integrity of the spacecraft structural and mechanical design and to provide data for establishing component/subsystem environmental test levels

b. *Thermal Model*—To develop and verify spacecraft temperature control techniques and to establish environmental test levels for components/subsystems.

2. *Qualification Testing*

To demonstrate the ability of prototype models to fulfill their performance requirements when subjected to environmental stresses more stringent than those expected during prelaunch, launch, and orbital flight.

3. *Flight Acceptance Testing*

To demonstrate the ability of flight hardware to fulfill performance requirements when subject to environmental stresses equal to those expected during prelaunch, launch, and orbital flight.

Implementation

The objectives of the preceding items 1a and 1b, and item 2 for the structure, thermal, and propulsion subsystems, were met by the testing of a combined thermal/structural model (TSM) spacecraft.

The TSM spacecraft was subjected to the following environmental tests, demonstrations, and measurements:

1. *Thermal/Structural Model Spacecraft (Prototype Propulsion Subsystem Installed)*

- a. Thermal balance test*
- b. Deployment testing
 - (1) Simulated zero-g testing of the solar array booms
 - (2) Deployment test of the 9.14-meter reflector in vacuum
 - (3) Release and first-motion test of the solar arrays
- c. Spacecraft assembly and alignment verification
- d. Launch vehicle compatibility tests at the prime contractor location and the Eastern Test Range
- e. Weight, center-of-gravity, and moment-of-inertia determinations
- f. Spacecraft/launch vehicle simulated zero-g separation test
- g. Static load test
- h. Launch configuration modal vibration survey
- i. Acoustic test (launch configuration and EVM only**)
- j. Launch configuration qualification vibration test
- k. Pyrotechnic/deployment/separation shock tests
- l. Leak tests
- m. Acceleration/pressure profile test*

2. *Protoflight Model Spacecraft*

Items 2 and 3 of the objectives of the test program were met by a combination of qualification and acceptance tests of a single protoflight model spacecraft. The protoflight spacecraft was subjected to the following environment tests, demonstrations, and measurements:

- a. Thermal balance tests**
- b. Thermal-vacuum performance test (thermal cycling)**

*These tests were performed only on the EVM of the TSM.

**These tests were conducted only on the Earth-viewing module. Items in other parts of the spacecraft were electrically connected for testing as appropriate.

- c. Deployment testing
 - (1) Simulated zero-g testing of solar array booms
 - (2) Deployment test of 9.14-meter reflector
 - (3) Release and first-motion test of solar arrays
- d. Spacecraft assembly and alignment verification
- e. Launch configuration electromagnetic compatibility test
- f. Deployed configuration electromagnetic compatibility test
- g. Mass property determination
- h. Launch configuration sinusoidal vibration test
- i. Launch configuration acoustic vibration test
- j. Pyrotechnic/deployment/separation shock tests
- k. Magnetic dc stray field surveys
- l. Leak tests
- m. Ground station and simulated ground station compatibility testing
- n. Prelaunch testing at the Eastern Test Range

Note: For protoflight spacecraft testing, the spacecraft was subjected to qualification level test exposures applied according to acceptance test durations. In addition, thermal performance was demonstrated at levels 10°C above and below expected temperature extremes.

SPECIAL TESTS

The ATS-6 design featured several unique mechanisms that were subjected to validation tests to demonstrate feasibility and capability to meet design requirements.

Spacecraft Separation

The spacecraft was cradled within the spacecraft adapter (Figure 5-2, Chapter 5) for launch. Release of the four restraint studs, one at each corner of a 142-cm (56-in.) square interface, permitted spring energy at each corner to initiate separation between the spacecraft and the launch vehicle.

Successful operation required the spacecraft to move in a manner that maintained the spacecraft centerline colinear with the adapter centerline during approximately 76 cm (30 in.) of travel while extracting the EVM lower module (experiments module) out of the adapter.

Guide rails and rollers along each edge of the EVM that parallel the EVM centerline maintained the required orientation. Design validation tests were configured to show that such variables as time of release for the explosive nut of the retention system, friction along each guide rail, center-of-gravity offset of transtage and spacecraft would be accommodated while attaining specified separation velocity with acceptable tip-off rates.

Adapter Release Test

The spacecraft retention/release system was validated by subjecting the TSM spacecraft in the launch configuration (with the adapter) to qualification level static loads and sinusoidal vibration loads. This test demonstrated the structural design capability. Following the vibration tests, the spacecraft/adapter was suspended above a cushion; the separation nuts were pyrotechnically actuated, and the adapter permitted to eject from the spacecraft. The test demonstrated the successful operation of the retention nut release system electrical design and the mechanical design after being subjected to launch qualification level loads.

Separation Test

The TSM was used as a vehicle to validate that the spacecraft/adapter separation system design would meet the separation velocity and tip-off rate criteria. A mass model of the Titan transtage, having mass properties similar to those expected at spacecraft separation, was mated to the spacecraft adapter. This assembly was supported with the centerline horizontal by a very low weight fixture that used air bearing pads to float on a smooth, level floor. A similar fixture provided support for the TSM. Figure 7-1 shows the TSM spacecraft mounted in the separation support cradle that is supported on an air bearing and aligned with the adapter/transtage mass simulator, similarly supported, prior to mating for the separation test series. The adapter/transtage assembly was mated to the TSM, with both in a flight configuration, and three spacecraft/adapter separation operations were performed to evaluate separation shock, spacecraft tip-off rates, and separation relative velocity.

The relative velocity and tip-off rates obtained from the test indicated that the separation event would provide the desired velocity and angular stability needed to ensure separation without subsequent impact between transtage and spacecraft. Relative velocities (corrected for air bearing and fixture drag) of approximately 106 centimeters per second and 109 centimeters per second (41.8 inches per second and 43.1 inches per second) were recorded in combination with respective spacecraft angular rotations of approximately zero degree per second and 0.34 degree per second. Spacecraft orientation about its centerline was rotated 90 degrees between these two tests.

Shock data instrumentation consisted of a charge amplifier and magnetic tape system for each shock accelerometer. Checkout of instrumentation before test runs verified that noise levels were acceptable. The signal/noise ratio was improved by isolating accelerometers from ground and from each other; however, test results were obscured, apparently by amplifier limitations. This test and

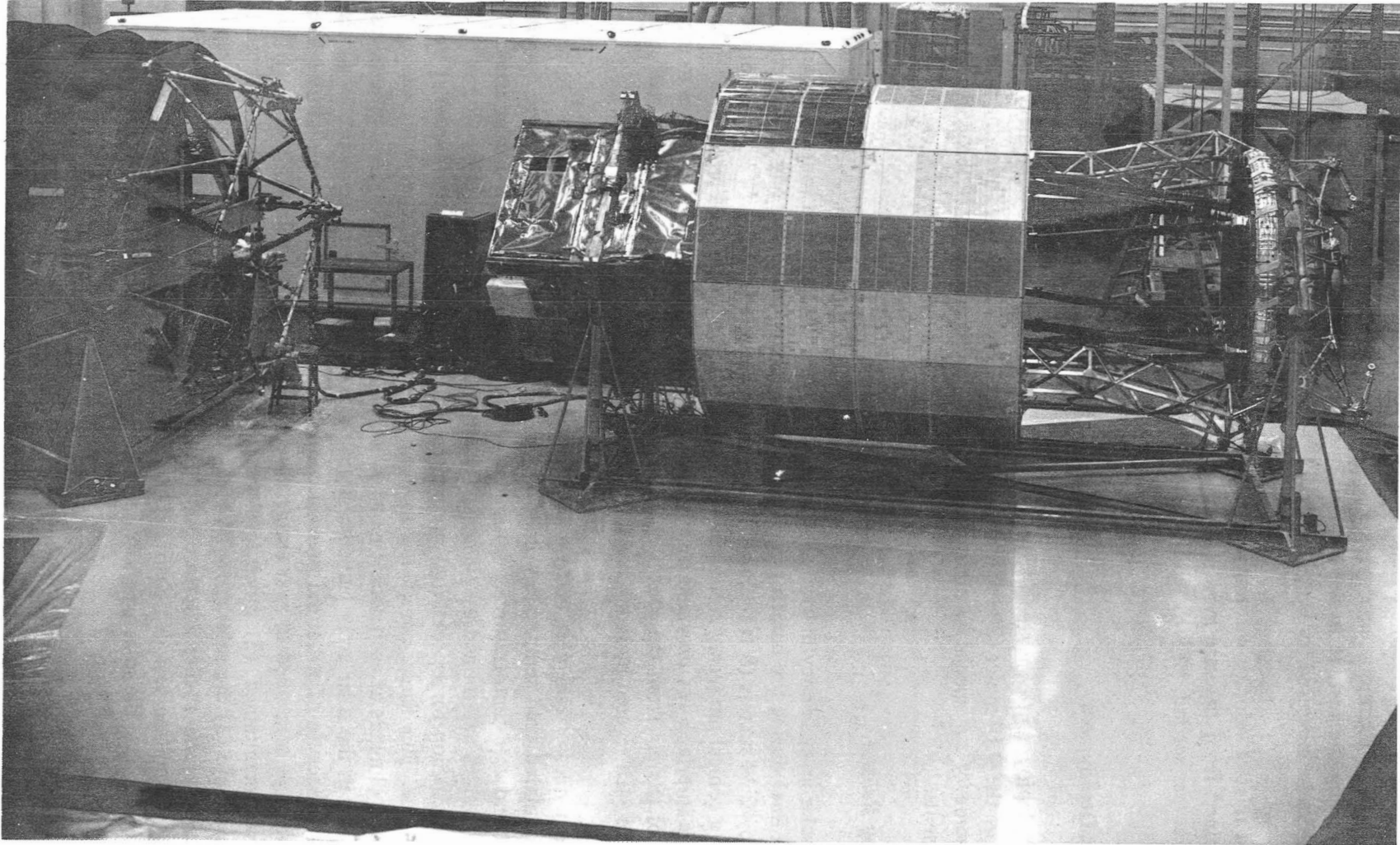


Figure 7-1. TSM and Adapter/Transtage Mass Simulator Configuration for Separation Tests

its results are a strong argument that all shock tests instrumentation should be checked out and calibrated using a technique employing shock pulses that exhibit the same characteristics as those expected during the test. It is also recommended that several standard shock pulses with known characteristics be measured for instrumentation calibration.

Separation relative velocity was not available for the flight separation event. Spacecraft tip-off rates were obtained from the rate gyro assembly following flight separation and were 0.13, 0.11, and -0.06 degree per second, all well within the specified 1 degree per second maximum allowable rate for all 3 axes.

Spacecraft Deployment

Spacecraft deployment consisted of three distinct motions of the two solar arrays and booms, and unfurling of the 9.14-meter (30-foot) diameter parabolic reflector. The following paragraphs briefly describe some of the special or unusual tests that were used to validate the design of the deployment elements.

Solar Array Release

The two solar array hemicylindrical assemblies were latched together at four positions (two on each separation line) during the launch phase to form a cylinder approximately 2.74 meters (9 feet) in diameter by 2.44 meters (8 feet) long. The cylinder was supported at each corner of the EVM top surface by a conical pin (array mounted) seated in a matching socket (EVM mounted). Pin axial preload at this interface was provided by strain energy within the solar array frames to prevent disengagement of the pin from the socket under inertial loadings during launch. The four stranded cable latches were each severed by redundant cable cutters.

First-motion release tests were performed to demonstrate release under ambient temperature conditions, simulated cold temperature conditions, and simulated hot temperature conditions. Simulated hot and cold temperature conditions were obtained by altering the solar array/EVM fitting preloads to values determined by analysis. The solar arrays first-motion drive springs of each boom produced separation forces totalling approximately 13 Newtons (3 pound-force) at the EVM/solar array interface. This force, considered to be insufficient to ensure separation, was augmented by spring-loaded plungers at each socket and by the rebound effect resulting from the release of strain energy stored in the solar array launch restraint preload. Cold temperature produced higher strain energy levels because of structural thermal contraction in the solar array structure while the EVM temperature was controlled to near ambient conditions. The test demonstrated that (1) structural integrity was maintained, (2) shock levels were not significantly increased over those at ambient temperatures, and (3) the solar array/EVM socket interface did not seize due to increased loads at the conical pin and socket interface and that separation was satisfactory. The simulated hot-temperature condition test demonstrated that the total separation forces, including the reduced strain energy level in the solar arrays, was sufficient to achieve separation at the array/EVM interface.

One solar array first-motion release test, conducted at ambient temperature and nominal load conditions, deviated from flight configuration in that only one of the two redundant cable cutters at each latch point (4) were actuated. The test confirmed the design release capability for this case of operation failure.

Damper and Hinge Cold Chamber Tests

A series of tests were conducted on the hinge and damper mechanism in a cold chamber at ambient pressure. The tests were of doubtful value because moisture condensed and froze on the mechanism that affected the operational characteristics.

Validation tests of the flight mechanisms were performed under hot and cold temperature extremes in vacuum. The solar array boom deployment and lock mechanism with complete hinge mechanisms at each end (hub hinge and 45 degrees skewed hinge), but with solar array removed, were tested operationally using solenoid release in lieu of pyrotechnic actuated pin pullers. The boom was secured as a base and the removable support assembly (hub-hinge end) and solar panel hinge fitting (solar-panel end) were permitted to move during the deployment events. Mass simulation and inertia characteristics were not simulated and were ignored in these tests. Deployment times were established for damper operation at temperature extremes, and lock-up operations were demonstrated.

Solar Array Zero-G Deployment Tests

The validation of the solar array deployment mechanisms presented many unusual problems. The large physical size of the array structures and the length of supporting booms caused handling problems and required that unique test support fixtures be developed. The boom was designed to have sufficient strength to be self-supporting in a one 'g' field; however, the deployment forces available were not of sufficient magnitude to overcome gravity-induced hinge pin friction, much less lift the array weight. It was necessary, therefore, to test solar array deployment mechanisms using a test setup that minimized gravitational effects. To this end, a facility was produced having a cast epoxy floor that was level to ± 0.1 cm over the working area. The solar array boom was mounted to a positioner mechanism at its field joint interface. (The field joint interface is located between the removable support assembly and the center support assembly of the hub bridge truss, Figure 5-3, Chapter 5.) The position mechanism was adjustable in azimuth and elevation and could rotate a boom mounted with the centerline horizontal about its centerline. The boom was also supported at a point approximately 2.8 meters (111 inches) from the hub hinge line.

Deployment torques for first-motion travel were quite modest, measuring from 34.6 Newton meters to 60 Newton meters (306 pound-inches to 530 pound-inches). This torque range translates to forces of 12.2 Newtons to 21.1 Newtons (2.75 pounds to 4.75 pounds) acting 2.84 meters (111.5 inches) from the hinge, the point at which the majority of the array and boom weight were supported. To ensure that forces tending to restrain or aid the deployment were minimized, the solar array and boom assemblies were supported by an air bearing approximately 2.8 meters (111 inches) from the first-motion hinge. This support reduced hinge pin friction loads induced by gravity to a negligible value and permitted the deployment first-motion mechanisms to be tested under ambient conditions.

The effects of the test fixture mass upon the deployment test were minimized by keeping the test fixture masses that were attached to the moving elements of the arrays and booms as small as possible. An air bearing was attached to the boom or array at the auxiliary support point (at a height of approximately 1.2 meters (4 feet) above the test floor) and rested on a level flat surface on a cart. The cart motion over the test floor was restricted by a radius arm to keep the cart on an arc to be traveled by the air bearing. The radius arm pivot and boom hinge had coincident centerlines. The cart was moved manually during deployment tests to maintain the air bearing on its mating support surface. Manual position control was feasible because of the relatively slow deployment rate.

Spacecraft deployment first and fourth motions used the test setup just described with the solar array latched in the launch position for first motion and deployed for fourth motion tests. For second motion tests, the boom and array were rotated about the boom centerline to place the boom/array skewed hinge centerline vertical.

The equipment described above was used early in the program to determine the effects of various parameters in the deployment system design, such as damping rates, deployment spring interleaf lubrication, hinge pin lubrication, lock and release characteristics and deployment time lines. The results of these early tests were reflected in design changes that corrected design deficiencies and established a baseline for predicting and measuring flight article performance.

Damper Development

The single-vane, rotary viscous dampers (Figure 6-9, Chapter 6) used to control the deployment rates of the solar array systems were developed from a two-vane commercial design with rotary travel limited to 90+ degrees. The flight damper design was undertaken to reduce the weight of the commercial design and to provide angular travel in excess of the 180 degrees that is required for the spacecraft deployment second-motion movement (rotation of solar array about the 45-degree skewed hinge). Direct drive of the damper shaft, rather than a 2:1 gear reduction from solar array 180-degree motion, was selected because it weighed less and resulted in a simpler thermal control system for damper temperature control.

The single-vane damper had one inherent major disadvantage: it produced unbalanced forces on the vane and shaft that were not present in a double-vane design. Higher strength shafts were required to withstand the loads. Tolerances on the housing, shaft, and vane, and on the fit of the seals used between vane and housing were decreased to obtain a design that functioned satisfactorily. The damper sealing system was also modified so that two redundant seals existed on all paths between the damping fluid and damper exterior.

Acceptance tests for each damper unit included characterization of the damping rate as a function of temperature, torque, and damping rate adjustment screw setting; damping rate as a function of shaft position and direction of rotation; and vacuum leak tests. These tests evolved from the development test program that determined these parameters to be crucial in damper operation and in predicting performance.

The dampers were assembled into each of four hinge assemblies, two dampers at each hinge, and tested under conditions of one and two dampers operational for each deployment motion. In all cases, the deployment events were successfully completed, verifying the capability to operate successfully over the temperature range and with one or two dampers operational.

THERMAL STRUCTURAL MODEL SPACECRAFT

A combined thermal structural model (TSM) spacecraft was fabricated essentially to flight model drawings and tested to demonstrate the integrity of the spacecraft structural and mechanical design and provide data for establishing subsystem environmentally induced loads for test levels, and to develop and verify spacecraft temperature control techniques and establish thermal test levels.

The TSM differed from the flight model primarily because the solar arrays contained mass loaded panels except for two live panels, and the components mounted in the EVM were replaced by mass models with heaters to simulate loads and heat dissipations.

The TSM spacecraft was subjected to the tests listed under the section heading "Spacecraft Environmental Testing Requirements" on the first page of this chapter. In addition to fulfilling the test objectives stated, the TSM tests validated the test procedures, equipment, and fixtures subsequently used on ATS-6. It was invaluable as a test model for proving spacecraft handling and transportation equipment and procedures.

IN-ORBIT PERFORMANCE AND OPERATIONS

Overview

The structural and mechanical subsystems met their basic flight requirements. The spacecraft successfully withstood the launch environment and deployed properly in space with no evidence of structural failures. Alignment of the various sensors (Earth sensor, interferometer, and monopulse) appeared to have been preserved to within 0.1 degree. The separation system worked very well; the spacecraft angular rates after separation were 0.13, 0.11, and -0.06 degree per second in roll, pitch, and yaw, compared to specified allowable rates of 1 degree per second about the three axes. Spacecraft deployment was successfully achieved, although a significant delay (approximately 15 minutes) was experienced before the north (-Y) solar array completed its unfolding operation (with respect to the supporting boom) and locked up. This anomaly is treated in a later section of this report.

Performance Evaluation of Structural/Mechanical/Reflector Subsystems

The structure of the spacecraft performed nominally from liftoff through orbit injection. At approximately 6h 33m 18s hours after launch, the deployment sequence was initiated by the Titan transtage command of "separation enable." This command powered all spacecraft deployment telemetry lines and the automatic deployment sequencer. At this time all telemetry indications were normal and the sequencer was automatically started upon receiving the separation-fire command from the Titan transtage. Separation from the launch vehicle occurred as planned and spacecraft deployment was nominal except for one event: the slow deployment of the north solar array with respect to its supporting boom.

Table 7-1 presents the ATS-6 separation/deployment timelines. Maximum predicted and actual times of events from liftoff are shown. The source of data was the printout of the normal telemetry history tape. The actual time listed is that at which the event was observed on the spacecraft telemetry that was updated every 3 seconds. Where more than one event (such as north boom lockup and south boom lockup) is covered by a single item, the time of the latest event is indicated. With the exception of the completion of the array unfold, all times were within a normal anticipated spread. Investigations that were conducted to determine the cause of slow deployment of the north solar array are discussed in the next section.

Table 7-2 presents the specified, predicted, and actual temperatures of the deployment mechanism components that were monitored. All were within predicted values.

Table 7-3 identifies the rotation rates of the spacecraft about the roll, pitch, and yaw axes before and/or after various deployment events that were obtained from the telemetered onboard rate gyro assembly (RGA) data.

Table 7-1
ATS-6 Separation/Deployment Timelines

Event	Expected Time From Liftoff (hours/min/s)	Actual Time From Liftoff (hours/min/s)	Delta Time (min/s)
Separation Enable	6/37/56	6/33/18	-4/38
Spacecraft Separation	6/37/59	6/33/21	-4/38
Start Solar Array Booms Release	6/43/59	6/39/23	-4/36
Complete Solar Array Booms Lockup	6/47/59	6/40/34	-7/25
Array Unfold Release	6/53/59	6/46/34	-7/25
Array Unfold Complete	7/00/59	7/02/00	+1/01
Start Reflector Deployment	7/06/59	7/08/03	+1/04
Complete Reflector Deployment	7/07/05	7/08/12	+1/07
Start Boom Drop	7/13/06	7/14/14	+1/08
Complete Boom Drop	7/14/05	7/14/32	+0/27

Table 7-2
ATS-6 Deployment Temperatures

Parameter	Specification	Predicted	Actual
Damper, Panel-End North	-48° to 46°C	-33° to 30°C	25°C
Damper, Panel-End South	-48° to 46°C	-33° to 30°C	26°C
S/A Boom 2nd Depl Hinge +Y	-140° to 150°C	-55° to 116°C	10° to 17°C
S/A Boom 1st Depl Hinge +Y	-140° to 150°C	-55° to 116°C	45° to 52°C
S/A Boom 2nd Depl Hinge -Y	-140° to 150°C	-55° to 116°C	2° to 7°C
S/A Boom 1st Depl Hinge -Y	-140° to 150°C	-55° to 116°C	48° to 55°C
Reflector Rib Sta 173 +Y	-18° to 34°C	-10° to 19°C	10°C
Reflector Rib Sta 110 +X	-18° to 34°C	-10° to 34°C	12°C
Reflector Rib Sta 110 -Y	-18° to 34°C	-10° to 34°C	5°C
Reflector Hub -Y	-160° to 60°C	-53° to 35°C	11°C

The mechanical operations of the spacecraft mission terminated with the successful deployment of solar arrays and the 9.14-meter parabolic reflector. The spacecraft structure maintained the spatial relationships between all components throughout the 5-year mission as far as is known. No alignment anomalies were reported. The structure performed its function of shielding components from the orbital environment and helped control energy within the EVM cavity. Structural elements also performed as expected in their capacity as integral parts of the thermal control subsystem.

IN-ORBIT ANOMALIES—NORTH ARRAY PANEL DELAYED DEPLOYMENT

The only in-orbit anomaly related to the structural and separation/deployment subsystems was the delay in the deployment of the -Y (north) solar panel. This anomaly resolved itself when the deployment was completed, approximately 10 minutes late, and no other anomalous behavior was observed.

Table 7-3
ATS-6 Deployment RGA Rates (Actual Values are in Degrees/Second)

Event	Roll	Pitch	Yaw
Before Separation	0.00	+0.04	+0.08
After Separation	+0.13	+0.11	-0.06
After Boom/Array Release	-0.03 to -0.18	-0.05	-0.06 to +0.06
After Boom Lock	-0.18	-0.02	+0.06
At Array Unfold Release	-0.18	-0.02	+0.07
Array Unfold Completed	-0.09	+0.02	+0.10
Reflector Release	-0.09	+0.03	+0.10
Reflector Deploy Completed	-0.09	+0.04	+0.10
Boom Drop Release	-0.09	+0.04	+0.10
Boom Drop Completed	-0.09	+0.06	+0.08

A number of questions were raised by the slow deployment of the north panel. Predicted deployment time of the panel/boom hinge was 3 to 4 minutes with a maximum of approximately 7 minutes. The actual deployment time was approximately 15 minutes and 26 seconds. Onboard instrumentation indicated the time of release, and hence the normal time of the start of deployment, and the completion of deployment motion. The start of deployment motion was assumed to have occurred with application of the firing current to the array release pyrotechnics. All ground tests of this release mechanism resulted in a nominal release of the array from the array restraint mechanism. Completion of deployment of the array was indicated by microswitches that were actuated upon correct seating of the deployment hinge lock pins. The position of the array during deployment, therefore, had to be determined by indirect means, since no direct readout of the position of the array was included in the spacecraft instrumentation.

Each deployment motion was unique; that is, only one type of motion occurred at any given time during the deployment sequence, although both north and south booms or panels were permitted to accomplish similar motions during the same period of time. The reaction of the spacecraft to the forces produced by deployment motions of the various array and reflector components was indicated by changes in the orientation of the spacecraft in inertial space.

The body rates of the quiescent spacecraft were quite low following separation and provided a baseline for study of spacecraft motions induced by solar array motions.

The studies strongly suggested that the north solar array panel motion occurred primarily during the period 19:58:00 and 20:02:03. There was some indication that the north panel may have moved through some portion (possibly 34 degrees) of the 180 degrees of deployment before halting. This possibility was based on sudden changes in body rates (Figure 7-2) at 19:47:52. The reversal of the

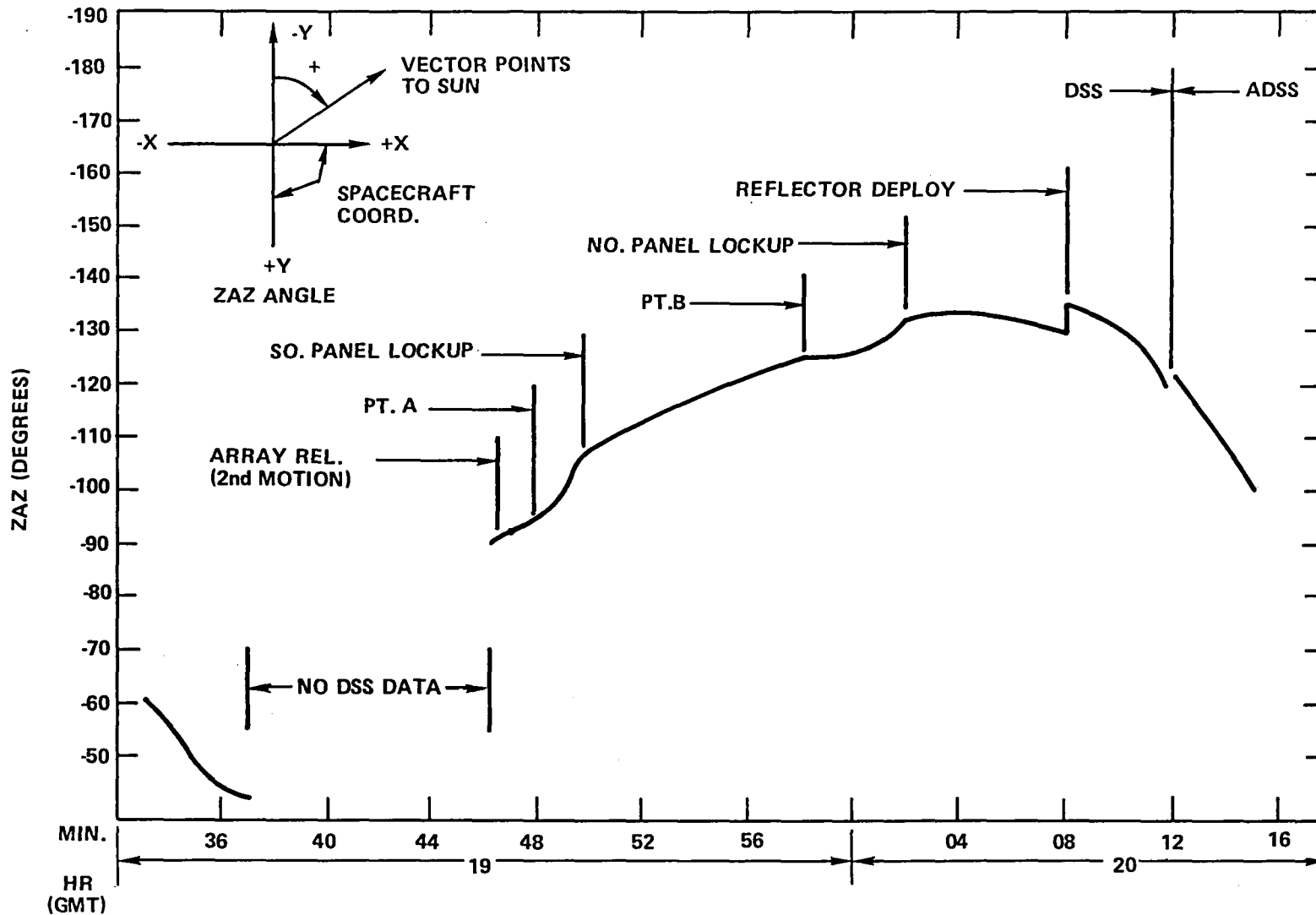


Figure 7-2. ZAZ During Deployment

ZAZ curve slope changes at 19:47:52 also indicated that the forces influencing the motion of the spacecraft body changed at this time (point A on the curve). The 34-degree position was significant, because it coincided with the closest approach of the corner of the solar array frame A to the boom structure during deployment. This clearance was about 2 inches under ambient conditions; however, the boom was wrapped with multiple-layer insulation and had several electrical cables attached outside of the insulation. It was possible that interference occurred between frame A and the boom because of thermal distortion, or the unexplained movement of the cable or insulation.

One advantage of the deployment drive systems used on the solar arrays was that the dampers, which controlled the deployment rate, were rate sensitive. Thus, when the north array ceased to move, the damper no longer restrained the deployment spring forces that were then permitted to act at full force against the obstruction. As was evident, the array eventually deployed completely.

CONCLUSIONS AND RECOMMENDATIONS

The established design criteria and the basic design implementation for the structural and separation/deployment subsystems were adequate to satisfy all of the ATS-6 mission requirements. However, as a result of investigations into the delayed deployment of the north panel, it was judged that the panel-boom design clearance may have been inadequate to allow for all thermoelastic deflections of the panel during deployment. Such effects should be carefully defined and accounted for when designing future spacecraft.

The reflector support truss, through satisfactory 5-year orbital performance, has demonstrated the feasibility of GFRP in space applications, and some of the advantages to be gained from the unique structural, thermal, and mass properties inherent in GFRP.

In-orbit tests were conducted in which the spacecraft was under monopulse control by the attitude control subsystem acting to null azimuth/elevation error signals developed from rf transmissions from a ground station relative to the rf boresight of the 9.14-meter diameter reflector. Spacecraft roll and pitch axes movement, as measured by the Earth sensor, during one period of approximately 19 hours, indicated an approximate change of 0.6 degree in roll and 0.3 degree in pitch. Roll and pitch axes movement, as seen by the interferometer during this period, correlated with the Earth sensor data. From these data, it was inferred that the diurnal variations of reflector temperature gradients, caused by the changing angle of solar flux, produced reflector distortions of such a magnitude as to cause the indicated "squinting" of the rf boresight off the spacecraft mechanical axes (sensor axes). The very small thermal deflection of the reflector support truss material, established by material characterization tests, indicated that truss deflections were so small that they could not cause distortions of a magnitude that could be detected by the test methods described above. Therefore, beam "squinting" was attributed to distortion of the parabolic reflector caused by thermal gradients. Such effects should receive careful attention in future, comparable spacecraft designs.

The program philosophy of performing a validation of the initial structural and thermal subsystem designs by using a combined thermal structural model (TSM) spacecraft resulted in numerous benefits that included the following:

- Validation of the spacecraft structural design for environmental conditions before integration and test of the flight spacecraft subsystems
- Validation of the design of the EVM thermal control subsystem
- Verification of analytically obtained spacecraft dynamic mode shapes, resonant frequencies, and load levels induced into components
- Validation of designs of separation and deployment mechanisms
- Validation of test fixture designs and characterization of test fixtures before use with the protoflight spacecraft
- Development and validation of ground support equipment for spacecraft handling and transportation, including compatibility of such equipment with transport aircraft and commercial carriers
- Proofing of production tooling and processes
- Validation of handling, integration, and test procedures, structural/mechanical assembly and alignment procedures, and thermal control subsystem process and installation procedures.

The TSM was used to perform these activities early in the program, leading by many months the similar operations of fabrication, installation, integration, and test of the protoflight spacecraft. Thus, the majority of program processes, procedures, and government supplied equipment were verified and validated before being used on the protoflight spacecraft. The result was that very few unexpected problems were encountered in operations on the protoflight spacecraft. The TSM concept was a very strong contribution to a relatively troublefree spacecraft program that culminated in a very successful mission that exceeded its 5-year design goal.

CHAPTER 8

TELEVISION CAMERA REFLECTOR MONITOR

FUNCTIONAL REQUIREMENTS

The television camera on ATS-6 was intended to verify that the 9.14-meter reflector and the solar arrays were properly deployed. During operations, the camera was used periodically to determine if any structural anomalies had occurred with respect to the reflector, and to determine if any visible indication of spacecraft static charge could be seen during eclipse.

DESIGN DESCRIPTION

The television (TV) camera was a subminiature black and white camera mounted on the top surface of the Earth-viewing module (EVM). Figure 8-1 is an outline drawing of the camera and lens, and the specifications for the camera were as follows:

- Sensor:

Type	GEC 1305 Vidicon
Tube diameter	12.70 mm (1/2 in.)
Photoconductor	S18
Scan diagonal	8.13 mm (0.32 in.)
Beam focus	Electrostatic
Beam deflection	Magnetic

- Camera Physical Dimension:

Size	3.81 cm (1.5 in.) × 3.81 cm (1.5 in.) × 12.7 cm (5 in.) (less lens)
Weight	9.27 kg (0.6 lb) (less lens)

- Camera Electronics:

Input voltage	12 Vdc, +1 V
Input power	6.0 watts @ 12 V
Aspect ratio	4:3
Scan format	525 lines, 30 frames per second
Interlace ratio	2:1
Horizontal frequency	15,750 Hz
Linearity	±5 percent

AGC/ALC	6 dB changeover 300:1 light range (image tube limited)
Video bandwidth	6 MHz
Preamp eq. input noise	Less than 2 NA
Video format	1 volt video into 75 ohms EIA Standard Composite Format RS 170
Scan failure-protection	Cathode blank within 1 frame of H&V sweep fail
● Environmental:	
Temperature	-20°C to +55°C
● Performance:	
Maximum resolution	425 lines
S/N @ 107.6 lumens per square meter (1m/m ²) or 10 foot-candles faceplate illumination	34 dB

The lens was selected to provide a view of the entire surface of the antenna and the solar arrays. It had a diameter of 10.5 centimeters and an optical field of view of 197 degrees that provided an overall camera field of view of 186 degrees by 140 degrees. The location of the camera and the extremely wide angle lens dictated that a photochromic lens be used to minimize the effects of flare from both incident and reflected light, which could be of varying intensity and duration, and could come from any direction depending on the aspect of the Sun with respect to the satellite.

To protect the camera from excessive light, the iris was designed to be fully closed or opened in seven steps; each one equal to one f stop. As a precaution, a built-in temperature sensor was incorporated. The output of the temperature sensor was multiplexed onto the fifteenth line on the video raster so that the temperature could be determined by looking at a video monitor or an oscilloscope prior to opening the lens iris.

Figure 8-2 shows the spacecraft configuration used for operating the TV camera and Figure 8-3 shows the ground station configuration used for monitoring and recording the data.

IN-ORBIT PERFORMANCE

The in-orbit performance of the TV camera was as designed. On June 3, 1974, the fourth day in orbit, the camera was turned on and the previous indications of successful deployment of the solar array booms and the 9.14-meter reflector were confirmed visually. During October 1974, the TV camera was turned on during eclipse to see if any visual indication of spacecraft charge could be seen. Even though there was a static charge build-up of 8000 volts, there was no visual indication from the TV camera. The camera was again turned on in March and April 1975 to verify the integrity

of the antenna. The pictures looked the same as the ones taken almost a year earlier. In July 1979, the TV camera was turned on as part of the end-of-life tests on ATS-6. It was still operating normally and the antenna and solar array booms still looked the same. Figures 8-4 through 8-7 show a series of TV camera pictures showing the progress of the EVM shadow across the antenna as the Sun moved with respect to the spacecraft.

IN-ORBIT ANOMALIES

No TV camera anomalies were noted during the life of ATS-6.

CONCLUSIONS AND RECOMMENDATIONS

The TV camera monitor was almost an afterthought in the design of ATS-6. It was built very inexpensively and provided a very simple and highly reliable assurance that the antenna had unfurled properly.

It is recommended that spacecraft employing large deployable antennas of the ATS-6 type consider the use of a TV camera for visual validation of successful deployment. A narrower field-of-view lens would provide a more detailed view of the antenna, solar panels, and struts; however, the mechanism for aiming the camera at various points of interest would add to the complexity and introduce additional possibilities for failures.

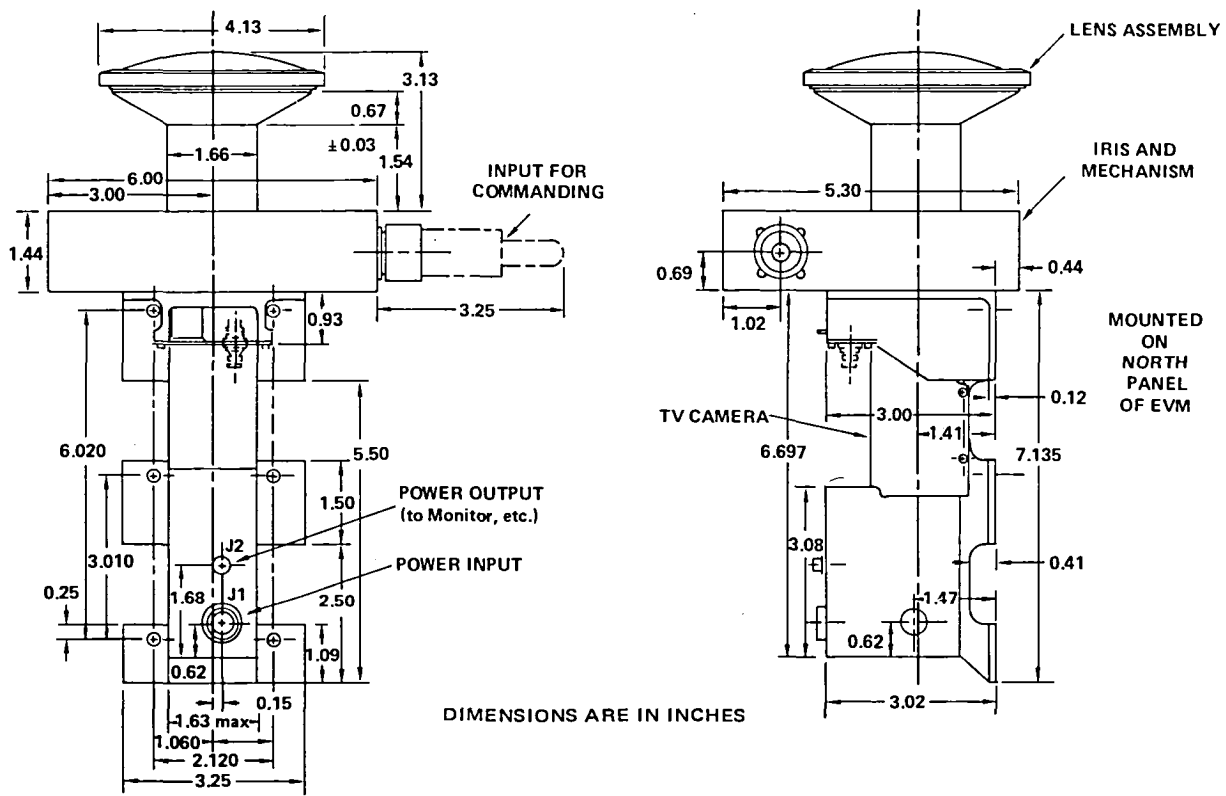


Figure 8-1. TV Camera Outline Drawing

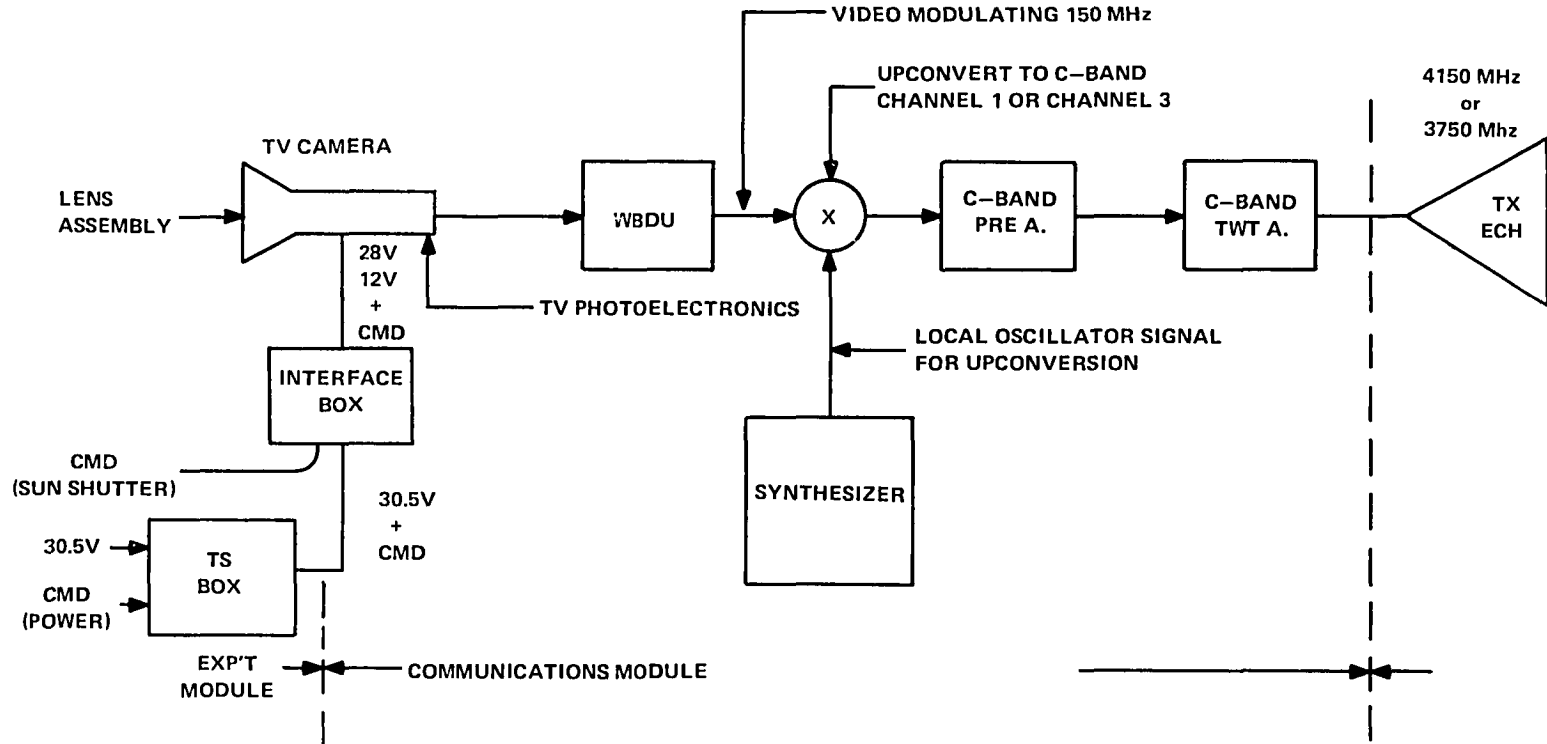


Figure 8-2. TV Camera Reflector Monitor Configuration

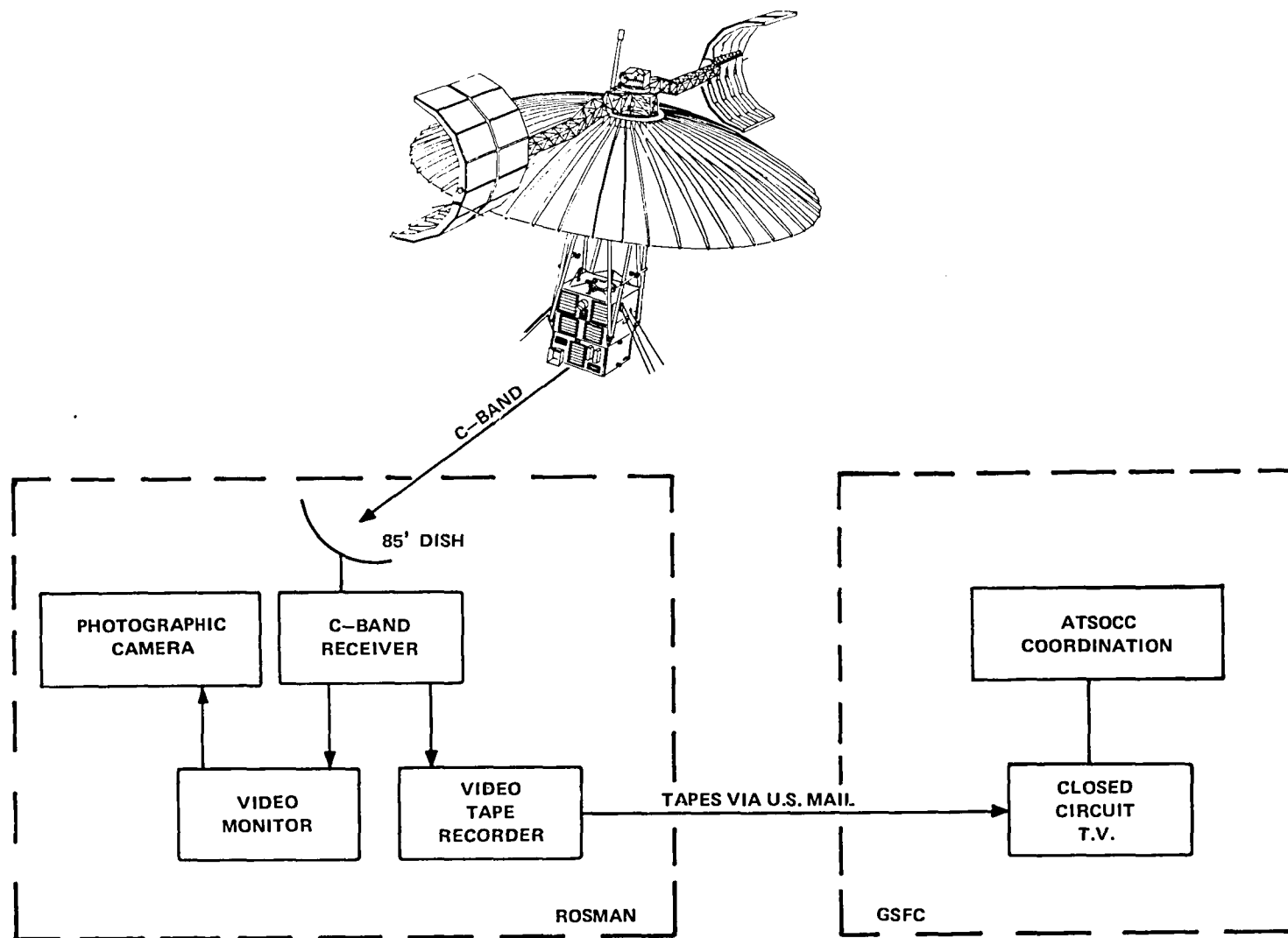


Figure 8-3. TV Camera Monitor Ground Station Configuration

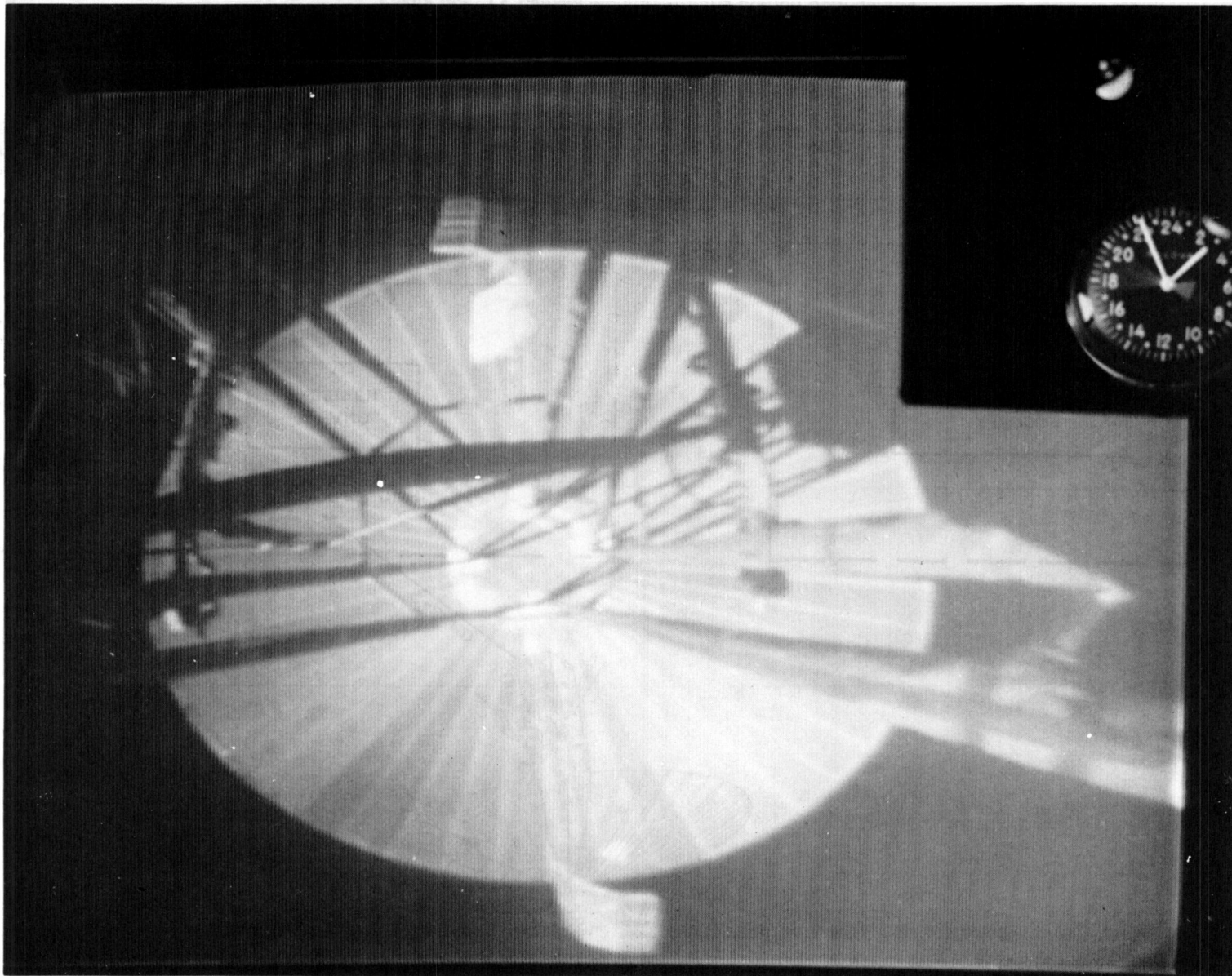


Figure 8-4. Progress of EVM Shadow Across Antenna—0255

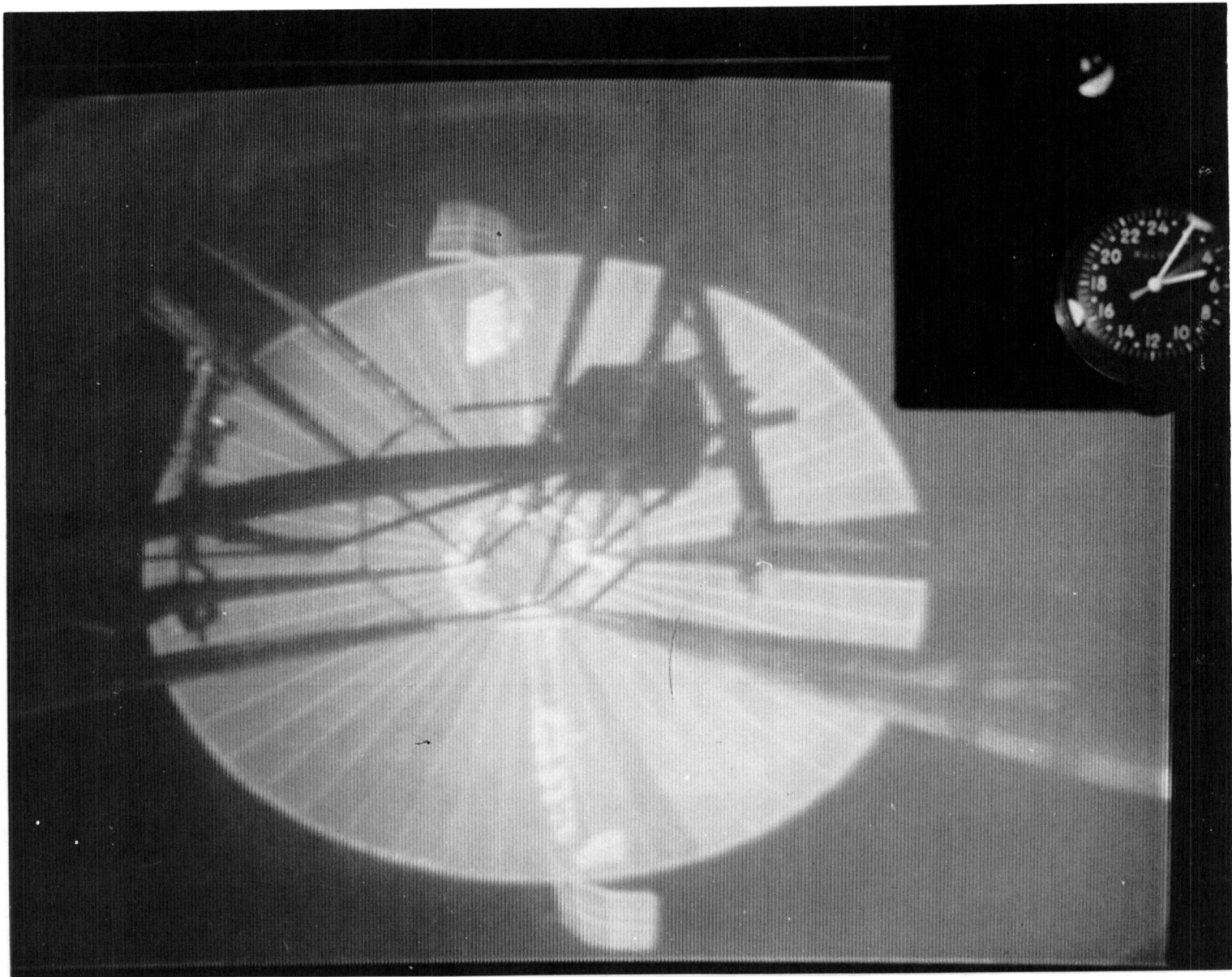


Figure 8-5. Progress of EVM Shadow Across Antenna—0505

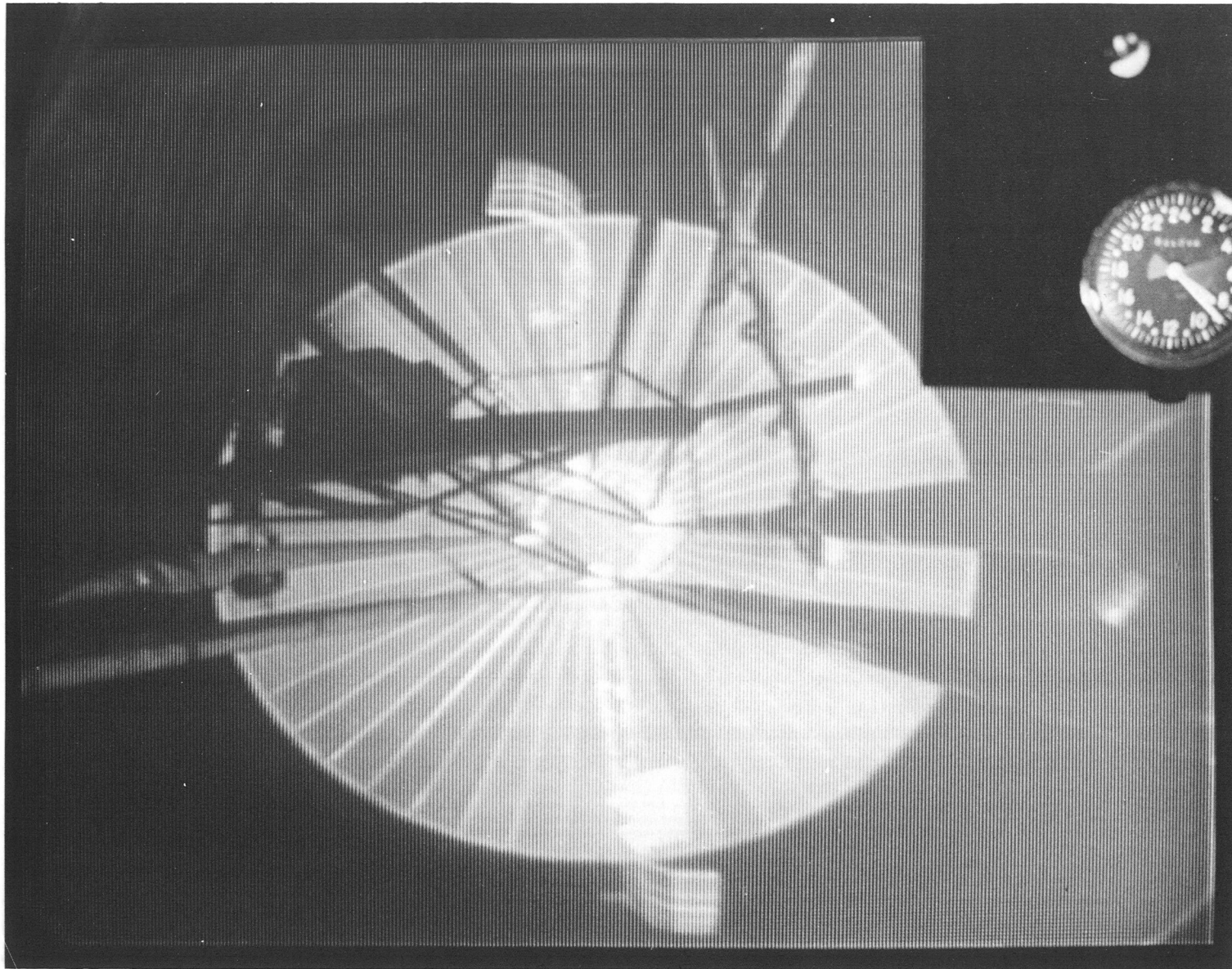


Figure 8-6. Progress of EVM Shadow Across Antenna—0822

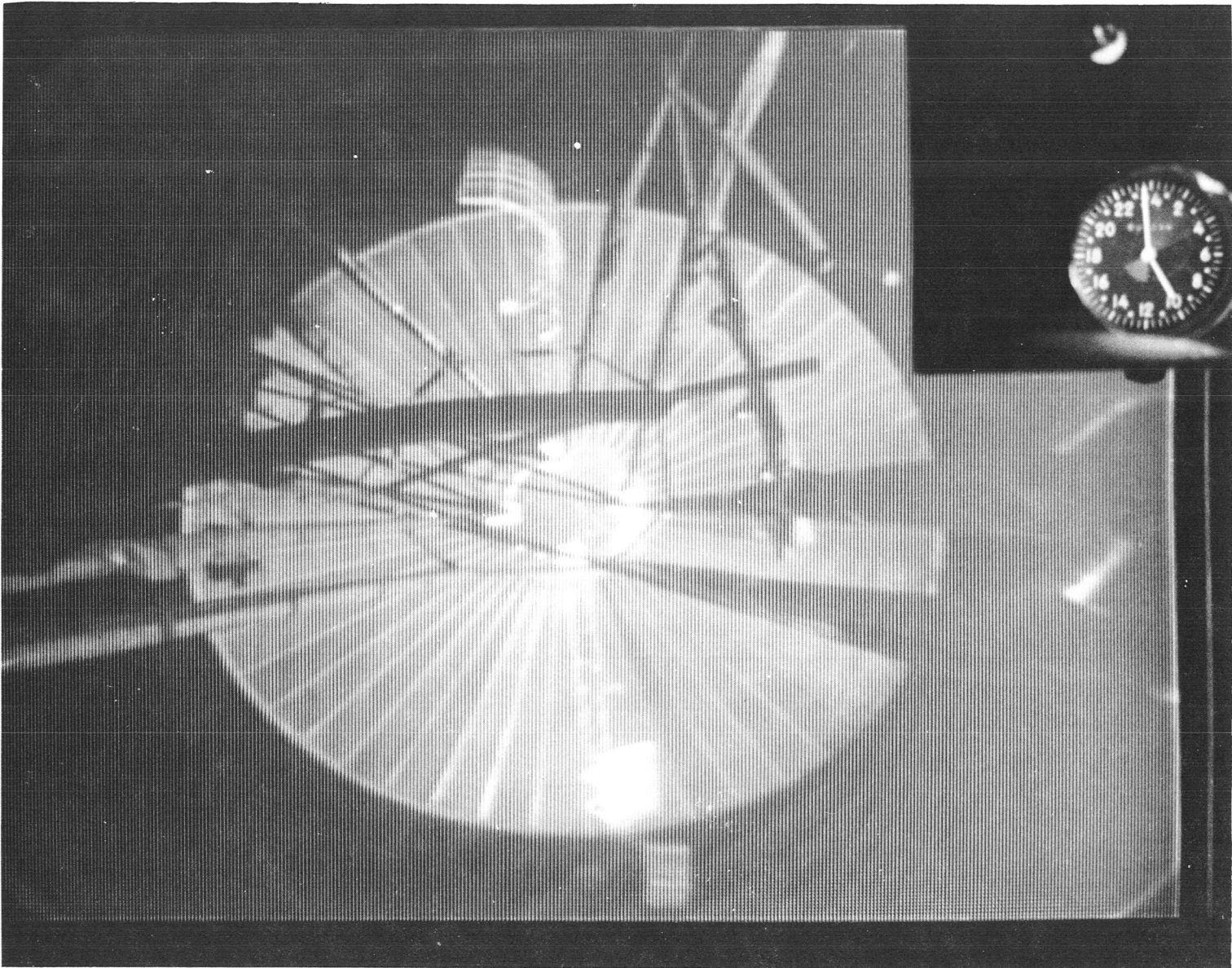


Figure 8-7. Progress of EVM Shadow Across Antenna—0959

Part C
Thermal Control
and
Contamination Monitor

CHAPTER 9

THERMAL CONTROL SUBSYSTEM

INTRODUCTION

The thermal control subsystem was designed to control the temperatures of all spacecraft elements (except the independently controlled Environmental Measurements Experiment¹), both internal and external to the EVM, consistent with the following requirements:

- Preserve the operational reliability of the electronic components by maintaining the mounting surfaces in the range of 5°C to 35°C during all modes of normal operation and spacecraft orientation.
- Minimize temperature variations and gradients on the structure external to the Earth-viewing module (EVM) during the launch/deployment phase when thermal distortions can have their greatest influence on the success of the mission.
- Control outgassing and long term deterioration due to excessive temperatures by selecting proven materials and by providing adequate temperature regulation.

The spacecraft temperature specifications that served as the basis for the thermal design are listed in Table 9-1.

Design Description

A schematic of the thermal control subsystem is given in Figure 9-1. The EVM thermal components are shown in Figure 9-2. The functional requirements were satisfied through the use of multilayer insulation, thermal louvers, heat pipes, coatings, and thermostatically controlled heaters.

General Considerations

One of the prime reasons for selecting a cubical shape for the EVM was its adaptability to a predictable and efficient thermal control system. Four of the six sides had considerable exposure to the Sun and therefore were covered with multilayer insulation. The two remaining sides, facing north and south, were honeycomb panels containing 3.2 square meters (m²) of thermal louvers. The louver arrays, coupled with the low absorptance (α)/emittance (ϵ) optical solar reflector wafers on the panels, provided a controlled radiative path from the EVM to space. Significant heat sharing within the EVM was accomplished through the high conductance of 17 triplets of heat pipes that connected the north and south faces by the transverse panels.

¹The EME subsystems are described in Volume VI of this report.

Table 9-1
ATS-6 Temperature Specifications (°C)

Component	In-Orbit	Launch/Ascent Acquisition	Acceptance	Qualification
Batteries (Mounting Surface)	0 to 25	0 to 25	0 to 25	0 to 35
Maximum Gradient Between Batteries	5	5	5	5
Earth Sensors				
(Mounting Surface)	3 to 40	3 to 40	3 to 45	-12 to 45
(Bolometer)	-7 to 42	-7 to 42	-7 to 50	-12 to 50
Polaris Tracker (Mounting Bracket)	5 to 37	5 to 37	-5 to 47	-10 to 52
Electronics Mounting Surface Within EVM (General)	5 to 35	5 to 35	-5 to 40	-10 to 50
Feed Farm Elements	-27 to 61	-27 to 61	-32 to 66	-37 to 71
Digital Sun Sensors	-60 to 65	-40 to 65	-50 to 75	-60 to 85
Analog Sun Sensors	0 to 40	0 to 40	-50 to 50	-65 to 65
Solar Arrays (Average Temperature)	-160 to 52	-140 to 75	-160 to 60	-160 to 60
Solar Array Booms (Average Temperature)	-40 to 135	-140 to 150		
GFRP Truss and Fittings	-80 to 60	-160 to 60		
Deployment Dampers	-46 to 54	-33 to 30		
Parabolic Reflector (Hub)	-140 to 75	-10 to 19 (Average at Deployment)		
Magnetometer Boom	-75 to 38	-75 to 38		
EME Bridge	-75 to 38	-75 to 38		
External Harness	-160 to 135	-160 to 135		
Squibs				
Titan/Adaptor		-50 to 59	-50 to 59	-65 to 74
All Others		-140 to 135	-140 to 135	-155 to 150
Thermal Blankets	-184 to 120	-184 to 120		
Louvers				
(Actuators)	5 to 35	5 to 35	-10 to 50	-20 to 60
(Blades/Frames)	-73 to 150	-73 to 150	-73 to 150	-75 to 180
Heat Pipes	5 to 35	5 to 35		
OSR	5 to 35	5 to 35	0 to 40	-10 to 50
SPS				
EVM Valves and Lines	5 to 45	5 to 45	5 to 102	5 to 112
OCJ Bar Valves	5 to 100	5 to 100	5 to 102	5 to 112
OCJ Bar Lines	5 to 70	5 to 70	5 to 90	5 to 100
Catalyst Bed	-50 to 800	-50 to 800	-100 to 950	-100 to 950

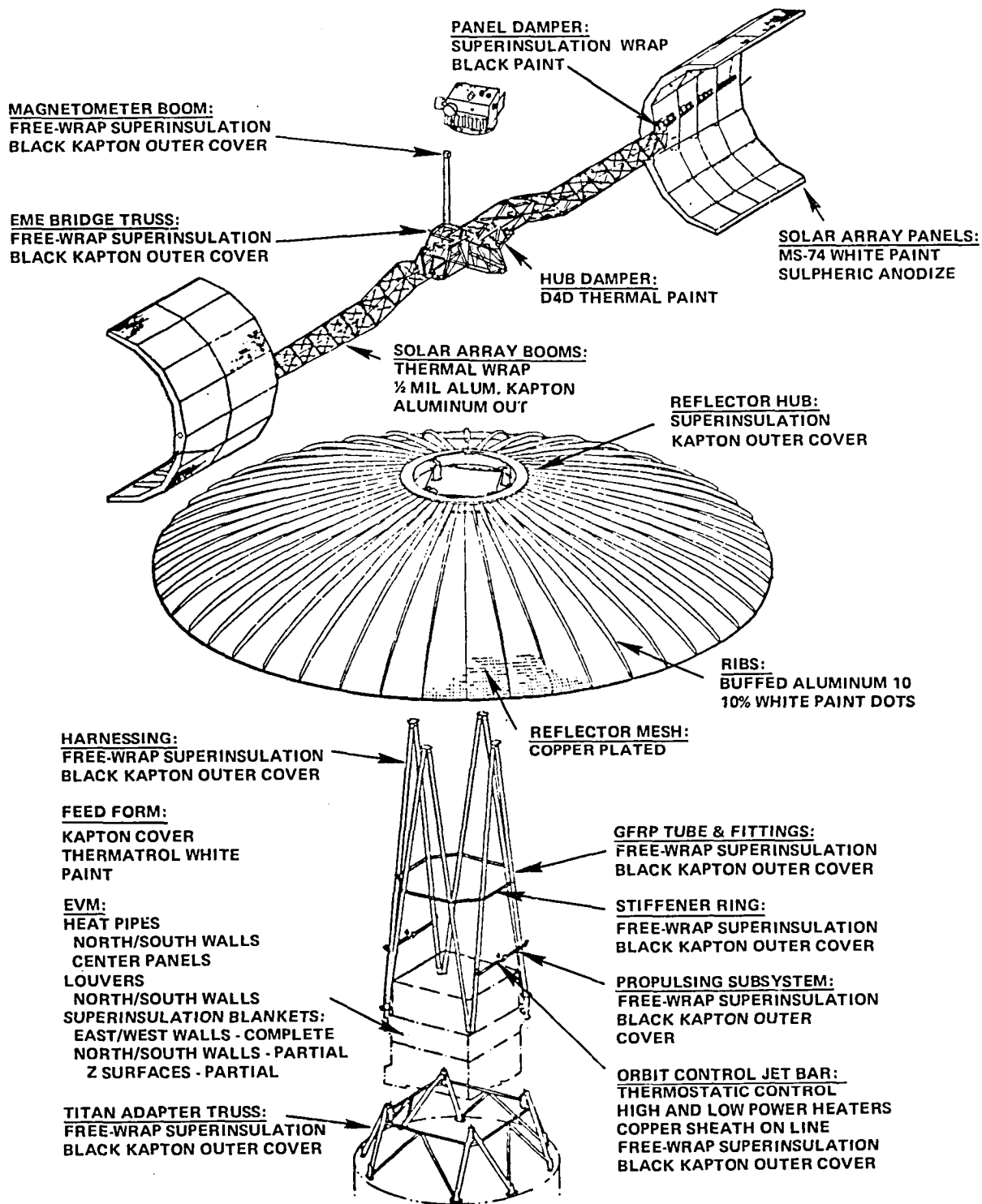


Figure 9-1. Thermal Control Subsystem

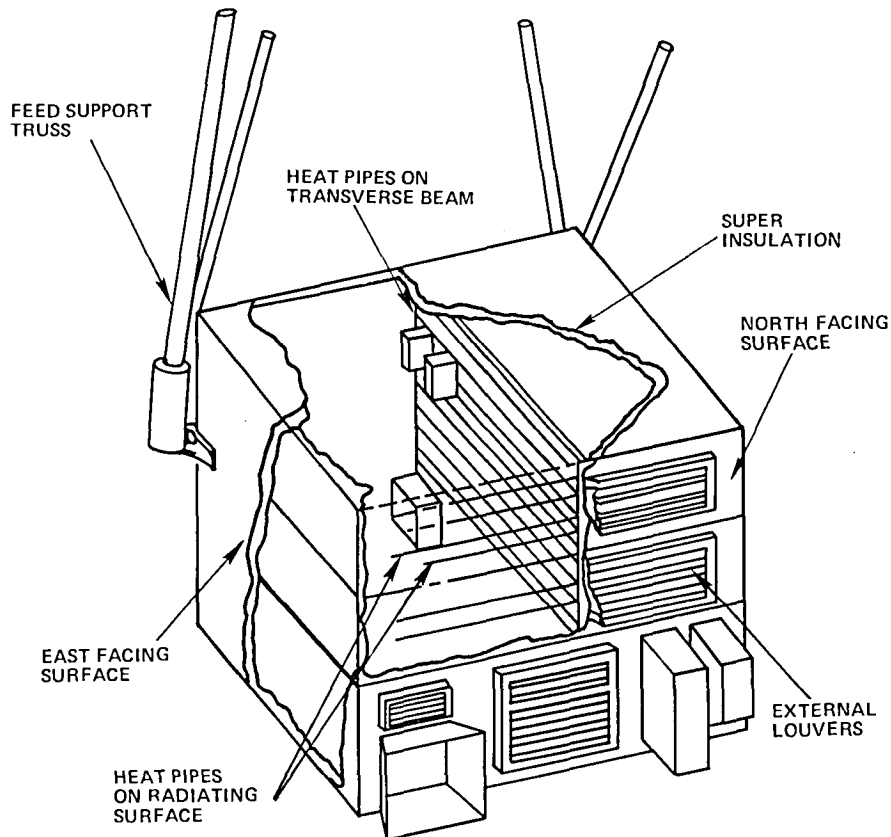


Figure 9-2. EVM Thermal Design

The communications module contained some of the highest dissipators associated with C-band traveling wave tubes; UHF, S-band, and L-band transmitters and power regulators, and ion engine electronics. The service module contained most of the housekeeping components and had a reasonably constant power profile under most normal operations. The experiments, Earth sensor, Polaris tracker, and the interferometer system were in the experiment module. The batteries were also located in this bay and their temperature had to be controlled effectively with little margin for error.

Placement of the electronic components on the EVM panels was exercised with the intention of balancing the dissipation of heat throughout the spacecraft. The uniformity of power was further enhanced by placing excess power shunts in key locations inside the EVM.

Thermal Design Hardware

The thermal control hardware elements were within the state-of-the-art and provided complete temperature control for the spacecraft during ground testing, prelaunch, ascent, and orbital phases.

Multilayer Insulation and Coatings—The design of the external structure was generally based on the passive approach of using coatings and multilayer insulation wrap or preformed blankets (aluminized mylar interspaced with nylon scrim cloth). Insulation also covered all but the north and south sides of the EVM with specially cut sections for the prime-focus feed elements and for the Earth-viewing surface.

The insulation consisted of 30 layers of 1/4-mil aluminized Mylar with a 2-mil aluminized Kapton cover sheet. The effective emittance was consistently verified (through testing) to be less than 0.02. A typical thermal blanket configuration is shown in Figure 9-3. The method of thermal control indicated in the figure was the general approach used on protruding components that had an interface with blankets.

The multilayer insulation cover on the reflector support truss was coated with Z-306 black paint that had an $\alpha = 0.85$ and $\epsilon = 0.92$. These properties tended to maintain the trusses at nominal temperatures for a wide range of orbits, and hence complemented the inherently low values of thermal expansion coefficient (on the order of 2×10^{-7} cm/cm/°C) of the graphite fiber reinforced plastic (GFRP) that practically eliminated thermal distortions. The GFRP tube/solar array harness interface is shown in Figure 9-4. Because the power losses along these cables were high, the harness only needed to be partially insulated.

The selection of a low absorptance/high emittance coating for ATS-6 was subject to the strict requirement that only minor degradation be permitted for a 5-year mission. Flight and laboratory data had consistently shown that optical solar reflector (OSR) wafers, made of vapor-deposited silver on 8-mil thick fused silica, would remain stable for indefinite periods of exposure to a synchronous altitude environment.

The purpose of applying an optical solar reflector (OSR) to the north and south panels of ATS-6 was to render the EVM as insensitive as possible to flux inputs from the Sun. Flight data taken between long time intervals indicate that the surface characteristics remained unchanged throughout the 5-year mission.

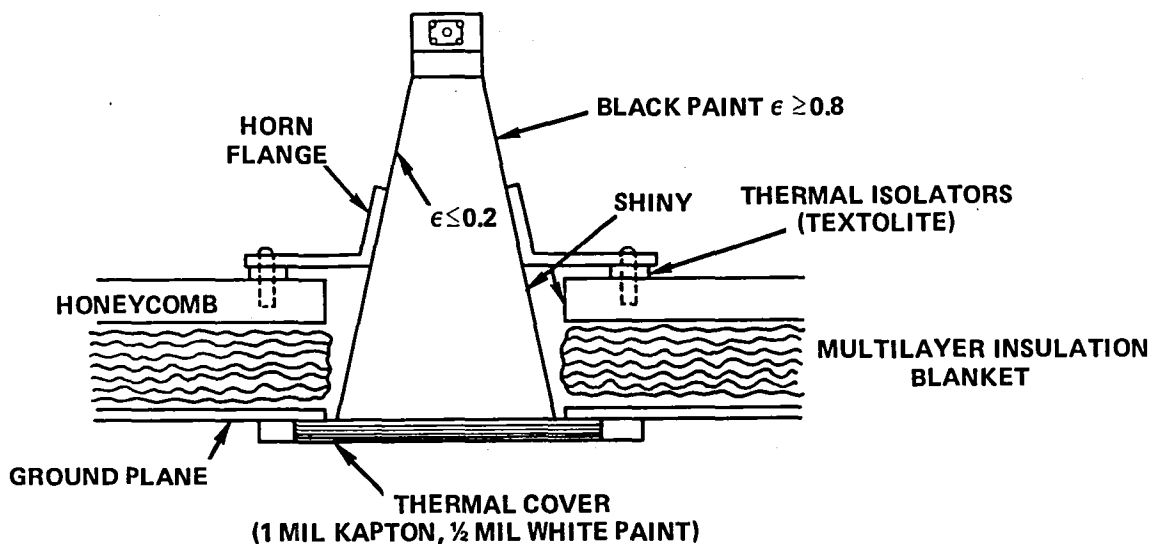


Figure 9-3. Interferometer Horn Thermal Design
(Typical Interface with EVM Blankets)

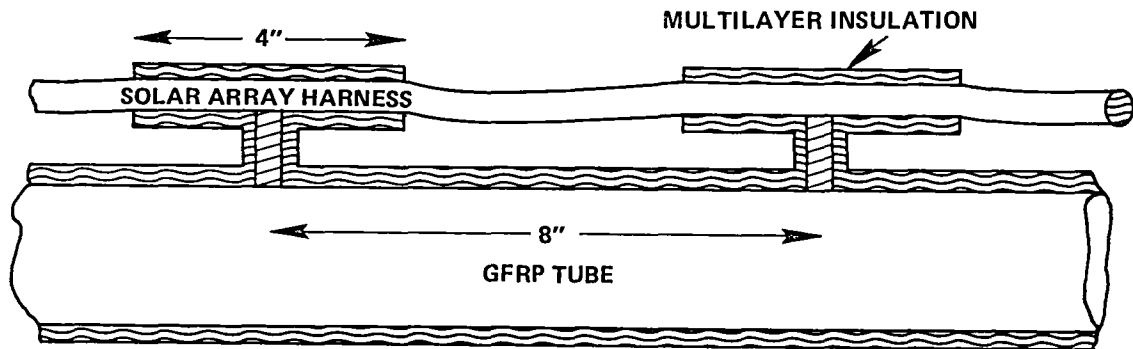


Figure 9-4. GFRP and Solar Array Harness Insulation

Other locations on ATS-6 requiring low solar absorptance and high emittance treatment included a few nonuniform surfaces on the panels where it was difficult to apply OSR, and the edges of the louver blades where such coatings would significantly reduce the temperatures resulting from solar impingement. Thermatrol S13G white paint was used in these areas. The limited use of this coating did not compromise the success of the mission despite the degradation in the absorptance.

Black paint Z-306 with primer was used on the outer cover of multilayer insulation throughout the structure external to the EVM. (The Kapton covers of the EVM itself were left free of paint in order to take advantage of their relatively low α/ϵ ratio.) The properties of Z-306 are $\alpha = 0.90, \pm 0.02$ and $\epsilon = 0.88, \pm 0.22$. These characteristics tend to yield benign average temperatures during normal orbits. Z-306 was also used on the spacecraft propulsion subsystem external to the EVM and inside the EVM.

The solar array booms were treated with high temperature aluminized Kapton tape that provided the uniformity of surface characteristics required during the launch/deployment phase. The tape was especially developed for ATS-6 application and featured extremely well controlled properties.

To minimize the temperature of the solar arrays, the spaceviewing side of the substrate was coated with MS74 white paint (degraded $\alpha = 0.40$ and $\epsilon = 0.90$). This coating was developed by NASA and is known to have one of the highest values of emittance associated with white paints. The high emittance leads to relatively cool solar cell temperature in orbit.

Louvers—The north and south faces of the EVM were honeycomb panels covered by a total of 3.2 square meters of thermal louvers. Figure 9-5 is a photograph of a typical set. The louvers were enclosed within rigid, lightweight, polished aluminum frames containing low-friction pivots for the blades. The blades were made of thin, highly polished, specular finish aluminum, and were individually actuated by bimetallic sensors located in a housing that was thermally isolated from the exterior environment. When the temperature of the interior panel rose, causing the bimetallic sensors to expand, the louver blades opened and allowed more heat to be radiated into space. A temperature change of 14°C would cause the louvers to rotate from fully open to closed positions.

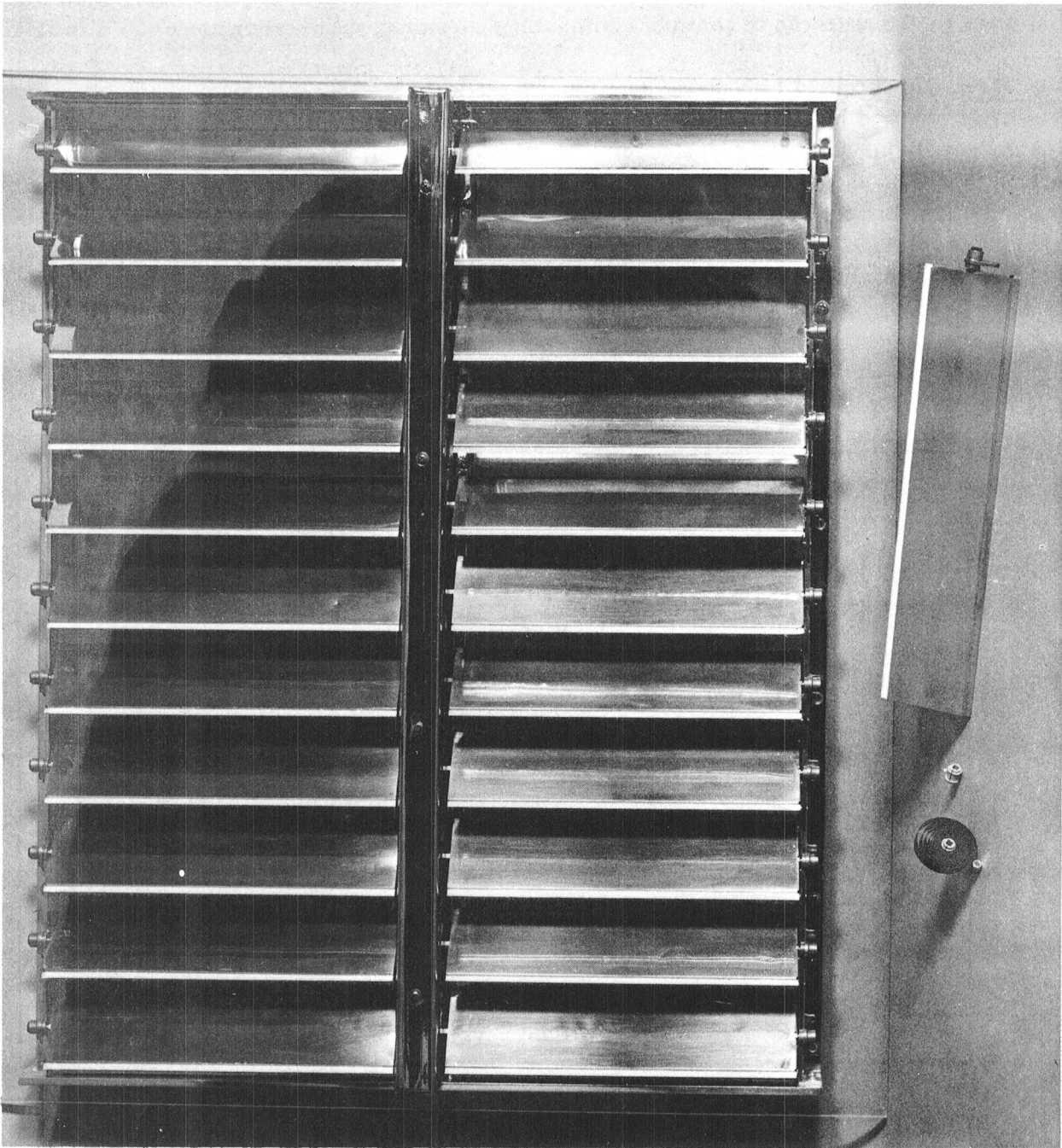


Figure 9-5. ATS-6 Louvers

The louvers provided the regulation of the temperature necessary to accommodate the wide fluctuation in power that resulted from the variety of operating modes. The effectiveness of the operation of the louvers is displayed in Figure 9-6. It is seen that a variation in power dissipation from 100 watts to 900 watts can be controlled within the temperature specification range of 5°C to 35°C.

Heat Pipes—The localized high power densities associated with ATS-6 solid state transponders were effectively removed by heat pipes. Their extremely high heat transport capability and the near isothermal conditions along their lengths resulted in smoothing out concentrations of power dissipation. In addition, the orbit inclination of ATS-6 produced solar heating loads on the north/south heat rejection surfaces during solstices and during spacecraft offset point conditions. Heat pipes provided the thermal path between the north and south faces so that the incident solar load on one face was transported to the other face that was in shadow.

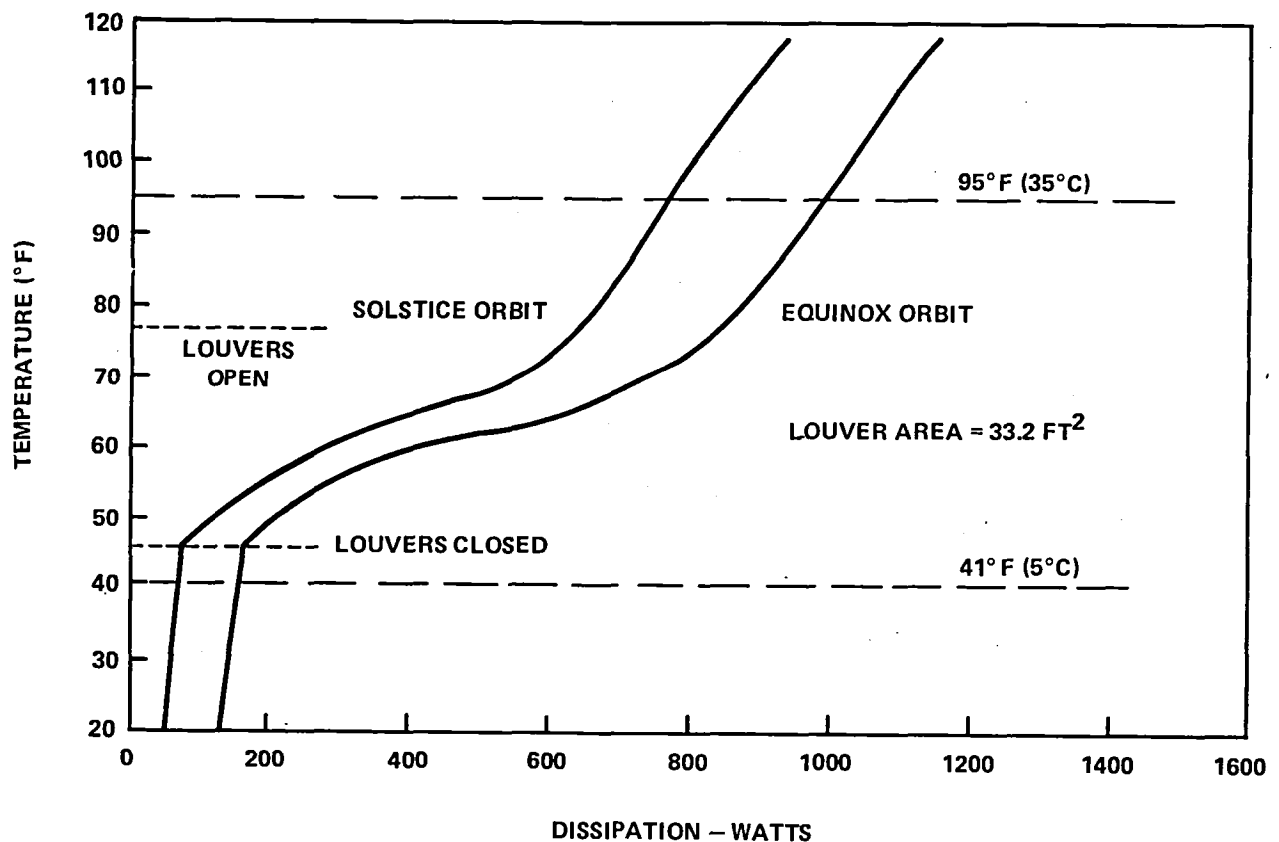


Figure 9-6. EVM Average Temperatures

The heat pipes were fabricated from 1.27-centimeter (1/2-inch) square aluminum tubes that were bonded as an integral part of the north and south honeycomb panels and of the transverse bulkheads connecting the north and south panels. In all cases the heat pipes ran parallel to the top and bottom surface of the EVM, which facilitated ground thermal testing. Ammonia was used as the working fluid because of its high heat transfer capability, its compatibility with aluminum, and the wide temperature range over which it can operate in a liquid-vapor phase. The layout within the spacecraft was as indicated in Figure 9-2.

Three configurations were used to conform with spacecraft and components envelopes. These are shown in Figure 9-7(a). The cross section is a grooved design as shown in (b). The design requirements were as follows:

Thermal Performance

Straight Pipes:

Heat load	60 watts
Input/output	30.48-cm (12-in.) evaporator/remainder of heat pipe condenser
Transport capability (maximum)	3810 W-cm (1500 W-in.)

Cee and Zee Pipes:

Heat load	20 watts
Input/output	15.2 cm (6-in.) evaporator/15.2 cm (6-in.) condenser
Transport capability	3175 w-cm (1250 W-in.)

All Pipes:

ΔT —Total	Less than 10°F (maximum) Evaporator to minimum (condenser)
ΔT —Within evaporator	3°F maximum
ΔT —Within condenser	3°F maximum
Tilt	Evaporator Elevated 2.54 mm (0.1 in.)

Ammonia Purity

99.995 percent

Maximum Liquid Slug Length

2.54 cm (1 in.)

Pressure

119.5 kg/cm² (1700 psia) at 270°F

Operating Temperature

5° to 40°C (41° to 104°F)

Qualification Temperature

-20° to 65°C (-4° to 149°F)

Weight

0.2 gm/cm (0.2 lb/ft)

Straightness

8.33×10^{-4} cm/cm (0.010 in./ft)

Operating Life

2 to 5 years

Reliability Goal

0.99999 for 2 years

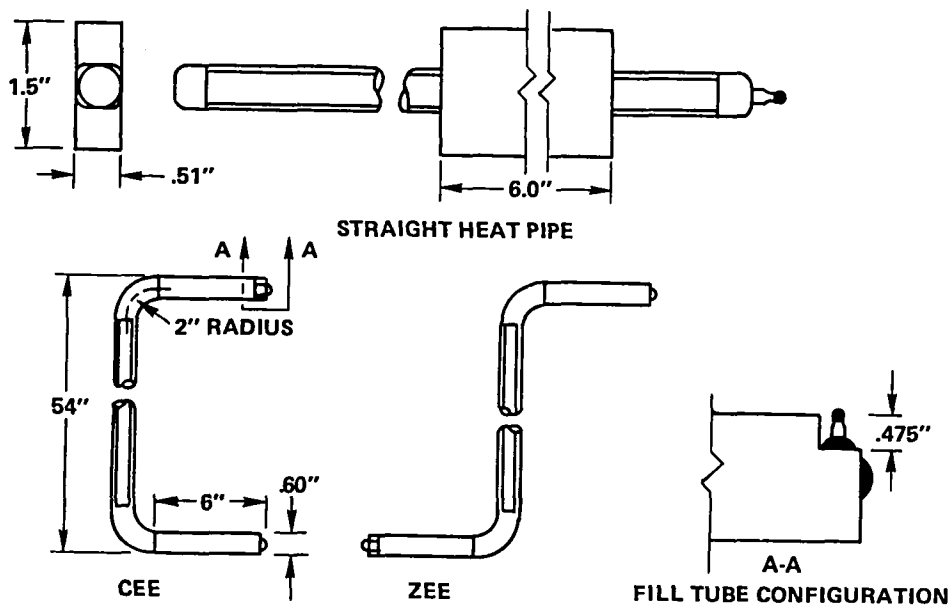
Vibration (all axes, qualification only)

PSD Level

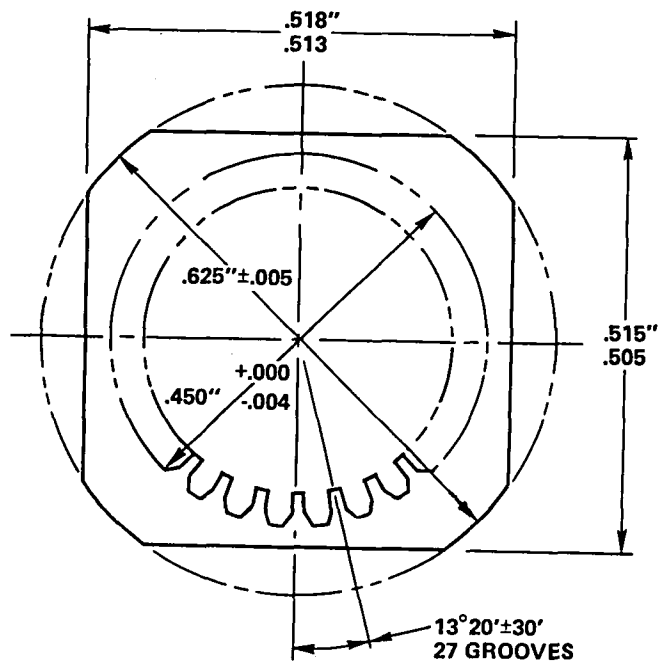
0.001 to 0.16 g²/Hz at 20 to 250 Hz
0.16 g²/Hz at 250 to 2000 Hz

Overall Acceleration

17.0 g—rms at 20 to 2000 Hz



(a) ATS-6 HEAT PIPE ENVELOPE DRAWING



(b) ATS-6 GROOVE HEAT PIPE DESIGN

Figure 9-7. Heat-Pipe Design

Heaters/Thermostats—The external components of the propulsion subsystem were maintained at the required temperature by using heaters and thermostats. The heater strips on the propellant line were activated by thermostatic control so as to keep the line at nominal temperatures during all phases of launch and orbit operations. A description of the spacecraft propulsion subsystem design and its operation are detailed in Volume II of this report.

CHAPTER 10

THERMAL CONTROL SUBSYSTEM DESIGN VALIDATION

INTRODUCTION

The variety of spacecraft operating modes resulted in a wide fluctuation in the amount of heat generated within the EVM. When the power variation occurred at a correspondingly biased spacecraft orientation, some of the electronics mounting surface temperatures could actually span the allowed specification ranges shown in Table 9-1, Chapter 9. In addition, it was agreed upon early in the program that maximum properties tolerances be considered realizable, and minimum restrictions be imposed on the launch profile and on the duration of spacecraft deployment. For these reasons, it was necessary to employ a high level of sophistication in analysis, and to provide an extensive thermal test and qualification program to verify the proper performance of all systems under the most adverse environmental conditions.

The thermal control subsystem was unique because it employed heat pipes and sunlit louvers as primary components for temperature control. Louvers used on satellites previous to ATS-6 were located in shadow or protected by sunshields. Earlier heat pipes were flown as experimental items or as secondary thermal hardware.

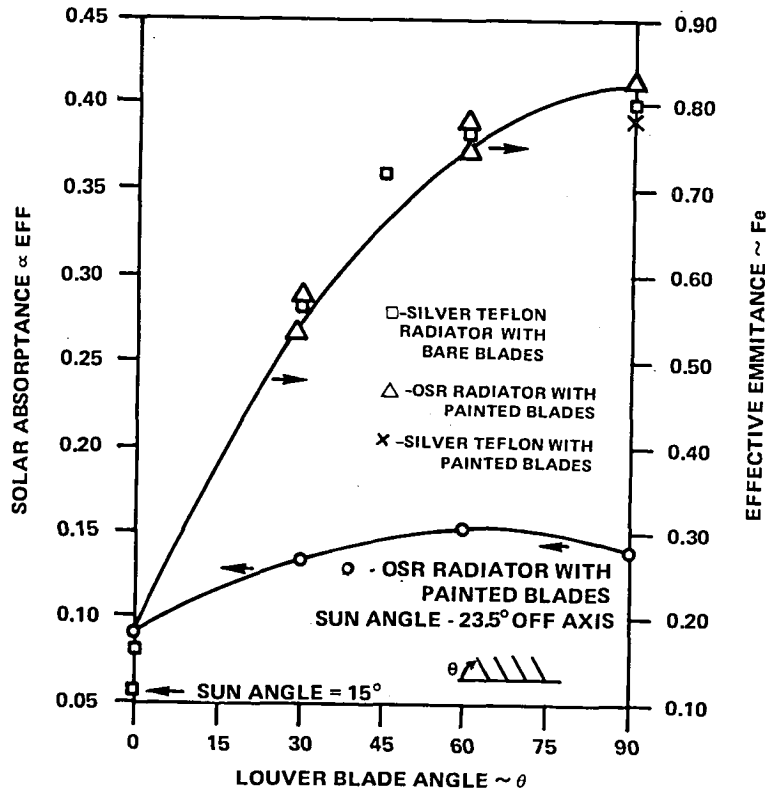
MATHEMATICAL MODELING

Louvers Analysis

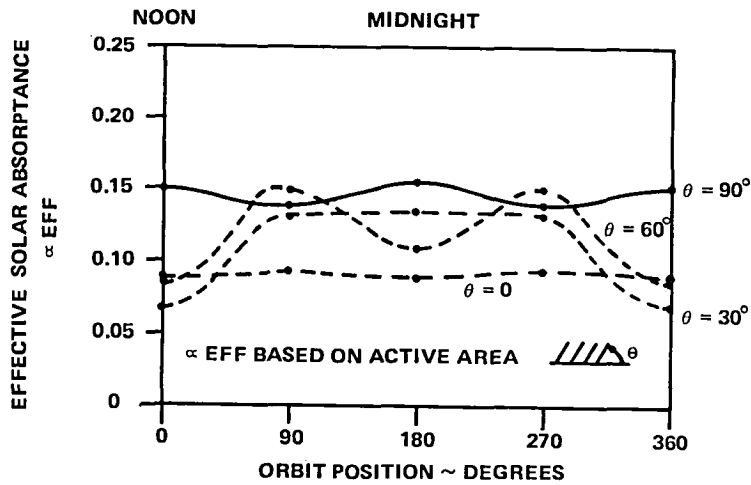
The complexity in modeling techniques introduced by louvered panels with variable emittance and absorptance was resolved by correlating analytical results to data from tests designed to determine the properties of louvers. The data most pertinent to the analysis are described in Figure 10-1 (a) and (b). Two techniques were used simultaneously in application to the EVM panels. First, the computer would calculate an average temperature of the panel and perform an interpolation on the effective emittance and absorptance curves per program iteration. The approach was very efficient in computer time but the error introduced in the temperature distribution was significant. However, the average temperature calculated for the panel was sufficiently accurate to serve as the basis for the first iteration on a multinode network as shown in Figure 10-2. As an example, the temperature of nodal point 17 was used to set the emittance on nodes 6 and 28. The EVM thermal model had 160 pairs of blades that were modeled in this manner. One significant finding was that the louvers caused a substantial reduction in the temperature gradient along the honeycomb/heat-pipe panels.

Heat Pipe Modeling

The method employed on modeling the heat pipes was based on generating a listing of effective conductances between the heat-pipe vapor and the walls of the pipe. The vapor core was modeled as an



(a) LOUVER SOLAR SIMULATION TEST RESULTS.



(b) LOUVER EFFECTIVE SOLAR ABSORPTANCE VS. ORBIT POSITION: 23.5° ORBIT INCLINATION.

Figure 10-1. Louver Characteristics

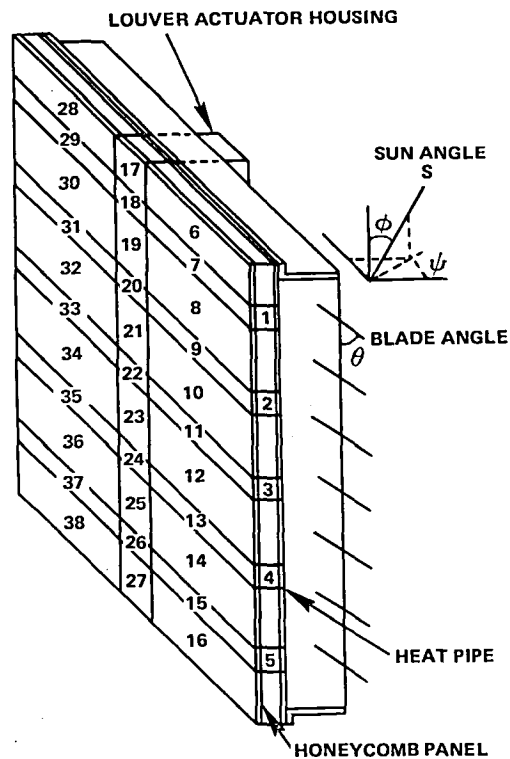


Figure 10-2. Thermal Model for Heat-Pipe-Honeycomb Panel with Exterior Louvers

isothermal node along the entire length of the pipe, and the honeycomb panel/heat-pipe wall interface was divided into a number of isothermal nodes. A typical arrangement is shown in Figure 10-2. The inner and outer facesheets of the honeycomb panel were combined into a set of single nodes connected to the heat-pipe vapor node. Because the pipes had only two sides, bonded to the facesheets, a fin effectiveness was introduced as a correction factor to account for a partial conduction path from the vapor to the panel through the heat pipe wall. The factor ranged between 0.37 and 0.48.

Effective conductances for heat-pipe/honeycomb panel heat transfer were calculated using test data derived from both heat-pipe acceptance tests and engineering tests run on individual panel sections. The conductance value used for the straight heat pipes was 0.18 W per degree C per linear cm of heat pipe. This value included a 0.0076-cm epoxy bond line thickness between the heat pipe and facesheet. Schematically, this value is the conductance between the heat-pipe vapor node 1 and the honeycomb facesheet node 7, Figure 10-2.

EVM Math Model

The EVM thermal math model consisted of more than 1000 nodal points. The primary heat-rejection surfaces were modeled as shown in Figure 10-2. In general, electronic components were modeled only up to the mounting surface. The baseplate (or bottom) of the box was modeled so that the

correct power dissipation profile was maintained. Detailed mounting surface temperature maps were prepared, and supplied to the electronic component subcontractors who performed internal box thermal analysis.

Various engineering tests were performed to determine heat leaks and gradients of specific hardware items such as antenna horns and Earth sensors. The results of these tests were incorporated into the math model as they became available. Multilayer insulation covered over 5.6 square meters of the EVM and was assumed in the model to have an effective emittance of 0.015 with a tolerance of ± 0.005 . The mathematical model was set up in SINDA format and was processed on an IBM 360-70 computer. The majority of math model runs were steady-state cases for the many power modes on the spacecraft. Selective orbital transient cases were executed to determine in-orbit temperature profiles on the batteries and gradient-sensitive experiments.

Black paints were applied to the internal panel surface and power dissipating components to increase internal radiation heat transfer. Because of a very large number of internal nodes and location changes, it was not practical to evaluate the configuration factors between nodes. Therefore, the interior cavities, divided by the transverse beams and three module interfaces of the EVM, were taken as dummy space nodes and radiatively coupled to all of the surrounding surface nodes. This method of calculating internal radiation was considered to be conservative if all internal surfaces were painted black.

The majority of computer runs were devoted to the three basic design cases for the spacecraft (hot, nominal, and cold) plus two special test evaluations cases. The hot case considered two operational modes: (1) the Health, Education, Telecommunications experiment power modes, and (2) the Millimeter Wave experiment. The cold design case was the power-off (except for telemetry) condition. The test points evaluated heat leaks with louvers fully open and closed.

TESTING

Thermal-Structural Model

The Thermal-Structural Model (TSM) was a full-scale engineering mockup of the ATS-6 spacecraft. The thermal control subsystem of the TSM EVM and the ATS-6 EVM were identical. A full set of 55 heat pipes was bonded into the TSM's honeycomb walls. Each heat pipe was subjected to a performance acceptance test before being implemented into the mockup's structure. Fifteen sets of thermal louvers were attached to the north and south walls of the TSM with the open and closed positions of the louver blades calibrated to flight specifications. Heaters were bonded to the north and south walls directly under the louvers and were used during thermal vacuum tests to simulate absorbed solar energy. Heaters also were bonded to the remaining four sides of the TSM to simulate the effects of the Sun. Dummy boxes, with heaters bonded to the baseplates, were installed into the TSM to simulate the weight and heat dissipation of flight electronic equipment. The mounting arrangement of these dummy boxes and the actual flight electronic boxes was identical.

Three design conditions for the spacecraft were tested to determine the performance of the thermal control subsystem and the predictability of the math model. In addition, two engineering tests were

performed to evaluate the total heat leak of the spacecraft. These tests were run at temperatures that forced all of the louvers either open (one test case) or closed. A comparison of predicted versus tests temperatures for the communication module heat pipes is shown in Figure 10-3, for the HET operational mode. The test temperatures of the three or more thermocouple readings were taken along each heat pipe. The predicted temperatures are the heat-pipe vapor temperatures. Excellent correlation between analytical and experimental temperatures is seen.

Verification and Qualifications Tests

Analysis and design were verified through an extensive thermal testing and qualification program. The most significant of these tests and their conclusions are summarized in Table 10-1. The monitored flight temperatures generally fall well within the qualification limits.

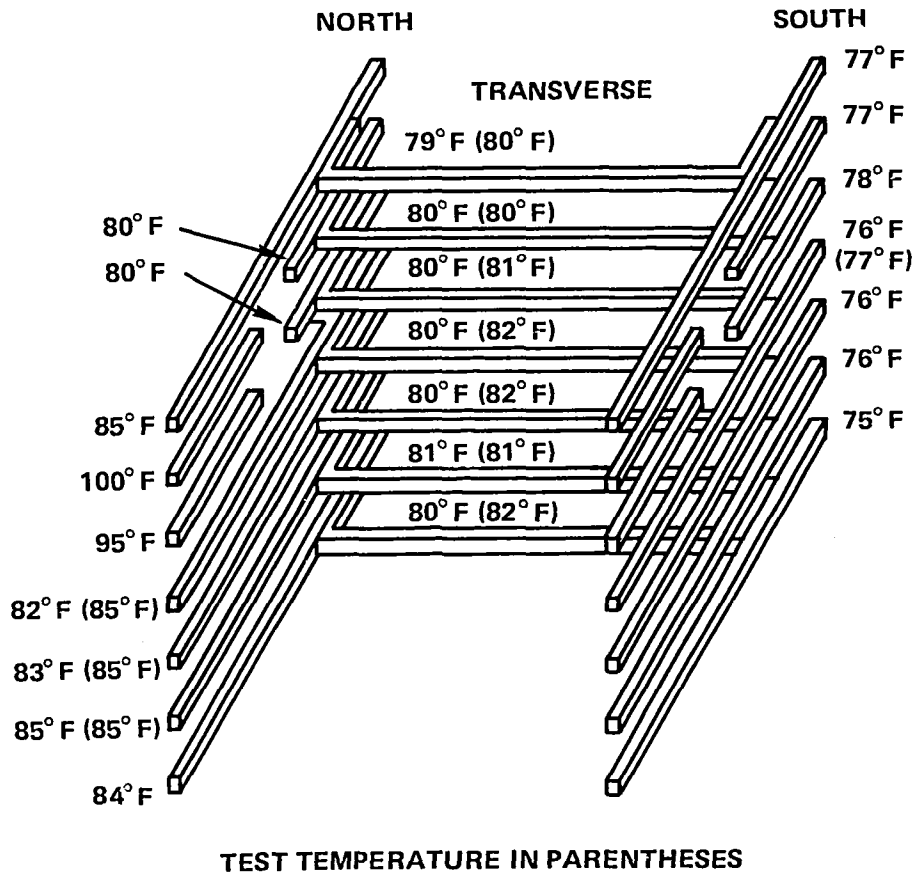


Figure 10-3. Predicted vs. Test Temperatures for Heat Pipes in Communications Module

Table 10-1
ATS-6 Components, Structure Qualification, and Actuals

COMPONENT	PREDICTION (°C)	ACTUALS FLIGHT (°C)	DESCRIPTION OF QUALIFICATION TESTING
EVM Electronics Mounting Panels (General)	5 to 35	20 to 30	<p><u>Component Level Thermal Cycling</u></p> <p>Individual components were mounted in vacuum on temperature controlled platforms in exactly the same fashion as in actual spacecraft. The component cover was wrapped with multilayer insulation and the chamber walls maintained at about 22°C. Functional tests were conducted at platform temperatures of -10°C for 6 hours and 50°C (35°C for the batteries) for 6 hours. The cycle was repeated three times.</p> <p><u>Spacecraft Level Thermal Vacuum Tests</u></p> <p>Functional performance of flight components was verified on protoflight spacecraft in vacuum. Infrared lamps were used to maintain the mounting panels at 50°C (35°C for the batteries) for 60 hours. Cryogenic walls aided in maintaining panels at -10°C also for 60 hours. Cycle was repeated 6 times.</p> <p><u>Spacecraft Thermal Balance Test</u></p> <p>Functional performance was verified on protoflight during a hot case, nominal case, and cold case thermal balance test.</p> <p>Units were qualified as above. The component level qualification was performed at mounting platform temperature range of -12°C to 50°C.</p>
Batteries (Mounting Panel) (Gradient)	0 to 25 5	15 to 25* 2 to 3	
Earth Sensors (Mounting Surface) (Bolometer)	3 to 45 -7 to 50	5 to 42 1 to 59**	

*The monitored flight temperature registered 29.1°C during November 1974. The high value was attributed to the effects of unusual combination of C/60 charge rates, spacecraft operations, and pointing maneuvers.

**The maximum monitored daily temperature increased at the rate of about 2°C per year due to degradation of white paint on the sensor head.

Table 10-1
 ATS-6 Components, Structure Qualification, and Actuals (Continued)

COMPONENT	PREDICTION (°C)	ACTUALS FLIGHT (°C)	DESCRIPTION OF QUALIFICATION TESTING
Earth Sensors (continued)			Additional component functional tests were performed in vacuum with solar simulation (three incident angles) and the mounting panel ranging in temperature between 0°C (cold case) and 45°C (hot case). The Earth sensor bolometer temperature during solar simulation was recorded at 55°C. No degradation or irreversible damage was observed.
Polaris Tracker (Mounting Bracket)	8 to 27	14 to 28	
Digital Sun Sensors	0 to 40	(not monitored)	The units were qualified as above at the component level between -45°C and 50°C. Workmanship and stress relief of solar cells (sensing element) were verified by thermal cycling between -83°C to 85°C (ten cycles in about 3 hours).
Solar Arrays (Local) (Average)	-160 to 52 -95 to 22	-150 to 56*	All flight panels were qualified while assembled within framed stringers which simulated the exact mechanical boundaries. The arrays were thermally cycled in vacuum (using Infrared lamps and cryogenic walls) 50 times in about 150 hours between -160°C and 60°C. Post test electric continuity and current data confirmed proper workmanship and adequate bonding of the cells.
Solar Array Booms (Local) (Predeployment Average)	-55 to 116 -23 to 93	-35 to 117 5 to 60	<p><u>Hinge Motion</u></p> <p>Hinge motion was demonstrated on the Thermal-Structural Model booms at acceptance level temperatures (-23°C to 93°C). The test configuration included a simulated solar array interface.</p> <p><u>Thermal Development Model Tests</u></p> <p>The thermal characteristics (including surface properties, cool-down rates, joint conductances, and harness interface properties) were verified using a 122-cm sample construction that featured flight material. Testing included solar simulation.</p>

*By the end of 1977 only one out of four solar arrays thermistors remained intact. The data from the last one became erratic by 1978 and no significance was any longer attached to the monitored values.

Table 10-1
ATS-6 Components, Structure Qualification, and Actuals (Continued)

COMPONENT	PREDICTION (°C)	ACTUALS FLIGHT (°C)	DESCRIPTION OF QUALIFICATION TESTING
GFRP Trusses and Rib Fitting	-73 to 35	-50 to 20	Two 40.6-cm specimens with flight type titanium fittings and bonding agent survived a soak test in LN ₂ (-160°C) while under 4535.9 kg (10,000 lb) compression load. The same specimens survived five thermal cycles between -73°C and 93°C with 20,411 kg (45,000 lb) compression load.
Deployment Dampers (During Deployment) (In Orbit)	-33 to 30 -46 to 54	14 to 22 -45 to 50	Dampening rates were confirmed in vacuum at -48°C, 20°C, and 46°C. No fluid leakage was detected during 12 hours soak at 70°C.
Parabolic Reflector (During Deployment)	-10 to 19	10 to ±5*	Deployment was confirmed for the flight unit in vacuum (at Houston) under three conditions: <ol style="list-style-type: none"> 1. Unfurling at steady state bulk temperature – 18°C (cold case) 2. Unfurling at steady state bulk temperature + 34°C (hot case) 3. Unfurling at steady state solar simulation with solar vector impinging on the edge (maximum peripheral gradient)
External Harness	-160 to 135	(not monitored)	No degradation was observed on flight type harness during EVM thermal balance tests and subsystem solar vacuum tests.
Multilayer Insulation and Adhesive Tapes	-184 to 120	(not monitored)	Effective emittance and resistance to degradation of blankets and associated tapes were verified during thermal balance and solar vacuum tests. East-west blankets performance was verified on a mockup of the communications module in vacuum. Development program confirmed effectiveness and technique of blanket “free wrapping” on trusses, EVM corner fittings, and external portions of the SPS.

*Thermistors location and installation techniques were intended for monitoring the average temperature in the unfurled configuration. Flight data after deployment does not indicate average temperature.

Table 10-1
ATS-6 Components, Structure Qualifications, and Actuals (Continued)

COMPONENT	PREDICTION (°C)	ACTUALS FLIGHT (°C)	DESCRIPTION OF QUALIFICATION TESTING
<p>Multilayer Insulation and Adhesive Tapes (continued)</p> <p>Thermal Louvers (Actuator) (Blades and Frames)</p>	<p>5 to 35 -73 to 150</p>	<p>15 to 35* (not monitored)</p>	<p>Proper venting of blankets was verified in high altitude chamber in which the pressure dropped from sea level to 45,720 m (150,000 ft) elevation in 30 seconds.</p> <p><u>Louvers Parts Tests</u></p> <p>(a) Vespel shafts survived 0.56 Nm (5 in-lb) moment tests at -100°C, 20°C, and 170°C. (b) Adhesive outgassing requirements were met in vacuum at -100°C to 190°C. (c) Blades thermal properties and structural integrity verified at -100°C to 190°C. (d) Actuator springs angular motion was verified at -5°C to 45°C. (e) No degradation was observed on paint and housing insulation materials in solar vacuum tests.</p> <p><u>Development Model Tests</u></p> <p>Effective emittance, absorptance, and blades motion were verified in solar vacuum. No degradation was observed.</p> <p><u>Flight-Type Qualification Model Tests</u></p> <p>Effective emittance and absorptance verified in solar vacuum at various Sun incident angles. Baseplate-to-actuator gradient was confirmed to be within ±3°C.</p> <p><u>Thermal Balance Tests</u></p> <p>The performance of flight louvers was verified during thermal balance tests of EVM.</p>

THERMAL CONTROL SUBSYSTEM DESIGN VALIDATION

*Flight thermistors are not located directly on the actuators. The data reported are those for the baseplate temperature in the vicinity of the actuator housing which, based on ground test results, runs at ±2°C from the mounting panel.

Table 10-1
 ATS-6 Components, Structure Qualifications, and Actuals (Continued)

COMPONENT	PREDICTION (°C)	ACTUALS FLIGHT (°C)	DESCRIPTION OF QUALIFICATION TESTING
Heat Pipes	5 to 35	20 to 30	<p>Qualification program on subsystem level included the following:</p> <ul style="list-style-type: none"> (a) Proof pressure tests at 132°C for 2 hours (b) Confirmation tests showing ammonia leakage less than 3×10^{-7} scc/sec (c) Three pipes of each ship set passed -10°C to 50°C performance tests (d) Two typical straight pipes functioned properly during zero G sounding rocket tests <p>Spacecraft level performance was verified during thermal balance and thermal cycling tests.</p>
Feed Farm Elements	-24 to 93	8 to 60*	<p>Performance confirmed in vacuum as follows:</p> <ul style="list-style-type: none"> (a) Hat coupler in place and inner panel 10°C colder than coupler. EVM was at 5°C and farm cavities viewed LN2 wall (b) Hat coupler in place and inner panel 10°C higher than coupler. EVM at 35°C and hat coupler heater adjusted to achieve cavity temp = 93°C.
Spacecraft Propulsion Subsystem (SPS)			<p><u>Blanket Wrap Technique</u></p> <p>Small diameter tube insulation technique verified by testing in vacuum of insulated simulated hydrazine lines.</p>
(EVM Valves & Lines)	5 to 45	20 to 28	
(OCJ Bar Valves)	14 to 96	10 to 92**	
(OCJ Bar Lines)	16 to 71	30 to 60†	
(Thruster CATBED)	-50 to 800	>-50	<p><u>External SPS Engineering Model Tests</u></p> <p>Thermal engineering model of the portion of SPS external to the EVM was tested in vacuum to verify the following:</p> <ul style="list-style-type: none"> (a) Insulation effectiveness and reproducibility (b) Valve-line and line-structure joint conductances (c) Adequacy of valves heater power

*Thermistor located inside EVM on upper panel of the communication module

**Valve heater failure on October 12, 1976 resulted in minimum valve temperature of about 2°C

†Manual operation of line heaters to improve valve temperatures after valve heater failure resulted in line temperature of about 105°C

Table 10-1
 ATS-6 Components, Structure Qualifications, and Actuals (Continued)

COMPONENT	PREDICTION (°C)	ACTUALS FLIGHT (°C)	DESCRIPTION OF QUALIFICATION TESTING
Spacecraft Propulsion Subsystem (SPS) (continued)			<p>(d) Line temperature dependence on line heater power (e) Performance in solar vacuum environment</p> <p><u>External SPS Qualification Model Test</u></p> <p>Thermal qualification model with flight type valve and line heaters and thermostats verified the performance of the system under worst environmental conditions. The cold case had no flux and minimum EVM temperature with system viewing LN2 walls. Hot case had maximum solar input, maximum voltage for heaters, and maximum EVM interface temperature.</p> <p><u>Components Tests</u></p> <p>(a) Valve seats survived soak in LN2 and 115°C heating (b) Valve black coating survived oven temperature of 1200°C (c) Insulation blanket survived expected levels of hydrazine products impingement</p>

CHAPTER 11

THERMAL CONTROL SUBSYSTEM PERFORMANCE

DATA COMPILATION AND EVALUATION

Two categories of thermistors were installed in key locations where the temperature was representative of the immediate surrounding. The temperature control unit thermistors were generally associated with the internal structure of the electronics and monitored through both data acquisition and control unit 1 (DACU 1) and DACU 2. The power control unit thermistors, which included DACU redundancy for the spacecraft propulsion subsystem, and telemetry and command, were generally intended to evaluate the spacecraft thermal performance.

Temperature telemetry data were continuously compiled and stored throughout the 5-year mission. Data analysis was conducted on a periodic basis and the thermal control subsystem evaluated by relating the predicted performance to the flight temperature profiles at various orbit conditions and spacecraft operational modes. Data comparisons of similar orbits and similar operations, separated by extended time intervals, were used for judging the extent of material degradation or system malfunction.

THERMAL CONTROL SUBSYSTEM PERFORMANCE

The thermal control subsystem functioned satisfactorily during all modes of operation from launch through the entire 5-year mission. No serious flight anomalies were found to be connected to a degradation in the thermal control elements, and all spacecraft components were maintained at temperature levels within the qualification ranges. The uniformity of performance is evident from Table 11-1 that lists some flight temperatures taken at different intervals during the mission, and Figure 11-1 that illustrates the insensitivity of the EVM modules to various power modes and to life in orbit.

Early Mission Performance

An essential requirement for successful deployment was that the external structure temperature remain within the constraints established by a structure thermal loads analysis that translated the relative thermal distortions of the solar arrays, the reflector support structure, and the solar array booms to compressive forces on the booms. The analysis led to the temperature specifications requirements listed under the launch-ascent-acquisition column given in Table 9-1, Chapter 9. Proper deployment was also dependent on a range of damper temperatures for which the damping rate was within the acceptable limits.

Table 11-1
Component Base Temperatures

Component	Temperature (°C)			Qualification
	1974 7 Sept	1976 20 May	1979 19 May	
<u>CM</u>				
TWTA 1	20 to 30	21 to 28	28 to 31	-10 to 50
Ion Engine	19 to 26	21 to 24	21 to 24	-10 to 50
RBE Osc 1	22 to 28	23 to 24	24 to 28	-10 to 50
S-Band Xmtr	23 to 31	21 to 35	22 to 35	-10 to 50
<u>SM</u>				
Xmtr 1	28 to 35	32 to 34	32 to 34	-10 to 50
Xmtr 2	30 to 32	29 to 32	30 to 32	-10 to 50
Xmtr 3	27 to 32	28 to 31	28 to 31	-10 to 50
Xmtr 4	24 to 27	24 to 27	24 to 28	-10 to 50
Yaw Wheel	27 to 28	26 to 28	26 to 28	-10 to 50
Pitch Wheel	20 to 26	21 to 27	21 to 27	-10 to 50
Roll Wheel	24 to 28	23 to 28	23 to 28	-10 to 50
PCU	24 to 28	23 to 27	23 to 26	-10 to 50
SPS Tank 1	20 to 25	17 to 26	17 to 26	5 to 50
SPS Tank 2	22 to 26	19 to 28	19 to 28	5 to 50
ACE	26 to 28	28 to 31	28 to 31	-10 to 50
<u>EM</u>				
Battery 1	15 to 24	16 to 25	16 to 25	-10 to 35
Battery 2	15 to 24	15 to 25	15 to 25	-10 to 35
ES Roll	1 to 43	1 to 50	1 to 50	-12 to 50
ES Pitch	2 to 41	1 to 49	1 to 47	-12 to 50

CM – Communications Module

SM – Service Module

EM – Experiment Module

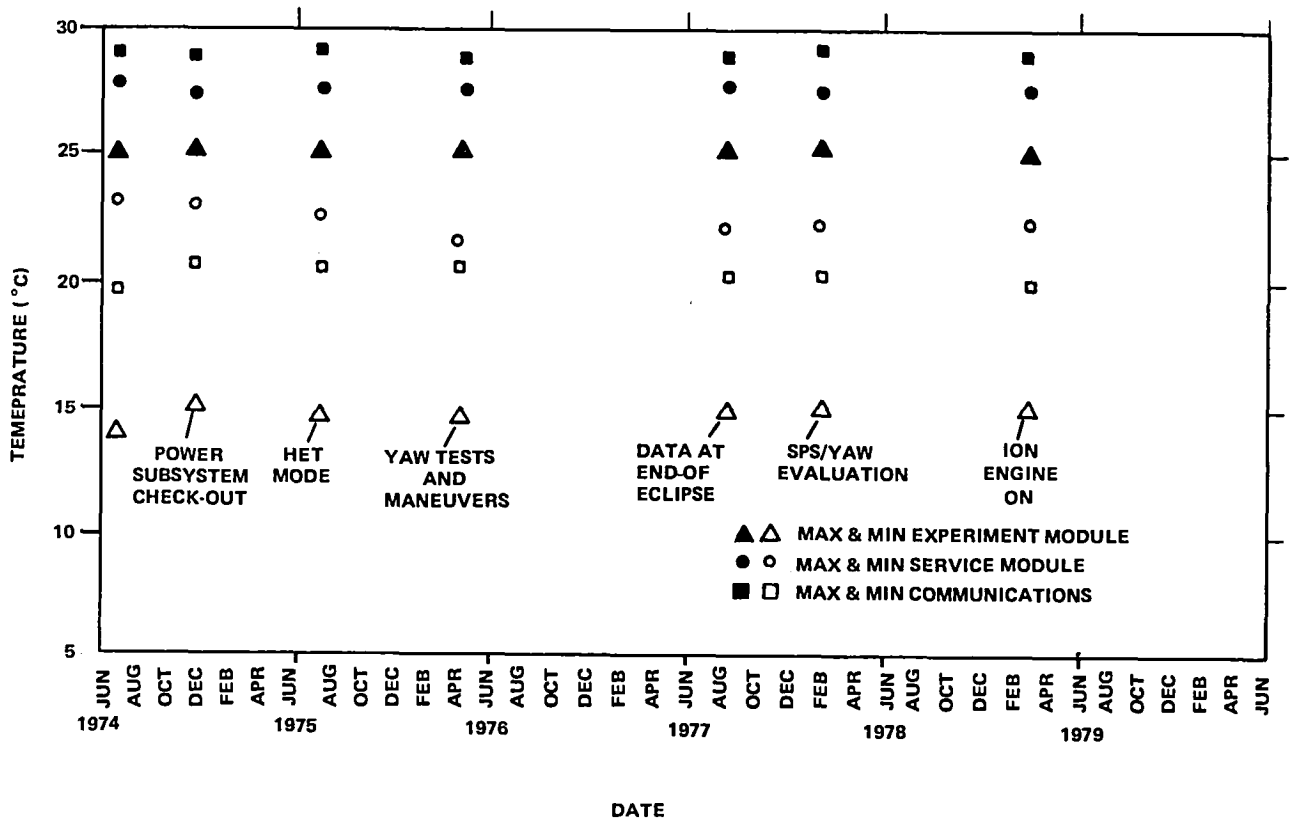


Figure 11-1. Average EVM Temperature (Heat Pipe Panels)

The external structure and the dampers were sufficiently instrumented to allow continuous monitoring of the temperatures during launch through final acquisition. The instrumentation provided the data necessary for making deployment decisions in the event of spacecraft disorientation.

Figures 11-2 through 11-6 give the launch-phase temperature profiles throughout the separation/deployment timeline. All of these met the specification requirements. Table 11-2 gives a comparison between expected and monitored temperatures.

Orbital Temperature

The EVM average temperature could be identified by thermistors located on the honeycomb face-sheets directly over the imbedded heat pipes. Each heat pipe triplet was designated by a number indicating its position along the spacecraft Z-axis. Some of the temperatures associated with the heat pipes are given in Figures 11-7 through 11-9. The orbit variation in temperature was reasonably small and falls within the specification requirements range of 20°C, ±15°C. The experiment module

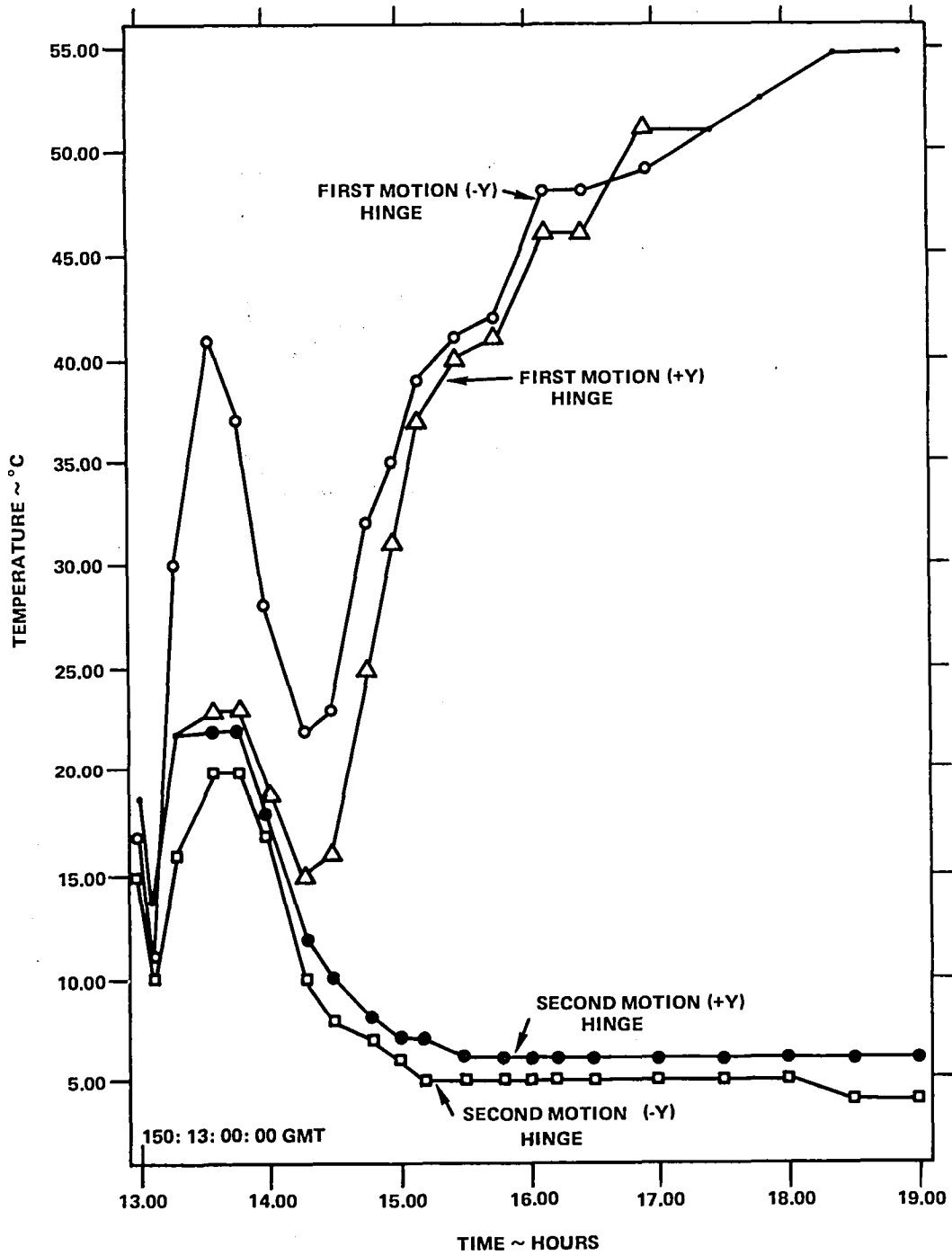


Figure 11-2. Launch Solar Array Boom Temperature (Sheet 1 of 2)

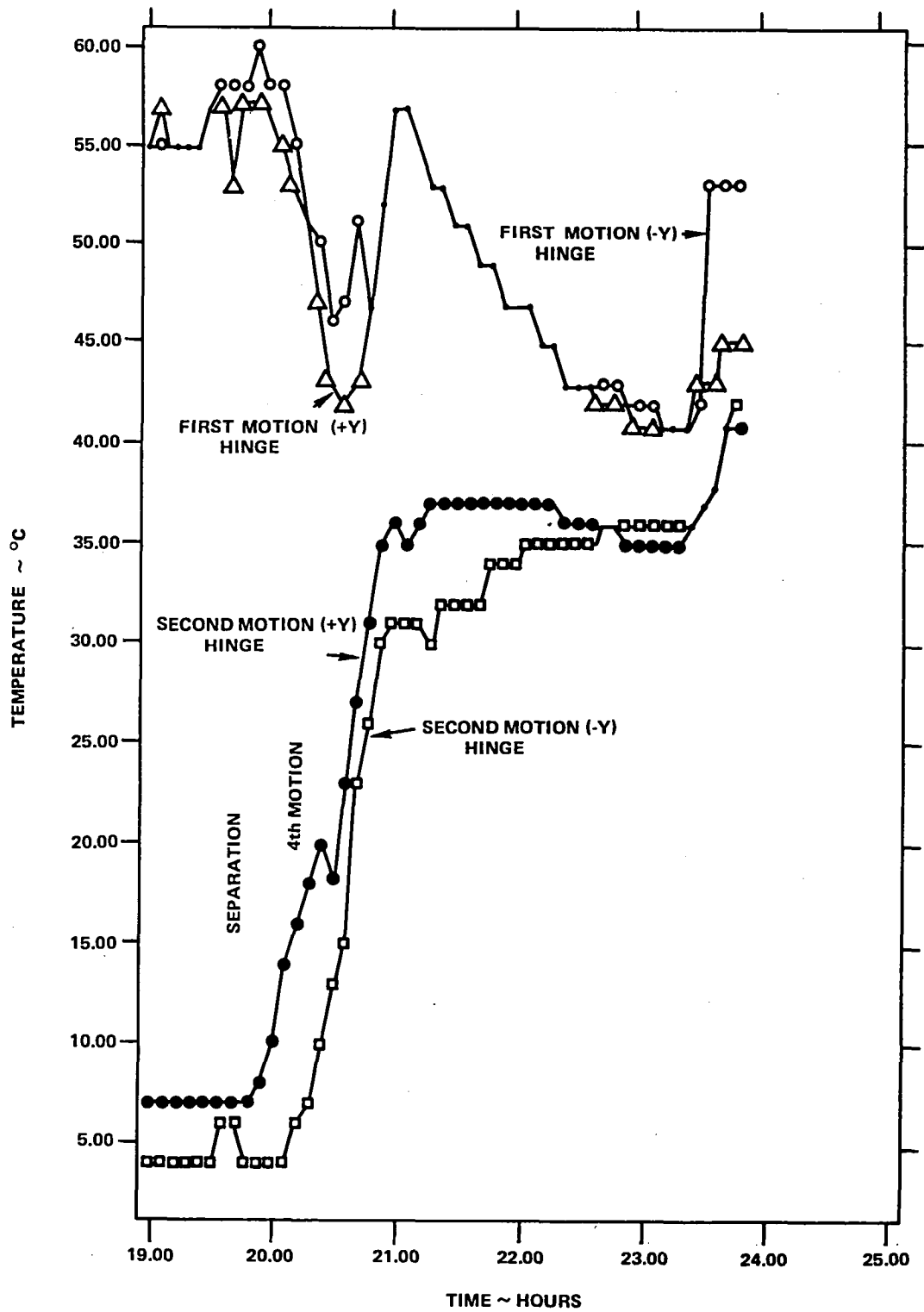


Figure 11-2. Launch Solar Array Boom Temperature (Sheet 2 of 2)

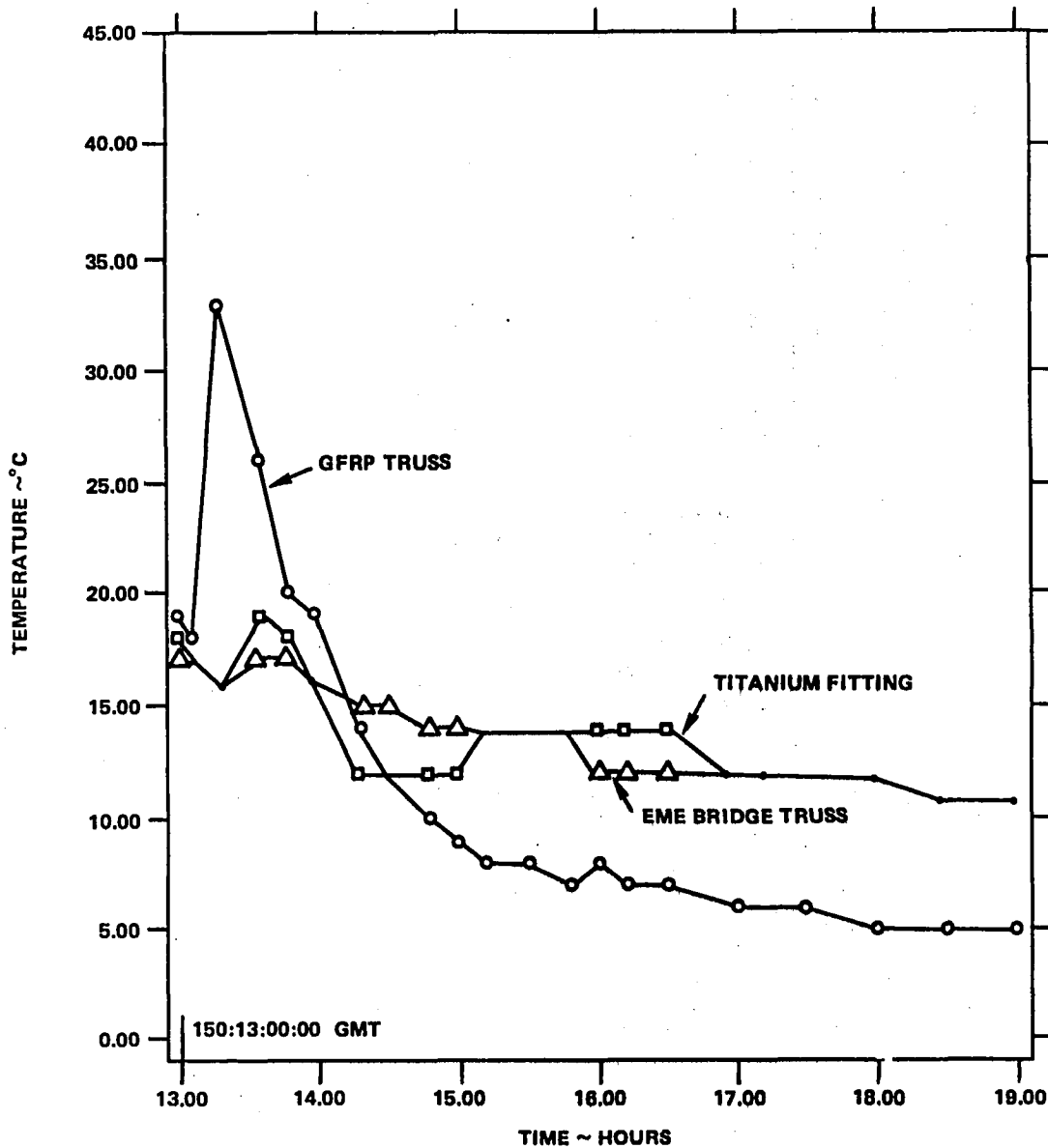


Figure 11-3. Launch GFRP, Fitting, and EME Truss Temperature (Sheet 1 of 2)

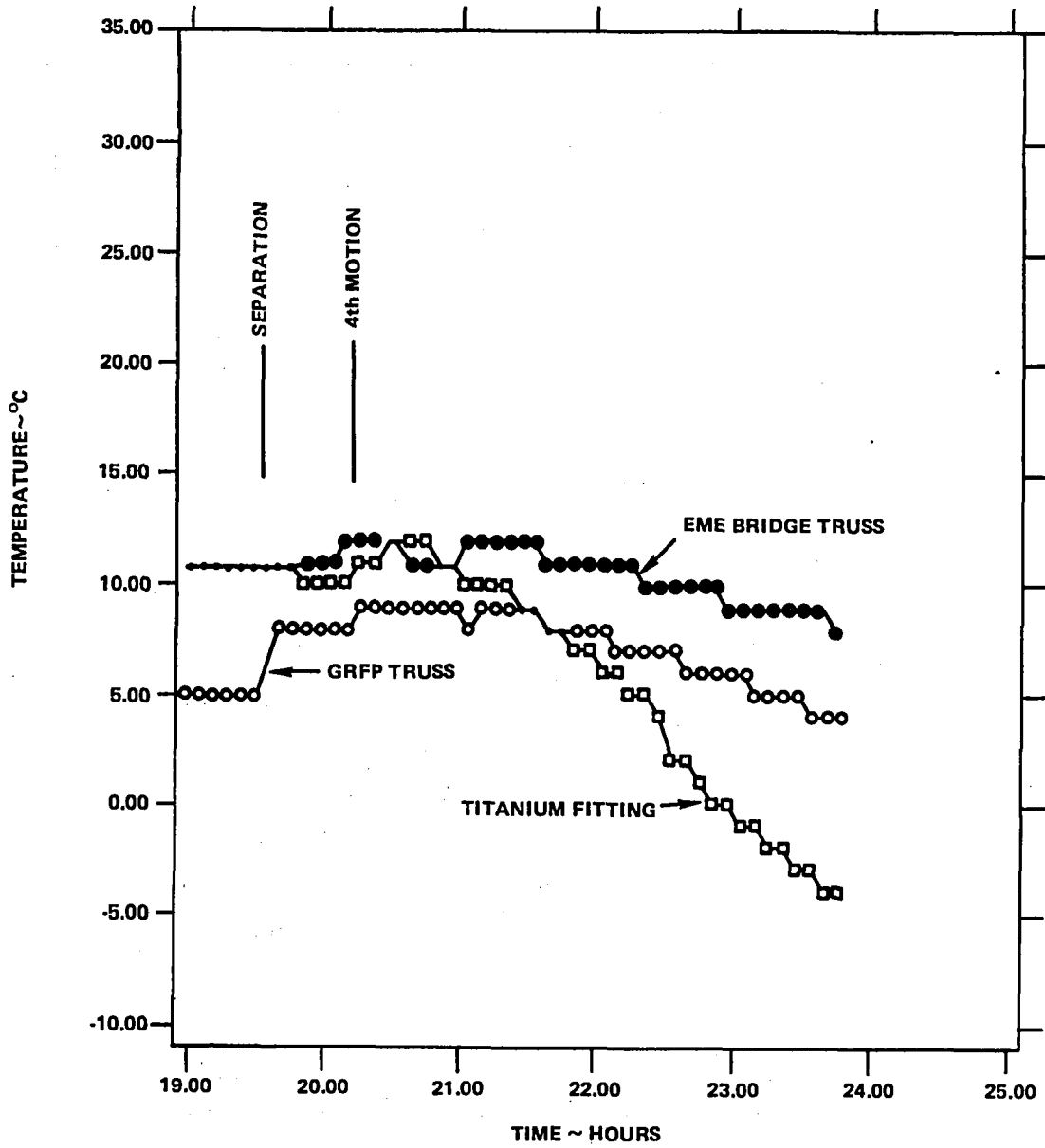


Figure 11-3. Launch GFRP, Fitting, and EME Truss Temperature (Sheet 2 of 2)

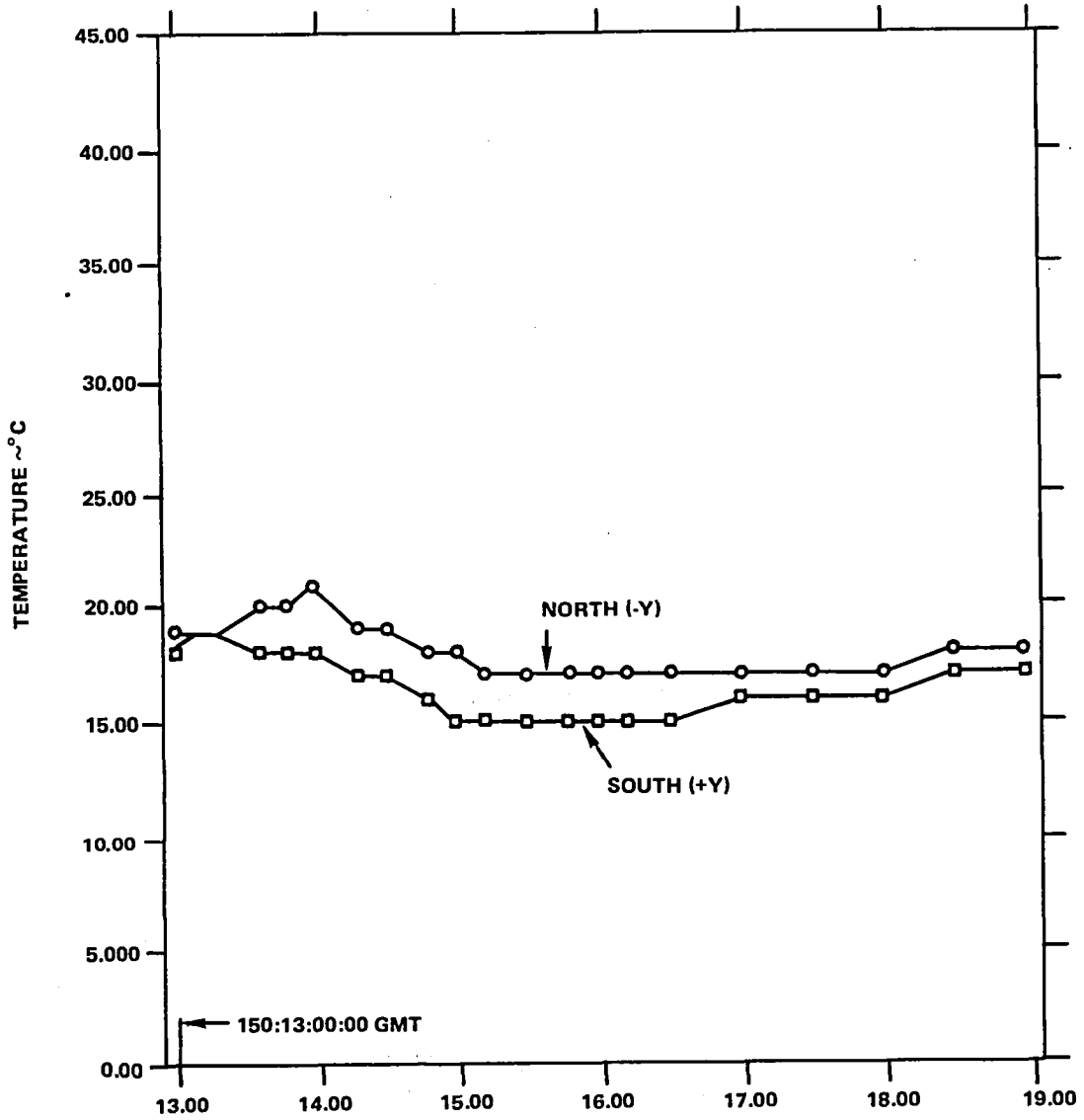


Figure 11-4. Launch Damper Temperature (Sheet 1 of 2)

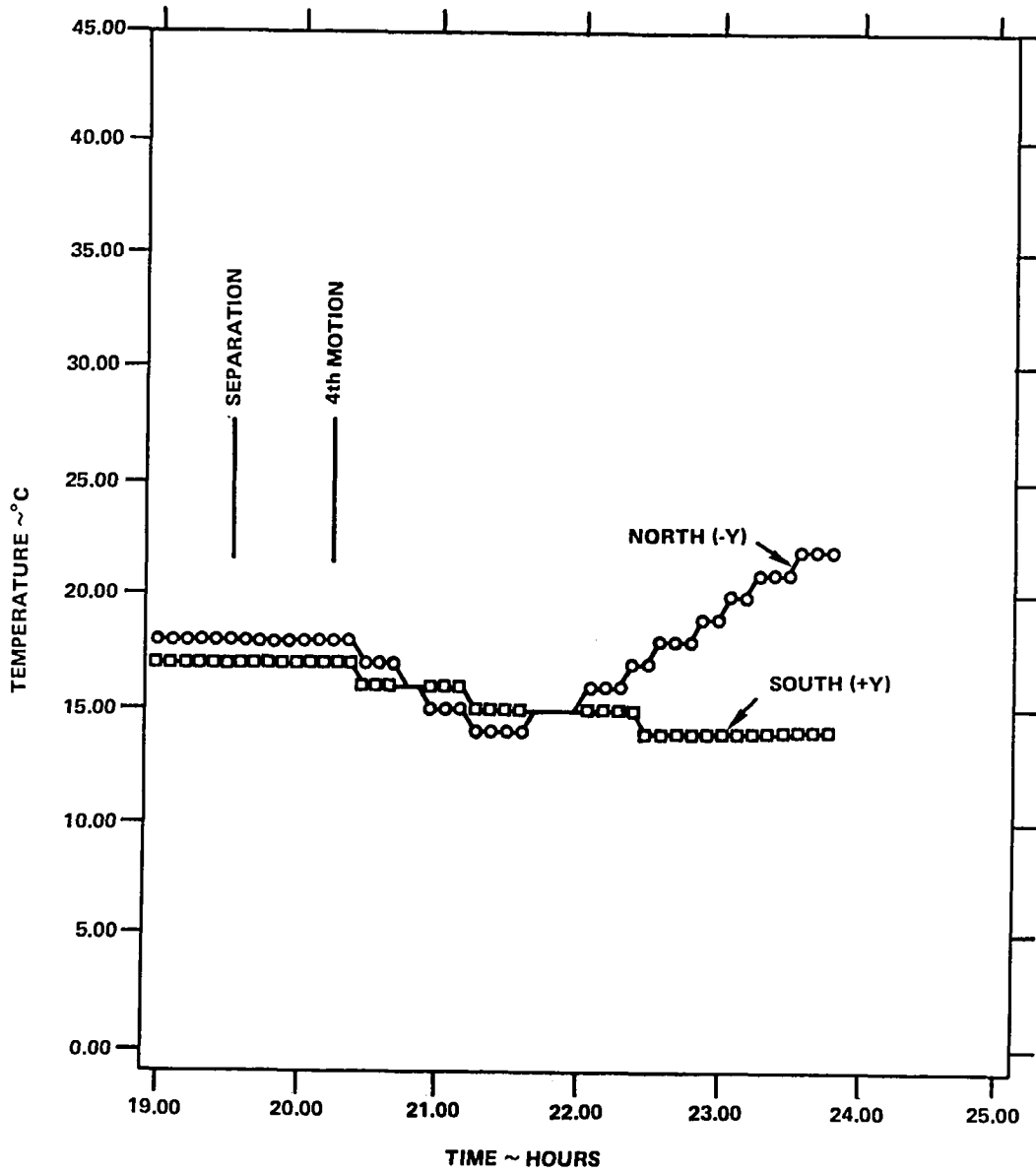


Figure 11-4. Launch Damper Temperature (Sheet 2 of 2)

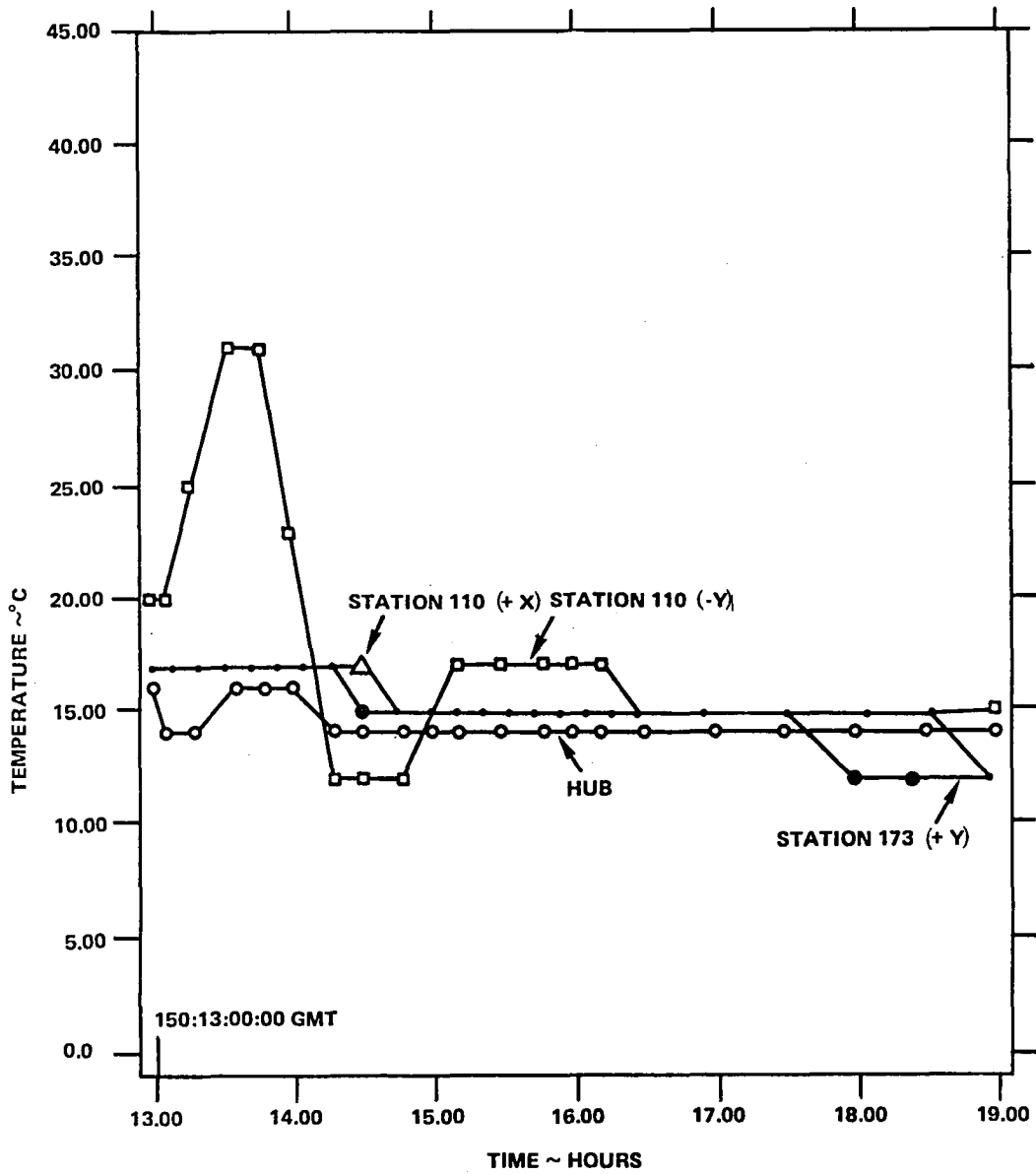


Figure 11-5. Launch Reflector Temperature (Sheet 1 of 2)

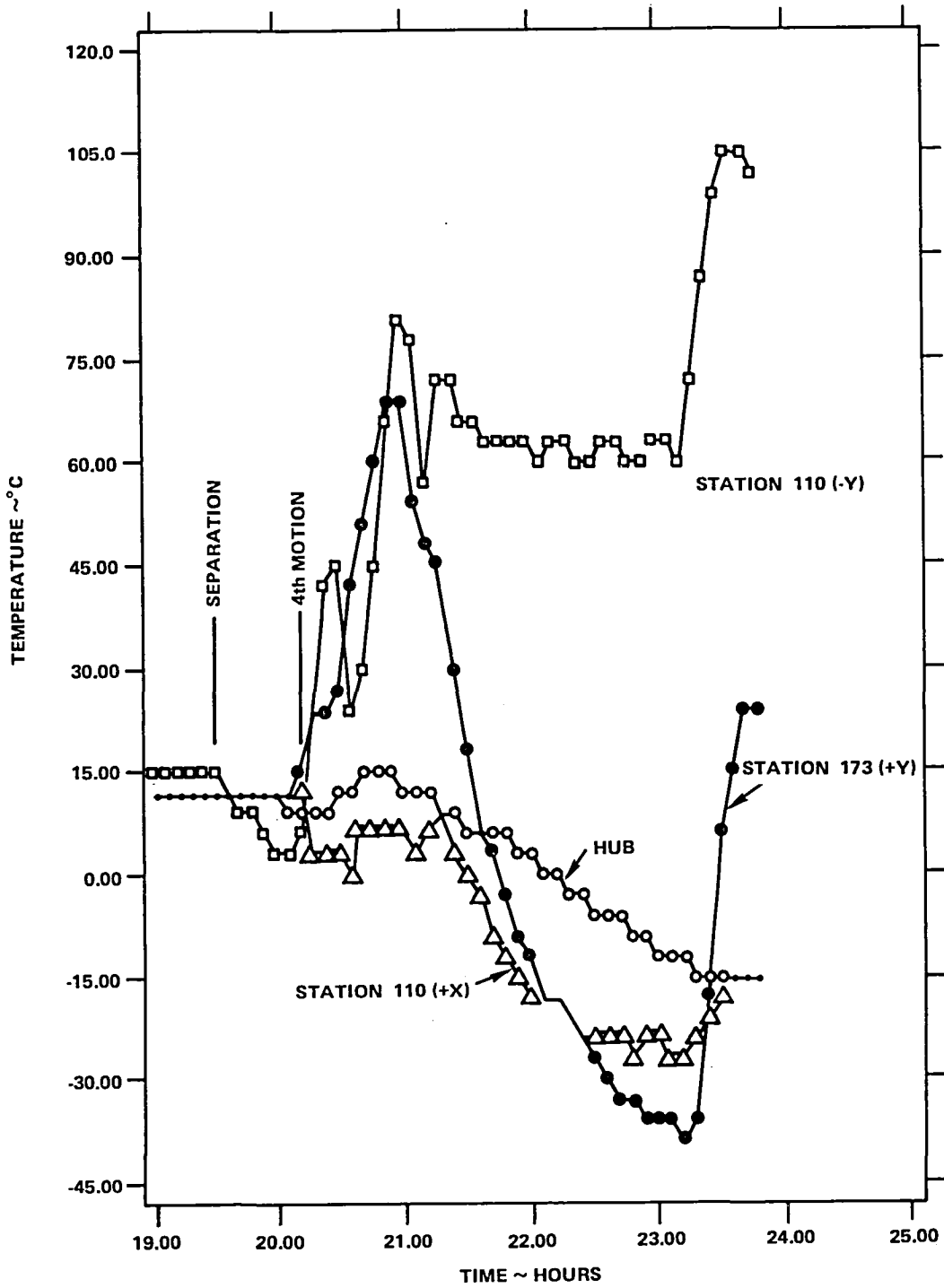


Figure 11-5. Launch Reflector Temperature (Sheet 2 of 2)

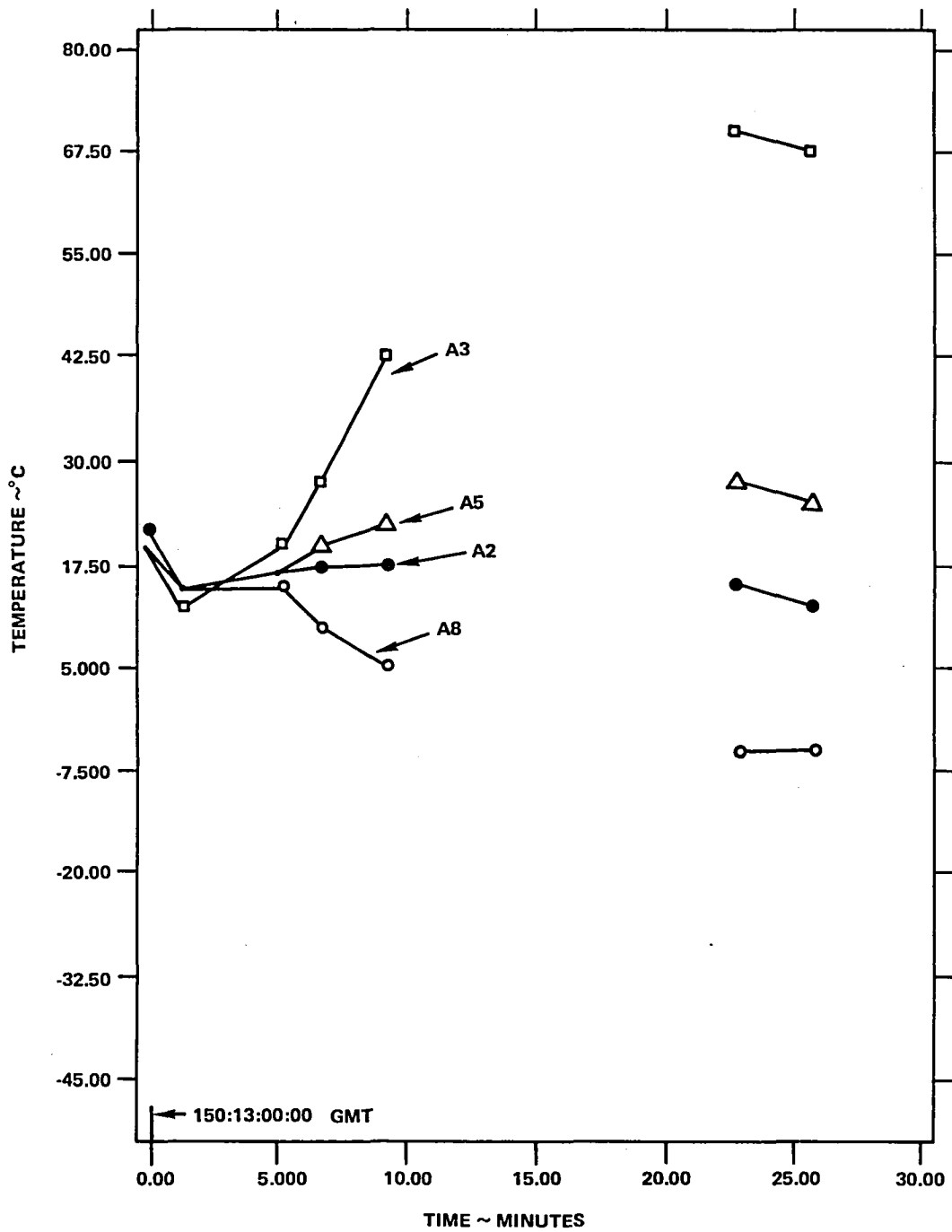


Figure 11-6. Launch Solar Array Temperature (Sheet 1 of 3)

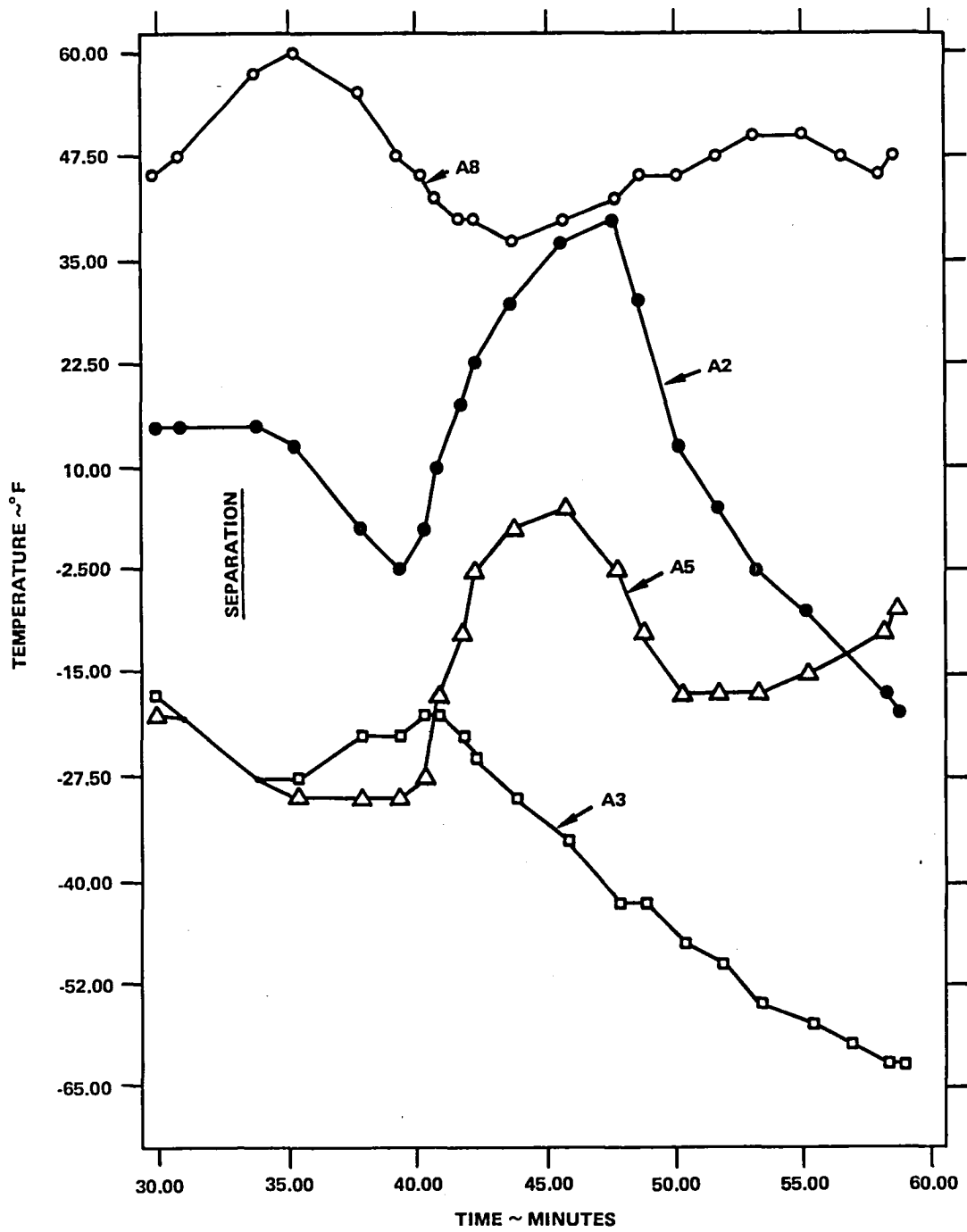


Figure 11-6. Launch Solar Array Temperature (Sheet 2 of 3)

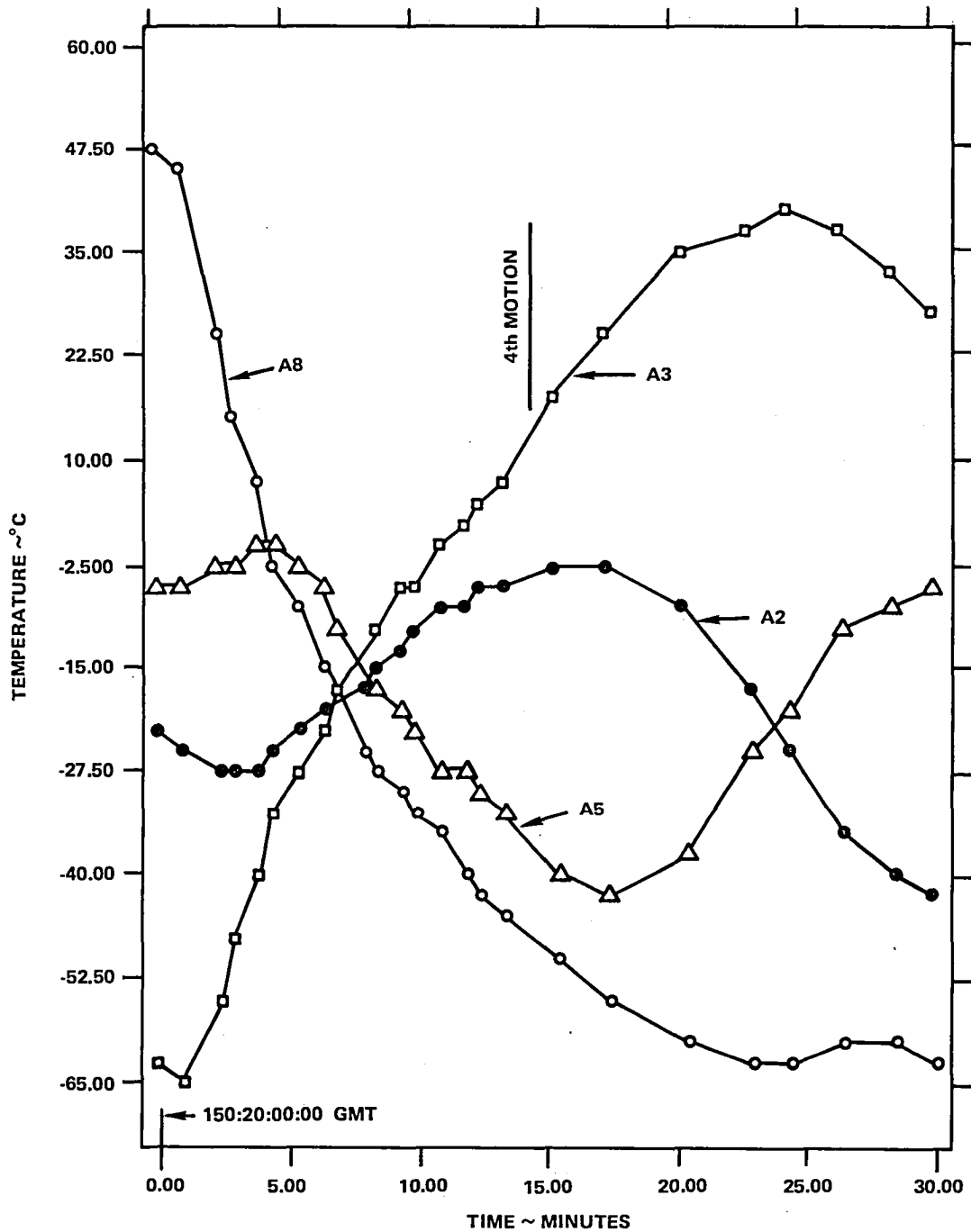


Figure 11-6. Launch Solar Array Temperature (Sheet 3 of 3)

Table 11-2
Launch Phase Temperatures

Component	Event	Temperature (Telemetry)	Expected Temperature	Qualification Limits
<u>Dampers</u>	T+1 hr	20°C	20°C	-40° to +40°C
	T+6 hrs	15°C	-4°C	
	Deployment	15°C	-7°C	
<u>Booms</u>				-60° to 140°C
2d Depl. Hinge	T+1 hr	12°C	10°C	
1st Depl. Hinge	T+1 hr	28°C	25°C	
2d Depl. Hinge	T+6 hrs	-4°C	-10°C	
1st Depl. Hinge	T+6 hrs	55°C	110°C	
2d Depl. Hinge	Deployment	-4°C	-10°C	
1st Depl. Hinge	Deployment	55°C	110°C	
<u>Reflector Hub</u>	T+1 hr	15°C	12°C	-18° to 35°C
	T+6 hrs	15°C	2°C	
	Deployment	15°C	1°C	
<u>Solar Arrays</u>	Deployment	-20°C to 40°C	0°C	-130° to 70°C

showed the widest excursion, mostly due to the sensitivity of the bottom shelf that contained a number of apertures of experiments and hence was affected by various orientations relative to the Sun. The temperature gradient along a heat pipe triad was small and was indicative of the expected operation of the heat pipes. This is clearly seen in Figure 11-8 that shows a maximum end-to-end temperature difference of less than 3°C.

Figure 11-10 shows the relative location of the thermistors in heat pipe 3 in the service module. The data for 1974 and 1976 pertain to approximately the same power mode (HET) with an attitude pointing differential of about 8 angular degrees. The data for 1979 were obtained during a 24-hour period in which the EME package was activated. The gradient along the triad had not shown any significant change throughout the mission. This indicates that there had been neither unusual leakage nor a generation of noncondensable gas. Both of these effects would have led to a noticeable deterioration in the temperature distribution.

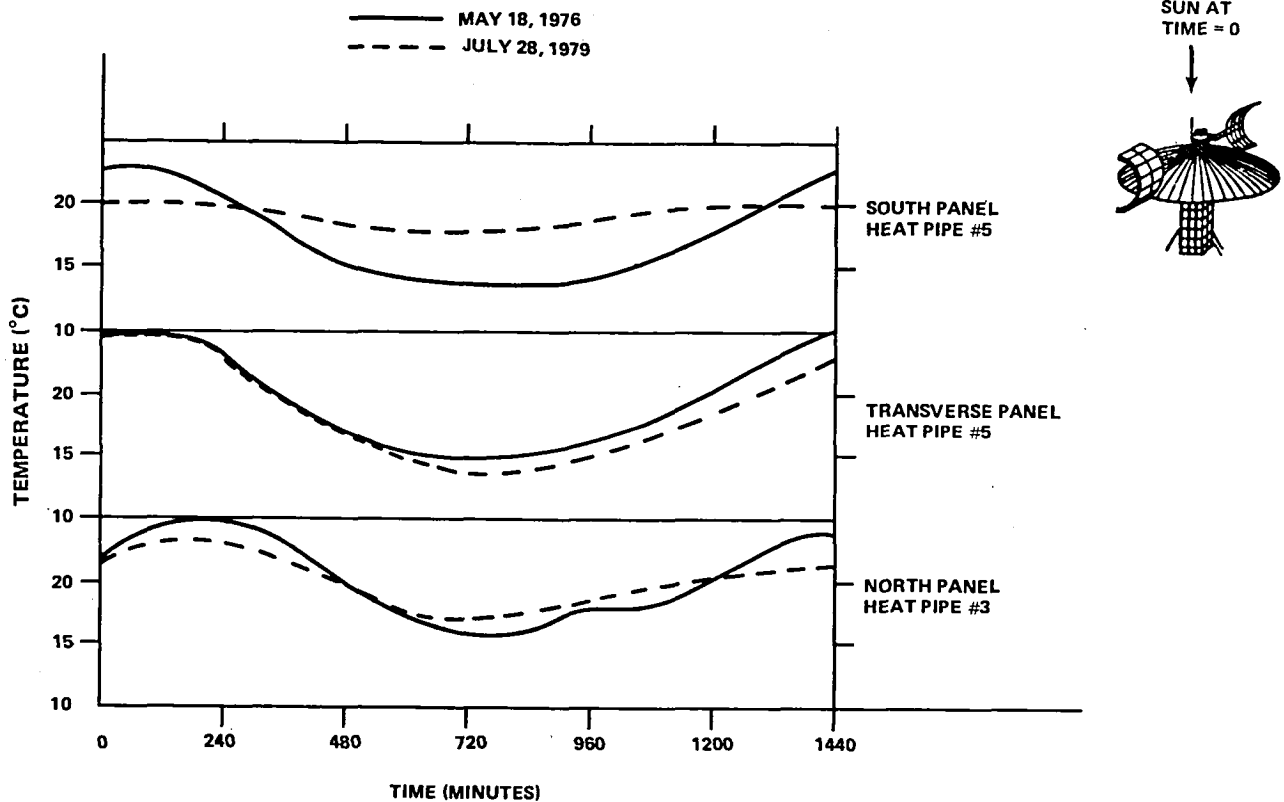


Figure 11-7. Experiment: Module Average Temperature

Additional data are given in Figure 11-11 that compared the temperature of one of the batteries, a telemetry transmitter, and the C-band traveling wave tube amplifiers for August 28, 1974, August 29, 1976, and June 20, 1979.

Components that were not mounted on heat pipe panels included the telemetry transmitters located on the upper cross beam of the service module. Figure 11-12 gives the orbital temperatures of the 136-MHz telemetry transmitters 1 and 3 and DOC 1. Transmitter 1 was the only transmitter in regular operation during November 1974 and 1975. The uniformity in the temperature of these components reflects the efficiency of heat distribution inside the EVM.

The temperature differential between the cases of the two batteries remained consistently below the specified 5°C. The daily temperature variation remained within 15°C to 28°C range with the peak temperature occurring during periods of Millimeter Wave Experiment (MMW) operation. A typical temperature profile of the batteries is given in Figure 11-13. The data for 1975 were taken during MMW operation.

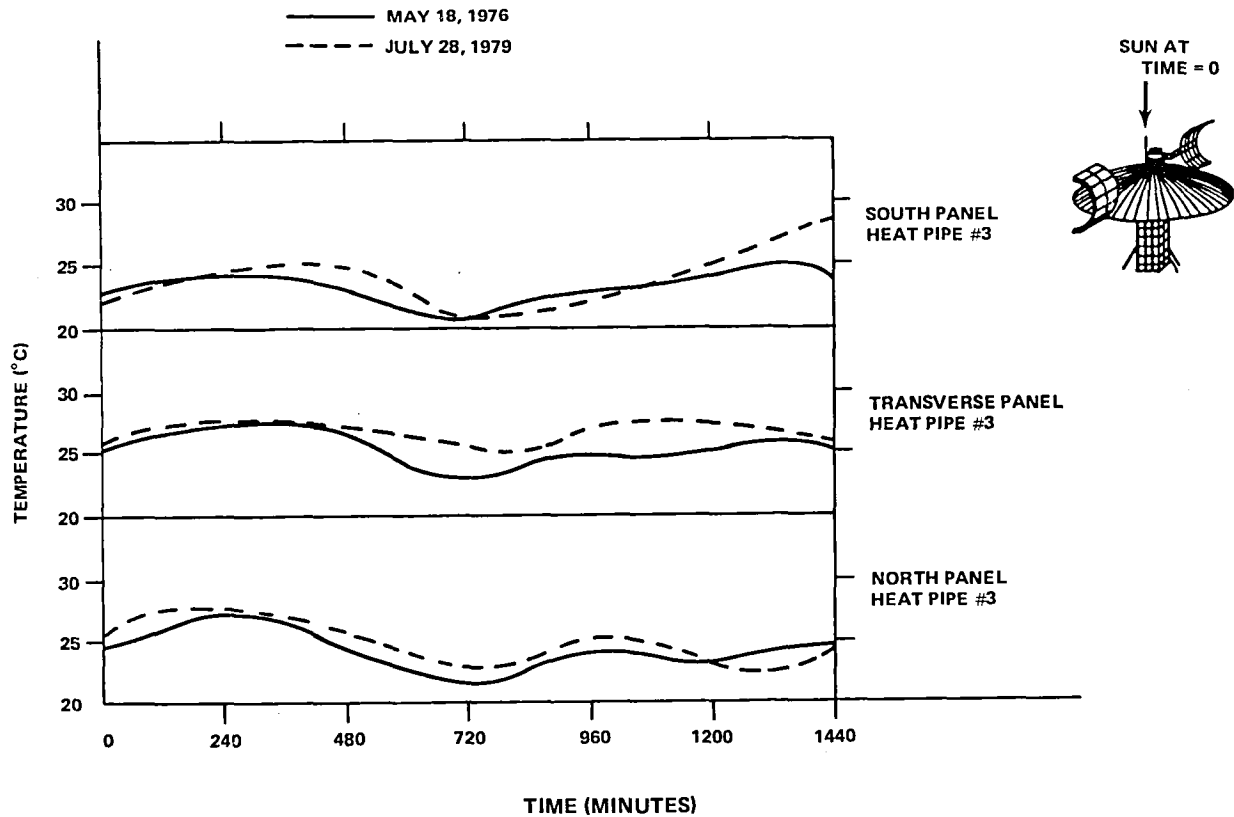


Figure 11-8. Service Module Average Temperature

On October 31, 1974, DACU 1 was operated in the normal mode for a 24-hour period to obtain diurnal temperature data on the structure external to the EVM. Of special interest were the solar array booms and the deployment dampers. The booms were treated with an aluminized Kapton cover secured by a film adhesive. Excessive temperatures (greater than 150°C) could lead to out-gassing of the adhesive and undesirable depositions on the spacecraft sensors. Severe temperatures on the dampers (greater than 70°C and less than -70°C) would result in failure of the seals that could also present a contamination problem. Figure 11-14 shows that these temperatures were maintained within acceptable limits. Figure 11-15 gives the orbital temperature profiles of the Environmental Measurements Experiment bridge, the graphite fiber reinforced plastic trusses and associated fittings, and two locations on the reflector dish. Comparative data were obtained on June 17, 1979. Many of the external thermistors had become erratic after long term cycling in orbit. The ones on the dampers and the solar array booms, however, still reflected normal response. Data are presented in Figure 11-14.

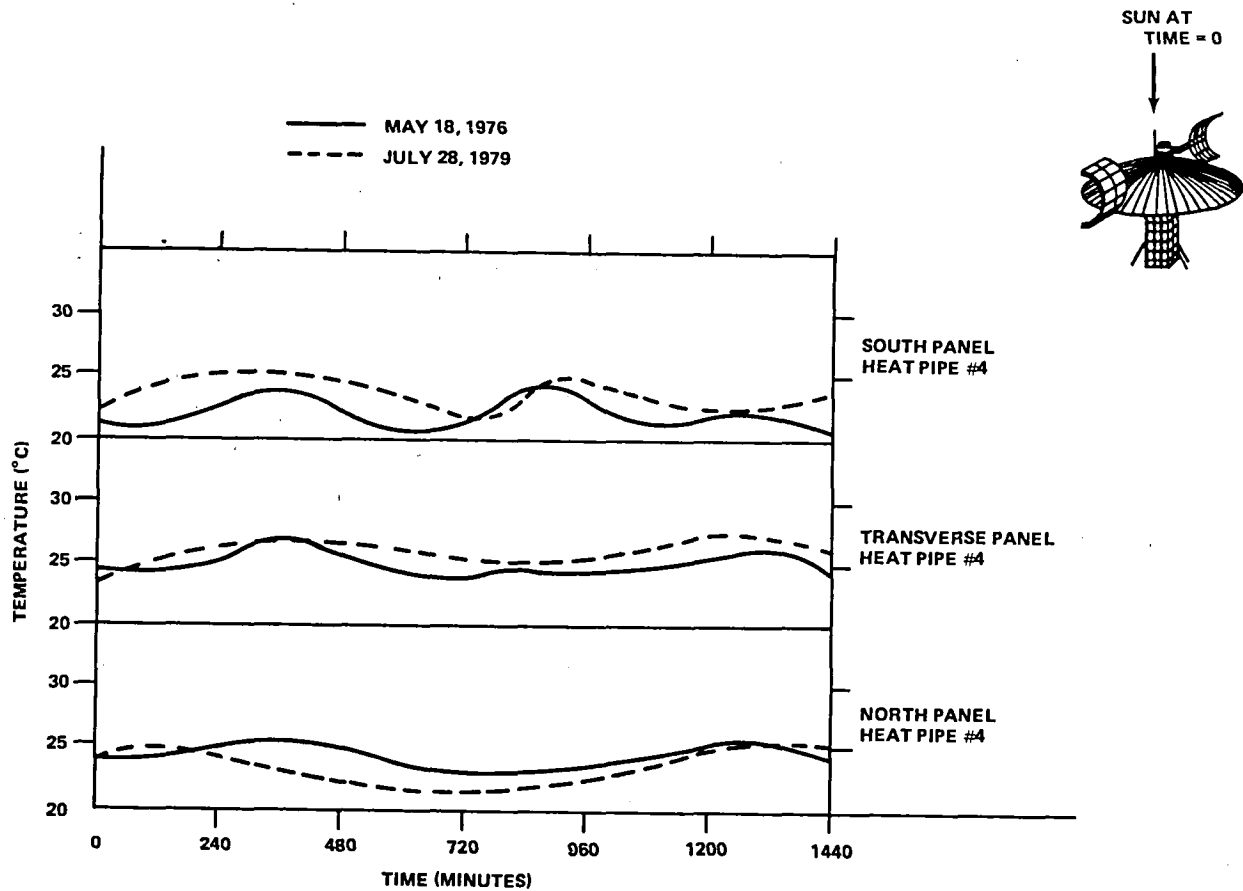


Figure 11-9. Communications Module Average Temperature

SPECIAL IN-ORBIT TESTS

During the six-week period just prior to ending the active life of ATS-6, final engineering tests were conducted to evaluate the performance of the spacecraft in terms of the long-time operation of its thermal hardware components. The tests were planned mainly to support future applications of louvers and heat pipes to spacecraft temperature control.

Heat Pipe Performance

Flight data taken intermittently throughout the 5-year mission indicated that the heat pipes functioned according to preflight specifications and predictions. There was no evidence of a detrimental leakage of ammonia or an increase in the amount of noncondensable gas.

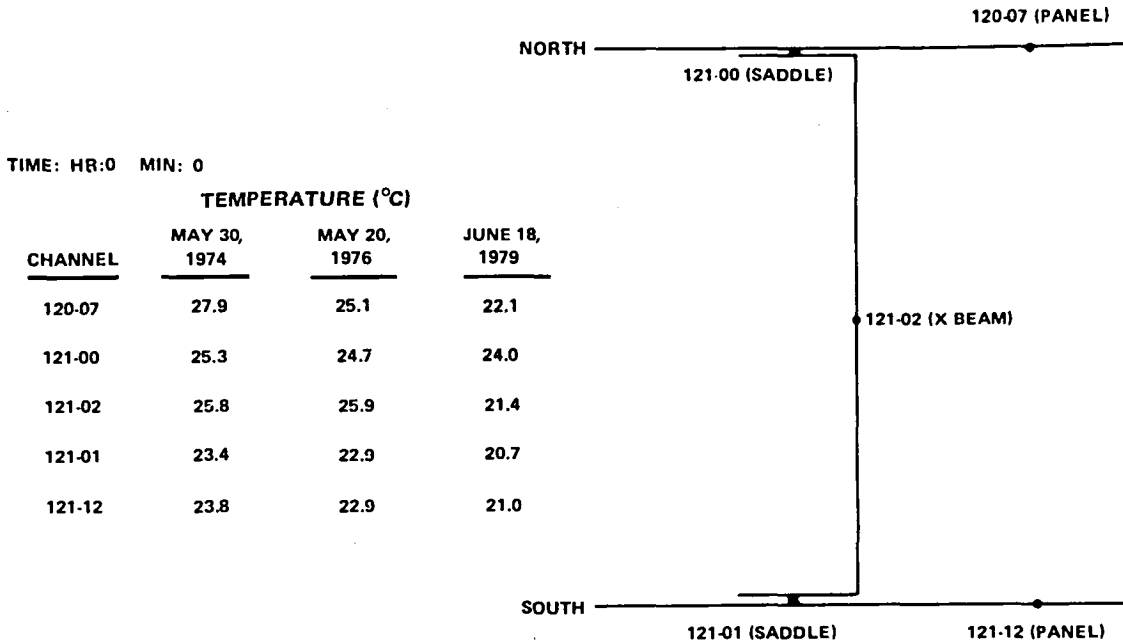


Figure 11-10. Service Module Heat Pipe No. 3 Flight Data

Data analysis was based on a comparison of temperatures and temperature gradients for compatible orbits and spacecraft operations falling several months apart. An overall increase in the temperature that could not be traced to failure of the louvers or to a degradation in coatings (optical solar reflector) and insulation characteristics would be construed to relate to a leakage in the ammonia. An increase in the gradient along the heat pipes would mean a probable increase in the generation rate of noncondensable gases.

The data collected include sets of temperatures registered on June 7, 1974, May 20, 1976, and June 20, 1979. The first two conditions were reasonably similar in orbits and power profiles. June 7, 1974, fell within a three-day period in which the dominant mode of operation was the Health, Education, Telecommunications experiment, although some short intervals were occupied by the Millimeter Wave experiment and a continuation of the spacecraft activation and checkout phase. May 20, 1976, was almost exclusively occupied by the Satellite Instructional Television Experiment (SITE). The apparent declinations of the Sun for both days were also very close (21 degrees to 23 degrees) even after adjustments were made to account for a 4-degree to 6-degree pointing maneuver required by SITE in broadcasting in India during 1976. June 29, 1979, was occupied by tests conducted on orbit control jets. This date also included tests of powered ion engine load interface circuits.

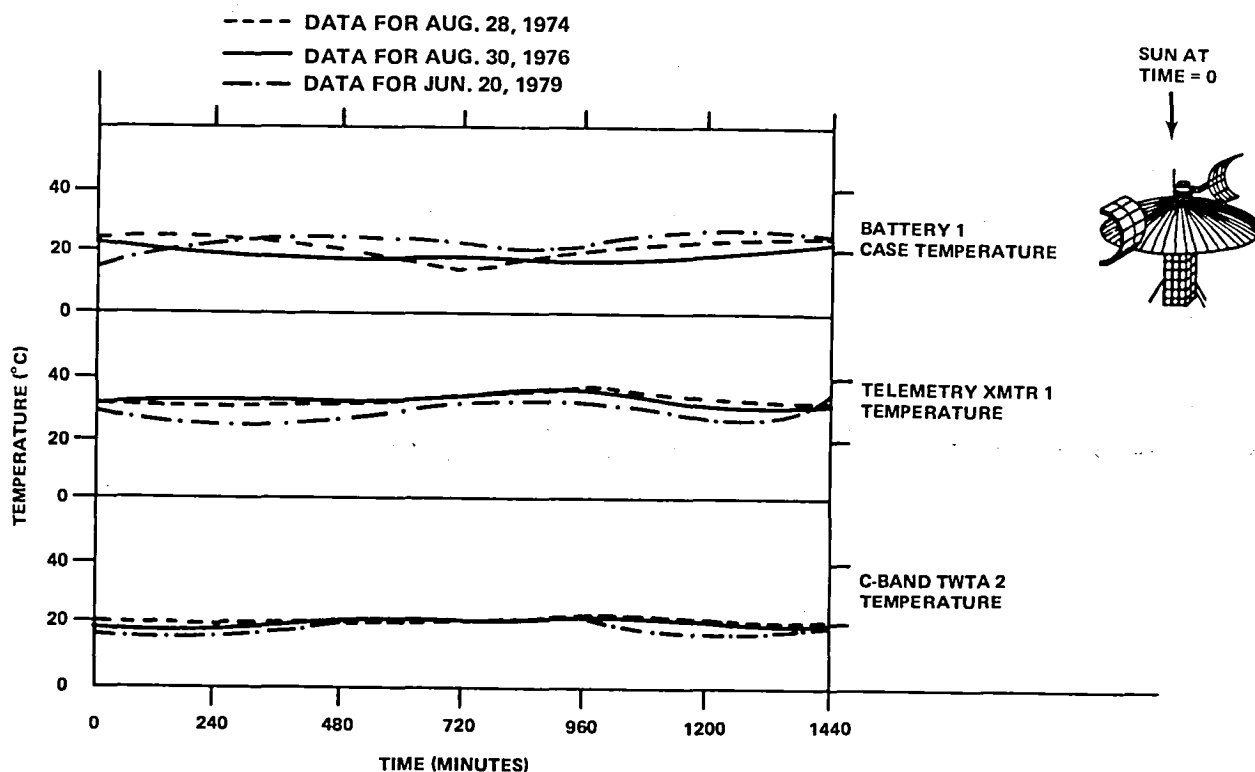


Figure 11-11. ATS-6 Five-Year Temperature Comparison

Temperature data for heat pipe No. 3 in the service module for the above dates are given in Figure 11-16. The decrease in temperature due to solar array power degradation, which led to a decrease in the service module shunt power, is evident. The temperature levels and gradients show proper heat pipe performance with no evidence of ammonia leakage or noncondensable gas buildup.

On July 28, 1979, a special test was performed to further verify heat pipe function and determine the effects of longtime operation on the ability to support uneven power dissipations. The test consisted of activating both C-band traveling wave tube amplifiers (TWTA) on the north wall of the communications module and monitoring the temperatures registered by the thermistors on heat pipe No. 6 in the communications module (Figure 11-17). The total net difference in the power between the north and south panels, before and after activating C-band, was estimated to be 42 watts. Ground testing results had indicated that a differential in power of this magnitude would result in minor changes in the overall heat pipe temperature gradient. Flight test data revealed that the situation remained practically unchanged after 5 years in orbit. Figure 11-18 summarizes these results. The increase in average temperature during the test is consistent with the communications module temperature versus power profile.

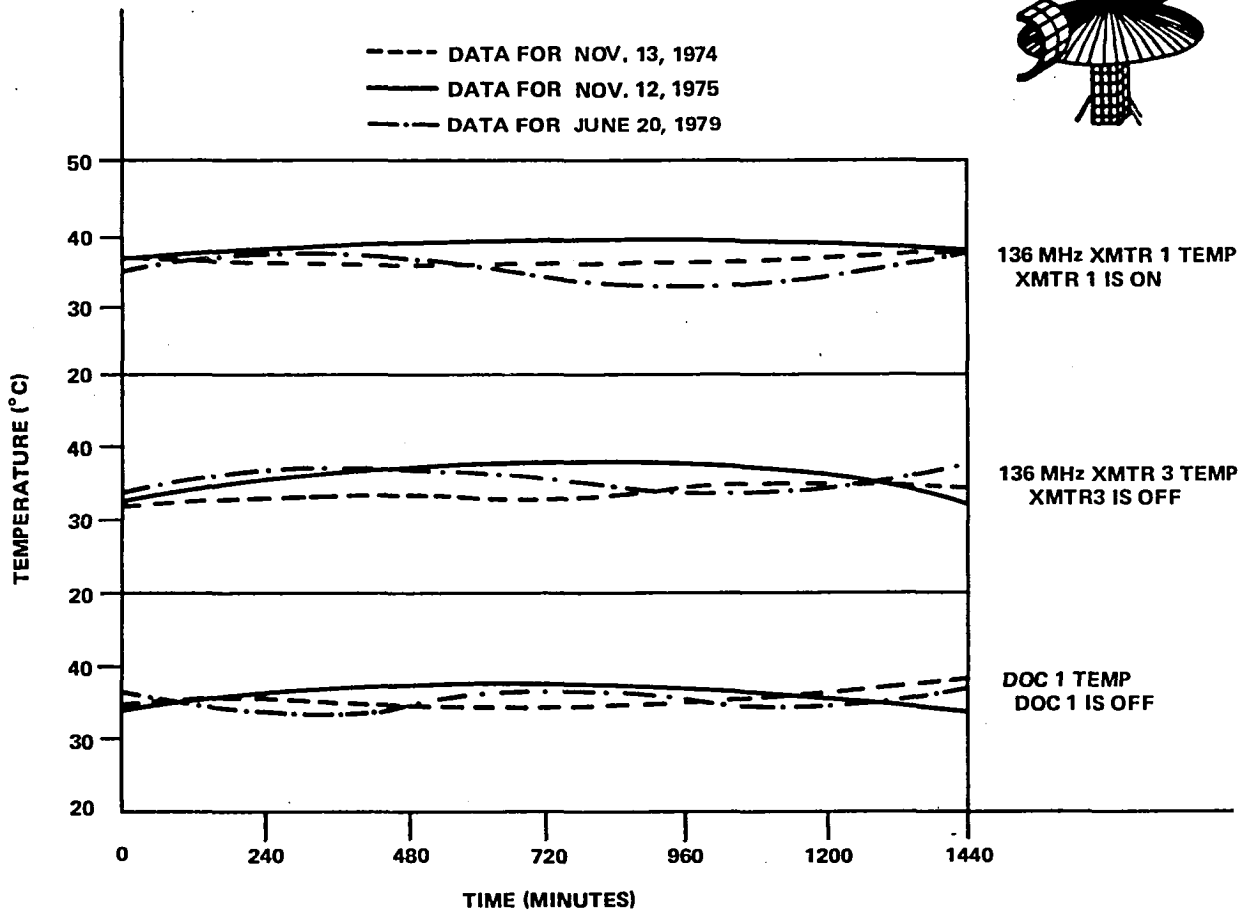


Figure 11-12. Telemetry Transmitters/DOC 1 Temperature

Louver Performance

The most distinctive indication of the excellent performance of the EVM thermal subsystem was the relative insensitivity of the temperatures in the three modules to the various power modes and to life in orbit. Throughout the spacecraft's active life, the north and south panels of all modules maintained a temperature within a few degrees of 20°C. The average temperature of the EVM changed very little from 25°C since launch. This tight control was attributed mainly to the louvers that compensated for variations in power and solar input by adjusting their heat rejection capability.

From the power profile of the arrays it was estimated that at 560-watt load power (new array), the total shunt dissipation was 105 watts of which 35 watts (one-third) were released in the service module. The power expended for housekeeping equipment remained approximately the same (78 watts in the service module) for almost all operations since the function of the service module components remained essentially constant throughout the mission. Hence it was concluded that in two years after launch, when the available power decreased to about 480 watts, only about 8 watts remained as shunt dissipation in the service module. At the end of the mission (available power

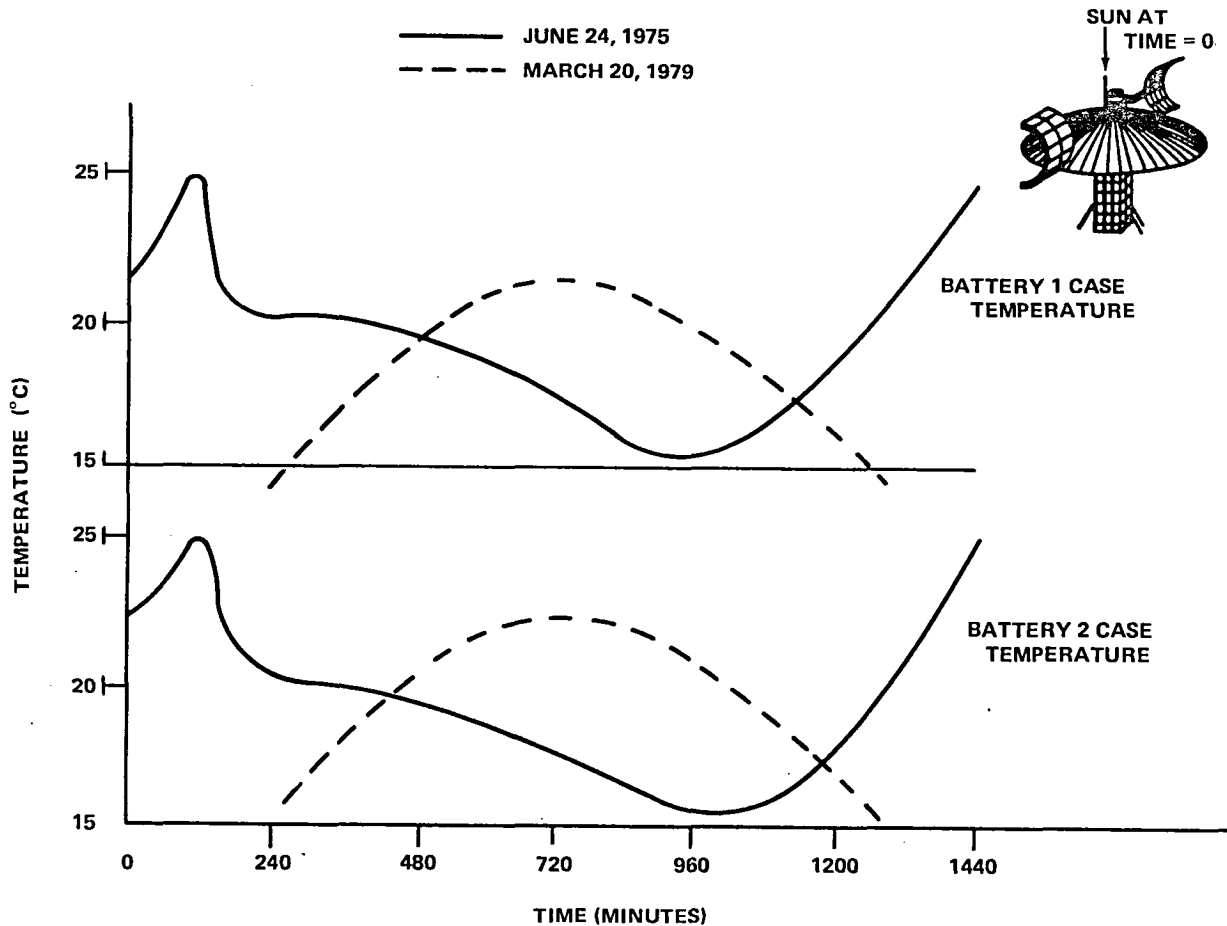


Figure 11-13. Battery Case Temperature

about 430 watts), very little heat was being generated in the shunts. A summary of the average service module temperature versus dissipation is given in Figure 11-19. The measured data clearly indicated proper compensation by louver operation.

ANOMALIES

No serious thermal control anomalies developed during the ATS-6 mission. The structure temperatures throughout the launch phase, including deployment, were nominal, and the electronics mounting surfaces in the Earth-viewing module maintained, for the duration of the mission, average temperatures that were within the operational reliability requirements of the components.

The orbital variation in the temperature of the experiment module was relatively wide when compared to service module and communications module data. The orbital average temperature of the mounting surfaces of the batteries and the Earth sensors remained as predicted and within preflight specification levels. However, the upper value of temperature during some phases of the orbit or during special operational and pointing maneuvers exceeded the upper limit recommended by

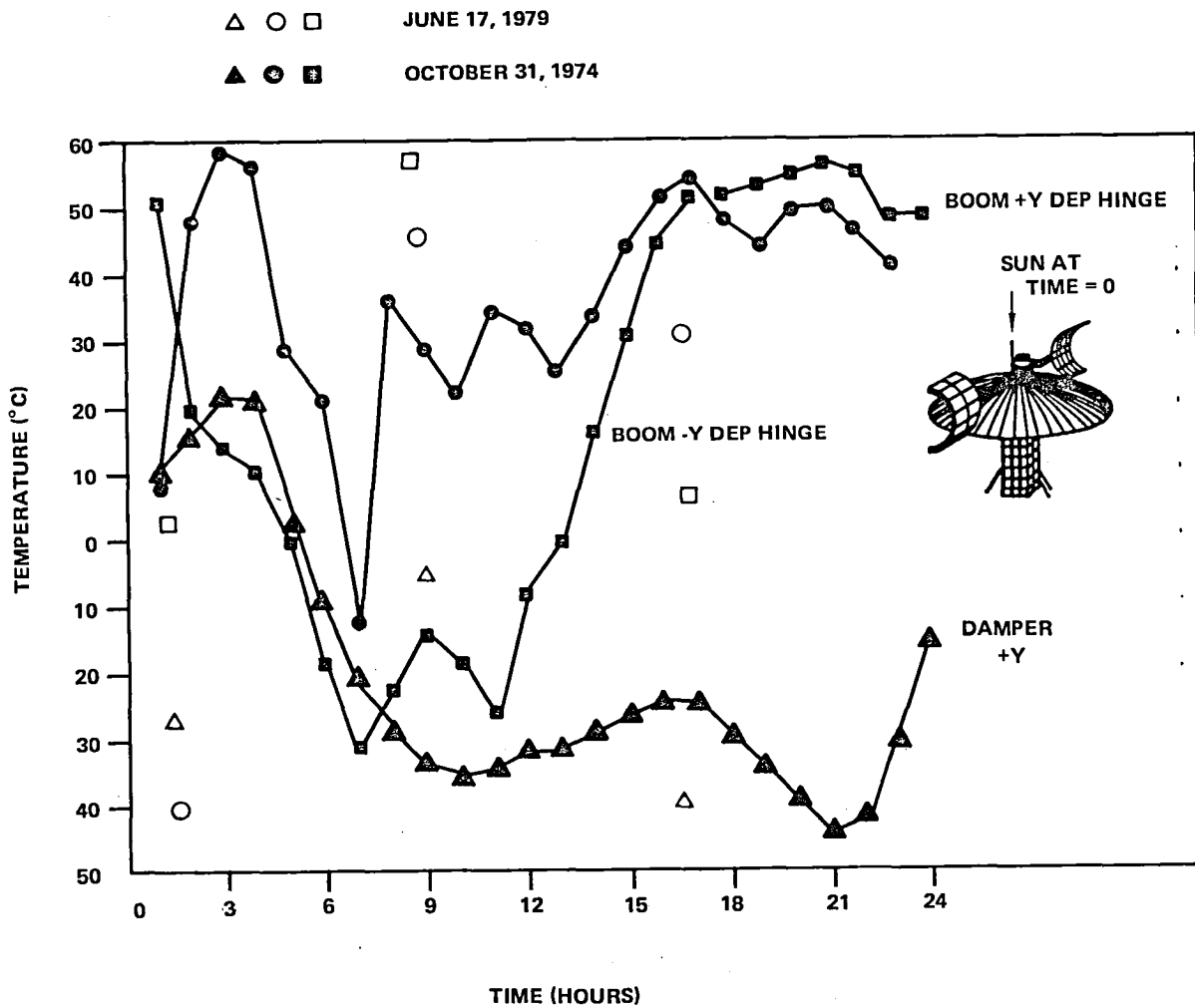


Figure 11-14. Solar Array Booms and Deployment Dampers Temperatures

vendors and adhered to by qualification tests. The high temperatures occurred for only short intervals during a given orbit, but they reflected the sensitivity of the experiment module to the thermal behavior of the bottom shelf on which was mounted a number of experiments with apertures or with exposure to direct sunlight.

Battery Temperature

Typical battery temperature profiles are shown in Figures 11-20 and 11-21. During the first week of November 1974, the temperatures exceeded the recommended 20°C. This prompted an investigation into the separate and combined effects of C/60 charge rates, shunt dissipation, spacecraft pointing, and MMW experiment operations.

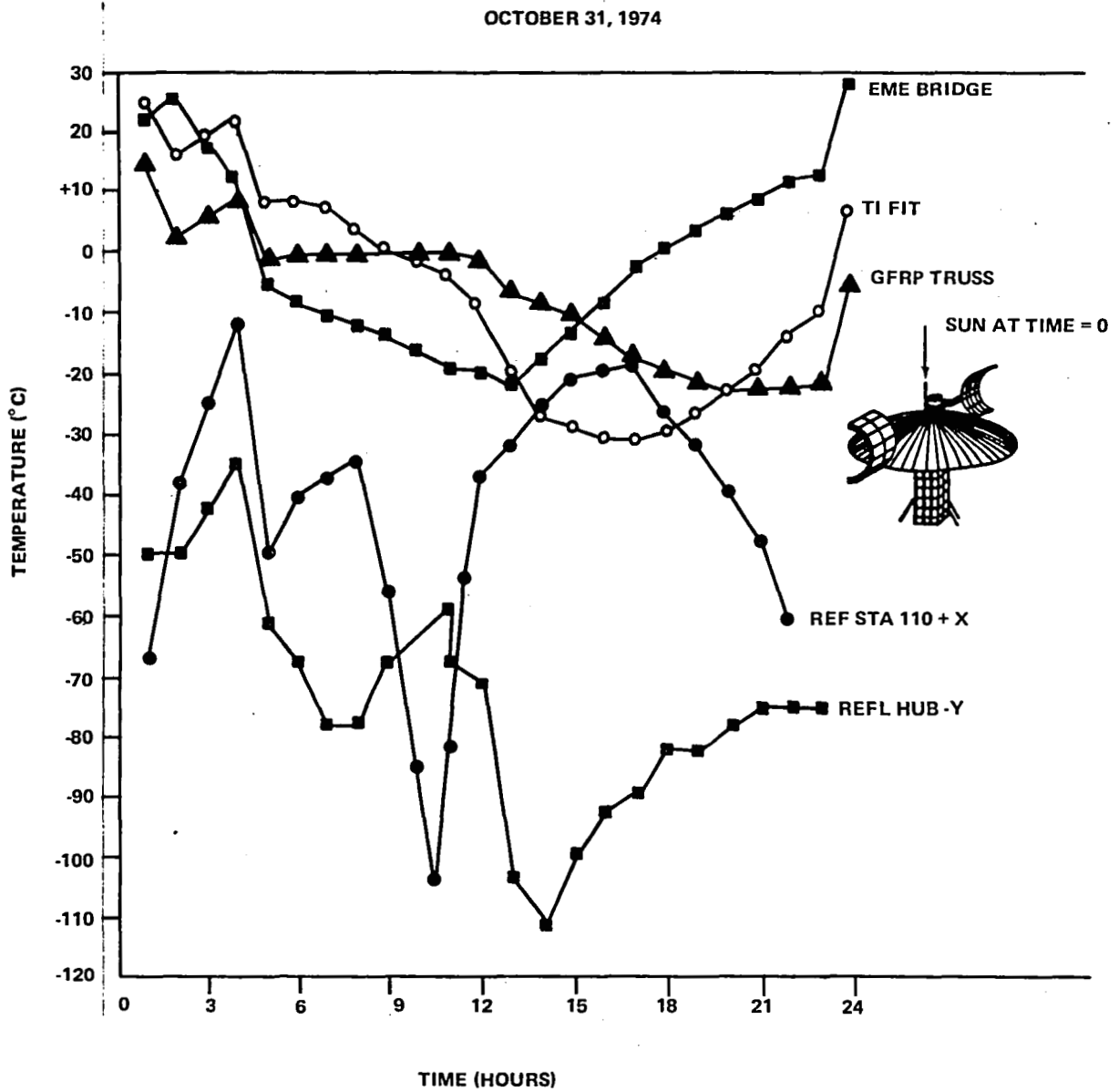


Figure 11-15. External Structure Temperature

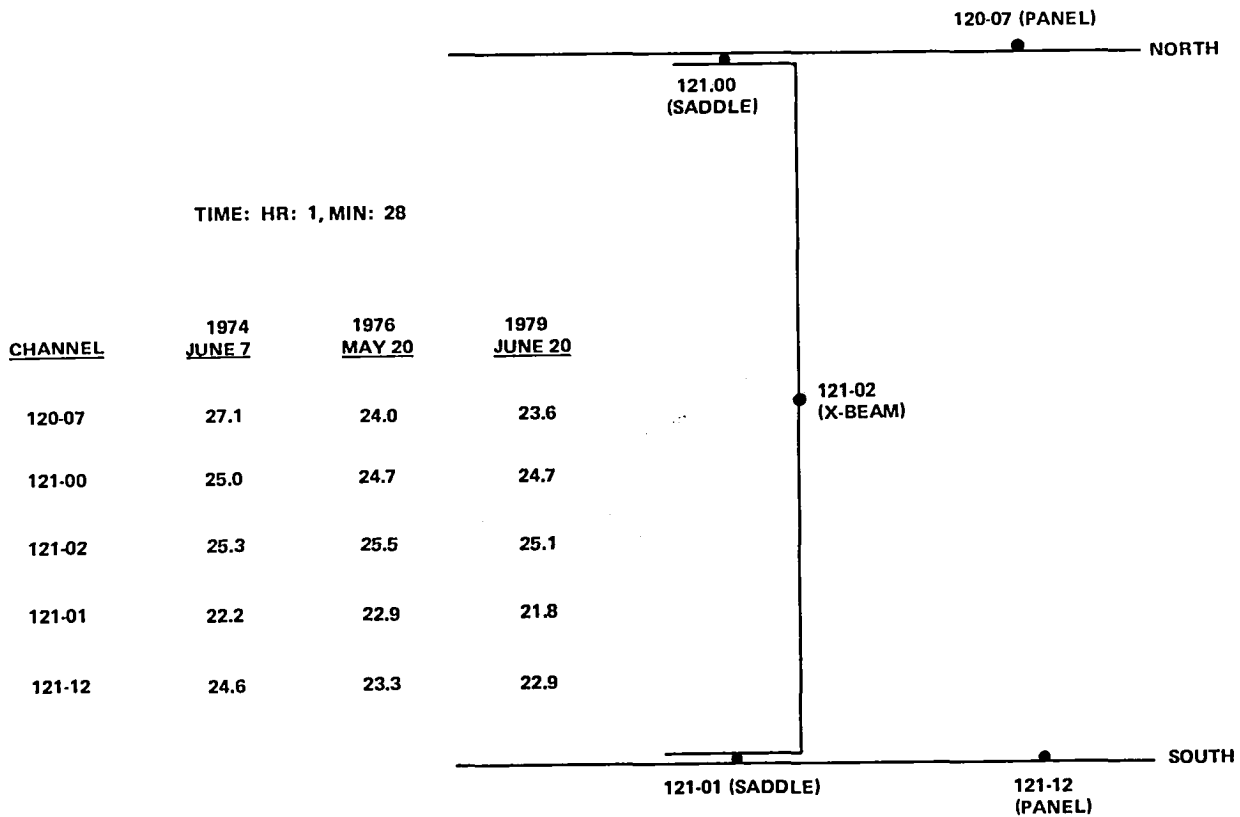


Figure 11-16. Service Module Heat Pipe No. 3 Flight Data

During the main charger rate tests, the temperature gradient between the battery cases and the nearest baseplate sensor was recorded. The test data are shown in Table 11-3. The gradient reached a peak value of 3.2°C for battery 2 and 2.5°C for battery 1. The main charge rates were 0.59/0.53 ampere (A) and the excess dissipation above the C/60 charge rate was 16.6 watts. Additional tests with C/60 charge rates at 0.25 A per battery resulted in a reduction in the gradients to 1.2°C per battery. Temperature gradients were also monitored through DACU 1 that provided telemetry from a temperature sensor located close to the battery baseplate. These data indicated that the C/60 temperature gradients across batteries 1 and 2 were 0.7°C and 1.4°C, respectively.

Data obtained during shunt dissipation tests are presented in Table 11-4. Reducing shunt dissipations at 0600 GMT to zero had a minor effect on battery peak temperatures, while a reduction to zero dissipation at 0100 GMT reduced peak temperatures from 26.3°C to 21.4°C.

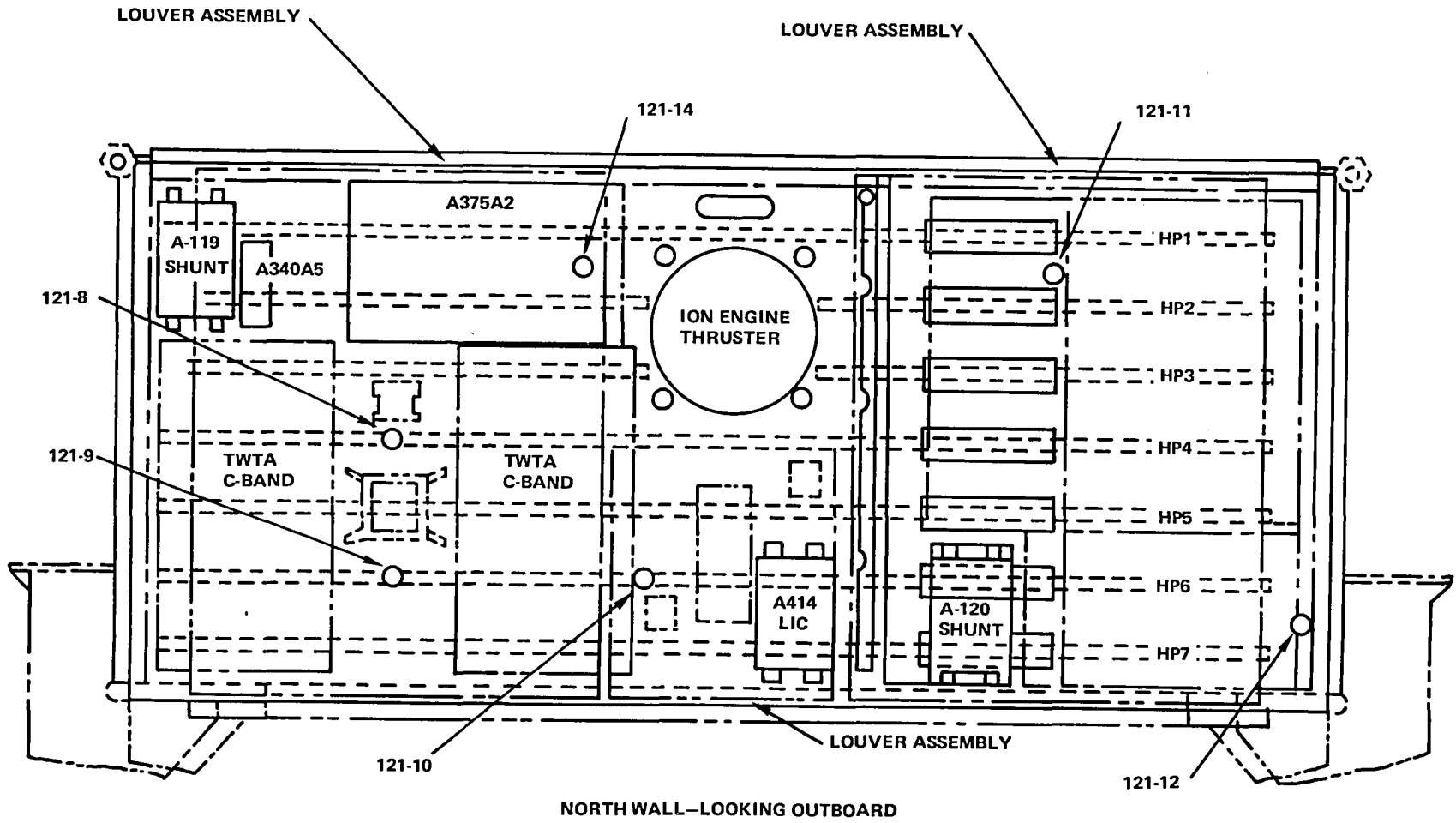


Figure 11-17. Communication Module—North Wall Temperature Sensor Locations

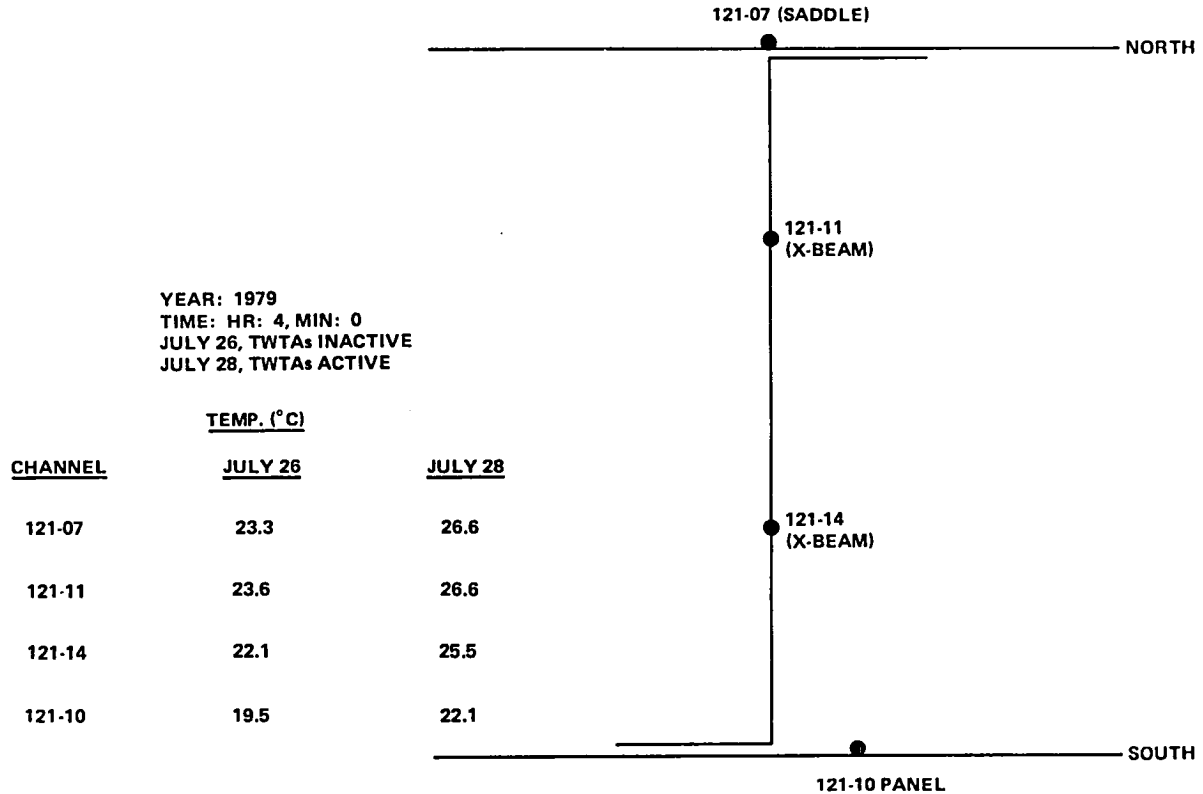


Figure 11-18. Communication Module Heat Pipe No. 3 Test

Tests conducted to determine the effects of roll attitude indicated that roll angle had the largest effect on battery temperatures from 0800 to 1000 GMT when the azimuth of the Sun varied from 30° to 60°. Empirical results obtained from the test data shown in Table 11-5 indicated that the effect of spacecraft roll angle on battery temperature was between 0.43°C and 0.84°C per degree roll.

Limited Millimeter Wave (MMW) experiment operations (less than or equal to 2-hour periods) were conducted to determine the MMW effect on battery temperatures. The data presented in Table 11-6 indicated that:

- MMW operations commencing at peak temperature periods (11:00 GMT) did not elevate battery peak temperatures but merely extended them.
- MMW operations starting at two hours before the peak (0900) and extending into the peak elevated battery peak temperatures from 22.8°C to 26.3°C at 1000.

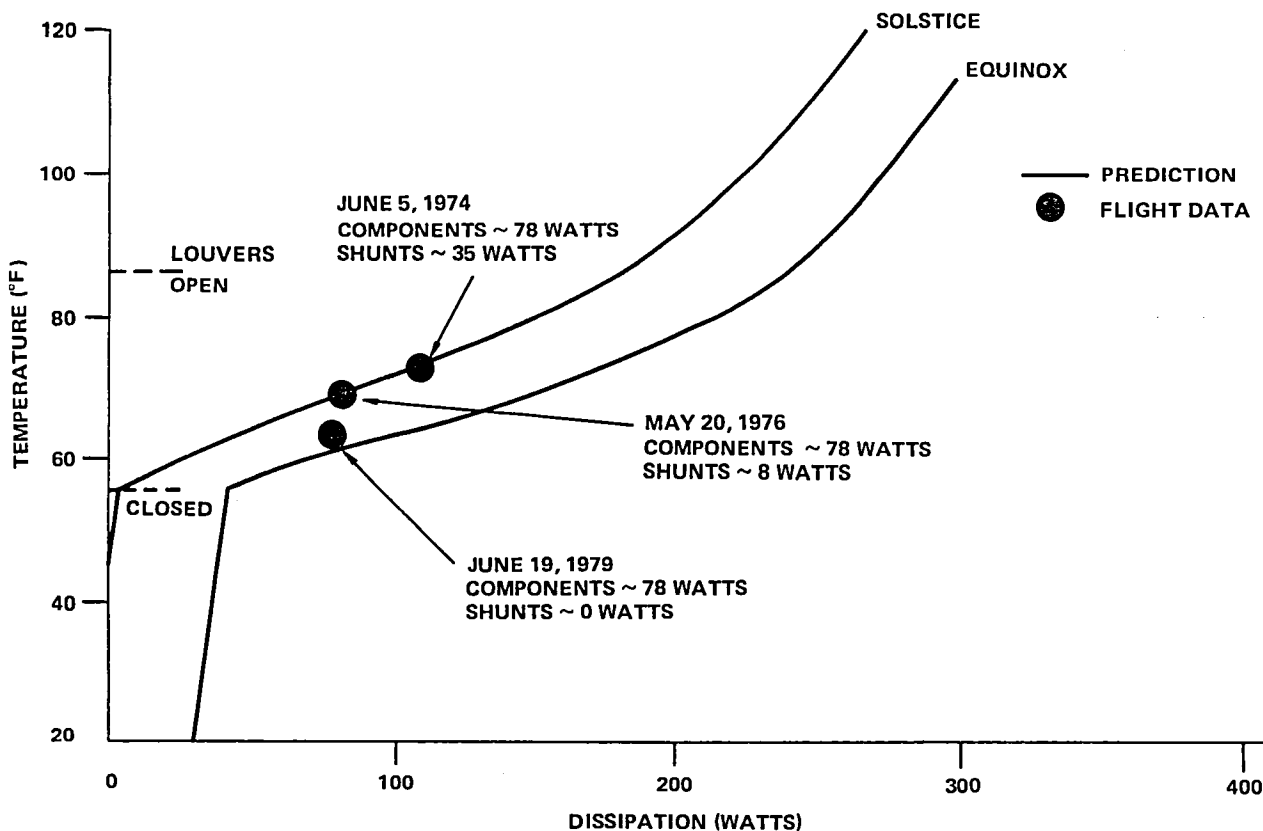


Figure 11-19. Service Module Temperature vs. Power Dissipation

Tests were also conducted to determine how hot the batteries would get under conditions simulating worst-case Sun elevation angle (23.5°) and spacecraft pointing. During the test, C/60 charge rates were used with the MMW experiment off and shunt dissipation set to zero with the spacecraft pointing 8 degrees off the local vertical in roll (Sun elevation = 24 degrees). Test results (Table 11-5, November 16, 1974) indicated that the combined effects of C/60 charge rate, MMW experiment off, and zero shunt dissipation ensured that battery temperatures were kept below 25°C during worst-case Sun elevation conditions that occurred during the winter solstice season.

Earth Sensor

The Earth sensor was located on the bottom shelf of the experiment module. Because of the absence of heat pipes in this shelf, the sensor was essentially thermally controlled by the radiation exchange with the rest of the EVM and with space. Preflight thermal analysis indicated that the bottom shelf

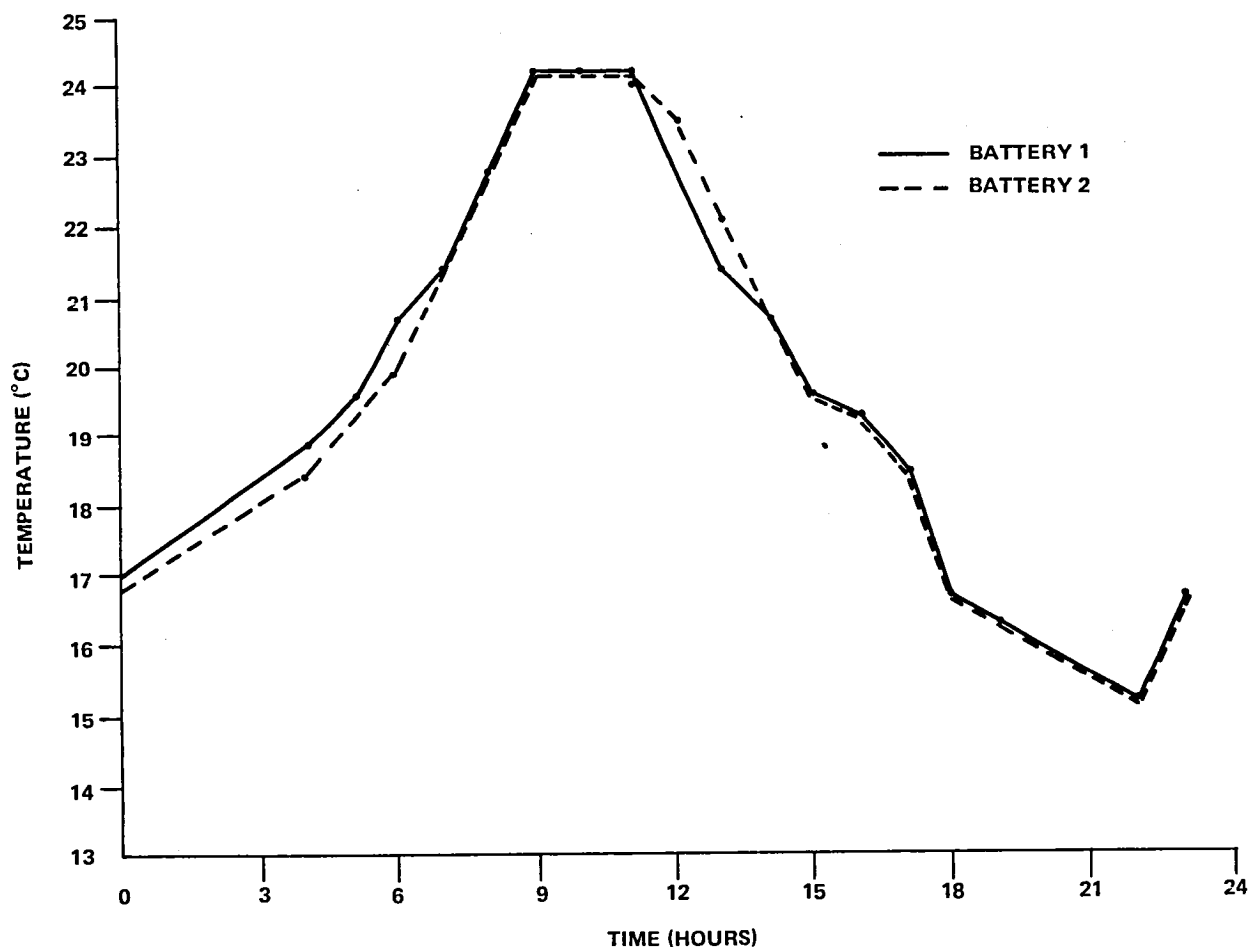


Figure 11-20. Battery Orbital Temperature (August 28, 1976)

could be maintained between 10°C and 30°C , and the qualification requirement for the Earth sensor mounting panel was established at -12°C to 50°C . The level was considered sufficient to bracket orbital temperature variations. In addition, a solar simulation test indicated that the bolometer temperature would not exceed 55°C during worst-case solar input (Table 10-1, Chapter 10). Typical Earth sensor orbital temperatures are shown in Figures 11-22 and 11-23.

Some portions on the perimeter of the sensor head were treated with thermatrol white paint to reduce solar input and maximize heat rejection to space. The maximum temperatures experienced at the end of the mission exceeded the recommended values at which no irreversible damage could occur on the bolometer. However, it was suspected that the short-time occurrence of high temperatures at separated time intervals (a few minutes once every twenty-four hours) was not detrimental. Further, no anomalous behavior was exhibited by the Earth sensor.

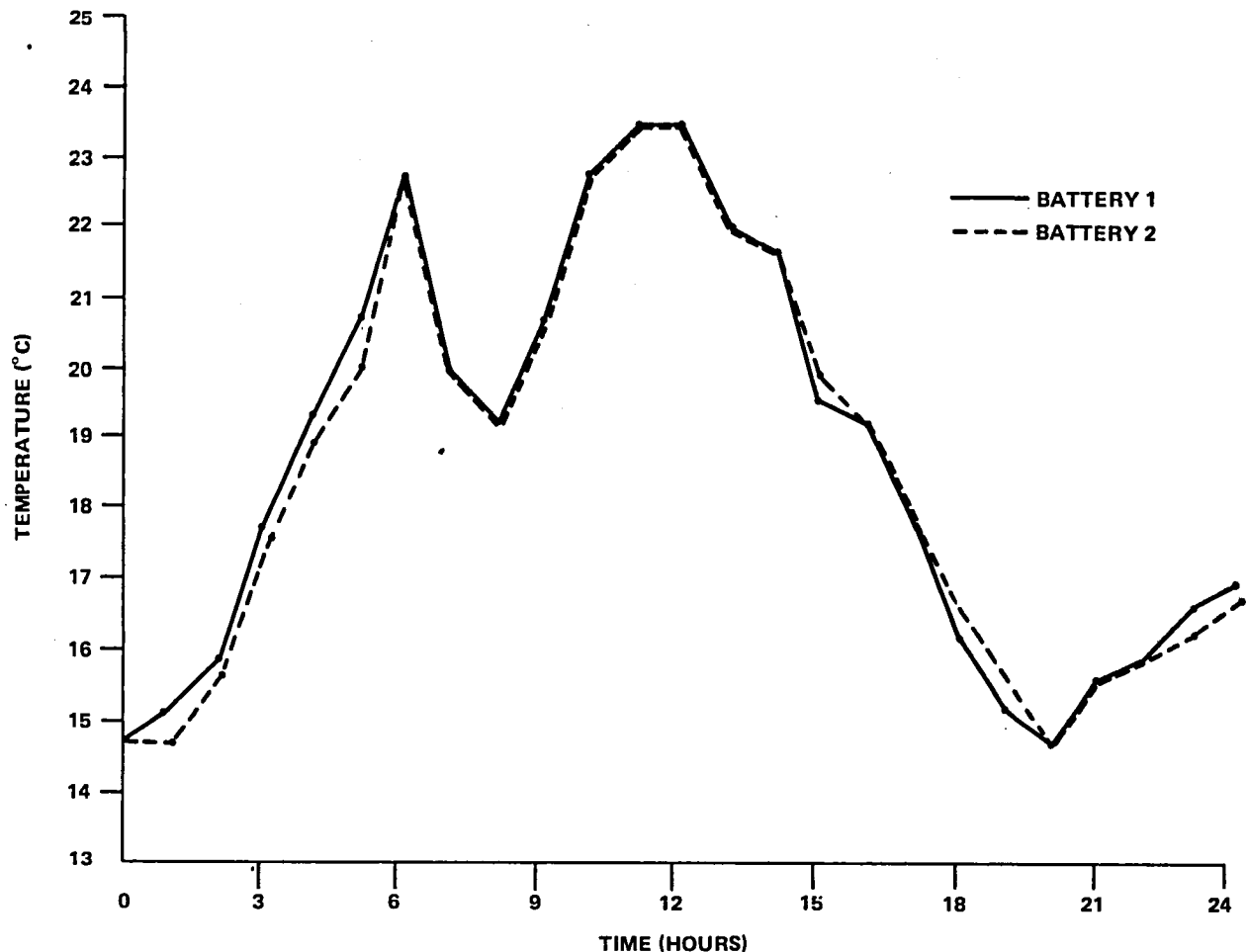


Figure 11-21. Battery Orbital Temperature (September 7, 1976)

CONCLUSIONS AND RECOMMENDATIONS

The thermal behavior of the spacecraft was as predicted and its temperatures were within preflight specification levels. EVM data for various orbital variations and power modes indicated that the elements of the thermal subsystem, particularly the louvers and the heat pipes, functioned properly throughout the mission. In-orbit tests confirmed the long-term reliability of the thermal control components.

In general, the temperatures followed closely the average registered by the heat pipes network on which most of the dissipators were located. Table 10-1, Chapter 10, gives a list of components acceptance and qualification levels and procedures and compares flight data with preflight analysis and ground test results. The temperatures during flight were within the limits imposed by ground testing. The temperatures of the batteries and Earth sensors approached the upper limits imposed by specifications and recommendations of the vendors, but no damage was observed.

Table 11-3
Battery Main and C/60 Charge Rate Temperature Gradients (°C)

Date, 1974*	C/60	Batt 1 Temp	Batt 2 Temp	Base- plate Temp	Batt 1 Gradient	Batt 2 Gradient	TLM
Nov. 10	OFF	29.1	29.8	26.6	2.5°	3.2°	DACU 2
Nov. 12	OFF	29.1	29.1	26.6	2.5°	2.5°	DACU 2
Nov. 16	ON	22.8	23.5	22.1	0.7°	1.4°	DACU 1
Nov. 20	ON	25.6	25.6	24.4	1.2°	1.2°	DACU 2

*Data taken at 1000 GMT

Table 11-4
Shunt Dissipation Data (°C)

Date, 1974	Total Shunt Dissipation (GMT Hr)	Battery 1 Temp. vs. GMT Hour				
		02	04	06	08	10
Nov. 11	114 watts (0100-1300)	17.8	20.7	25.7	29.1	29.1
Nov. 12	114 watts (0000-0600)	18.1	22.1	26.3	28.4	29.1
	0 watts (0600-1300)					
Nov. 13	0 watts (0100-1300)	17.0	18.9	21.4	23.5	24.2*

*Spacecraft roll angle changed from 5.4° to 3.2°C.

Table 11-5
Spacecraft Roll Angle vs. Battery Temperature

Date, 1974	(Temperature in °C)				
	Battery Temp/ESA Roll Angle Versus GMT Hour				
	02	04	06	08	10
Nov. 14	17.4°/5.8°	18.9°/5.8°	20.0°/5.8°	22.1°/3.2°	22.8°/3.2°
Nov. 16	16.7°/8.0°	18.5°/8.0°	20.7°/8.0°	24.2°/8.0°	24.9°/8.0°
Nov. 17	16.3°/5.4°	17.8°/5.4°	19.6°/5.4°	22.1°/5.5°	23.5°/5.5°

Table 11-6
Millimeter Wave Experiment

Date, 1974	Battery Temperatures (°C) Versus GMT Hour							MMW On Time (GMT)
	02	04	06	08	10	12	13	
Nov. 14	17.4	18.4	20.0	22.1	22.8	22.8	20.0	OFF
Nov. 17	16.3	17.8	19.6	22.1	23.5	23.5	23.5	1100 to 1300
Nov. 18	18.9	22.8	22.8	24.2	26.3	25.6	--	2300 to 0344

The largest variations in in-orbit temperatures occurred in the experiment module that necessarily contained a number of cut-outs to accommodate the experiments and the sensors. The reaction of the module to the alternating solar input and radiation to space through the apertures was partly responsible for these excursions. However, the major effect appeared to be a result of the severe oscillation in the temperature of the ground plane whose thermal coupling to the Earth-viewing panel had not been fully evaluated prior to flight. Last minute changes were made in the attachment design just before shipment to the launch pad and several days after a final thermal balance test was completed.

Minor modifications can be made on future similar spacecraft to reduce the daily variations in the temperatures of an Earth-viewing surface. The improvement would be significant for any Earth sensors and any batteries whose flight temperatures may be quite close to their upper qualification

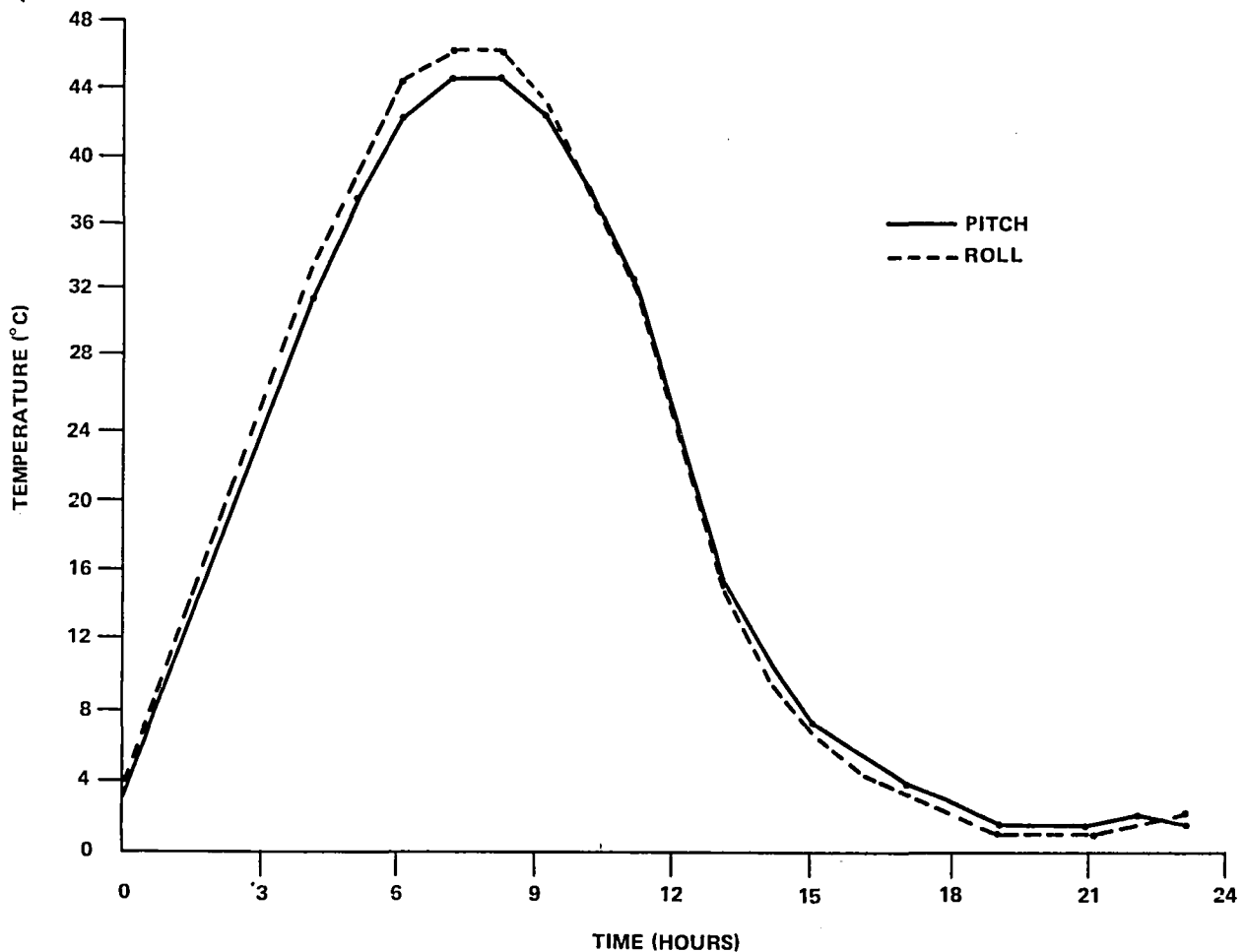


Figure 11-22. Earth Sensor Temperature (August 28, 1976)

levels. A doubler plate can be used to provide a good conductive path between the outer casing of any Earth sensors and the north/south wall whose temperature should be relatively stable (ATS-6 remained below 30°C). A preliminary design of such a doubler was considered early in the ATS-6 program but was discarded after thermal testing showed satisfactory performance of the sensors in the region of the upper temperature limits. Further reduction in any battery temperature may not be readily feasible; however, an evaluation should be made to determine if a partial replacement of the louvered area facing the batteries by passive radiators could lower the temperatures; e.g., from the ATS-6 range of 15°C to 25°C to a more desirable 5°C to 15°C.

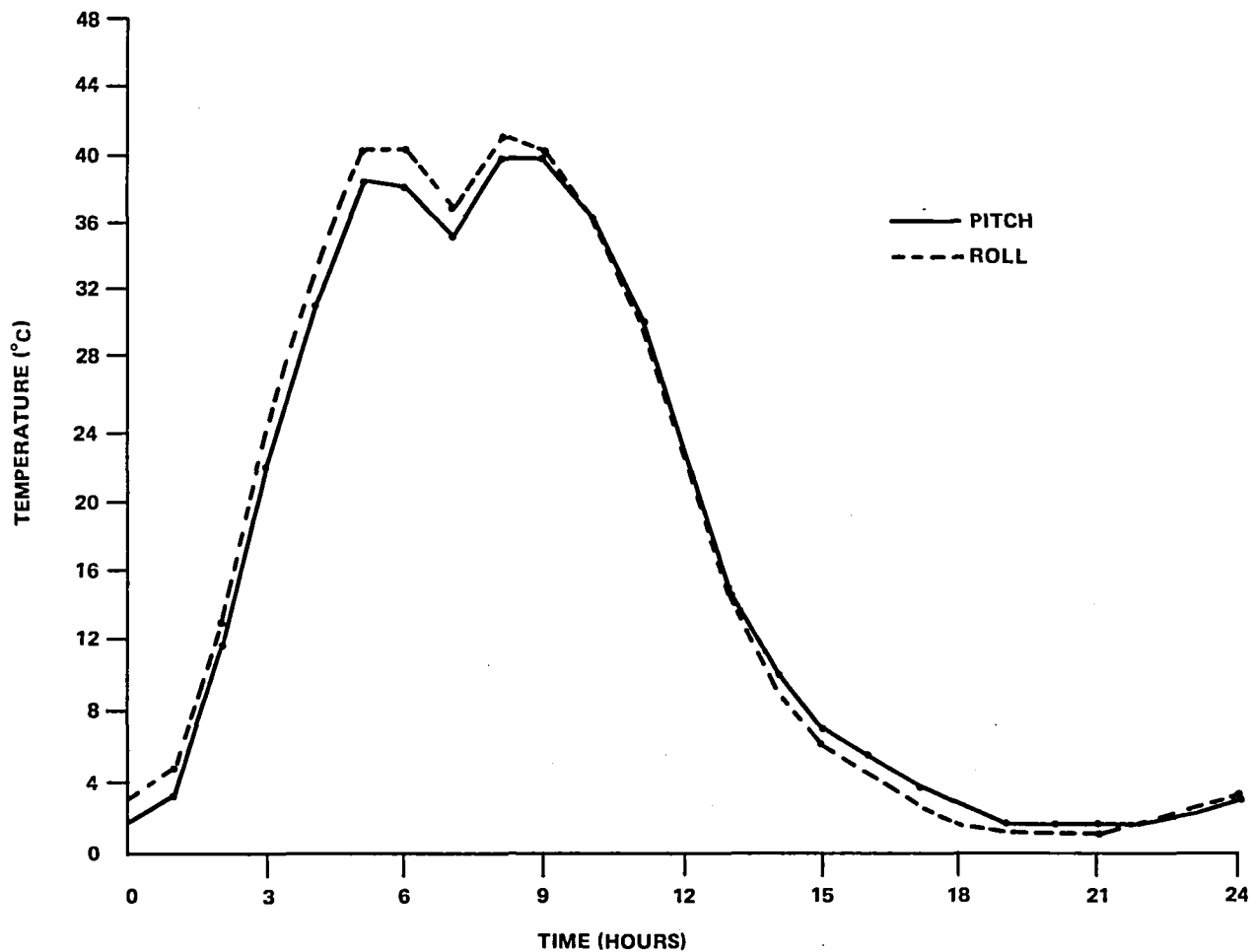


Figure 11-23. Earth Sensor Temperature (September 7, 1976)

CHAPTER 12

ADVANCED THERMAL CONTROL FLIGHT EXPERIMENT

INTRODUCTION

The Advanced Thermal Control Flight Experiment (ATFE) provided the first zero-g-flight data (Earth synchronous orbit) for the performance and evaluation of a thermal-diode heat pipe and an electrical feedback-controlled heat pipe. The temperature stability derived from the melting and freezing of a substance, octadecane, was also evaluated.

EXPERIMENT OBJECTIVES

The ATFE was designed to demonstrate the thermal control capability of a thermal-diode (heat passed in one direction) heat pipe, a phase-change material (PCM) for thermal storage, and a feedback-controlled variable conductance heat pipe (FCHP).

These components were evaluated individually and collectively to develop flight-qualified hardware for future thermal control applications. The ATFE performance objectives were as follows:

- Thermal Diode—Demonstrate reverse-mode diode operation, determine the effect of zero-g environment on diode shutdown characteristics and demonstrate forward-mode heat pipe operation. See Figure 12-1.
- Phase-Change Material—Demonstrate stability derived from the melting and freezing of a PCM. Determine the stability of the melting and freezing points in a zero-g environment, and evaluate the effect of the zero-g environment on the thermal conductance of the PCM package. See Figure 12-2.
- Feedback Controlled Heat Pipe—Demonstrate the ability of the FCHP to provide temperature stability with variations in the heat load and effective sink temperature. Demonstrate the ability of the FCHP to perform as an on/off thermal switch and establish its variable conductance behavior in flight. See Figures 12-3 and 12-4.

SYSTEM DESCRIPTION

The ATFE consisted of a solar absorber, a thermal diode, a simulated equipment package that contained phase-change material, a feedback controlled variable conductance heat pipe, and a space radiator. See Reference 1.¹ Supporting hardware were a solid state electronics module, temperature

¹Refer to references at the end of this chapter.

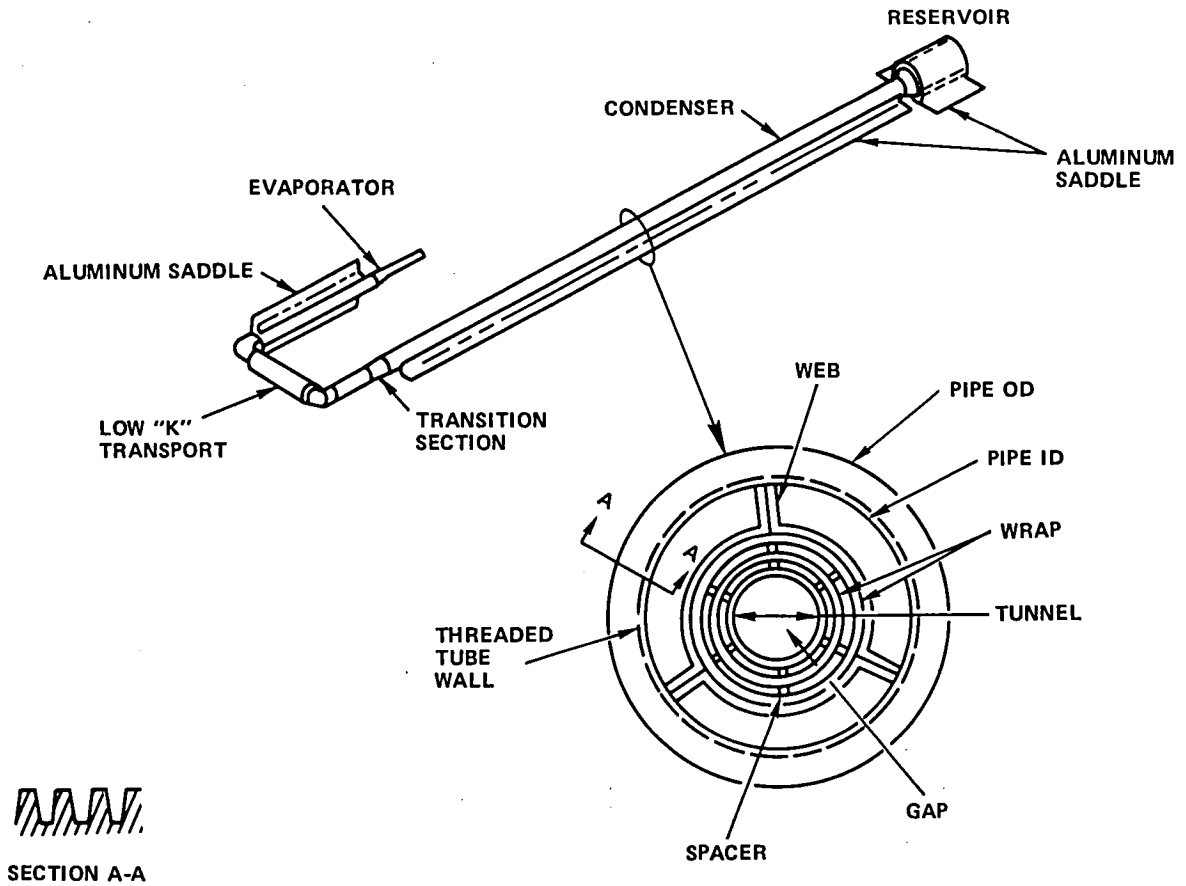


Figure 12-1. Diode Heat Pipe

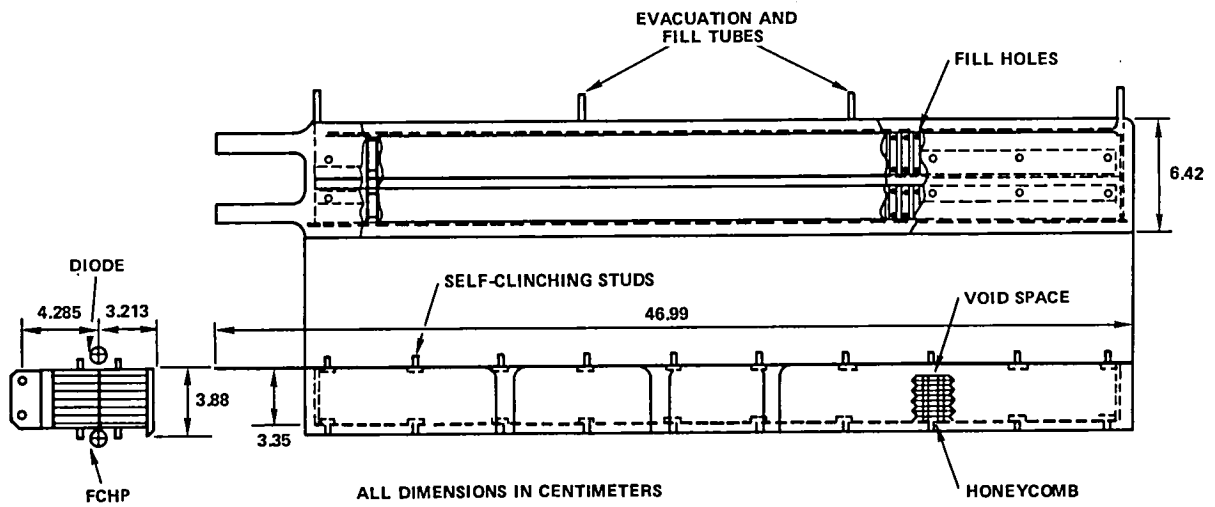


Figure 12-2. PCM Box

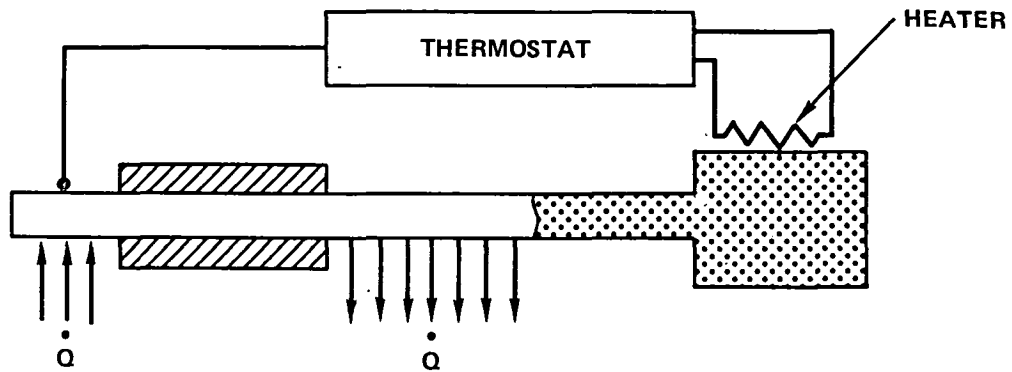


Figure 12-3. Feedback Control

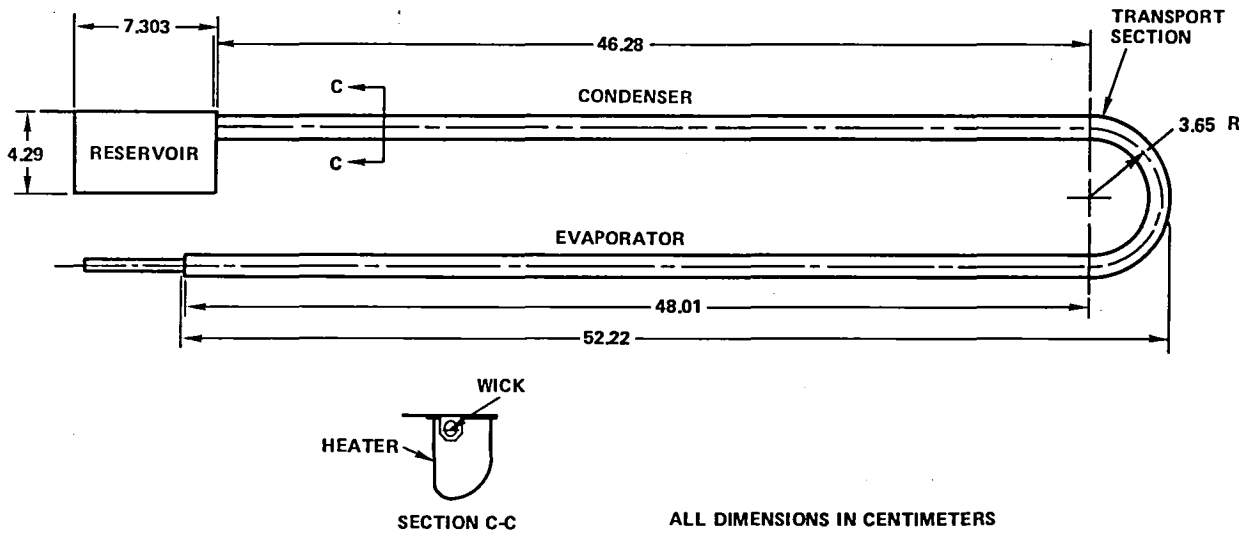


Figure 12-4. Feedback Control Heat Pipe

sensors, foil heaters, multilayer thermal insulation blankets, and a support structure. The electronics module contained the controller for the feedback controlled heat pipe, signal conditioning circuitry, and command relays. The functional relationship of the ATFE components is represented in Figure 12-5.

The ATFE was mounted in the east wall of the Earth-viewing module of ATS-6 with only the out-board surfaces of the solar absorber and radiator exposed to the external environment. Solar input was used as the primary heat source to the experiment. Because of the geosynchronous orbit and three-axis stabilization, the solar flux incident upon the east wall and the AFTE rose and set with an approximately sinusoidal variation over the 12-hour period, followed by 12 hours of shadow (Figure 12-6). The solar cycle was essentially the same as that experienced by a fixed point on the Earth's surface.

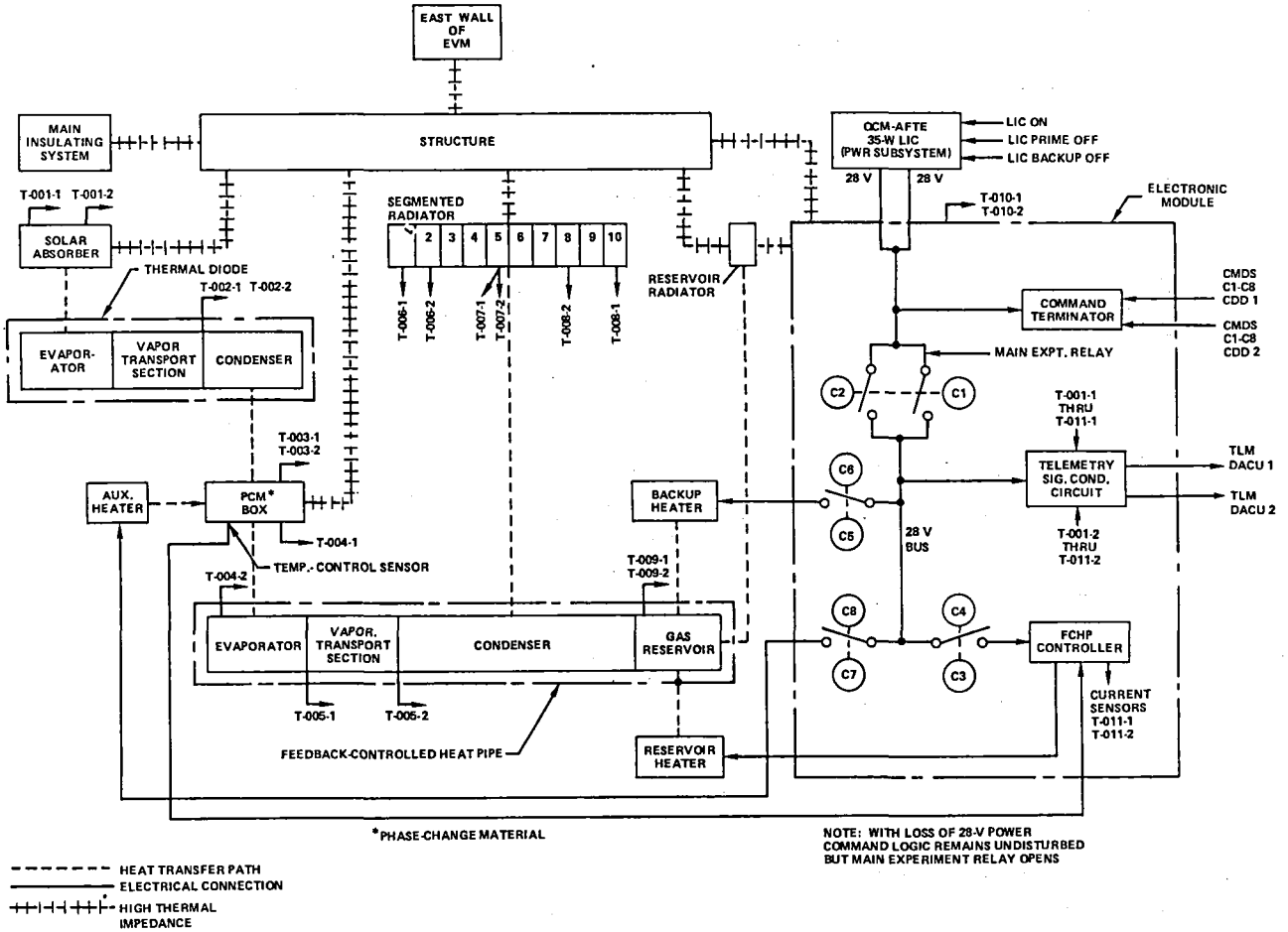


Figure 12-5. Functional Diagram

During the period of solar input, energy collected by the absorber was transported by the diode heat pipe to the PCM box. This energy was equivalent to power dissipation during an electrical duty cycle, with the PCM package serving as a simulated temperature-controlled equipment shelf. Initially, the energy melted the PCM, which was octadecane with a melting point of 28°C. When all of the PCM had melted, the energy from the absorber passed through the equipment shelf to the FCHP, which transported it to the space radiator. During this part of the cycle, temperature control of the diode/PCM box interface was provided by the FCHP. A sensor at this interface enabled the FCHP to regulate the heat rejection to space and thereby accommodate variations in both the thermal load and the thermal boundary conditions at the radiator. The feedback system was designed to control the diode side of the PCM box at 29°C, ±3°C.

As a shadow period approached, the diode and FCHP decreased their conductance to minimize the heat loss from the PCM box to space. This occurred in the following manner: as the heat input to the system diminished, the absorber radiator and PCM box began to cool. When the absorber temperature dropped below the temperature at the diode side of the PCM, passive shut-down of the diode occurred that thermally decoupled the cold absorber from the PCM box. Similarly,

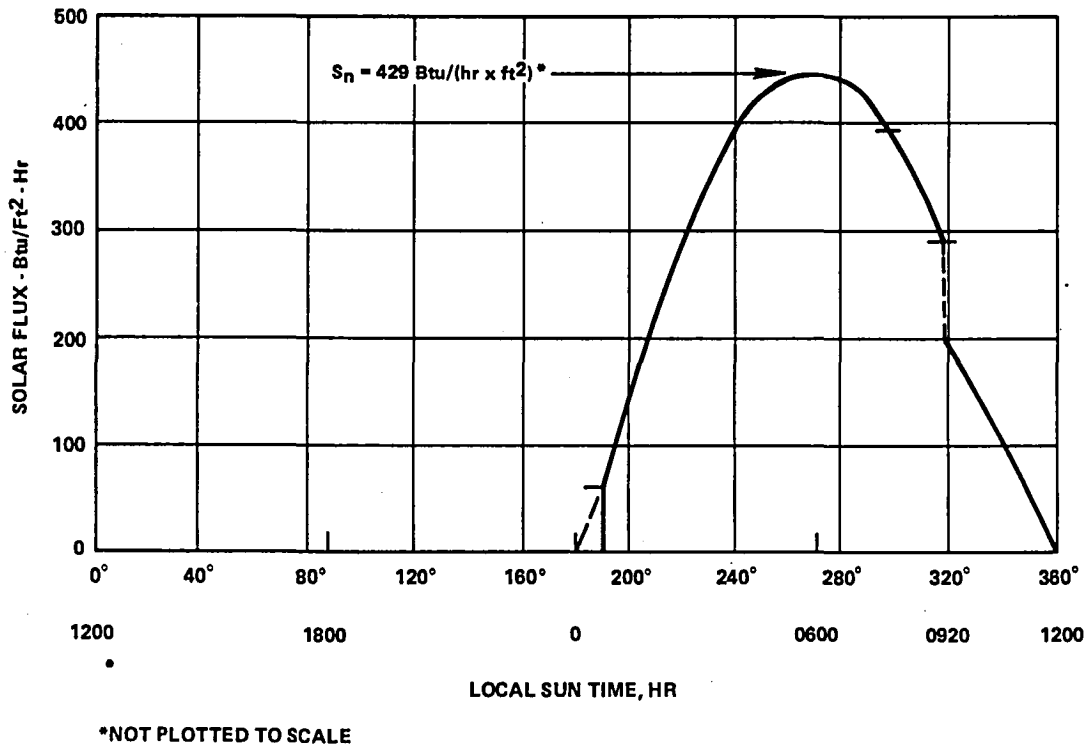


Figure 12-6. Typical Daily Solar Cycle for ATFE

under normal FCHP operation, when the PCM temperature dropped below 29°C , the FCHP shut down and decoupled the box from the cold radiator. With no thermal throughput, the PCM continued to cool to 28°C and then began to freeze.

The release of thermal energy by the freezing of the octadecane was used to compensate for the heat loss during transient shutdown of the diode and the FCHP, and to provide for temperature stability over part of the 12-hour shadow period. When all the octadecane had frozen, the temperature of the equipment shelf decreased at a rate consistent with the thermal capacitance of the PCM box and its parasitic heat leaks. There was 0.363 kg of octadecane that provided temperature stability for about 5 hours of shadow, after which the PCM box cooled to approximately 0°C . The temperature of the PCM was allowed to decrease to 0°C to evaluate the effect of subcooling on the stability of the melting point of the octadecane.

ATFE had five operational modes in addition to the normal mode just described. Each of these modes is defined in Table 12-1. Several modes permitted continued operation in the event that the thermal diode or FCHP controller failed. The passive and passive-auxiliary modes were used to obtain performance data with the FCHP operating as a conventional gas-controlled heat pipe. Finally, the auxiliary and backup heaters could be used to demonstrate extended performance capability by the FCHP at temperatures different from the controller set point (29°C).

Table 12-1
ATFE Operational Modes

Mode	Description	Command Status
Normal	Normal operation of system: Controller provided automatic regulation by FCHP.	Experiment turn on FCHP controller on
Auxiliary	Auxiliary heater on. Provided additional exercise of FCHP or redundancy if thermal diode should fail.	Experiment turn on FCHP controller on PCM box auxiliary heater on*
Passive	FCHP controller turned off: FCHP acted as a passive variable conductance heat pipe.	Experiment turn on
Passive-Auxiliary	FCHP controller off and auxiliary heater on as in auxiliary mode: To evaluate system with passive control.	Experiment turn on PCM box auxiliary heater on
Backup	Manual control of the backup reservoir heater: Provided redundancy in the event the FCHP controller should fail, or operation at an alternate set point.	Experiment turn on FCHP backup reservoir heater on/off**
Backup/Auxiliary	This mode was redundant to the auxiliary mode, with manual control of the backup heater. It could also be used to demonstrate additional FCHP performance at temperatures different from the FCHP controller's set point.	Experiment turn on FCHP backup reservoir heater on/off** PCM box auxiliary heater on

*The auxiliary heater was attached to the diode side of the PCM box and had a 20-watt electrical output.

**The backup heater was attached to the FCHP's reservoir and was redundant to the reservoir heater regulated automatically by the controller. It had a 2.8-watt output and was turned on or off by command, as needed, to maintain control at the desired set point.

FLIGHT PERFORMANCE AND EXPERIMENT RESULTS

The ATFE was tested extensively over the first 3 years after being launched into orbit on May 30, 1974. Each of the test modes identified in Table 12-1 was exercised. Major emphasis was on normal and passive mode operation. The data presented were derived from 10 analog telemetry channels that measured temperatures at different positions throughout the ATFE. An additional analog channel measured electric current to determine the status of the FCHP controller/reservoir heater.

Many of the results presented in this report were derived from previous reports on ATFE. (See References 1 to 16).² Information obtained from these reports was modified and updated as required to best reflect the current understanding of the ATFE's performance.

Normal Mode Performance

The operation of the ATFE in the normal mode was previously described under "System Description." The characteristic transient orbital performance of the experiment is presented in Figure 12-7 for the normal mode 10 days after launch.

As the ATFE moved from the end of the shadow period into sunlight, the absorber (T-001) rapidly rose from -60°C to a maximum of 36°C near maximum solar input. As the Sun "went down," the temperature of the absorber dropped below the PCM melt temperature (28°C) and diode reversal was initiated. Once diode shutdown was completed, the absorber cooled rapidly and its temperature approached its minimum steady-state condition asymptotically.

The PCM box (T-003) also increased rapidly in temperature once the diode began transferring energy. It then reached a plateau as the octadecane began to melt. A gradient of approximately 3°C developed across the PCM box as the octadecane melt front advanced from the diode to the FCHP side of the box. The further increase in temperature from 31°C to 35°C was an overshoot resulting from inadequate cooling by the FCHP. This result relates to the performance of the FCHP reservoir (T-009), which at launch was 10°C warmer than the nominal design value and the temperature experienced during acceptance tests.

The higher reservoir temperature required a higher vapor temperature for the FCHP to open and conduct heat. The resulting increase in vapor temperature was reflected directly in an increase in the temperature of the PCM box. A discussion of the potential cause of the elevated reservoir temperature is presented in a later section.

Beyond 0700 Sun time, the thermal energy transferred by the diode began to decrease and the PCM temperature started to drop. As the solar input decreased further, the absorber temperature dropped below the PCM temperature and there was no longer any heat input from the diode (0945). The PCM continued to cool until it reached 27.7°C , at which time freezing began. The latent heat released by the octadecane's freezing compensated for any transient losses during the diode and FCHP shutdowns. Further freezing compensated for the conductive losses through the diode and FCHP and any other parasitic losses from the PCM box. When all of the octadecane had frozen, the PCM box cooled consistent with its parasitic heat leaks and its heat capacitance to just below 0°C before the start of the next daily cycle.

The solar input to the FCHP reservoir radiator, during the initial portions of the cycle, supplemented the heat power applied to the reservoir by the controller and resulted in a rapid increase in reservoir temperature (T-009). When the temperature of the diode side of the PCM box (controller sensor location) reached the set point (29°C), the reservoir heater turned off and the reservoir temperature began to decrease. As the reservoir temperature decreased, the control gas in the FCHP receded into

²See references at the end of this chapter.

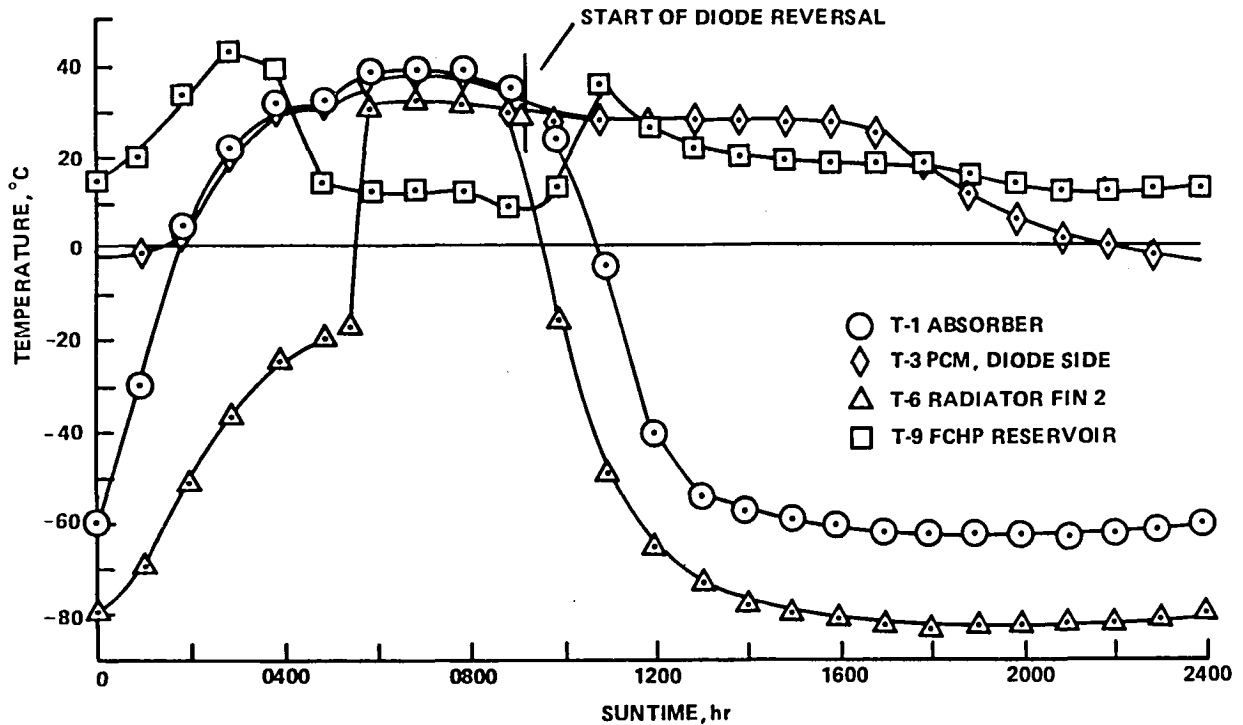


Figure 12-7. Typical Transient Response in Normal Mode
(10 Days Post-Launch)

the reservoir. This unblocked the FCHP condenser section and permitted the heat pipe to transport energy from the PCM to the radiator fins. Once all of the PCM had melted, the FCHP began to transfer the energy to the radiator (T-006) where it dissipated to space.

When the diode-side PCM temperature dropped below 29°C the controller turned the reservoir heater back on with a resulting increase in reservoir temperature. This caused the FCHP to shut down and resulted in a corresponding cooling of the radiator. Continued cooling of the radiator and subsequent cooling of the reservoir resulted from diminishing solar input as the shadow period was approached.

The ATFE's thermal performance is further illustrated by the axial temperature distributions shown in Figure 12-8. At the time of maximum energy throughout (0700), there were slight temperature drops across the absorber/diode, the PCM box, and the active portion of the FCHP. Radiator fins 5 through 10, which were located at the inactive portion of the FCHP, exhibited thermal gradients consistent with the conduction losses from the active portion and the gas reservoir. For this cycle, the reservoir heater had been off since 0400, and at 0700 the reservoir had reached a quasi-steady-state temperature of 11.5°C. At maximum conditions, the radiative coupling from the hot absorber inhibited cooling of the reservoir, and caused its temperature to be higher than the effective sink temperature (e.g., fin 8).

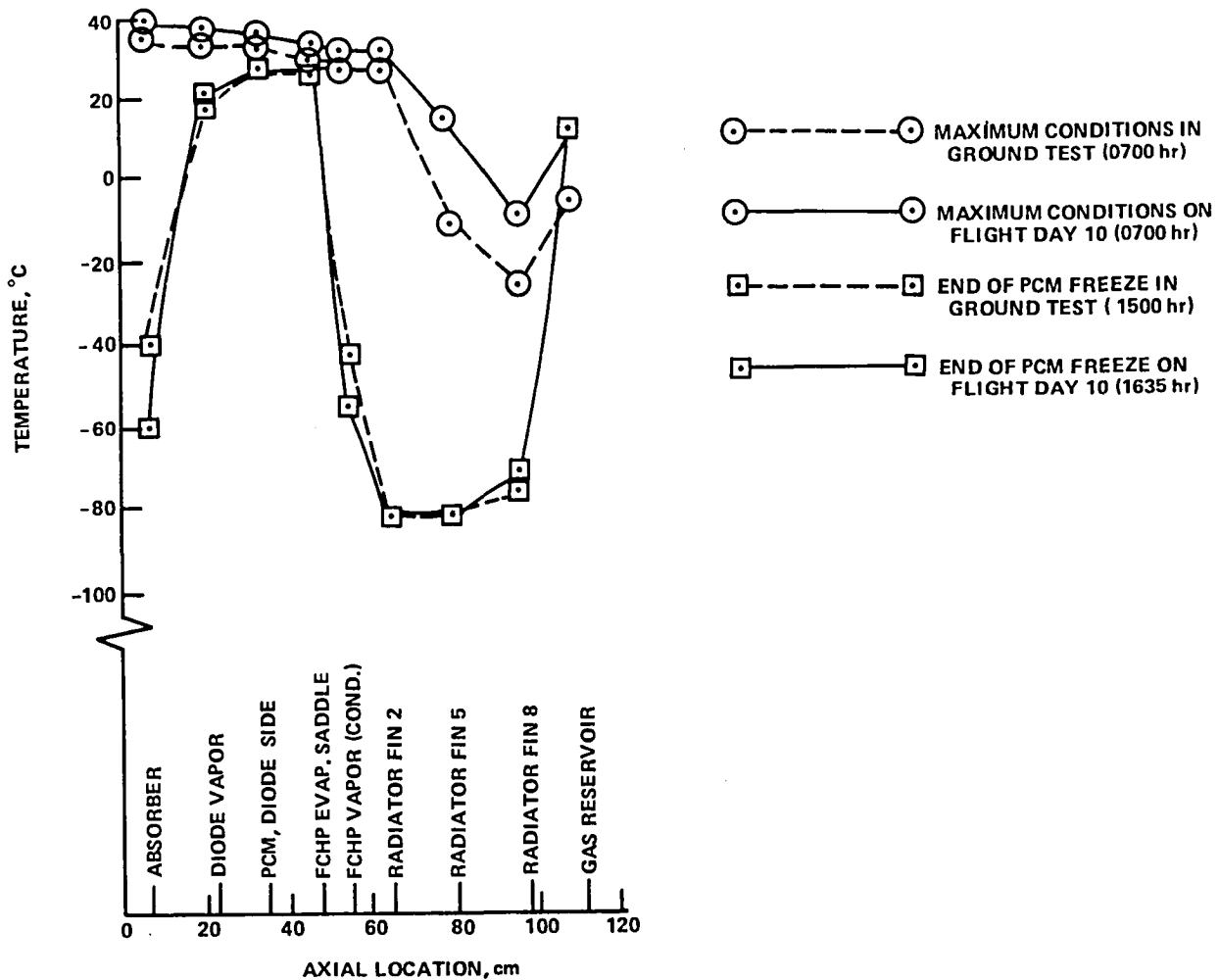


Figure 12-8. Axial Temperature Profiles, June 9, 1974

During the shadow period, the PCM box was essentially isothermal and large gradients developed between the PCM, the absorber, and radiator as the diode and FCHP shut down. In the normal mode, conditions were such that the PCM had completely frozen by 1630. At this time the PCM was at 27°C, and the absorber and radiator had reached equilibrium temperatures of -62° and -82°C, respectively. The 6°C gradient between the PCM and the diode transport section (T-002) indicated that the diode was fully shut off, with liquid blockage extending through the “low-k” and at least part of the transport section (Reference 7). The -55°C temperature in the FCHP transport (T-005), and the 82°C gradient between it and the PCM was indicative of gas blockage back into the FCHP evaporator.

Throughout the entire shadow period, the reservoir heater was on continuously and the reservoir temperature achieved an equilibrium value of 14°C, which was sufficient to maintain complete shut-off of the FCHP. At the end of the shadow, the PCM box was still isothermal but had dropped to 0°C. The absorber and radiator temperatures showed a slight increase that was due apparently to infrared inputs from the spacecraft antenna, which were at a maximum at the beginning and end of shadow.

Feedback Versus Passive Control

The operation of an electrical feedback-controlled heat pipe was the same, in principle, as that of a passive "cold-reservoir" variable conductance heat pipe (VCHP). The only difference was that the FCHP's reservoir temperature was regulated to provide the desired control. In the passive system, the reservoir followed the sink temperature and the heat-pipe vapor and heat-source temperatures adjusted accordingly. The normal and passive modes provided a comparison of the ATFE's performance with the two types of control. In addition, operation at an elevated set point could be effected by using the auxiliary and backup heaters. This test gave a direct comparison of the temperature stability afforded by a gas-controlled VCHP with and without feedback.

Normal Versus Passive Mode Performance

In Figure 12-9 the ATFE's transient performance in the normal mode is compared with its performance in the passive mode. The diode's performance (i.e., T-001) is not included since its transient behavior was the same in both modes. In the passive mode, the controller was turned off and the feedback pipe operated as a conventional "cold-reservoir" system. Hence, during the period of solar input, the reservoir had a sinusoidal temperature profile that increased from -75°C to a maximum of 10°C and then cooled back to -75°C and held through the shadow period. At approximately 0400, the VCHP began to open and transport energy to the radiator. This was evidenced by the sharp rise in the pipe's transport temperature (T-005). The more rapid increase in the temperature of the reservoir compared to the heat pipe caused a partial shutdown of the VCHP at 0500. As the solar input condition was approached, the conditions were such that the VCHP opened up again and remained open through 1100 in the passive mode. Freezing of the PCM occurred between 1000 and 1100 as the open VCHP transferred the PCM's latent heat. Subsequent cooling by the VCHP reduced the PCM and pipe temperature to the point where the heat pipe shut down even though the reservoir was very cold. This was indicated by the sharp decrease in T-005.

The major difference in the performance of these two modes of operation was due to the passive VCHP's being open when the PCM started to freeze. As a result, all the stored latent heat was transmitted to the radiator. In the normal mode, where feedback was employed, the reservoir was heated when T-003 dropped below 29°C. This caused the FCHP to shut down prior to freezing, and it remained shut off until the next day's solar input brought the PCM to above 29°C. Consequently, temperature stability was provided for 6 to 7 hours in the normal mode, versus 1 hour with passive control.

Axial temperature profiles for these modes are compared in Figure 12-10 at the end of each of their respective freezing periods. The end of freezing occurred at 1111 in the passive mode. The heat-piping action during this time was evidenced by the isothermal region of the VCHP that extended

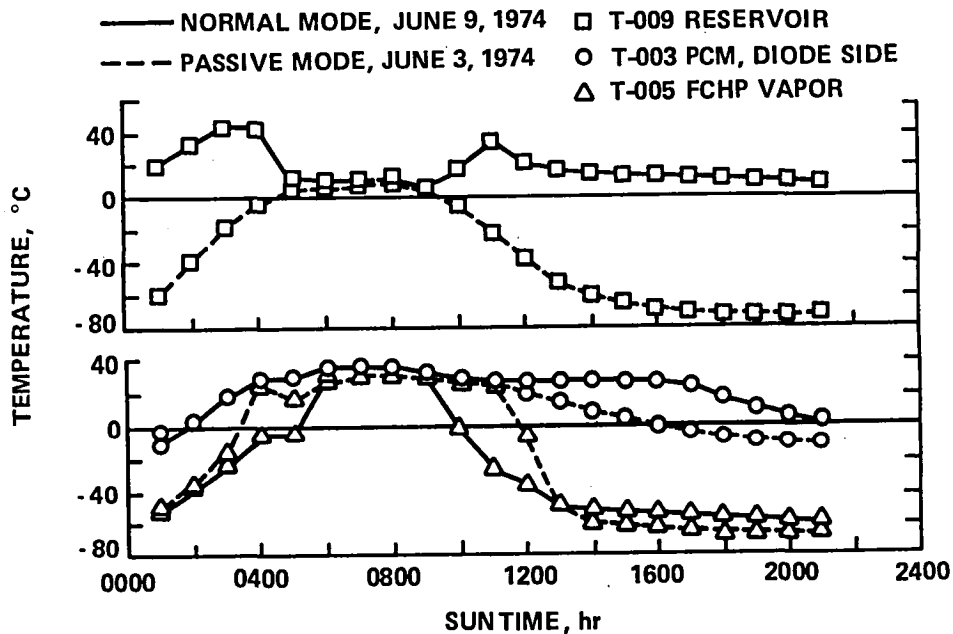


Figure 12-9. Comparison of Feedback and Passive Transient Control

through the second radiator fin. At the same time, in the cycle with feedback control, the FCHP was shut off back to the downstream end of the evaporator. Freezing was completed at 1635 in the normal mode, and the pipe was still completely shut off. The passive mode profile at this time also showed the VCHP shut off, but this was because the PCM's latent energy had been dissipated more than 5 hours earlier and its temperature had dropped below 0°C.

Feedback Control at an Elevated Set Point

The operation of the FCHP in the normal mode just discussed was essentially that of an "on-off thermal switch." The ATFE was designed to demonstrate regulated FCHP energy dissipation during solar input at a nominal 29°C set point (measured at the PCM). However, because the in-flight reservoir temperatures exceeded the maximum reservoir design temperature of 5°C, an overshoot of PCM temperature occurred and regulated control at 29°C was not possible.

A demonstration of the FCHP's ability to provide temperature regulation was obtained by running the system at an elevated set point. This was accomplished by operating in the backup/auxiliary mode. In these tests, the control temperature was preset to 46°C and the backup reservoir heater was then manually commanded on or off consistent with the prevailing PCM temperature (T-300). As in the case of the automatic control, the backup heater was on when T-003 was below the set point and the FCHP shut down. Conversely, the heater was off when T-003 was above the set point.

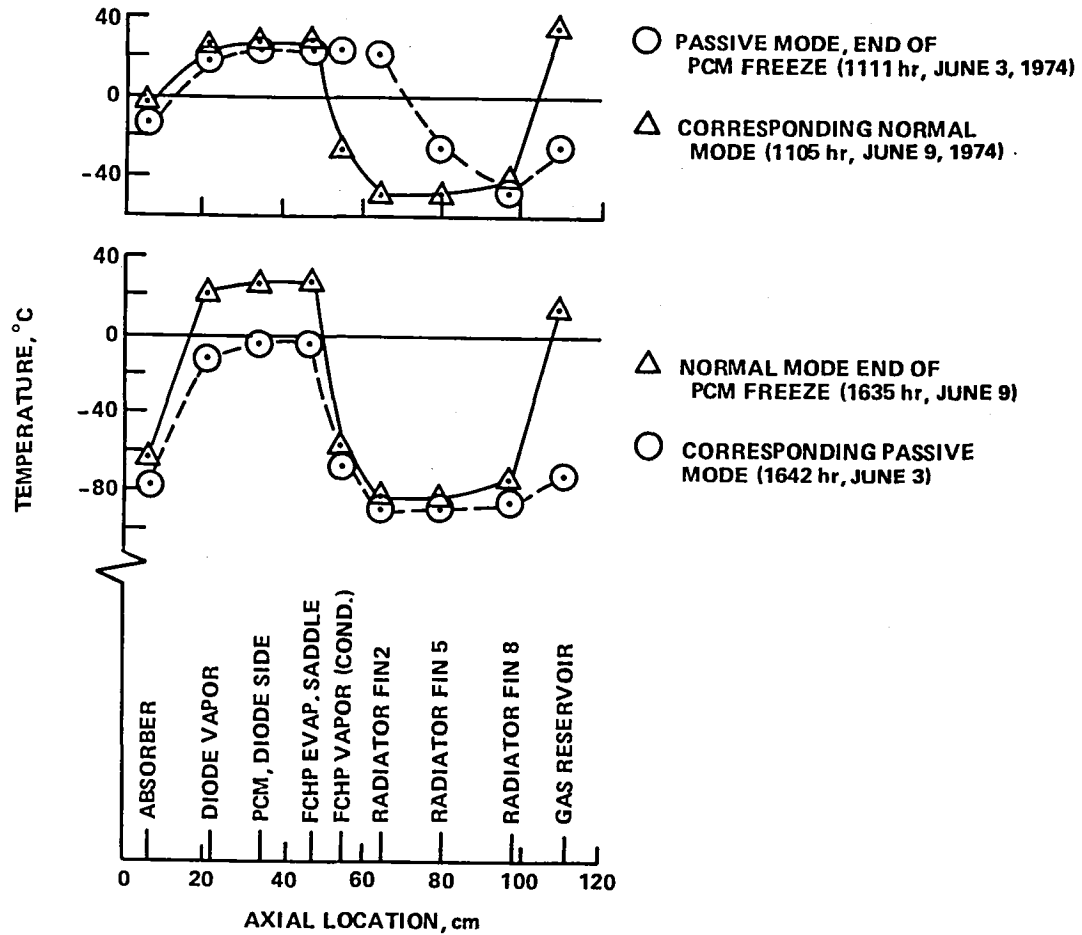


Figure 12-10. Comparison of Axial Profiles in Normal and Passive Modes

The auxiliary heater was used in this test to provide thermal throughput during shadow and the early and late portions of the solar cycle when the thermal diode was off. This heater had a 20-watt output and was attached to the diode side of the PCM box. It replaced or supplemented the thermal energy transferred by the diode during its forward-mode, heat-pipe operation.

A comparison of the temperature stability provided with feedback versus passive control during the elevated set-point tests is presented in Figure 12-11. The results show that with feedback, the PCM temperature was controlled at 46°C, ±2°C throughout the entire cycle. Tests were conducted through only a portion of shadow since quasi-steady operation was obtained then. Passive control, under the same conditions, resulted in a peak PCM temperature of 45°C and a steady-state shadow condition with the PCM box at 25°C.

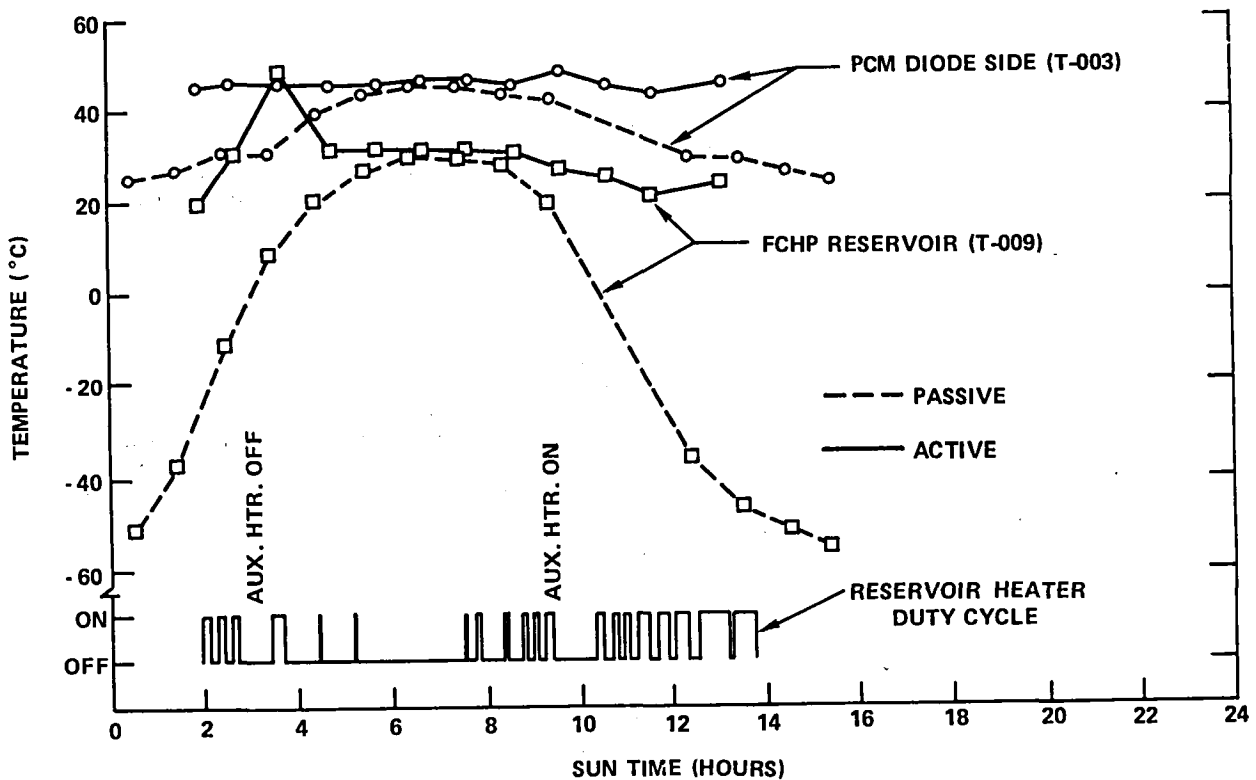


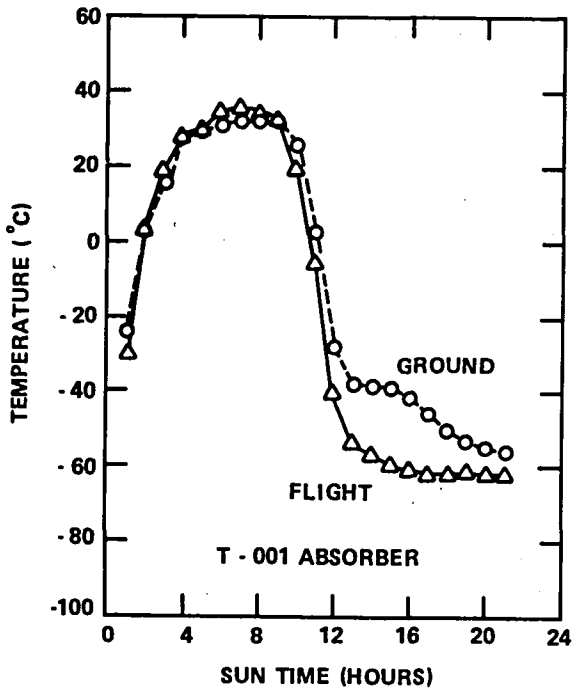
Figure 12-11. Comparison of Feedback and Passive Control at an Elevated Set Point

The major control provided by the FCHP during these tests lay in its regulation of the heat dissipation throughout a very broad variation in sink temperature. Radiator fin 10, which was in the inactive region of the heat pipe, was a good measure of the effective sink temperature. It varied from -56°C during the shadow to a maximum of 26°C . The feedback system therefore provided control to within $\pm 2^{\circ}\text{C}$ corresponding to an 82°C variation in sink temperature.

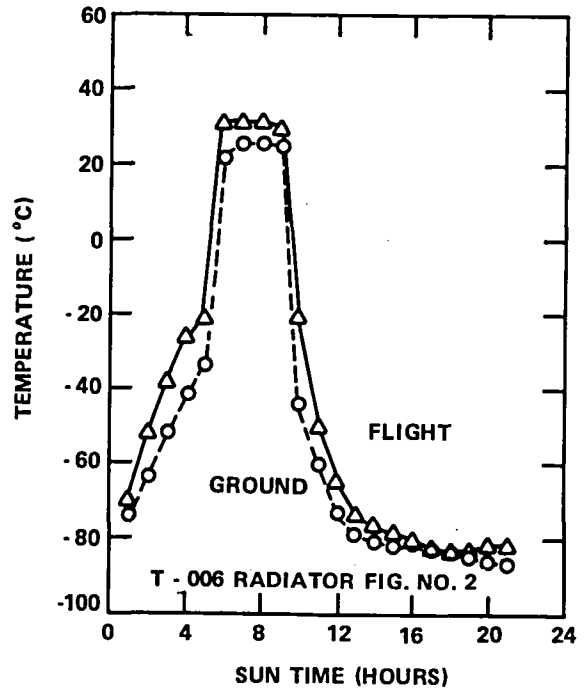
COMPARISON OF FLIGHT AND 1-g PERFORMANCE

Flight data for the normal mode on June 9, 1974, is compared with data obtained with the preflight thermal vacuum acceptance tests in Figures 12-12 and 12-13. Solar input during the ground tests was simulated by electrical heaters attached to the inboard side of the absorber, radiator, and FCHP reservoir surfaces. The input for this ground test was based on a solar intensity of 1245 W/m^2 (395 Btu/hr-ft^2), whereas the actual solar intensity on June 9th was 1201 W/m^2 (281 Btu/hr-ft^2). An absorptivity of 0.96 was used for the absorber's black paint. The radiator and reservoir were covered with second-surface mirrors, for which a nominal design absorptivity of 0.10 was used to establish the heater input.

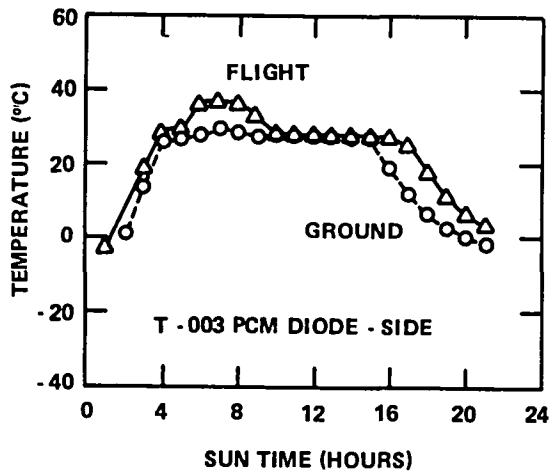
The transient response of the ATFE presented in Figure 12-12 was similar in the flight and ground tests. There were some discrepancies worth noting, however. As can be seen in both Figures 12-12



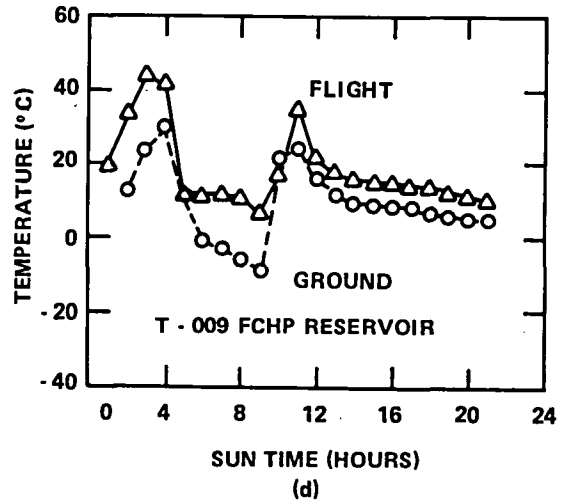
(a)



(c)



(b)



(d)

Figure 12-12. Comparison of Flight and Ground Transient Performance—Normal Mode

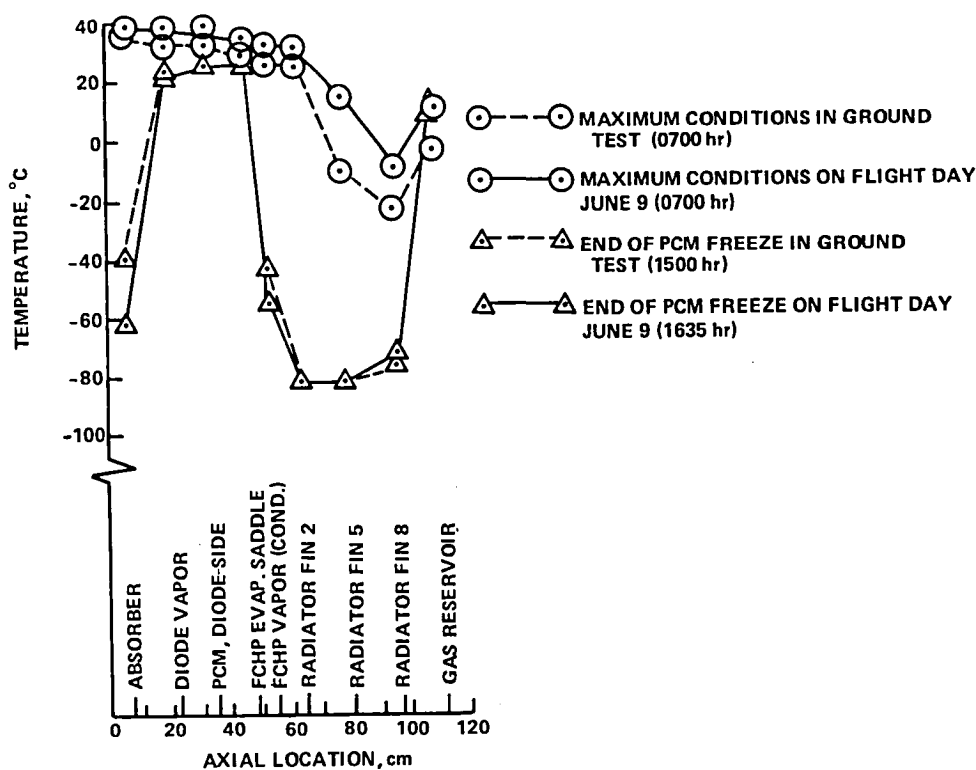


Figure 12-13. Comparison of Flight and Ground Axial Temperature Profiles

and 12-13, the flight temperatures during the hours of peak solar insolation (peak at approximately 0700) were higher at all locations. The most noticeable increase occurred at the FCHP gas reservoir (T-009) that was running approximately 15°C warmer on June 9, 1974. The hotter reservoir caused the entire FCHP to operate at a higher temperature (Section 4) and this, in turn, caused the PCM (T-003) to run warmer. Thus, the efficiency of the entire absorber-to-radiator heat transfer path was impaired by the higher reservoir temperature. The higher reservoir temperature was due to degradation of the second-surface mirrors that acted at the reservoir's radiating surface. This was discussed in the section on feedback versus passive control.

Another difference in thermal performance between the flight and ground tests was indicated by lower absorber temperatures (T-001) on June 9th during the shadow period. See Figure 12-12(a). This lower temperature implied that the diode was conducting less heat between the PCM and the absorber subsequent to diode shutdown. This was further supported by the fact that the time required for complete freezing of the PCM increased from 5.5 hours during ground tests to 6.5 hours on June 9th. See Figure 12-12(b). A lower diode off conductance would decrease the parasitic losses from the PCM and increase its freeze interval. This is discussed in more detail in the following section.

The behavior of the PCM was the same in both ground and flight tests. The melting and freezing points were both approximately 28°C and the gradient across the box, less than 3°C during peak solar conditions, indicated that the thermal conductance was unaffected by the 0-g environment.

Long Term Performance

Telemetry

Certain anomalies were encountered while reducing the flight data for the ATFE and it was suspected that some of the telemetry data was unstable. An analysis was performed to determine the validity of this data (Reference 1). By comparing the long term trends of all the channels and by examining quasi-steady-state results derived from auxiliary-mode tests, it was deduced that the channels on the radiator (T-006, -007, -008) and absorber (T-001) were indeed drifting.

These channels had very sensitive signal conditioning networks. This was necessary to accommodate the low temperature (approximately 190 K) and broad range that they monitored. Low resistance platinum transducers, which required amplification of their output signals, were used for these channels. All other channels (T-002, -003, -004, -005, and -009) used thermistors and resistance divider circuits which were much more stable.

A shift in the calibration that caused higher readings than normal was observed during the flight acceptance tests. At that time resistors were replaced in the circuits that provided a constant-current source to the transducers. It is possible that the telemetry shift in flight was also due to a drift in this constant-current source. This drift could have been caused by the electronics module running as high as 40°C during maximum conditions, while the components were typically rated at 20°C.

The analysis reported in Reference 1 was performed after a year and a half of flight time. After that time, it appeared that these channels had stabilized and were no longer drifting. Adjustments were made in all subsequent analyses to account for these shifts.

One further problem with the telemetry data was that some of the channels became saturated at maximum conditions. Specifically, channels T-006, -007, and -008 in DACU 2 did not read any higher than 37°C, 16°C, and 26°C, respectively. However, sufficient data existed and this did not impair the analytical efforts.

Degradation of Second-Surface Mirrors

As noted previously, the temperature of the ATFE during the hours of peak solar insolation was higher immediately following launch than in the ground tests and it continued to increase with time. The probable cause of this was a degradation of the second-surface mirrors, optical solar reflectors (OSR), that were employed as radiator surfaces for the FCHP's condenser and reservoir.

Selected flight data for the first 2.5 years of orbit are presented in Figure 12-14(a). The data show the maximum daily temperature (at approximately 0700 hr Sun time) for the PCM (T-003) and the FCHP reservoir (T-009) versus days in orbit. The reservoir temperature near the end of the PCM freeze period (approximately 0600 hr) is also shown in this figure. At both locations the maximum daily temperatures increased with time: T-003 increased from 36°C at launch to 54°C on flight day 949, while T-009 increased from 11°C to 47°C over the same interval.

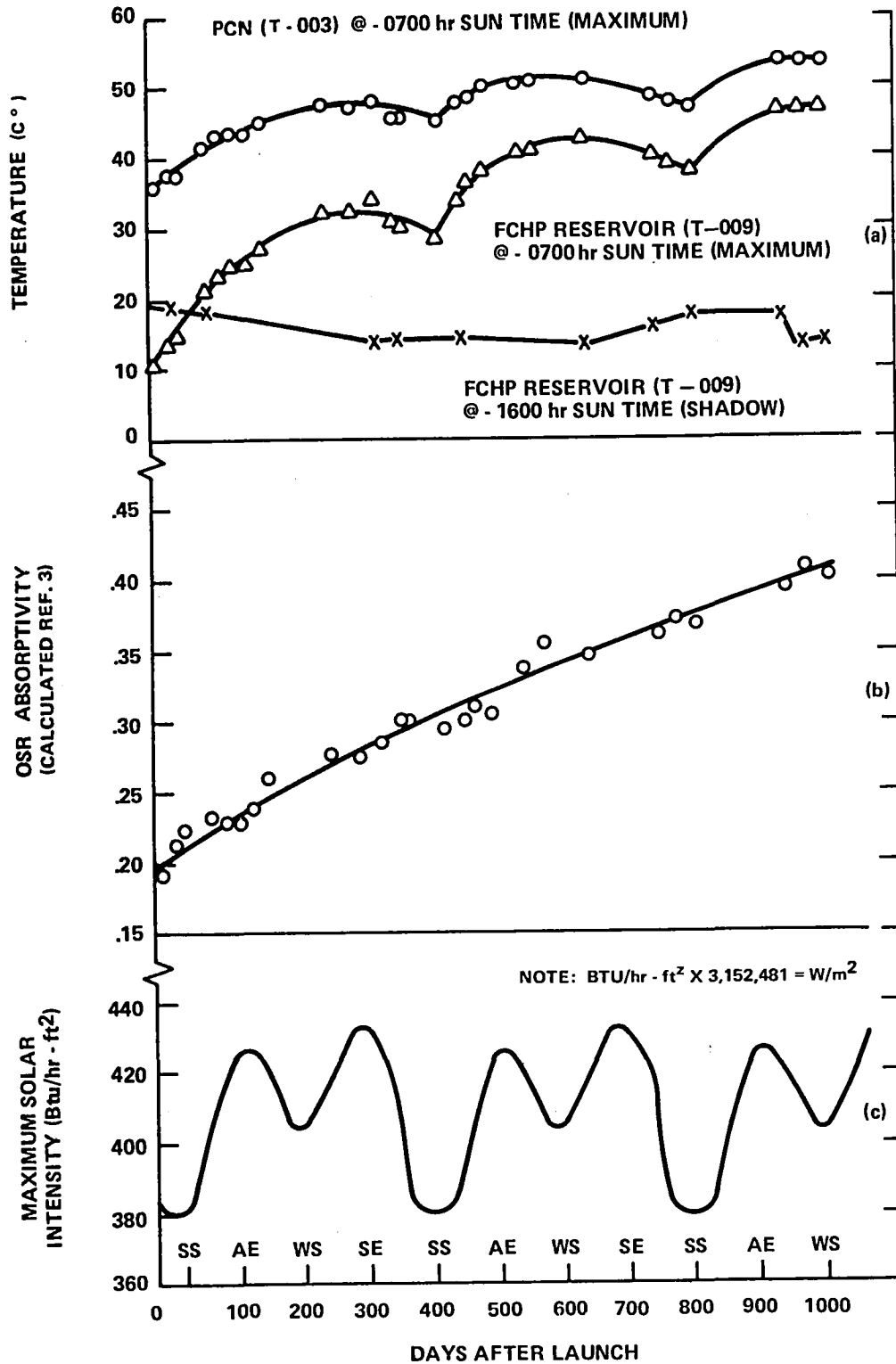


Figure 12-14. Daily Temperatures, OSR Absorptivity, and Maximum Solar Intensity vs. Days in Orbit

The FCHP reservoir temperature (T-900) during the shadow period in the normal mode, remained constant at about 16°C. This supports the earlier conclusion that this channel was stable and that the trends were due to causes other than telemetry drift.

The seasonal variation of solar intensity incident on ATFE is shown in Figure 12-14(c). The variations of both incident solar angle and solar irradiance were used in calculating the intensity. If Figures 12-14(a) and 12-14(c) are examined concurrently, it can be observed that the rates of increase of the maximum temperatures for both T-003 and T-009 were greatest during the period of increasing solar intensity prior to the spring and autumn equinoxes (SE and AE). The temperatures tended to decrease slightly prior to the summer and winter solstice (SS and WS).

During maximum Sun conditions, the PCM was completely melted and the absorbed heat was transported from the PCM box to the radiator via the FCHP. The higher the gas reservoir temperature during this time, the more difficult it was for the FCHP to open; i.e., to increase its thermal conductance. The operating temperature of the FCHP increased 1°C for every 2°C increment in reservoir temperature in order to continue transporting the heat input. The increase in FCHP temperature was reflected directly in the temperature of the PCM box.

The outboard face of the reservoir was in the plane of the radiator and viewed deep space continuously. Its surface, like the radiator's, was covered with OSR's to permit maximum cooling with solar input. Design values used for the mirror's optical properties were $\alpha/\epsilon = 0.10/0.82$.

A thermal analysis of the reservoir was conducted to determine the cause of the elevated temperatures (Reference 3). The heat balance included solar and infrared inputs, radiation to space, and parasitic radiative and conductive heat flows. Flight data were used in the analysis. The OSR absorptivity, which satisfied the thermal balance at each selected data point, was calculated. The results of this analysis are plotted in Figure 12-14(b).

The effective absorptivity of the OSR's increased from approximately 0.19 at launch to 0.41 two and one-half years later. The oscillation of the individual data points around the mean was due to the sinusoidal variation of the maximum solar intensity. The high points occurred at the solstices, when the intensity was lowest. See Figure 12-14(b) and (c). This was due to the inverse relationship between α and the solar input that occurred in the equation defining the reservoir heat balance. This equation slightly over-compensated for seasonal effects, thus causing the variance from the mean.

The conclusion that the measured ATFC temperatures were due to a degradation of the OSR's was further supported by flight simulation tests conducted with the ATFE Flight Backup Unit at NASA/ARC. During these tests, electrical inputs were applied to the radiator system, including the FCHP gas reservoir, to simulate a solar input corresponding to an $\alpha = 0.20$ (Reference 4). This was the effective absorptivity calculated for an early flight day. The temperature profiles exhibited by the ATFE during this test were in much closer agreement with the early flight temperature profile than those exhibited during the flight acceptance tests, during which an $\alpha = 0.10$ was used to determine heater input.

There is no well-defined reason for the high degradation rates experienced by the ATFE's OSR panels. It is possible that the mirrors were cracking due to discharge of the silver coating. This phenomenon may have occurred because of a difference in electrical potential between the mirror and the substrate to which it was bonded.

In any case, a larger reservoir on the FCHP would have provided a greater margin. The added mass would result in slightly slower response, but overall it would represent an improvement.

Phase-Change Material

The function of the phase-change material package was to provide the ATFE with temperature stability. It accomplished this by absorbing or rejecting heat nearly isothermal as the fusible material melted and froze in the course of its orbital cycle. The fusible material chosen for the AFTE was octadecane because its melting temperature (28°C) was within the desired operating range and because it had a high heat of fusion and a stable melting point.

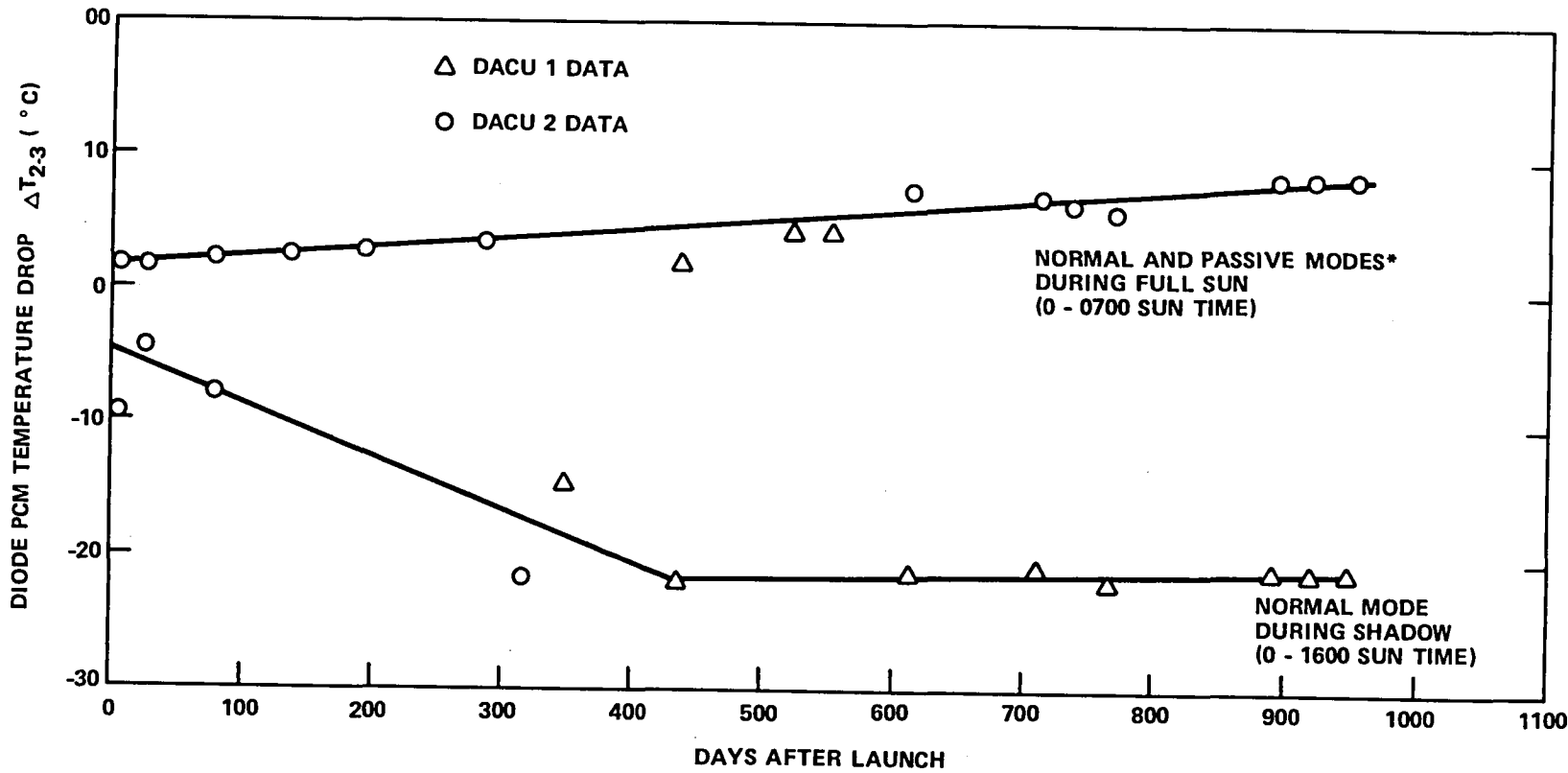
Flight data indicated that the PCM performed as predicted through more than 1800 melt/freeze cycles in a 0-g environment. The PCM melting point was stable at 27.9°C . The normal mode melting interval was 1.3 hours when the PCM was subjected to a thermal throughput of approximately 20 watts. This is consistent with the 26 watt-hours of latent heat energy that the 384 gram charge of octadecane was predicted to supply.

The freezing point remained stable at 27.4°C . The normal mode freezing interval was consistently 6.4 hours. In the passive mode, without the benefit of FCHP shutdown to prevent the heat from escaping through the radiator, PCM freeze occurred in 1.3 hours. The subcooling averaged 0.5°C and was less than 0.7°C in all cases.

Thermal Diode Heat Pipe

The thermal-diode heat pipe effectively performed its major functions during its exposure to the 0-g environment. Every day it transported an average of 20 watts of solar input between the absorber and PCM during its forward mode of operation. Then when the absorber temperature dropped below the PCM temperature during the daily shadow period, it shut down, minimizing the reverse flow of energy. This behavior is illustrated in Figures 12-4 and 12-5 that show the axial temperature profiles and transient response at the beginning of flight. While the absorber stabilized at about -60°C throughout the shadow period, the PCM dropped only slightly below 0°C at the end of the shadow period. This was directly due to low off conductance of both the diode and the FCHP which isolated the PCM from heat sinks at the absorber and radiator.

The diode behavior, nevertheless, did indicate some apparent degradation. Figure 12-15 shows the temperature and the PCM for Sun and shadow conditions in the passive and normal modes as a function of time. During the maximum solar input (approximately 0770 Sun time), the temperature drop was increasing steadily at a rate of 0.007°C per day. However, in the shadow period the temperature drop increased initially and then leveled off after approximately 1 year.



*NORMAL AND PASSIVE MODE ARE THE SAME DURING FULL SUN SINCE FCHP RESERVOIR HEATER IS OFF

Figure 12-15. Diode PCM Temperature Drop vs. Days in Orbit

These two trends indicated that noncondensable gas blockage was occurring. In the shadow period, the shutdown blockage advanced from the transition/low k mitre joint (Figure 11-22, Chapter 11) to somewhere in the forward-mode condenser. The temperature drop remained constant after the gas front reached the condenser section, because at this point all two-phase transfer beyond the condenser was inhibited. The amount of axial-heat conduction was independent of the degree of gas blockage and remained constant; thus, the temperature drop ($\Delta T_{2,3}$) in shadow stabilized as indicated in Figure 12-15.

However, during the forward mode of operation (at approximately 0700 Sun time), the temperature gradient continually increased. This was because the effective conductance decreased proportionally with the increased gas blockage and decreased effective condenser length; hence, forward-mode performance was degrading slightly.

Feedback-Controlled Heat Pipe

The FCHP experienced a steady increase in its operating temperature throughout the flight tests. As noted previously, this was due to the degradation of the second surface mirrors that covered the reservoir's radiator. This led to a higher reservoir temperature that caused the entire heat pipe to run warmer; however, the heat pipe itself did not degrade while in orbit. It transported as much as 30 watts in the forward mode. It performed effectively as an off/on thermal switch to minimize temperature fluctuations at the PCM control point and, at an elevated set point, it was capable of providing temperature stability with variations in heat load and effective sink temperature.

END OF MISSION

During the last 2 to 3 years of its mission, the ATFE was operated primarily in the passive mode. It was without electrical power and the acquisition of telemetry data was suspended. However, the ATFE was subjected to a daily solar cycle with all components responding in the passive mode.

A final set of telemetry data was obtained in early July 1979, after more than 5 years in orbit. The ATFE was operated in both the normal and passive modes during the data acquisition period. The data indicated that the ATFE was functioning much the same as it was during the first 2.5 years. The trends observed with respect to the OSR degradation and the diode's noncondensable gas generation are elaborated below.

The peak temperatures after 1859 days in orbit had increased to 58°C and 53°C at the PCM (T-003) and gas reservoir (T-900), respectively, compared to 53°C and 47°C on day 949 (Figure 12-14). This indicated that while the temperatures were still increasing due to the degradation of the second surface mirrors, the rate of increase had slowed. The effective absorptivity of the OSR's had degraded from 0.41 on day 949 to 0.47 on day 1859.

The 5-year data also indicated that the noncondensable gas generation in the diode had stopped. The temperature gradient between the diode's vapor and the PCM was essentially the same as it was after 2.5 years (Figure 12-15). Finally the behavior of the PCM was virtually unchanged from ground tests after 5 years of daily freeze/thaw cycles in space.

SUMMARY

The Advanced Thermal Control Flight Experiment contained a thermal diode, a phase-change material package and a feedback-controlled heat pipe that were integrated with a solar absorber and a space radiator in a thermal control system. For more than 5 years this system was in a geosynchronous orbit aboard the Applications Technology Satellite-6. Its outboard surface, which viewed deep space, received a daily solar exposure similar to that experienced by a fixed point on the Earth's surface. This solar input continuously exercised the ATFE components with the end-of-mission data being obtained July 3, 1979.

The thermal diode performed effectively as an off/on thermal switch. It carried an average of 20 watts in the forward mode and demonstrated an off conductance of less than 0.03 watt per degree Celsius. It exhibited some apparent noncondensable gas generation that subsided after the first 2.5 years. This increased the forward-mode temperature drop and led to an initial decrease in the reverse-mode conductance.

The octadecane PCM package provided temperature stability in accordance with its design. Its melting and freezing points remained stable at 27.9° and 27.4°C, respectively, through 5 years of daily cycles. Its thermal conductance was unaffected by the 0-g environment and any subcooling effects were negligible. The 26 watt-hour of latent heat energy that it supplied allowed the simulated equipment package to stabilize at the freezing point after 6.4 hours in the shadow period in the normal operational mode.

The FCHP also demonstrated its effectiveness as a thermal control component. It daily transported a forward-mode heat load of approximately 20 watts and carried up to 30 watts in auxiliary mode tests. It operated as an on/off thermal switch by isolating the PCM from the radiator during the shadow period. Its off conductance was also less than 0.03 watt per degree Celsius.

The FCHP was unable to control at the 29°C design set point because the gas reservoir ran hotter than the nominal design conditions. It was determined that the higher reservoir temperatures were caused by degradation of the second surface mirrors (optical solar reflectors) that cover the reservoir's radiator. The effective absorptivity of the OSR's steadily increased throughout the mission. Their nominal value was taken as 0.10, whereas they demonstrated an absorptivity of 0.19 initially in space that increased to approximately 0.47 at the end of the mission. The FCHP's temperature control capability was demonstrated, however, by tests in which a higher control point (46°C) was used to overcome the limitation imposed by the hot reservoir. The feedback system in this test provided control to within $\pm 2^\circ\text{C}$ while the sink temperatures varied 82°C.

In conclusion, the ATFE met all design objectives throughout more than 5 years of flight operation. It can be concluded that feedback controlled heat pipes, thermal-diode heat pipes, and phase-change materials are flight worthy. Their designs are readily available and their behavior is well understood. Finally, their long term performance is well established and on the basis of the ATFE experience, highly reliable.

REFERENCES

1. Brennan, P. J., "Summary Report for Thermal Analysis of ATFE Flight Data," prepared for NASA/ARC under P.O. A 15055 B(KT), December 1975.
2. Kirkpatrick, J. P. and P. J. Brennan, "The Advanced Thermal Control Flight Experiment," AIAA Paper 73-757, *Proceedings of AIAA 8th Thermophysics Conference*, Palm Springs, California, July 16-18, 1973.
3. Suelau, H. J. and P. J. Brennan, "Advanced Thermal Control Flight Experiment Thermal Analysis—First Progress Report," prepared for NASA/ARC under P.O. 8380 B(KT), December 1974.
4. Suelau, H. J. and P. J. Brennan, "Advanced Thermal Control Flight Experiment Thermal Analysis—First Progress Report," prepared for NASA/ARC under P.O. 8380 B(KT), March 1975.
5. Kirkpatrick, J. P. and P. J. Brennan, "Performance Analysis of the Advanced Thermal Control Flight Experiment," AIAA Paper 75-727, March 1975.
6. Kirkpatrick, J. P. and P. J. Brennan, "ATS-6: Flight Performance of the Advanced Thermal Control Flight Experiment," *IEEE Transactions on Aerospace and Electronic Systems*, Vol. AES-11, No. 6, November 1975.
7. Swerdling, B., et al., "Development of a Thermal Diode Heat Pipe for the Advanced Thermal Control Flight Experiment (ATFE)," AIAA Paper 72-260, *Proceedings of AIAA 7th Thermophysics Conference*, San Antonio, Texas, April 10-12, 1972 (also in *AIAA Progress in Astronautics and Aeronautics: Thermal Control and Radiation*, Vol. 31).

CHAPTER 13

QUARTZ-CRYSTAL MICROBALANCE CONTAMINATION MONITOR

INTRODUCTION

The primary objective of the quartz-crystal microbalance (QCM) contamination monitor was to provide data on the return of contaminants to the exterior surfaces of ATS-6.

The QCM measured the deposition of material on the surface by measuring the change of frequency of the quartz crystal due to the increase in the surface mass of the crystal. The crystal frequency was mixed with a reference frequency and the difference frequency was correlated to a mass accretion on the surface of the quartz crystal.

SYSTEM DESCRIPTION

The QCM was a mass measuring device, with the relationship between increased mass deposition on the active area of the crystal to the resonant frequency, Δf , given by:

$$\Delta f = -k f^2 \Delta m$$

where:

Δf = change in resonant frequency

k = calibration constant

f = resonant frequency

Δm = delta mass

The change in resonant frequency, Δf , was measured as a variation from a fixed-frequency reference crystal so that changes in resonant frequency up to 50 kHz were measured with a 1-Hz resolution. Active thermal control of the crystal at 200 K, ± 2 K was used to eliminate the temperature effects on crystal performance. The sensitivity of the QCM was on the order of 10^{-9} grams using a 10-MHz resonant crystal. This allowed detection of less than one equivalent monomolecular layer of water. The beat frequency (Δf) was digitized and returned through spacecraft telemetry with a 1 Hz accuracy.

DATA MEASUREMENT AND EXPERIMENT RESULTS

Results of performance to April 5, 1975, are shown in Figure 13-1. The small accretion on June 3rd to 5th (day 4 to 6) could be attributed to a large outgassed flux that occurred on early orbits. On

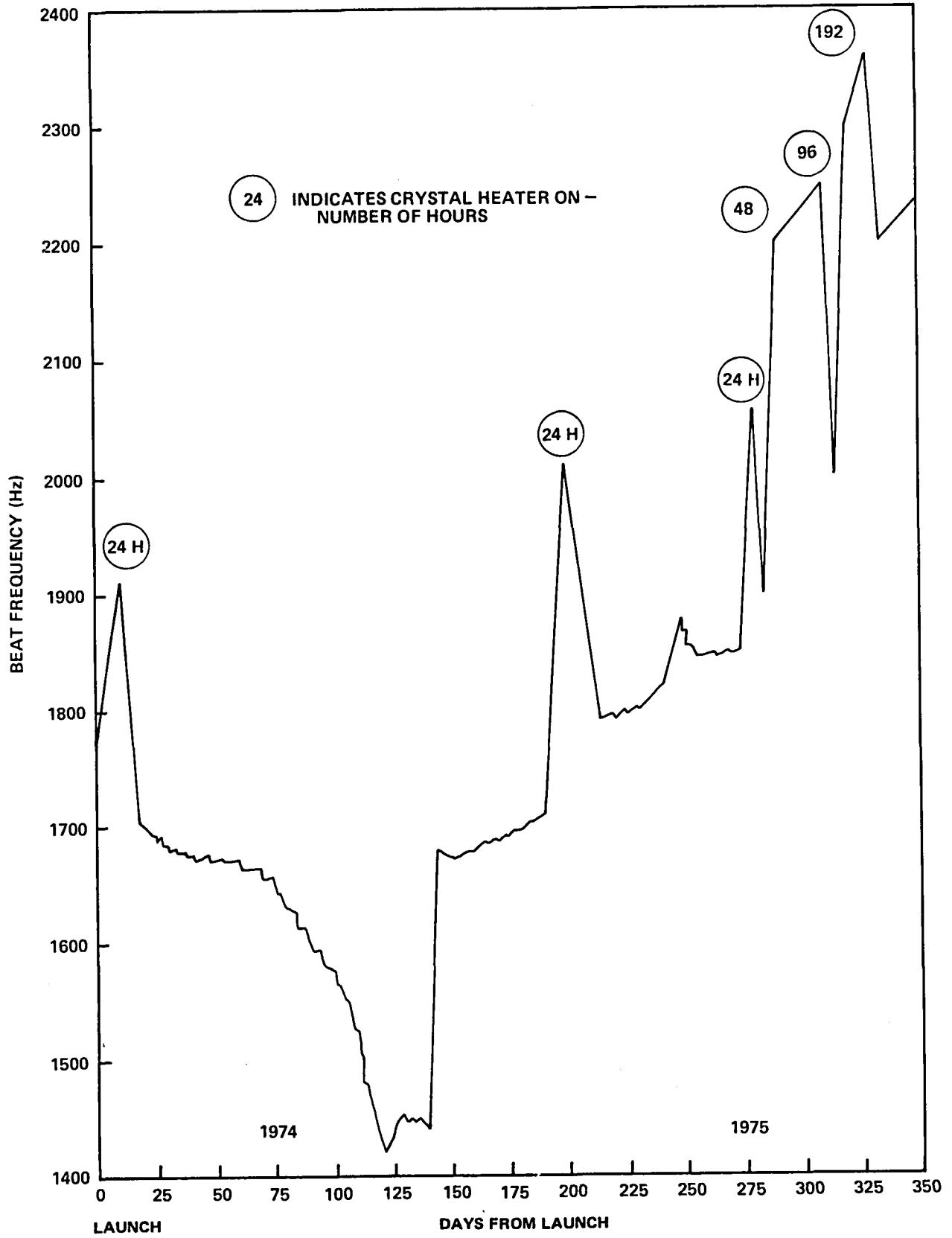


Figure 13-1. Quartz-Crystal Microbalance Data

June 6 (day 7), the crystal was baked out at 50°C with a subsequent loss of $4.45 \times 10^{-13} \text{ g}\cdot\text{cm}^{-2}\cdot\text{s}^{-1}$. This occurred in spite of the fact that the momentum wheels were unloaded many times using the hydrazine thrusters on the north side of the spacecraft.

On October 7, 1974 (day 130), the north cesium ion engine was fired and an accretion rate of $1.0 \times 10^{10} \text{ atoms}\cdot\text{cm}^{-1}\cdot\text{s}^{-1}$ was observed. Between November 1974 and April 1975, mass accretion continued at different rates. The five heating periods can be seen in Figure 13-1. It should be noted that heating periods did not cause a mass desorption to occur.

SIGNIFICANT RESULTS AND SUMMARY

There was no significant accretion due to the firing of the hydrazine thrusters; however, there were accretions due to the cesium ion engines and they appeared to contaminate the surfaces of the QCM.

The QCM was energized on June 30, 1979, during the ATS-6 end-of-life testing and found to be operational.

APPENDIX
ACRONYMS AND ABBREVIATIONS

A

A	ampere
Å	Angstrom
ABC	analog backup controller
AC	attitude control
a.c.	alternating current
ACE	actuator control electronics
ACP	acquisition control program
acq.	acquisition
ACS	attitude control subsystem
ACSN	Appalachian Community Service Network
A/D	analog to digital
ADC	analog-to-digital converter
ADPE	automatic data processing equipment
ADS	automatic deployment sequencer
ADSS	auxiliary digital Sun sensor
ADVM	adaptive delta voice modulation
A/E	absorbitivity to emissivity
Aerosat	aeronautical satellite
AES	Ahmedabad Earth Station
AESP	Appalachian Education Satellite Project
af	audio frequency
AFC	automatic frequency control
AFTE	Advanced Thermal Control Flight Experiment
AGC	automatic gain control
AGE	aerospace ground equipment
Ah	ampere-hour
AID	Agency for International Development
AIDSAT	Agency for International Development Television Demonstration
AIR	All India Radio
ALC	automatic level control
ALED	Alaska Education Experiment
am, AM	amplitude-modulation
AMP	amplifier
AOS	acquisition of satellite
APM	antenna pattern measurement

APT	automatic picture transmission
ARC	Appalachian Regional Commission
ASC	Aerospace Corporation
ASP	automated sequential processor
ASSY	assembly
ASTP	Apollo-Soyuz Test Program
ASTP-TV	ASTP television coverage experiment
ATA	automatic threshold adjust
AT&T	American Telephone and Telegraph (Spacecraft)
ATC	air traffic control, active thermal control
ATFE	Advanced Thermal Control Flight Experiment
atm, ATMOS	atmosphere(s)
ATS	Applications Technology Satellite
ATS-6	Applications Technology Satellite-6
ATSOCC	ATS Operations Control Center
ATS-R	ATS ranging
ATSSIM	ATS simulator
Atten	attenuator (attenuation)
Aux	auxiliary

B

B&E	Broadcast and Engineering
BAM	building attenuation measurement
BB	baseband
BER	bit error rate
bps	bits per second
BRC	Balcones Research Center
BSA	bit synchronization acquisition
BTC	binary time code
BTE	bench test equipment
Btu	British thermal unit
BW	bandwidth

C

C	Celsius
Cap Com	Capsule Communicator
CCIR	International Radio Consultative Committee
CDD	command/decoder distributor
CEE	designator for "career education course for elementary-grade teachers"
CES	designator for "career education course for secondary-grade teachers"
CESP	computer executive system program
CFSS	coarse/fine Sun sensors

CIC	command interface control
CIE	cesium ion engine
C/L	capacitance-to-inductance
cm	centimeter
CM	communications module
C/M	carrier-to-multipath
CMD	command
CMOS	complimentary metal oxide semiconductor
C/N_0	carrier power to spectral noise density ratio
CNR, C/N	carrier-to-noise ratio
cntr	center
Comsat	Communications Satellite Corporation
ConUS,	Continental United States
CONUS	
CONV	converter
COSMOS	complimentary symmetry metal oxide semiconductor
CPI	cross polarization isolation
CPR	cross polarization ratio
CPU	central processing unit
CRT	cathode-ray tube
CSM	command-service module
CSP	command service program
CSS	coarse Sun sensor
CTNE	Companie Telefonica Nacional de Espana
CW	carrier wave, continuous wave

D

DA	design adequacy
D/A	digital to analog
DACU	data acquisition and control unit
DAF	Data Acquisition Facility
dB	decibel
dBi	decibel isotropic (gain relative to an isotropic antenna)
dB/K	decibel per degree Kelvin
dBm	decibels referred to 1 milliwatt
dBW	decibel (reference level 1 watt)
DC	downconverter
d.c.	direct current
DCP	data collection platforms
DDDF	duplex digital data formatter
DDS	digital Sun sensor
DECPSK	differentially encoded coherent phase shift key (modulated)
DEG, deg	degree

DEM	digital evaluation mode
Depl	deployment
DES	Delhi Earth Station
DESA	double electrostatic analyzer
DIB	data input buffer
div	division
DIX	data interface transmitter
DJS	Dzhusaly (designator)
DLO	dual local oscillator
DM	docking module
DOC	digital operational controller
DOD	depth-of-discharge
DOT	Department of Transportation
DOT/FAA	The Department of Transportation/Federal Aviation Administration
DOT/TSC	The Department of Transportation/Transportation Systems Center
DPRI	diagnostic and prescriptive reading instruction
DR	Copenhagen (designator)
DRR	data recorder/reproducer
DRS	direct reception system
DSS	digital Sun sensor
DSU	data switching unit
DTS	data transmission system
DUT	Denver Uplink Terminal

E

EBU	European Broadcast Union
ECH	Earth-coverage horn
ECI	Earth centered inertial
e.d.t., EDT	eastern daylight time
e.i.r.p.	effective isotropic radiated power
EME	Environmental Measurements Experiments
emi, EMI	electromagnetic interference
EML	equivalent monomolecular layer
enc	encoder
Eng.	engineering
EOL	end-of-life
EPIRB	Emergency Position Indicating Radio Beacon
EPS	electrical power subsystem
ERP	effective radiated power
ES	Earth sensor
ESA	Earth sensor assembly, European Space Agency
ESA/PSA	Earth sensor assembly/Polaris sensor assembly
e.s.t., EST	eastern standard time

ETR	Eastern Test Range
eV	electronvolt
EVM	Earth-viewing module
EVT	Eupatoria (designator)

F

f	frequency
F	Fahrenheit
FAA	Federal Aviation Administration
FCC	Federal Communications Commission
FCHP	feedback-controlled variable conductance heat pipe
FCP	flight computer program
FCT	fixed calibration terminal
f/d	ratio of focal distance to diameter
FDM	frequency diversity modulation; frequency division multiplexer
fm, FM	frequency modulated
FOV	field-of-view
FOWG	Flight Operations Working Group
Freq.	frequency
FRMS	Federation of Rocky Mountain States
fsk	frequency shift keying
FSS	fine Sun sensor
ft	foot, feet
FT	frequency translation
ft-lb	foot-pound
FTO	functional test objective
FTS	Federal Telecommunications System

G

g	grams, gravity
G	gain
GAC	ground attitude control
GEOS-3	Geodetic Earth-Orbiting Satellite-3
GFRP	graphite fiber reinforced plastic
GHz	gigahertz
gm	gram
G.m.t., GMT	Greenwich mean time
GRD	ground
GRP	group
GSFC	Goddard Space Flight Center
G/T	dB/K, antenna gain over system noise temperature
GTT	ground transmit terminal
GVHRR	Geosynchronous Very High Resolution Radiometer

H

HAC	Hughes Aircraft Company
HDRSS	high data rate storage system
HET	Health, Education, Telecommunications (experiment)
HEW	Department of Health, Education, and Welfare
hf	high frequency
HGA	high gain antenna
HI	Honeywell International
HPBW	half power bandwidth
HR	hour
HSE	high-speed execute
HTR	heater; high-time resolution
Hz	hertz

I

IBM	International Business Machines
IDT	image dissector tube
IEB	interface electronics box
i.f.	intermediate frequency
IFC	in-flight calibration
IHS	Indian Health Service (Alaska)
IHSDL	interferometer high speed data link
IM	intermodulation
IMF	interplanetary magnetic field
IMP	Interplanetary Monitoring Platform
in.	inch
in.-oz	inch-ounce
Intelsat	International Telecommunications Satellite
INTF	interferometer
I/O	input/output
IPD	Information Processing Division
IR	infrared
IRAC	Interdepartment Radio Advisory Committee
ISRO	Indian Space Research Organization
IT	intensive terminal
ITS	Institute of Telecommunications Sciences
ITU	International Telecommunications Union
I-V	current voltage
IW	inertia wheel
IZMIRAN	Institute of Terrestrial Magnetism, Ionosphere and Radio Wave Propagation

J

JAM	jet-assist mode
Joburg	Johannesburg (designator)
JSC	Johnson Space Center

K

K	Kelvin
kbps	kilobits per second
keV	kiloelectronvolt
kg	kilogram
kHz	kilohertz
km	kilometer
KSC	Kennedy Space Center
kW	kilowatt

L

lb	pound
LC	inductive-capacitance
LD	linear detector
LFT	long form test
LIC	load interface circuit
LLD	lower level discriminator
LO	local oscillator
LOS	line-of-sight
LRIR	limb radiance inversion radiometer
LSB	least significant bit
LT	local time
LV	local vertical
L.V.	latch valve

M

m	meter
m ²	square meter
mA	milliamperes
Mad	Madrid
MAD-HYB	Madrid Hybrid
Mage	U.S./U.S.S.R. Magnetometer Experiment
Marad	Maritime Administration
MASEP	main sequential program
Max.	maximum

MCC-H	Mission Control Center, Houston
MCC-M	Mission Control Center, Moscow
MDAC	McDonnell-Douglas Aircraft Corporation
MDHS	meteorological data handling system
MESC	magneto-electrostatic plasma containment
MeV	megaelectronvolts
MHz	megahertz
μ f	microfarad
μ m	micrometer (micron)
μ s, μ sec	microsecond
MILA	Merritt Island Launch Annex
min, MIN	minute
mlb	millipound
MMW	Millimeter Wave Experiment
mN	millinewton
MOCC	Multisatellite Operations Control Center
MOCR	Mission Operations Control Room
MONO	monopulse
MOR	Mission Operations Room
MOS	metal oxide semiconductor
MSB	most significant bit
ms, msec	millisecond
m/s	meters per second
MT	multitone
mV	millivolts
mW	milliwatt
MWE	Millimeter Wave Experiment
MW XMTR	microwave transmitter

N

N	Newton
NAFEC	National Aviation Facilities Experiment Center
NASA	National Aeronautics and Space Administration
Nascom	NASA Communications Network
NBFM	narrowband frequency modulation
NCC	Network Coordination Center
NCE	normal command encoder
NDR	Hamburg (designator)
nm	nanometer
NMRC	National Maritime Research Center
NOAA	National Oceanic and Atmospheric Administration
N/P	negative/positive
NRL	Naval Research Laboratories

ns nanosecond
 NTSC National Television System Committee color (U.S.)

O

O&M operations and maintenance
 OC orbit control
 OCJ orbit control jet
 OCP operational control program
 o.d. outside diameter
 OD Operations and Distribution (Center)
 omni omnidirectional
 OSR optical solar reflectors
 OSU Ohio State University
 OYA Helsinki (designator)

P

PA power amplifier, preamplifier
 PAL phase alternation live color (Europe)
 PAM pulse amplitude modulated
 PAO Public Affairs Office
 PARAMP parametric amplifier
 PB phonetically balanced
 PBS Public Broadcasting Service
 P_c course phase measurement
 pcm, PCM pulse code modulation
 pcm/fsk/am pulse code modulation/frequency shift keying/amplitude modulation
 PCT portable calibration terminal
 PCU power control unit
 PDM pulse duration modulation
 pf picofarad
 PFD power flux density
 PFF prime-focus feed
 PGE PLACE ground equipment
 PIC power interface circuit
 PLACE Position Location and Aircraft Communications Experiment
 PLU Project Look-Up
 PM phase-modulated
 PN pseudo-noise
 POCC Project Operations Control Center
 p-p peak-to-peak
 PPK Petropavlovsk-Kamchatski (designator)
 ppm parts per million

P_R	reference (phase) signal
P_{rgi}	power received at ground into an isotropic antenna
P_{rsi}	power received at spacecraft into an isotropic antenna
PRU	power regulation unit
PSA	Polaris sensor assembly
P_{SE}	probability function
psia	pounds per square inch absolute
PSK	phase shift keyed
Pv	vernier phase measurement
pW	picowatt
PWR	power

Q

QCM	Quartz-crystal microbalance contamination monitor
Q-M	quadrature phase modulation

R

Radsta	U.S. Coast Guard Radio Station
R&RR	range and range rate
RBE	Radio Beacon Experiment
RCA	Radio Corporation of America
RCC	Resource Coordinating Center
RCV	receive
RDA	rotating detector assembly
REC	receive
Ref., REF	reference
Rel	release
RESA	Regional Education Service Agency
rf	radio frequency
RFC	radio-frequency compatibility
rfi	radio frequency interference
RFIME	Radio Frequency Interference Measurement Experiment
RGA	rate-gyro assembly
RME	Rocky Mountain East
RMPBN	Rocky Mountain Public Broadcast Network
rms	root mean square
RMW	Rocky Mountain West
ROT	receive-only terminal
rpm	revolutions per minute
RR	rain rate

S

S/A	solar array
SAPPSAC	Spacecraft Attitude Precision Pointing and Slewing Adaptive Control (Experiment)
SAR	search and rescue
S&R	surveillance and ranging
Satcom	Satellite Communications
SC	sudden commencement
S/C	spacecraft
SCAMA	switching, conferencing, and monitoring arrangement
SCAMP	small command antenna medium power
SE	system effectiveness
sec, s	second
SECAM	Sequential Couleurs a Memoire (III) color (U.S.S.R.)
SEL	Space Environment Laboratory
SENS	sensor
S.G.	signal generator
SITE	Satellite Instructional Television Experiment
SITEC	sudden increase in total electron content
SIU	squib interface unit
S-IVB	Saturn IB second stage
SMSD	spin motor sync detector
SNR, S/N	signal-to-noise ratio
Spec	specification
SPS	spacecraft propulsion subsystem
SPU	signal processing unit
sr	steradian
SR	Stockholm (designator)
SRT	SAPPSAC remote terminal
SSC	sudden storm commencement
SSEA	Sun sensor electronics assembly
SSR	Staff Support Room
STA	station
STADAN	Space Tracking and Data Acquisition Network
STDN	Spaceflight Tracking and Data Network
STRUCT	structural
SWBT	Southwestern Bell Telephone Company
SYN	synthesizer
SYNC	synchronous
SYSSIM	system simulator

T

T&C	telemetry and command
TACH	tachometer
T&CS	telemetry and command subsystem
T&DRE	Tracking and Data Relay Experiment
TART	transmit and receive terminal
TASO	Television Allocation Study Organization
TBC	time base corrector
TCD	transponder command decoder
TCS	telemetry and command subsystem, thermal control subsystem
TDA	tunnel diode amplifier
TDRE	Tracking and Data Relay Experiment
TEMP	temperature
THIR	temperature-humidity infrared radiometer
TID	traveling ionospheric disturbances
TLM, TM	telemetry
TORQ	torquer
TRUST	Television Relay Using Small Terminals
TSM	thermal structural model
TSP	telemetry service program
TSU	temperature (control) and signal (conditioning) unit
TT/N	test-tone signal-to-noise ratio
TTY	teletype
TV	television
TVOC	Television Operational Control Centers
TWT	traveling wave tube
TWTA	traveling wave tube amplifier

U

UC	upconverter
UCLA	University of California at Los Angeles
UCSD	University of California at San Diego
uhf	ultrahigh frequency
UK	United Kingdom
UKTV	University of Kentucky Television
ulf	ultralow frequency
UNH	University of New Hampshire
U.S.	United States
USA	ubiquitous spectrum analyzer
USAF	United States Air Force
USCG	United States Coast Guard
USK	Ussuriisk (designator)

U.S.S.R. Union of Soviet Socialist Republics
 UT universal time
 UV ultraviolet

V

v velocity
 V volt
 VA Veterans Administration
 VCA voltage controlled amplifier
 VCHP passive "cold-reservoir" variable conductance heat pipe
 VCXO voltage controlled crystal oscillator
 Vdc volts direct current
 V/deg volts per degree
 Vert. vertical
 vhf, VHF very high frequency
 VHRR very high resolution radiometer
 VIP versatile information processor
 VIRS vertical interval reference signal
 VITS vertical interval test signals
 VPI Virginia Polytechnic Institute
 vs. versus
 VSWR voltage standing-wave ratio
 V/T voltage/temperature
 VTR video-tape recorder
 VU MTR VU meter

W

W watt
 WAMI Washington, Alaska, Montana, Idaho (medical education)
 WBDU Wideband Data Unit
 WBVCO wideband voltage-controlled oscillator
 WHL, WH wheel

X

XMIT transmit
 XMTR transmitter
 XTAL crystal
 XTAL DET. crystal detector

Y

YIRU yaw inertial reference unit

Z

ZAZ Z-axis azimuth
Zcoel Z-coelevation

BIBLIOGRAPHY

1. Afifi, M., and B. Keiser, "ATS-6 EMI Field Measurements Techniques and Results," *Proceedings of IEEE EASCON*, 1974.
2. Alexander, J., R. Luzier, and T. Swales, "ATS-F Notching Criteria as Determined by Analysis and Test," 20th Annual Meeting of Institute of Environmental Sciences, Washington, D.C., April 1974.
3. "Applications Technology Satellite-6," *IEEE Transactions on Aerospace and Electronics Systems*, Vol. AES-11, Number 6, November 1975.
4. Bentilla, E. W., et al., "Research and Development Study on Thermal Control by Use of Fusible Materials," Northrop Space Laboratories, NASA N66-26691, April 1966.
5. Bienert, W. and P. J. Brennan, "Transient Performance of Electrical Feedback Controlled Variable Conductance Heat Pipes," ASME Paper 71-Av-27, July 1971.
6. Bienert, W., P. J. Brennan, and J. P. Kirkpatrick, "Feedback Controlled Variable Conductance Heat Pipes," AIAA Paper 71-421, 1971 (also in *AIAA Progress in Astronautics and Aeronautics: Fundamentals of Spacecraft Thermal Design*, Vol 29).
7. Brennan, P. J., "Study to Evaluate the Feasibility of a Feedback Controlled Variable Conductance Heat Pipe," Technical Summary Report NASA CR-73475, September 1970.
8. Corrigan, J. P., "ATS-6 Experiment Summary," *IEEE Transactions on Aerospace and Electronic Systems*, Vol. AES-11, No. 6, November 1975, pp. 1004-1014.
9. Depew, C. A., et al., "Construction and Testing of a Gas-Loaded Passive-Control Variable Conductance Heat Pipe," NASA CR-114597, June 1973.
10. Eby, R., "Performance Verification of ATS-6 Heat Pipes," 2nd Aerospace Testing Seminar, Institute of Environmental Sciences, March 1975.
11. Hale, D. V., et al., "Phase Change Material Handbook," NASA CR-73475, September 1970.
12. Hall, R., and W. Redisch, "ATS-6 Spacecraft Design/Performance," *Proceedings of IEEE EASCON*, 1974.
13. Johnston, Jr., W., "ATS-6 Experimental Communications Satellite—A Report on Early Orbital Results," AIAA 11th Annual Meeting, February 1975, published as reprint in *AIAA Journal of Spacecraft and Rockets*, Vol. 13, No. 2, February 1976.

BIBLIOGRAPHY (continued)

14. Johnston, Jr., W., and A. Whalen, "ATS-6—A Satellite for Human Needs," AIAA Communication Satellite Conference, July 1975.
15. Kampinsky, A., B. Keiser, and P. Mondin, "ATS-F Spacecraft: An EMC Challenge," *IEEE 1974 Symposium on EMC*, Publication No. IEEE 1974 CH0803-7 EMC.
16. Keiser, B., "ATS-6 Spacecraft Surface Treatment for Control of Electrical Discharges," *IEEE Transactions on Electromagnetic Compatibility*, Vol. EMC-17, No. 4, November 1975.
17. LaVigna, T., "The ATS-6 Power System—An Optimized Design for Maximum Power Source Utilization," *Tenth Intersociety Energy Conversion Engineering Conference Proceedings*, 759157, August 18-22, 1975, p. 1048.
18. LaVigna, T., and F. Hornbuckle, "The ATS-6 Power System: Hardware Implementation and Orbital Performance," presented at Intersociety Energy Conversion Conference, 1976.
19. LaVigna, T., and F. Hornbuckle, "The ATS-6 Power System: Hardware Implementation and Orbital Performance," NASA Technical Paper 1023, September 1977.
20. Marcus, B. D., "Theory and Design of Variable Conductance Heat Pipes," NASA CR-2018, April 1972.
21. Marsten, R. B., "ATS-6 Significance," *IEEE Transactions on Aerospace and Electronic Systems*, Vol. AES-11, No. 6, November 1975, pp. 984-993.
22. Patterson, G., "ATS-6 Television Camera Reflector Monitor," *IEEE Transactions on Aerospace and Electronics Systems*, Vol. AES-11, No. 6, November 1975, pp. 1202 thru 1205.
23. Rogers, John F., "ATS-6 Quartz-Crystal Microbalance," *IEEE Transactions on Aerospace and Electronic Systems*, Vol. AES-11, No. 6, November 1975, pp. 1185-1186.
24. Schreib, R., "ATS-6 Propulsion: Two Years in Orbit," AIAA Paper 76-629, *Proceedings of AIAA/SAE 12th Propulsion Conference*, Palo Alto, California, July 26-29, 1976.
25. Schreib, R., "ATS-6 Propulsion Performance: Four Years in Orbit," AIAA Paper 78-1062, *Proceedings of AIAA/SAE 14th Joint Propulsion Conference*, Las Vegas, July 25-27, 1978.
26. Schreib, R., "Flow Anomalies in Small Hydrazine Thruster," AIAA Paper 79-1303, *Proceedings of AIAA/SAE/ASME 15th Joint Propulsion Conference*, Las Vegas, Nevada, June 18-20, 1979.
27. Smith, A., T. LaVigna, and L. Pessin, "Design Impact of a Unique Solar Array Configuration for the ATS-F Electrical Power Subsystem," *Proceedings of Eighth IECEC*, August 1973.

BIBLIOGRAPHY (continued)

28. Smith, A., F. Hornbuckle, and F. Betz, "Evaluation of Flight Acceptance Thermal Testing for the ATS-6 Solar Array," presented at the 11th IEEE Photovoltaic Specialist Conference, 1975.
29. Swerdling, B. and R. Kosson, "Design, Fabrication and Testing of a Thermal Diode," NASA CR-114526, November 1972.

BIBLIOGRAPHIC DATA SHEET

1. Report No. NASA RP-1080	2. Government Accession No.	3. Recipient's Catalog No.	
4. Title and Subtitle ATS-6 Final Engineering Performance Report Volume I - Program and Systems Summaries; Mechanical and Thermal Details		5. Report Date November 1981	
		6. Performing Organization Code 415	
7. Author(s) Robert O. Wales, Editor		8. Performing Organization Report No. 81F0034	
9. Performing Organization Name and Address Goddard Space Flight Center Greenbelt, Maryland 20771		10. Work Unit No.	
		11. Contract or Grant No. NAS 5-25464	
		13. Type of Report and Period Covered Reference Publication	
12. Sponsoring Agency Name and Address National Aeronautics and Space Administration Washington, D.C. 20546		14. Sponsoring Agency Code	
15. Supplementary Notes			
16. Abstract The Applications Technology Satellite 6, an experimental communications spacecraft, operated for five years in a geosynchronous orbit. The six volumes of this report provide an engineering evaluation of the design, operation, and performance of the system and subsystems of ATS-6 and the effect of their design parameters on the various scientific and technological experiments conducted. This volume (I) covers the mission and system summaries, the mechanical subsystems design details and performance, the thermal design details and performance, the heat pipe experiment, and contamination monitor.			
17. Key Words (Selected by Author(s)) SPACE COMMUNICATION, SPACECRAFT COMMUNICATION, EVALUATION, SPACE- CRAFT PERFORMANCE, COMMUNICA- TIONS TECHNOLOGY SATELLITE		18. Distribution Statement Unclassified - Unlimited Subject Category 18	
19. Security Classif. (of this report) Unclassified	20. Security Classif. (of this page) Unclassified	21. No. of Pages 271	22. Price* A13

*For sale by the National Technical Information Service, Springfield, Virginia 22161.

GSFC 25-44 (10/77)

National Aeronautics and
Space Administration

Washington, D.C.
20546

Official Business

Penalty for Private Use, \$300

SPECIAL FOURTH CLASS MAIL
BOOK

Postage and Fees Paid
National Aeronautics and
Space Administration
NASA-451



NASA

POSTMASTER: If Undeliverable (Section 158
Postal Manual) Do Not Return
